

THE X-RAY SCATTERING BEHAVIOR OF MOLECULAR FLUIDS

Thesis by

Paul Frederick Morrison

In Partial Fulfillment of the Requirements

for the Degree of

Doctor of Philosophy

California Institute of Technology

Pasadena, California

1972

(Submitted May 18, 1972)

ACKNOWLEDGMENTS

I would like to express my sincere appreciation for the patient guidance and encouragement given me by my advisor, Dr. C. J. Pings, during the course of this project.

I owe a note of thanks to several people with whom I have had many enlightening conversations. These include Dr. Raymond Schmidt, Dr. Anthony Collings, Dr. George Wignall, Dr. Vincent Gutschick, Dr. William Steele, Mr. Bruce Kirstein, Mr. Joseph Karnicky, and Mr. Hollis Reamer. Mr. and Mrs. Gulari and Mr. Ronald Brown are also owed thanks for making my stay pleasant.

During the course of my research, I have received support from the California Institute of Technology, the Office of Naval Research, and the Air Force Office of Scientific Research. I wish to express my appreciation for these various fundings to both the granting agencies and to Dr. C. J. Pings for making the monies available to me.

Special thanks go to my wife, Sandra, for her cheerful smile, her understanding and her encouragement.

ABSTRACT

The Steele-Pecora equation describing the x-ray scattering behavior of molecular fluids has been investigated. Several molecular scattering factor coefficients, molecular distribution functions for chlorine according to the Percus-Yevick theory, and intensity functions for chlorine have been evaluated using orthonormal expansion methods.

Molecular scattering factors for H_2 , N_2 , LiH, and HF have been obtained as spherical harmonic expansions. The coefficients of the expansions and corresponding gas scattering intensities have been evaluated using both the molecular orbital and isolated atom approaches, and significant differences have been found to exist between the two methods. Chlorine scattering factor coefficients were calculated for the isolated atom approximation only. Expressions for the two-centered Gaussian scattering integral coefficients were derived, and the harmonic expansion technique was shown to be a practical method of calculation.

The Percus-Yevick equation was solved for chlorine by an extension of the Hankel transform method of Chen and Steele. Chlorine was represented by an appropriate two-centered Lennard-Jones potential, the σ and ϵ parameters having been determined from second virial data. Higher order expansions of $f(\underline{R}_1, \underline{R}_2)$, $C(\underline{R}_1, \underline{R}_2)$, and $H(\underline{R}_1, \underline{R}_2)$ were used here than in previous work as well as a more complete representation of the product of two harmonic series. Pair correlation functions

were obtained over the density range $\rho^* = 0.1$ to 1.2 for $T^* = 0.75$, 1.00 , and 1.30 . It was concluded that the first two expansion coefficients of $f(\underline{R}_1, \underline{R}_2)$, $C(\underline{R}_1, \underline{R}_2)$, and $H(\underline{R}_1, \underline{R}_2)$ were sufficient to obtain accurate pair correlation functions over this range of states. For certain states, use of the more complete product expression reduced the error in g_{000} by several percent. Evidence for a chlorine critical point was obtained in the vicinity of $(\rho^*, T^*) = (0.65, 0.70)$.

A version of the Steele-Pecora equation suitable for use with diatomic molecules was derived. Substitution of the chlorine scattering factor coefficients and Percus-Yevick distribution functions into this equation led to the determination of total scattered intensity functions expressed as sums of gas scattering, spherical, and angular intensity contributions. The angular contributions were shown to be experimentally significant in the regions of the first and second peaks at high densities ($\rho^* \gtrsim 1.2$). Temperature was shown to have only a slight effect on total intensity. g_{000} , g_{200} , and g_{220} were found to be the principal contributors to the intensity.

TABLE OF CONTENTS

<u>PART</u>	<u>TITLE</u>	<u>PAGE</u>
	ACKNOWLEDGMENTS	ii
	ABSTRACT	iii
	TABLE OF CONTENTS	v
	LIST OF TABLES	viii
I	INTRODUCTION	1
	A. Liquid State Review	6
	B. Statistical Mechanics of Linear Molecules	11
	C. Molecular X-Ray Scattering	21
	D. Bibliography	31
II	MOLECULAR SCATTERING FACTORS	34
	1. Introduction	35
	2. Theory	36
	3. Results	44
	4. Discussion	47
	5. List of Figures	53
	6. Figures	54
	7. Tables	59
	8. Bibliography	64
III	PERCUS-YEVICK SOLUTIONS FOR THE TWO-CENTERED LENNARD-JONES POTENTIAL	66
	1. Introduction	67
	2. Theory	69
	A. The Percus-Yevick Solution	69

<u>PART</u>	<u>TITLE</u>	<u>PAGE</u>
	B. Expansions of the Pair and Direct Correlation Functions	79
	C. Potential Parameters for Chlorine	82
	3. Numerical Evaluation	90
	4. Results	97
	5. Discussion	138
	6. List of Figures	142
	7. Figures	144
	8. Bibliography	155
IV	X-RAY SCATTERING FROM DIATOMICS	157
	1. Introduction	158
	2. Theory	161
	3. Numerical Evaluation and Results	167
	4. Inversion of Data	180
	5. Discussion	184
	6. List of Figures	188
	7. Figures	190
	8. Bibliography	197
	APPENDICES	199
	1. Scattering Integral Expansions	200
	2. Rederivation of the Steele-Pecora X-ray Scattering Equation	209
	3. Restrictions on the Percus-Yevick Hankel Transforms	219
	4. Clebsch-Gordan Coefficients	221

<u>PART</u>	<u>TITLE</u>	<u>PAGE</u>
	5. Second Virial Coefficients	226
	6. Trigonometric Forms of Spherical Bessel Functions	227
	PROPOSITIONS	228
	1.	229
	2.	241
	3.	253
	4.	261
	5.	272

LIST OF TABLES

<u>PART</u>	<u>TABLE</u>	<u>TITLE</u>	<u>PAGE</u>
II	1	Harmonic Coefficients of Scattering Factor Integrals	59
	2	Scattering Factor Coefficients and Gas Scattering Intensities	61
	3	J Values Required for Convergence of Gas Scattering Intensity	63
III	I	Coefficients of Simultaneous Equations for $H(2002), H(2200), H(2202), H(2204)$	78
	II	Second Virial Coefficients for the Two-Centered Lennard-Jones Potential	84
	III	Parameters of the Kapoor-Martin Second Virial Coefficient	85
	IV	Second Virial Data for Chlorine	87
	V	Two-Centered Lennard-Jones Parameters for Chlorine	88
	VI	$H_{\ell\ell'm}(r)$ Coefficients for $\rho^* = 0.60, T^* = 0.75$	98
	VII	$H_{\ell\ell'm}(r)$ Coefficients for $\rho^* = 1.20, T^* = 0.75$	100
	VIII	$g_{\ell\ell'm}(r)$ Coefficients for $\rho^* = 0.40, T^* = 1.30$	102
	IX	$g_{\ell\ell'm}(r)$ Coefficients for $\rho^* = 0.60, T^* = 1.30$	104
	X	$g_{\ell\ell'm}(r)$ Coefficients for $\rho^* = 0.80, T^* = 1.30$	106
	XI	$g_{\ell\ell'm}(r)$ Coefficients for $\rho^* = 1.00, T^* = 1.30$	108
	XII	$g_{\ell\ell'm}(r)$ Coefficients for $\rho^* = 1.20, T^* = 1.30$	110
	XIII	$g_{\ell\ell'm}(r)$ Coefficients for $\rho^* = 0.40, T^* = 1.00$	112
	XIV	$g_{\ell\ell'm}(r)$ Coefficients for $\rho^* = 0.60, T^* = 1.00$	114
	XV	$g_{\ell\ell'm}(r)$ Coefficients for $\rho^* = 0.80, T^* = 1.00$	116
	XVI	$g_{\ell\ell'm}(r)$ Coefficients for $\rho^* = 1.00, T^* = 1.00$	118

<u>PART</u>	<u>TABLE</u>	<u>TITLE</u>	<u>PAGE</u>
	XVII	$g_{\ell\ell^m}(r)$ Coefficients for $\rho^* = 1.20$, $T^* = 1.00$	120
	XVIII	$g_{\ell\ell^m}(r)$ Coefficients for $\rho^* = 0.40$, $T^* = 0.75$	122
	XIX	$g_{\ell\ell^m}(r)$ Coefficients for $\rho^* = 0.60$, $T^* = 0.75$	124
	XX	$g_{\ell\ell^m}(r)$ Coefficients for $\rho^* = 0.80$, $T^* = 0.75$	126
	XXI	$g_{\ell\ell^m}(r)$ Coefficients for $\rho^* = 1.00$, $T^* = 0.75$	128
	XXII	$g_{\ell\ell^m}(r)$ Coefficients for $\rho^* = 1.20$, $T^* = 0.75$	130
	XXIII	Main Peak Heights of the $g_{\ell\ell^m}(r)$ for $R^* = 0.53$	133
	XXIV	Isothermal Compressibility Values ($R^* = 0.53$)	137
IV	I	Chlorine Molecular Scattering Coefficients	168
	II	X-ray Scattering Functions, $\rho^* = 0.50$, $T^* = 0.75$	170
	III	X-ray Scattering Functions, $\rho^* = 0.80$, $T^* = 0.75$	171
	IV	X-ray Scattering Functions, $\rho^* = 1.20$, $T^* = 0.75$	172
	V	X-ray Scattering Functions, $\rho^* = 1.50$, $T^* = 0.75$	173
	VI	X-ray Scattering Functions, $\rho^* = 1.20$, $T^* = 1.00$	174
	VII	X-ray Scattering Functions, $\rho^* = 1.20$, $T^* = 1.30$	175

-1-

PART I

INTRODUCTION

I. INTRODUCTION

The scattering of x-rays may be used to obtain information about pair distribution functions in fluids. A rigorous theory¹ exists for the treatment of fluids composed of spherical atoms and has been employed with success for over thirty years. The same theory has also been applied to fluids composed of nonspherical molecules² with the major assumption that the x-ray scattering is determined entirely by a spherical molecular pair distribution. This application has met with only partial success because the distribution function of such molecules is not spherical but is dependent upon orientational correlations as well.

A recent theory developed by W. Steele and R. Pecora³ shows the details of the correct form of the x-ray scattering cross-section. In particular, a specific expression for the orientational contribution of the pair distribution function to scattered intensity now exists. It is of interest to know just how large a contribution orientation makes to the total scattering, but at present no numerical information is available. This work therefore undertakes the task of evaluating the total scattering for a nonspherical system from a theoretical standpoint. So as not to complicate the equations and expressions to be evaluated any more than necessary in this initial treatment, we have restricted our attention to linear diatomic molecules. Although other molecules are discussed, the bulk of the work which follows is for chlorine.

When one attempts to evaluate the x-ray intensity, one finds that two quantities must be known as input. The first is the molecular

scattering factor, defined as the spatial integral over the product of the electronic density and its phase factor $e^{i\mathbf{k}\cdot\mathbf{r}}$. The second is the pair distribution function, including its angular correlations over a large temperature and density range. Two methods exist for the calculation of the molecular scattering factor. In one, the atoms of the molecule are assumed spherical and independent of one another⁴. In the other, the molecule is viewed as a whole and is treated quantum mechanically in a manner analogous to atomic scattering factors. Bonding effects are specifically taken into account. As presently formulated, neither approach presents the molecular scattering factor in the form of a harmonic expansion, yet the Steele and Pecora equation demands it to be in this form. We have therefore derived equations for harmonically expanded scattering factors in both treatments. The quantum mechanical treatment (at least for small molecules) was expected to be the most accurate, as had been indicated by earlier work on hydrogen^{6,7} and carbon^{8,9}. However, an investigation over a variety of different molecules and bond types had not been done and the differences between the two treatments were still largely unknown. Harmonically expanded factors have thus been calculated for the four first row molecules, H_2 , N_2 , LiH , and HF using both methods of calculation, and differences have been presented and discussed.

Calculation of the pair distribution function for a nonspherical molecule presents a difficult problem. No such data for a temperature and density dependent function have been previously calculated, and until quite recently no technique was available that might be adapted for the determination of such quantities. The recent

advance that does allow one to calculate these pair distributions is the work of Chen and Steele¹⁰ in which distribution functions in harmonically expanded form were evaluated for a two-centered hard sphere ("dumbbell") potential by solving the Percus-Yevick equation. We have adapted this technique for use with a temperature dependent two-centered Lennard-Jones potential and have evaluated distribution function coefficients for three temperatures and a variety of densities ranging from zero to moderately high values. Behavioral trends of the coefficients as determined by these temperature and density variations are presented and discussed.

The x-ray equation itself was adapted for use with diatomics, both homonuclear and heteronuclear. As indicated above, it was evaluated by using the molecular scattering factor results and pair distribution function coefficients previously obtained. The resulting intensity curves were decomposed into their three main components, the contribution of each being studied as a function of temperature and density. Particular attention was paid to the component composed of the angle-dependent fluid interference terms, the primary interest being to determine if those terms collectively contributed enough to the total intensity to be measurable.

Some theoretical background is called for before the detailed analysis is begun. We therefore devote the remainder of this introduction to a presentation of that background. Since this research ultimately reduces to a study of the fluid state and methods useful for discovering new information about fluid structure, a brief review of fluid (or liquid) state theory is in order and is found in the section

immediately following this one. Nearly all the main theoretical equations evaluated in this work depend on the method of orthonormal D-function expansion advanced by Steele¹¹. Consequently a section is devoted to this, followed by results obtained from its application to hard core Percus-Yevick cluster and integral equations. Lastly, early work on the x-ray scattering from spherical and nonspherical molecules is reviewed. Scattering factor treatments are discussed, and some results for specific systems are considered.

A. Liquid State Review

A continuing problem in statistical mechanics is the prediction of macroscopic properties from microscopic configurational properties. Restricting oneself to equilibrium properties, the thermodynamic properties typically of interest include pressure and volume relationships, isothermal compressibility, the heat capacities C_p or C_v , and molar free energy. The scattering behavior of visible light, neutrons, and x-rays is also of interest since this provides detailed information about the microscopic structure of the fluid as well as further information about the macroscopic thermodynamic properties.

Predicting these fluid properties from theory has been the subject of a great number of studies, beginning with Van der Waals¹². Even the most modern theories still predict certain properties incorrectly, notably pressure and critical state phenomena, and it is apparent that unlike the gaseous or solid states, the liquid state is still far from being solved.

In the region of low density, the theory of Mayer and coworkers¹³ has proven quite accurate. This is the cluster expansion approach and results from an expansion of the configurational integral in Mayer f functions. Virial coefficients and a density expanded version of the pair correlation function have been derived and evaluated for a variety of spherical potentials including the Lennard-Jones (LJ) potential. The theory is only valid at low densities, however, since at higher densities the series apparently becomes nonconvergent¹⁴. It is useful for evaluating higher density theories by comparing their prediction of

virial coefficients against the accurate Mayer values.

The modern theories which have been developed and applied to the moderate and high density region are all distribution function theories¹⁵, these having replaced the older cell theories¹⁶. Distribution functions are desirable because they have direct integral relations to the macroscopic equilibrium properties and for certain systems they are given directly by the Fourier transform of the x-ray scattering intensity. The accuracy of a particular distribution function may thus be assessed by carrying forth the required integrations for a bulk property and comparing the results with experimental data. Within the error bands of present x-ray data, a point by point comparison might be made.

The first dense fluid theories included the Born, Green, and Yvon (BGY) theory¹⁷ and the similar Kirkwood theory¹⁸. These theories led to an open-ended coupled set of integro-differential equations for the set of n^{th} order distribution functions $g^{(n)}(r)$. The set of equations was closed by employing the superposition approximation of Kirkwood. Unfortunately the theory fails badly in predicting the equation of state at liquid densities. A recent attempt¹⁹ has been made to revive this theory by using a higher order superposition approximation, but while an improvement has been made in the results, computation time is nearly prohibitively high.

One of the most successful and widely investigated theories is the Percus-Yevick (PY) theory²⁰. It is similar to the marginally successful hypernetted chain (HNC) theory²¹. In integral form, the PY theory provides an approximation for the direct correlation function

which when solved with the Ornstein-Zernike equation provides a solution for $g(r)$. In spherical form this approximation is

$$c(r) = g(r)[1 - \exp(\beta u(r))]$$

or

$$c(r) \exp[-\beta u(r)] = f(r) g(r)$$

It has been applied at low and high densities²²⁻²⁵ and found to give distribution functions which generally agree with experimental curves and which yield thermodynamic properties that agree well with Monte Carlo and molecular dynamics values. Pressure is a notable exception to this good agreement. Perhaps significantly it also predicts a critical point which agrees quite closely with that for fluid argon and, unlike earlier theories, predicts an infinite isothermal compressibility at the critical point.

Still another approach to the liquid equation of state is the perturbation theory originally set forth by Zwanzig²⁶. The theory expands the Helmholtz free energy as a sum consisting of a contribution from a hard sphere reference potential and a contribution from a term which represents the perturbation of the hard sphere potential to a more complicated potential such as the Lennard-Jones potential. Originally a high temperature expression, it has been modified by Barker and Henderson²⁷ and applied to true liquids. Accurate results require the inclusion of the $g^{(3)}(r)$ and $g^{(4)}(r)$ hard sphere distribution functions which can be only roughly approximated. Dense fluid applications are encouraging but a final evaluation awaits further research.

The aforementioned theories have been applied to a great extent to the spherical molecules composing what is usually termed simple fluids. Theories suitable for application to more complicated fluids composed of nonspherical polyatomic molecules must be capable of explaining the quantitative changes which occur from simple fluid behavior. These include the changes which occur in the equation of state (particularly in the location of phase boundaries), the small changes in the virial coefficients (especially third), the increase of heat capacity values, and the changes in dielectric behavior (especially in the second dielectric virial coefficient). Orientational correlations, rotation, and vibration all contribute to these changes. The latter two effects may be separated and evaluated by standard statistical mechanical expressions, whereas orientational effects must be included specifically in the configuration integral or pair correlation function. If orientation is taken into account, the theories above can be properly generalized for application to nonspherical systems.

Pople and Buckingham²⁸ have used cluster theory with dipole and quadrupole forces included in treating second ordinary and dielectric virial coefficients. They included nonspherical repulsive effects by adding on an arbitrary r^{-12} term multiplied by the sum of two second order Legendre functions depending on orientation angles. More recently, Levine and McQuarrie²⁹ and Stogryn³⁰ have presented general treatments for the evaluation of virial coefficients up through the third for a multipole potential. The repulsive core is spherical, however. Recently Chen and Steele³¹ have evaluated the virial coefficients and density expansion coefficients of the pair correlation

function for linear hard core molecules following cluster theory. They expanded the pair correlation function and cluster integrals in harmonic expansions of the orientational angles, a technique proposed by Steele¹¹ and developed by Sweet and Steele^{32a} in evaluating zero density pair correlation functions for the two-centered Lennard-Jones potential. Chen and Steele¹⁰ also adapted the Percus-Yevick theory for use with linear hard core molecules using harmonic expansions. This work, along with earlier cluster work, was the first to specifically determine the size of the contributions of the orientational effects at moderate densities. Most importantly, it is a general theory and may be further adapted for use with other potentials. It is incapable of yielding very high density results due to convergence problems. Forms of perturbation theory have been applied to slightly nonspherical molecules by Pople³³ in early work and more recently by Kong³⁴ in the calculation of second ordinary and dielectric virial coefficients.

B. Statistical Mechanics of Linear Molecules

Orthonormal Expansions

If a microscopic pair property of a substance, such as its potential or pair distribution function, is expressed in terms of the distance separating two molecules and their mutual Euler angles of orientation, then a very complicated expression often develops. Steele¹¹ advanced a general theory for handling such expressions in which they are orthonormally expanded in the rotational D-functions (or symmetric top functions). An important assumption in this approach is that the molecules are rigid, since if they were to bend freely the Euler angles would lose their meaning. If the position and Euler angles of orientation of a molecule are denoted by \underline{r} and Ω , or collectively by $\underline{R} = (\underline{r}, \Omega)$, then a general function $X(\underline{R}_1, \underline{R}_2)$ may be expressed as

$$X(\underline{R}_1, \underline{R}_2) = 8\pi^2 \sum_{\underline{N}_1} \sum_{\underline{N}_2} X_{\underline{N}_1, \underline{N}_2}(r_{12}) D_{\underline{N}_1}(\Omega_1) D_{\underline{N}_2}(\Omega_2) \quad (1)$$

where the coefficients $X_{\underline{N}_1, \underline{N}_2}(r_{12})$ depend only on the scalar distance between molecules. $\underline{N}_1 = \{K_1, M_1, J_1\}$ and $\sum_{\underline{N}_1} = \sum_{J_1=0}^{\infty} \sum_{M_1=-J_1}^{J_1} \sum_{K_1=-J_1}^{J_1}$. In the case of dealing with linear molecules, the D functions reduce to the usual spherical harmonics since $M_1, M_2 = 0$, $K_1 = -K_2$, and one obtains

$$X(\underline{R}_1, \underline{R}_2) = 4\pi \sum_{\ell=0}^{\infty} \sum_{\ell'=0}^{\infty} \sum_{\underline{m} \in \underline{\ell} \cap \underline{\ell}'} X_{\ell \ell' m}(r_{12}) Y_{\ell, m}(\Omega_1) Y_{\ell', -m}(\Omega_2) \quad (2)$$

where $\underline{\ell} = \{-\ell, -(\ell-1), \dots, (\ell-1), \ell\}$. (In the harmonics the Ω_i represent only two angles instead of a full Euler set of three; i.e.,

$\Omega_i = \{\theta_i, \phi_i\}$.) The Euler angles are always expressed relative to a coordinate system in which the Z axis corresponds to the vector \underline{r}_{12} . This allows one to make use of molecular symmetry in determining the allowable values of ℓ, ℓ', m . This work employs the D function normalization of Steele¹¹ and the harmonic definitions of Rose³⁵ . The factor of 4π is present so that if $X(\underline{R}_1 \underline{R}_2)$ is freely averaged over all orientations, $X_{000}(r)$ is equal to this average. The $X_{\ell\ell', m}$ coefficients may be obtained by multiplying both sides of (2) by $Y_{\ell, m}^*(\Omega_1)$ and $Y_{\ell', -m}^*(\Omega_2)$ and integrating over angles, i.e.,

$$X_{\ell\ell', m}(r) = \frac{1}{4\pi} \int_0^\pi \int_0^\pi \int_0^{2\pi} \int_0^{2\pi} X(\underline{R}_1 \underline{R}_2) Y_{\ell, m}^*(\theta_1 \phi_1) Y_{\ell', -m}^*(\theta_2 \phi_2) d\Omega_1 d\Omega_2 \quad (3)$$

where $d\Omega = \sin \theta d\theta d\phi$.

Symmetry imposes several additional restrictions on the allowable $\ell\ell', m$ values. The orientation angles of two linear molecules are shown in Figure 1. It is clear that the azimuthal functionality of $X(\underline{R}_1 \underline{R}_2)$ depends only on the absolute difference $|\phi_1 - \phi_2|$. If this observation is applied to (3), one can see that the $X_{\ell\ell', m}$ coefficient is invariant to the sign of m . For homonuclear molecules, a restriction on the allowable values of ℓ, ℓ' may be obtained if it is noticed that the $X(\underline{R}_1 \underline{R}_2)$ should be invariant to an end for end switch of either molecule provided the molecular center is taken at the internuclear midpoint. This implies a $(\theta, \phi) \rightarrow (\pi - \theta, \pi + \phi)$ change in the coordinates of one of the spherical harmonics in (2). Since

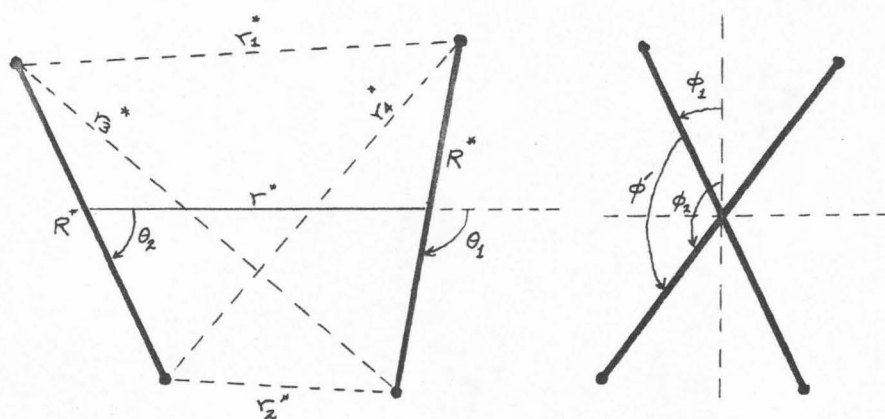


Figure 1

$$\begin{aligned}
 Y_{\ell,m}(\pi-\theta, \pi+\phi) &= P_{\ell,m}(-\cos \theta) e^{im\phi} e^{im\pi} \\
 &= (-)^{\ell+2m} P_{\ell,m}(\cos \theta) e^{im\phi} \\
 &= (-)^{\ell} Y_{\ell,m}(\theta, \phi),
 \end{aligned}$$

it is apparent that if $X(\underline{R}_1, \underline{R}_2)$ is to remain invariant, ℓ (and ℓ') must be even. In the case of heteronuclear molecules, a similar approach shows that the sum $\ell+\ell'$ must be even.

The usual statistical mechanical expressions for spherical molecules may be taken over for nonspherical use by including angles of orientation in the potential, various pair properties, or integrals involved. The configurational integral becomes

$$Z_N = \int \exp[-\beta U(\underline{R}_1, \underline{R}_2, \dots, \underline{R}_N)] d\underline{R}_1 d\underline{R}_2, \dots, d\underline{R}_N \quad (4)$$

and the pair distribution function becomes

$$\begin{aligned}
 \rho^{(2)}(\underline{R}_1, \underline{R}_2) &= \frac{\rho^2}{64\pi^4} g^{(2)}(\underline{R}_1, \underline{R}_2) = \frac{N(N-1)}{Z_N} \int \exp[-\beta U(\underline{R}_1, \dots, \underline{R}_N)] \\
 &\quad \times d\underline{R}_3 \dots d\underline{R}_N
 \end{aligned} \quad (5)$$

In systems whose potential energy derives only from pair interactions, an ensemble averaged configurational property becomes

$$\langle X \rangle = \int X(\underline{R}_1, \underline{R}_2) \rho^{(2)}(\underline{R}_1, \underline{R}_2) d\underline{R}_1 d\underline{R}_2 \quad (6)$$

The standard thermodynamic properties may be obtained by applying (6) to the usual spherical equations. Some results are:

$$\begin{aligned}
 E &= E_{\text{trans}} + E_{\text{vib}} + E_{\text{rot}} + \frac{\rho^2}{128\pi^4} \int \int u(\underline{R}_1 \underline{R}_2) g(\underline{R}_1 \underline{R}_2) d\underline{R}_1 d\underline{R}_2 \\
 P &= \rho kT - \frac{\rho^2}{384\pi^4 V} \int \int \frac{\partial u(\underline{R}_1 \underline{R}_2)}{\partial r_{12}} g(\underline{R}_1 \underline{R}_2) r_{12} d\underline{R}_1 d\underline{R}_2 \\
 \kappa &= \beta \left\{ \rho^{-1} + \frac{1}{64\pi^4 V} \int \int [g(\underline{R}_1 \underline{R}_2) - 1] d\underline{R}_1 d\underline{R}_2 \right\} \quad (7)
 \end{aligned}$$

The isothermal compressibility may be further evaluated by using (1) for the pair correlation function. Because the $D_{\underline{N}}(\Omega)$ are orthogonal functions and $D_{\underline{0}}(\Omega) = (8\pi^2)^{-1/2}$, (7) becomes

$$\kappa = \beta \left\{ \rho^{-1} + \int [g_{\underline{00}}(r) - 1] 4\pi r^2 dr \right\} \quad (8)$$

and the isothermal compressibility depends only on the spherical average of $g(\underline{R}_1 \underline{R}_2)$.

Sweet³² has applied the method of orthonormal expansion to the intermolecular potential and zero density pair correlation function. The Kihara core potential, modified Stockmayer potential, and two-centered Lennard-Jones potential were treated. The latter was employed in this work and has its variables defined by Figure 1 and is given by:

$$u(\underline{R}_1 \underline{R}_2) = \epsilon \sum_{k=1}^4 (r_k^{*-12} - r_k^{*-6}) \quad (9)$$

where

$$r_k = [a_k + (-)^k b \cos \phi']^{1/2}$$

and where

$$a_1 = r^2 + rR(\cos \theta_1 - \cos \theta_2) + \frac{R^2}{2}(1 - \cos \theta_1 \cos \theta_2)$$

$$a_2 = r^2 + rR(\cos \theta_1 - \cos \theta_2) + \frac{R^2}{2}(1 + \cos \theta_1 \cos \theta_2)$$

$$a_3 = r^2 - rR(\cos \theta_1 - \cos \theta_2) + \frac{R^2}{2}(1 - \cos \theta_1 \cos \theta_2)$$

$$a_4 = r^2 - rR(\cos \theta_1 - \cos \theta_2) + \frac{R^2}{2}(1 + \cos \theta_1 \cos \theta_2)$$

$$b = \frac{1}{2} R^2 \sin \theta_1 \sin \theta_2$$

and

$$r_k^* = r_k / \sigma$$

In this potential, the Lennard-Jones type potentials at all four interaction centers are taken to be identical, i.e., have the same σ and ϵ . The σ and ϵ values were determined for a variety of substances by Sweet by fitting theoretical virial data to experimental values.

N_2 , O_2 , CO, and short chain hydrocarbons were treated.

The $u_{\ell\ell'm}$ were evaluated for linear molecules beginning with (3). The ϕ' integration was performed analytically and the theta integrations were done numerically. The zero density $g_{\ell\ell'm}$ were done the same way except that all integrations were done numerically by Gaussian quadrature. The results, which were obtained for a variety of R^* and T^* values, showed that the series were fairly rapidly convergent; even for relative lengthy molecules with $R^* = 0.6$, convergence required only the 200 and some of the 400 series coefficients. The $u_{000}(r)$ and $g_{000}(r)$ functions were always the largest terms. As R^* became longer, the primary effects were to broaden the peaks of the $g_{000}(r)$ and shift them to higher r^* and to generally increase the size of the other $g_{\ell\ell'm}(r)$. The bowl depth of u_{000} became shallower and shifted to higher r^* . The Stockmeyer potential produced

$g_{111}(r)$ and $g_{110}(r)$ functions which for the parameter set $R^* = 0.4$, $T^* = 1.0$, $t^* = \mu^2 / \sqrt{8} \epsilon \sigma^3 = 1.0$ were the largest of the angular correlations and were nearly as large as $g_{000}(r)$.

Percus-Yevick Solutions

The method of orthonormal expansion has been applied by Chen and Steele^{10,31} to the problem of calculating pair correlation functions for linear hard core molecules at moderate densities. They were calculated by two methods, one being the cluster density expansion of the pair correlation function and the other being the integral equation approach. In each case the Percus-Yevick approximation was employed.


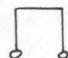
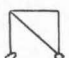
The density expansion for nonspherical systems is

$$g(\underline{R}_1 \underline{R}_2) = g^0(\underline{R}_1 \underline{R}_2) \{ 1 + \rho \text{ (bridge diagram)} + \rho^2 (\text{ (parallel diagram)} + 2 \text{ (bridge diagram)} + \frac{1}{2} \text{ (crossed diagram)} + \frac{1}{2} \text{ (crossed diagram)}) + \dots \} \quad (10)$$

where all Mayer diagrams now include integrations over all the Euler angles of the field points. Application of the Percus-Yevick approximation to (10) required that the bridge and parallel diagrams be neglected, i.e., $(\text{crossed diagram} + \text{crossed diagram}) = 0$ through second order. Chen and Steele truncated the expansion after ρ^2 .

To evaluate (10), $g(\underline{R}_1 \underline{R}_2)$, $g^0(\underline{R}_1 \underline{R}_2)$, and each of the Mayer diagrams were expanded according to (2), the indicated summations and multiplications were carried out, and corresponding coefficients on either side of the equation were identified with one another. The diagrams themselves were evaluated by equating the expansion of the full diagram (expressed relative to \underline{r}_{12}) to the integral over the

expansions of the component Mayer f_{ij} values (each expressed relative to a \underline{r}_{ij} coordinate system), multiplying both sides of the equation by the 1,2 harmonics, and then integrating over the angles of these harmonics. Since each f_{ij} was expanded in a coordinate system relative to the \underline{r}_{ij} vector, each f_{ij} had to be transformed to the 1,2 system in which the entire diagram was expanded by using the rotation matrices of Rose³⁵. The integrations were carried out by a lengthy Fourier transform process.

These calculations showed that the expressions converged rapidly at low to moderate densities. The angular dependent contributions from the cluster integrals were shown to be small at all densities considered, with the bulk of the angular effects of $g(\underline{R}_1 \underline{R}_2)$ being determined by the zero density limit. The 200 coefficient of the  diagram proved to be the largest angular contributor, becoming as much as 10% of the 000 coefficient at $R^* = 0.6$. The  and  diagrams possessed angular coefficients which were negligible. The $g_{000}(r)$ term was composed of contributions from $g^0(\underline{R}_1 \underline{R}_2)$ and from all the cluster diagrams. It was found to become a smoother and more long-ranged function as the molecule became more nonspherical at a fixed reduced density.

Diatomic hard-core virial coefficients were also determined. It was found that the virial coefficients, if reduced by a factor proportional to the molecular volume, changed very slowly with increasing R^* . The $(PV/nRT - 1)$ values derived from evaluation of the virial equation of state showed differences from hard sphere values of 6% for

$R^* = 0.4$ and 13-14% for $R^* = 0.6$ over the entire density range (to $\rho^* = 0.7$). The properties of these nonspherical molecules were thus found to be primarily a function of molecular volume.

The integral equation approach to pair correlation function calculations involved a generalization of the Percus-Yevick (PY) approximation and Ornstein-Zernike equation, i.e.,

$$c(\underline{R}_1 \underline{R}_2) = f(\underline{R}_1 \underline{R}_2) [H(\underline{R}_1 \underline{R}_2) + 1] \quad (11)$$

$$h(\underline{R}_1 \underline{R}_2) = g(\underline{R}_1 \underline{R}_2) - 1 = c(\underline{R}_1 \underline{R}_2) + \frac{\rho}{4\pi} \int c(\underline{R}_1 \underline{R}_3) h(\underline{R}_2 \underline{R}_3) d\underline{R}_3 \quad (12)$$

where $H(\underline{R}_1 \underline{R}_2) + 1$ is the density dependent part of the pair correlation function. (11) was substituted in (12), and both sides of the resulting Percus-Yevick equation were Fourier transformed. By expanding each Fourier kernel according to (2), the PY transform equation was converted to a form where spherical harmonic expansions appeared on both sides of the equation. By equating corresponding coefficients, an infinite series of coupled integral equations was obtained. By truncating the series, a solution was obtained from the remaining series numerically by iteration techniques similar to those employed in spherical systems.

The $H(\underline{R}_1 \underline{R}_2) + 1$ could be identified with the bracketed term of (10) at low densities. Since the cluster terms were described by just the 000 and 200 coefficients, only coefficients with these indices were included in the integral equation calculations. It was noted that a source of probable error at high densities was the neglect of coefficients with indices higher than 200.

Pair correlation functions, inverse isothermal compressibilities, and pressure were calculated for the hard core potential. In general the results were the same as derived from the cluster expansion. Such differences as did occur were the largest at high density, where the cluster approach would be expected to be breaking down. The $g_{000}(r)$ function was a bit more structured in the integral-equation method. The angular $g_{\ell\ell'm}(r)$, however, were in quite close agreement. No critical point was found. The equation of state was only moderately affected by molecular shape, the difference between hard sphere and diatomic hard core values being less than 20% at the highest values of $R^* = 0.6$ and $\rho^* = 1.6$.

C. Molecular X-ray Scattering

X-ray scattering data have been used to supply information about distributions of molecular distances for some time. The relation of the pair distribution function to the diffraction pattern for spherically symmetric fluid systems was developed by Zernike and Prins¹. They showed how the Fourier integral theorem could be applied to obtain the radial distribution function for a single component spherical fluid. Their treatment is to start with the standard expression for scattering from any rigid atomic system

$$I_1(\kappa) = \sum_{n,m}^N f_n(\kappa) f_m^*(\kappa) \exp(i\kappa \cdot \underline{r}_{nm}) \quad (13)$$

where N is the number of atoms in the system and $f_n(\kappa)$ is the atomic scattering factor. To obtain an expression for a fluid system in which the atoms are free to move, (13) must be averaged over space and time. This implies an ensemble average over the n, m pairs. The terms with $n=m$ are split out of (13) and singlet averaged, whereas the other terms remain together and are pair averaged. Thus,

$$\begin{aligned} \langle I_1(\kappa) \rangle &= N |f(\kappa)|^2 + \int |f(\kappa)|^2 \exp(i\kappa \cdot \underline{r}) \rho^{(2)}(\underline{r}_1, \underline{r}_2) d\underline{r}_1 d\underline{r}_2 \\ &= N |f(\kappa)|^2 + V |f(\kappa)|^2 \int \rho^{(2)}(\underline{r}) \exp(i\kappa \cdot \underline{r}) d\underline{r} \end{aligned} \quad (14)$$

Since $\rho^{(2)}(\underline{r}_1, \underline{r}_2) = \rho^2 g^{(2)}(\underline{r}_1, \underline{r}_2)$ and since for spherical fluids the pair distribution function depends only on scalar distances between molecules, one may write

$$V^{-1} \langle I_1(\kappa) \rangle = \rho |f(\kappa)|^2 + \rho^2 |f(\kappa)|^2 \int g(r) j_0(\kappa r) 4\pi r^2 dr \quad (15)$$

where $j_0(Kr) = \sin Kr/Kr$ and the integration has been carried out over the angular variables. To insure convergence of the integral, a term equal to $\rho^2 |f(K)|^2 \int j_0(Kr) 4\pi r^2 dr$ (zero or surface scattering) has been subtracted from (15); the left hand side of (15) remains unchanged except at very low values of K which are outside the experimental range. Thus

$$V^{-1} \langle I_1(K) \rangle = \rho f^2(K) + \rho^2 f^2(K) \int [g(r) - 1] j_0(Kr) 4\pi r^2 dr \quad (16)$$

In application one often sees the identifications

$$i_1(K) = \frac{\langle I_1(K) \rangle - N f^2(K)}{N f^2(K)} = \rho \int [g(r) - 1] j_0(Kr) 4\pi r^2 dr = \rho \hat{h}(K) \quad (17)$$

where $(\hat{})$ signifies the exponential 3-dimensional Fourier transform of $h(r)$. Fourier inversion of (17) leads to

$$r[g(r) - 1] = \frac{1}{2\pi^2 \rho} \int_0^\infty K i_1(K) \sin Kr dK \quad (18)$$

Applications of the Zernike and Prins theory have been many, and reviews by Gingrich³⁶, Furukawa³⁷, Kruh³⁸, and Pings and Paalman³⁹ summarize the results. Some of the most recent work has been done by Pings, et al.⁴⁰ on liquid argon in which distribution functions have been obtained over a relatively large temperature and density range. Mikolaj and Pings have also derived Percus-Yevick potentials from the data by noting that the Fourier transform of the direct correlation function is simply related to $i_1(K)$ by the Fourier transform of the Ornstein-Zernike equation, i.e.,

$$\hat{c}(\kappa) = \frac{\hat{h}(\kappa)}{1 + \rho \hat{h}(\kappa)} = \frac{1}{\rho} \frac{i_1(\kappa)}{1 + i_1(\kappa)}$$

The potential $u_{PY}(r)$ is obtainable directly from the Percus-Yevick approximation if the $c(r)$ derived from $\hat{c}(\kappa)$ is substituted into it; i.e.,

$$u_{PY}(r) = kT \ln \left| 1 - \frac{c(r)}{g(r)} \right|$$

The x-ray scattering from molecules, if given as a function of molecular distribution functions, requires several modifications of the Zernike-Prins development since the scattering centers are no longer spherical and the atoms within molecules are fixed at specific distances and orientations. Until quite recently the molecular equations derived by Menke² were standard. However, orientational effects were only treated approximately, the more complete treatment being developed by Steele and Pecora³. We present both derivations and contrast the two.

Menke began with the atomic sum given by (13) but formed separate sums over the atoms in each molecule. Thus (13) becomes

$$I_1(\kappa) = \sum_{\ell, m}^N \sum_{\mu, \nu}^{N_a} f_{\mu}^{\ell}(\kappa) f_{\nu}^m(\kappa) \exp(i\kappa \cdot \underline{r}_{\mu}^{\ell}) \exp(-i\kappa \cdot \underline{r}_{\nu}^m) \quad (19)$$

where N is the number of molecules and N_a is the number of atoms per molecule. If \underline{r}_{ℓ} is now the location of the molecular center (assumed to be as near as possible to a spherical center), b_{μ}^{ℓ} is the distance to atom μ in molecule ℓ , and f_{μ}^{ℓ} is the atomic scattering factor of atom μ in molecule ℓ .

$$\underline{r}_\mu^\ell = \underline{r}_\ell + \underline{b}_\mu^\ell \quad (20)$$

Introducing the molecular scattering function

$$F_\ell(\kappa) = \sum_\mu f_\mu^\ell(\kappa) \exp(i\kappa \cdot \underline{b}_\mu^\ell), \quad (21)$$

(19) can be rewritten to give

$$I_1(\kappa) = \sum_{\ell, m}^N F_\ell(\kappa) F_m^*(\kappa) \exp[i\kappa \cdot (\underline{r}_\ell - \underline{r}_m)] \quad (22)$$

Noting the similarity between (22) and (13), one may define $F_\ell(\kappa)$ as a molecular scattering factor. In general, it depends on the orientation of molecule ℓ (i.e., on the Euler angles Ω_ℓ) since the \underline{b}_μ^ℓ depend on the orientation.

As in the spherical case, $I_1(\kappa)$ must be ensemble averaged to get the experimentally measurable intensity. Splitting out the $\ell = m$ terms as above, we singlet and pair average over both intermolecular distances and orientations to obtain

$$\begin{aligned} \langle I_1(\kappa) \rangle = & \frac{N}{8\pi^2} \int F_1(\kappa) F_1^*(\kappa) d\Omega_1 + \int F_1(\kappa) F_2^*(\kappa) \\ & \times \exp(i\kappa \cdot \underline{r}_{12}) \rho^{(2)}(\underline{r}_1 \Omega_1; \underline{r}_2 \Omega_2) d\Omega_1 d\Omega_2 d\underline{r}_1 d\underline{r}_2 \end{aligned} \quad (23)$$

An approximation in the Menke approach is that there is no correlation between two molecules and their respective orientations. This is equivalent to stating that $\rho^{(2)}$ is a function of \underline{r}_1 and \underline{r}_2 only; the angular $\rho^{(2)}$ is replaced by a $(8\pi^2)^{-2} \rho^{(2)}(\underline{r})$ spherical term. Hence in (23) the Ω_1 and Ω_2 integrations are carried out over F_1 and F_2 only, each integration corresponding to a random orientational

average over (21). Thus

$$\frac{1}{8\pi^2} \int F(\kappa) d\Omega = \sum_{\mu} f_{\mu}(\kappa) j_0(\kappa b_{\mu})$$

and defining $F_e(\kappa)$

$$\begin{aligned} F_e(\kappa) &= \left(\frac{1}{8\pi^2}\right)^2 \int F_1(\kappa) d\Omega_1 \int F_2^*(\kappa) d\Omega_2 \\ &= \sum_{\mu} \sum_{\nu} f_{\mu}(\kappa) f_{\nu}(\kappa) j_0(\kappa b_{\mu}) j_0(\kappa b_{\nu}) \end{aligned} \quad (24)$$

Also

$$\frac{1}{8\pi^2} \int F_1(\kappa) F_1^*(\kappa) d\Omega_1 = \sum_{\mu} f_{\mu}^2(\kappa) + 2 \sum_{\mu, \mu'} f_{\mu}(\kappa) f_{\mu'}(\kappa) j_0(\kappa b_{\mu\mu'}) = i_g(\kappa)$$

where $b_{\mu\mu'} = |\underline{b}_{\mu} - \underline{b}_{\mu'}|$. Thus (23) in the Menke approximation

becomes

$$\frac{1}{N} \langle I_1(\kappa) \rangle = i_g(\kappa) + 4\pi\rho F_e(\kappa) \int_0^{\infty} [g(r) - 1] r^2 j_0(\kappa r) dr \quad (25)$$

where the angular integrations over \underline{r}_{12} have been carried out.

Steele and Pecora begin their derivation with (22) but define their molecular scattering factor analogous to the way the atomic scattering factors are defined in (13). Using the symbol $a(\kappa\Omega^K)$ for this scattering factor, where the Ω^K are the Euler angles of molecular orientation relative to $\underline{\kappa}$,

$$a(\kappa\Omega^K) = \int \rho(\underline{x}) \exp(i\underline{\kappa} \cdot \underline{x}) d\underline{x} \quad (26)$$

where $\rho(\underline{x})$ is the electronic density within the molecule. Also,

$$I_1(\kappa) = \sum_{\ell, m}^N a_{\ell}(\kappa\Omega_1^K) a_m(\kappa\Omega_2^K) \exp(i\underline{\kappa} \cdot \underline{r}_{\ell m}) \quad (27)$$

The ensemble average of (27) can now be written as in (23) but, unlike Menke, $\rho^{(2)}(\underline{R}_1 \underline{R}_2)$ is left as an orientational dependent function.

In order to carry out the orientational averaging, each of the functions are expanded using the D function orthonormal expansion of Steele. $\rho^{(2)}(\underline{R}_1 \underline{R}_2)$ is expanded according to (1); the exponential of (27) is expanded in spherical waves; and the $a(\kappa \Omega^K)$ are expanded into the harmonic series

$$a(\kappa \Omega^K) = (8\pi^2)^{1/2} \sum_{M,J} a_{0,M}^J(\kappa) D_{0,M}^{*J}(\Omega^K) \quad (28)$$

Both $\rho^{(2)}(\underline{R}_1 \underline{R}_2)$ and the pair $a_1(\kappa \Omega_1^K), a_2(\kappa \Omega_2^K)$ involve Euler angles of molecules 1 and 2, but the angles are given relative to two different coordinate systems. Hence the rotational matrices of Rose must be employed to express these angles in a common coordinate system. Substitution of the resulting scattering factor, $\rho^{(2)}$, and exponential expansions, followed by lengthy integrations over the Euler angles of Ω_1, Ω_2 , and the angular variables of \underline{r}_{12} , lead to the result

$$\begin{aligned} \frac{1}{N} \langle I_1(\kappa) \rangle = & \sum_{M,J} |a_{0,M}^J|^2 + \rho |a_{00}^0|^2 \int [g_{00}(r) - 1] j_0(\kappa r) 4\pi r^2 dr \\ & + \rho \sum_{\substack{N_1, N_2 \\ \neq 0}} (-)^{K_1 - M_1} a_{0, -M_1}^{J_1} a_{0, M_2}^{J_2} \sum_J i^J \frac{2J+1}{2J_2+1} c(JJ_1J_2; 00) c(JJ_1J_2; 0K_2) \\ & \times \int g_{-K_2 M_1 K_2 M_2}^{J_1 J_2}(r) j_J(\kappa r) 4\pi r^2 dr \end{aligned} \quad (29)$$

Details and corrections of the original work may be found in Appendix

2. If $|a_{00}^o|^2$ is identified with the $F_e(\kappa)$ of (24), then it is apparent that the first two terms of (29) are identical with those of (25). For molecules with nearly spherical symmetry such as methane, it would thus appear that the Menke equation is adequate, whereas for less spherical molecules the longer expression of (29) must be employed. The Steele and Pecora result has been applied to only one system, water⁴¹. Only the $a_{00}^o(\kappa)$ scattering coefficient was taken as non-zero and hence the treatment effectively reduced to the Menke approach.

We now mention another technique which may be used to calculate the intensity for a molecular fluid. It is to treat the fluid as a mixture of atomic species in which the intensity is determined by summing over all the atomic scattering factors, ensemble averaging the intensity by using the appropriate two species pair correlation function, i.e., $\rho_{ij}^{(2)}(r)$ functions. The assumption is made that the atoms within the molecules remain as spherically symmetric scattering centers. Following the work of Waser and Schomaker⁴² one may scale the intensity to the gas scattering of a free molecule⁴³ or alternatively to the square of the sum of atomic scattering factors over a molecular stoichiometric unit⁴¹ and Fourier transform the resulting scaled function to give a linear combination of convoluted true radial pair distribution functions. The intensity formula is

$$I(\kappa) = \sum_i x_i f_i^2(\kappa) + \rho \sum_i \sum_j x_i x_j f_i(\kappa) f_j(\kappa) \int [g_{ij}(r) - 1] j_0(\kappa r) 4\pi r^2 dr$$

where i, j denote atomic species and x_i, x_j are mole fractions derived from the molecular stoichiometry. If $[I(\kappa) - \sum_i x_i f_i^2(\kappa)] / [\sum_i x_i f_i(\kappa)]^2$ is denoted by $i_m(\kappa)$, it can be shown that the Fourier

transform of $\kappa i_m(\kappa)$,

$$\rho r H(r) = \frac{1}{2\pi^2} \int_0^\infty \kappa i_m(\kappa) \sin \kappa r \, d\kappa,$$

is given by

$$H(r) = \sum_i \sum_j x_i x_j H_{ij}(r)$$

where

$$H_{ij}(r) = r^{-1} \int_{-\infty}^{\infty} y [g_{ij}(y) - 1] T_{ij}(r-y) dy$$

and

$$T_{ij}(r) = \frac{1}{\pi} \int_0^\infty f_i(\kappa) f_j(\kappa) / \left[\sum_i x_i f_i(\kappa) \right]^2 \cos \kappa r d\kappa$$

The $H(r)$ function is thus not equal to a molecular distribution function of the type used in (23) and requires some careful and often difficult interpretation. Furthermore, as discussed by Pings and Waser⁴⁴, it is not possible to obtain the component $\rho_{ij}^{(2)}(r)$ atomic pair distributions from one experiment, since it provides only enough information to characterize one function. It should be noticed that orientational variables never appear in this treatment. The Waser and Schomaker approach has been applied to several systems in slightly varying form. Carbon tetrachloride, carbon tetrafluoride, bromine, benzene, water, ammonia, t-butyl ammonium fluoride, and methane are a representative few.

In (25) and (29), molecular scattering factors are required. In the former, the molecule is viewed as a collection of independent atoms and the evaluation proceeds from (21). Accurate atomic scattering factors have been given by Cromer and Mann⁴⁵. The most general

expression, however, is (26) and the electronic density $\rho(\underline{r})$ is to be determined from quantum mechanics in order to account for molecular bonding effects. The scattering integrals which result from (26) when $\rho(\underline{r})$ is expanded into Gaussian basis molecular orbitals were first treated by McWeeny⁴⁶. By a contour integration he was able to give integral results for s,s; s,p; and p,p integrals. The same integrals were treated by Krauss and Miller⁴⁷ in which the integrals were expressed as a finite sum of Hermite polynomials. Previous calculations of molecular scattering factors have been restricted for the most part to H_2 ^{6,7} and C-H, C-N, C-O, or C-C bond factors^{8,9}. Hydrogen represented an extreme case since all the electrons are bonding, and thus the MO results were greatly different from isolated atom results. McWeeny showed that good results were obtained by employing just s and p type basis functions, and that the inclusion of configuration interaction had no appreciable effect on the scattering factor values. Stewart was able to show that a good representation for hydrogen was obtainable by using spherical atomic scattering factors for each H atom and floating the centers of these spherical factors 0.07Å off each proton into the bond.

The McWeeny work on carbon bond factors pointed out the need to use the correct valence state (hybrid orbital) when dealing with carbon. Bond distortions were shown to affect the inner part of the scattering factor curve most heavily, while temperature and vibrational effects were greatest in the high κ region. The more recent work of Stewart confirmed the effects of distortion and pointed out that certain integrals, notably $2p\sigma$ integrals, were more anisotropic than indicated

by McWeeny. The general conclusion was reached that scattering factors which rigorously included bonding effects had smaller amplitudes than those calculated from the assumption of independent atomic scatterers. Calculations of molecular scattering factors for complete organic molecules have not generally been performed.

-31-
Bibliography

1. F. Zernike , J. A. Prins, Z. Physik 41, 184 (1927)
2. H. Menke, Z. Physik 33, 593 (1932)
3. W. A. Steele, R. Pecora, J. Chem. Phys. 42, 1863 (1965)
4. P. Debye, Phys. Zeits. 31, 419 (1930)
5. R. W. James, The Optical Principles of the Diffraction of X-Rays
Cornell Univ. Press, 1965
6. R. McWeeny, Acta. Cryst. 5, 463 (1952)
7. R. F. Stewart, E. R. Davidson, W. T. Simpson, J. Chem. Phys. 42,
3175 (1965)
8. R. McWeeny, Acta. Cryst. 7, 180 (1954)
9. R. F. Stewart, J. Chem. Phys. 51, 4569 (1969)
10. Y. D. Chen, W. A. Steele, J. Chem. Phys. 54, 703 (1971)
11. W. A. Steele, J. Chem. Phys. 39, 3197 (1963)
12. J. A. Pryde, The Liquid State, Hutchinson and Co., London, 1966,
p. 13
13. J. E. Mayer, J. Chem. Phys. 5, 67 (1937); with M. G. Mayer,
Statistical Mechanics, J. Wiley, New York, 1940
14. S. A. Rice, P. Gray, The Statistical Mechanics of Simple Liquids
J. Wiley, New York, 1965, Ch. 2
15. T. L. Hill, Statistical Mechanics, McGraw-Hill, New York, 1956,
Ch. 6
16. J. A. Barker, Lattice Theories of the Liquid State, Pergamon Press,
Oxford, 1963
17. M. Born, H. S. Green, Proc. Roy. Soc. (London) A188, 10 (1946);
J. Yvon, Actualités scientifiques et industrielles, Hermann and
Cie, Paris, 1935
18. J. G. Kirkwood, J. Chem. Phys. 14, 180 (1946); 15, 72 (1947)
19. F. H. Ree, Y. T. Lee, T. Ree, J. Chem. Phys. 55, 234 (1971)

20. J. K. Percus, G. J. Yevick, Phys. Rev. 1, 110 (1958); J. K. Percus, Phys. Rev. Letters 8, 462 (1962)
21. (a) J. M. J. Van Leeuwen, J. Groeneveld, J. DeBoer, Physica 25, 792 (1959); (b) E. Meeron, J. Math. Phys. 1, 192 (1960); (c) G. S. Rushbrooke, Physica 26, 259 (1960)
22. (a) A. A. Broyles, J. Chem. Phys. 35, 493 (1961); (b) A. A. Broyles, S. U. Chung, H. L. Sahlin, J. Chem. Phys. 37, 2462 (1962); (c) A. A. Khan, A. A. Broyles, J. Chem. Phys. 43, 43 (1965)
23. (a) G. J. Throop, R. J. Bearman, Physica 32, 1298 (1966); (b) F. Mandel, R. J. Bearman, M. J. Bearman, J. Chem. Phys. 52, 3315 (1970)
24. D. Levesque, Physica 32, 1985 (1966)
25. R. O. Watts, J. Chem. Phys. 48, 50 (1968)
26. R. W. Zwanzig, J. Chem. Phys. 22, 1420 (1954)
27. J. A. Barker, D. Henderson, J. Chem. Phys. 47, 4714 (1967)
28. A. D. Buckingham, J. A. Pople, Trans. Far. Soc. 51, 1173 (1955)
29. H. B. Levine, D. A. McQuarrie, J. Chem. Phys. 44, 3500 (1966)
30. D. Stogryn, J. Chem. Phys. 50, 4967 (1969)
31. Y. D. Chen, W. A. Steele, J. Chem. Phys. 50, 1428 (1969); 52, 5284 (1970)
32. (a) J. R. Sweet, W. A. Steele, J. Chem. Phys. 47, 3022, 3029 (1967); (b) 50, 668 (1969)
33. J. A. Pople, Disc. Far. Soc. 15, 35 (1953)
34. C. L. Kong, J. Chem. Phys. 53, 1516, 1522 (1970)
35. M. E. Rose, Elementary Theory of Angular Momentum, J. Wiley, New York, 1957
36. N. S. Gingrich, Rev. Mod. Phys. 15, 90 (1943)

37. K. Furukawa, Rept. Prog. Phys. 25, 395 (1962)
38. R. F. Kruh, Chem. Rev. 62, 319 (1962)
39. C. J. Pings, H. H. Paalman, Rev. Mod. Phys. 35, 389 (1963)
40. P. G. Mikolaj, C. J. Pings, J. Chem. Phys. 46, 1401, 1412 (1967)
41. A. H. Narten, J. Chem. Phys. 55, 2263 (1971)
42. J. Waser, V. Schomaker, Rev. Mod. Phys. 25, 671 (1953)
43. R. W. Gruebel, G. T. Clayton, J. Chem. Phys. 46, 639 (1967);
47, 195 (1967)
44. C. J. Pings, J. Waser, J. Chem. Phys. 48, 3016 (1968)
45. D. Cromer, J. Mann, Los Alamos Scientific Lab. Report LA-3816
(1968)
46. R. McWeeny, Acta Cryst. 6, 631 (1953)
47. K. J. Miller, M. Krauss, J. Chem. Phys. 47, 3754 (1967)

PART II

MOLECULAR SCATTERING FACTORS

Introduction

Molecular scattering factors in X-ray analysis are most often calculated from the isolated atom equation originally derived by Debye.^{1,2} In this equation a polyatomic molecule is viewed as being composed of independent atoms located at the ends of interatomic vectors known primarily from spectroscopic data. The molecular scattering factor is then a weighted sum over the atomic scattering factors held at these interatomic distances.

As first discussed by McWeeny³ and most recently by Tavard^{5,6} and Stewart,^{7,8} this approach ignores distortions in the electronic density due to bonding. In this paper we calculate molecular scattering factors for the ground states of H_2 , N_2 , LiH , and HF using Gaussian Hartree-Fock SCF results so as to include the effects of bonding. The factors are expressed as harmonic expansions, a formalism having several advantages over other approaches, the principal one being that all orientational information may be stored in a small number of coefficients. Most previous work^{4,7,8} has recalculated the results for each orientation of the molecule with respect to the scattering vector κ . The expansion technique was first suggested by McWeeny⁴ and was recently developed as an expansion of equivalent symmetric top functions by Steele and Pecora.⁹ Steele and Pecora also derived the most complete fluid

X-ray scattering equation to date, and in order to be compatible with their work we have followed their scattering factor formula closely. We compare our results to isolated atom results and, in the case of hydrogen, to the earlier MO results of Stewart.⁷

These four molecular cases were chosen so as to represent a great variety of bonding cases. Below we present the harmonic expansions for the scattering factor integrals based on two-center Gaussian wavefunctions and their relation to Pecora's equation. Specific results for the scattering factor coefficients for the molecules studied come next, followed by comparisons with the isolated atom results. Lastly convergence of the series representations of the coefficients and the choice of two-center expansions is discussed.

Theory

It is our primary purpose to evaluate the coefficients in the molecular scattering factor derived by Steele and Pecora, i.e., the $a_{0,M}^J(\kappa)$ in

$$a(\kappa, \Omega^K) = (8\pi^2)^{1/2} \sum_J \sum_{M=-J}^J a_{0,M}^J(\kappa) D_{0,M}^{*J}(\Omega^K), \quad (1)$$

where κ is the usual scattering parameter $4\pi \sin\theta/\lambda$, Ω^K is the set of Euler angles of the molecule giving its orientation relative to a laboratory coordinate system,

and $D_{\kappa, M}^J(\Omega)$ is the rotational or symmetric top function.¹⁰ In this paper we study only diatomic molecules and therefore have the symmetry restrictions on (1) that $M=0$ and that, for homonuclear diatomics, J is even. Thus $D_{0M}^{*J}(\Omega^K)$ reduces to a spherical harmonic and

$$a(\kappa, \Omega^K) = (4\pi)^{1/2} \sum_J a_J(\kappa) Y_{J,0}(\Omega^K) . \quad (2)$$

In the case of closed shell diatomics we may write an alternative formula for $a(\kappa, \Omega^K)$ in terms of doubly occupied spatial molecular orbitals.⁵ By definition,

$$a(\kappa, \Omega^K) = \int \rho(\underline{r}) \exp(i\kappa \cdot \underline{r}) d\underline{r} \quad (3)$$

where $\rho(\underline{r})$ is the one electron density for the molecule expressed in a molecular fixed coordinate system. For our closed-shell cases we may express $\rho(\underline{r})$ in Hartree-Fock orbitals as

$$\rho(\underline{r}) = 2 \sum_n \phi_n \phi_n^* . \quad (4)$$

Thus,

$$a(\kappa, \Omega^K) = 2 \sum_n \langle \phi_n | \exp(i\kappa \cdot \underline{r}) | \phi_n \rangle . \quad (5)$$

In this work we have assumed the molecular orbitals to be expanded in two-center Gaussian basis functions. This choice was made because, in general, two-center functions are more accurate than one-center functions, and

Gaussian scattering factor integrals are analytic. From (5) we are therefore led to a sum of integrals of the form

$$a(\kappa, \Omega^{\kappa}) = 2 \sum_n \sum_i \sum_j c_i^n c_j^n \langle B_i | e^{i\vec{\kappa} \cdot \vec{r}} | B_j \rangle, \quad (6)$$

where B_i represents real s, x, y or z Gaussian basis functions. Although it is possible to do so, like McWeeny, we have not included d orbitals as we expect their effect on electronic density to be minimal. The integrals in (6) have been evaluated by McWeeny.³

It is our purpose to expand these integrals into harmonic series. However, McWeeny's results are not in this form and must be transformed to it. This can be done most easily for diatomics by taking the center of the coordinate system as the mid-point of the internuclear axis, and then noting that each integral of McWeeny's is a product of a factor of the form $e^{i\vec{\gamma} \cdot \vec{R}}$ and a factor expressible as a first or second power function of $\hat{\vec{\kappa}} \cdot \vec{R}$. If the exponential is then plane wave expanded, the $\hat{\vec{\kappa}} \cdot \vec{R}$ function is expressed as a spherical harmonic, and the resulting product of spherical harmonics is combined into one by the spherical harmonic coupling rule, then the desired expansion can be obtained.

We will show this derivation for the single case of $I = \langle s_A | e^{i\vec{\kappa} \cdot \vec{r}} | z_B \rangle$. The coordinate system used is in Figure 1. I is the integral denoted by McWeeny as $(1s, a|f|2p, b)$ and, after allowing for our coordinate change, is found equal to

$$I = A(-2\alpha\beta R \cdot \hat{k} + i\kappa\beta\hat{k} \cdot \hat{k}) / (\alpha+\beta) \exp(i\hat{k} \cdot \hat{R}q) \quad (7)$$

where \hat{k} and \hat{k} are unit vectors along the scattering vector and z-axis respectively, α is the Gaussian exponent on center A, β is the Gaussian exponent on center B, R is the internuclear distance,

$$A = \frac{1}{2} \beta^{-1} \left(\frac{\pi}{\alpha+\beta} \right)^{\frac{3}{2}} \exp \left(\frac{-4\alpha\beta R^2 - \kappa^2}{4(\alpha+\beta)} \right), \quad (8)$$

and

$$q = \frac{\kappa R(\beta-\alpha)}{2(\alpha+\beta)} \quad (9)$$

Now notice that $R \cdot \hat{k} = R$ and $\hat{k} \cdot \hat{k} = \cos\theta = \left(\frac{4\pi}{3} \right)^{\frac{1}{2}} Y_{1,0}(\theta)$.

If these identities are then substituted into (7) and the complex exponential is expanded into spherical waves, then there results

$$I = \frac{-2A\alpha\beta R}{\alpha+\beta} \sum_{\ell=0}^{\infty} [4\pi(2\ell+1)]^{1/2} j_{\ell}(q) Y_{\ell,0}(\theta) \quad (10)$$

$$+ \frac{iA\kappa\beta}{\alpha+\beta} \left(\frac{4\pi}{3} \right)^{\frac{1}{2}} \sum_{\ell=0}^{\infty} [4\pi(2\ell+1)]^{1/2} j_{\ell}(q) Y_{\ell,0}(\theta) Y_{1,0}(\theta)$$

In the second summation in (10) we may use the identity¹⁰

$$Y_{\ell_1 m_1}(\theta\phi) Y_{\ell_2 m_2}(\theta\phi) = \sum_{\lambda} \left[\frac{(2\ell_1+1)(2\ell_2+1)}{4\pi(2\lambda+1)} \right]^{1/2} c(\ell_1 \ell_2 \lambda; m_1 m_2) c(\ell_1 \ell_2 \lambda; 00) \quad (11)$$

$$+ Y_{\lambda, m_1+m_2}(\theta\phi),$$

where the range of λ is $|\ell_1 - \ell_2|$ to $\ell_1 + \ell_2$ and the $c(\ell_1 \ell_2 \lambda; m_1 m_2)$ are Clebsch-Gordon coefficients. These coefficients are

readily available.¹¹ Thus we obtain

$$I = \frac{-2A\alpha\beta R}{(\alpha+\beta)} \sum_{\ell=0}^{\infty} [4\pi(2\ell+1)]^{1/2} j_{\ell}(q) Y_{\ell,0}(\theta) \quad (12)$$

$$+ \frac{A\kappa\beta}{\alpha+\beta} (4\pi)^{1/2} \sum_{\ell=0}^{\infty} (2\ell+1) i^{\ell+1} j_{\ell}(q) \sum_{\lambda=|\ell-1|}^{\ell+1} \frac{[c(\ell 1 \lambda; 00)]^2}{(2\lambda+1)^{1/2}} Y_{\lambda,0}(\theta)$$

(2)

Note that because of the symmetry of Clebsch-Gordon coefficients that λ goes in steps of two. Finally, the second series in (12) can be rearranged to give a single series by regrouping the indices and one is led to

$$\frac{A\kappa\beta}{\alpha+\beta} (4\pi)^{1/2} \left[-j_1(q) Y_{00}(\theta) + \sum_{J=1}^{\infty} \sum_{\ell=J-1}^{J+1} (2\ell+1) i^{\ell+1} j_{\ell}(q) \frac{[C(\ell 1 J; 00)]^2}{(2J+1)^{1/2}} Y_{J,0}(\theta) \right] \quad (13)$$

(2)

The case $J=0$ must be treated as a special case since $\ell=J+1=1$ only. Putting (13) into (12) we obtain the desired single harmonic expansion and the coefficient of a particular harmonic is easily identified.

Similar expansions to the one for $\langle s_A | e^{i\mathbf{k} \cdot \mathbf{r}} | z_B \rangle$ may be carried out for $\langle s_A | e^{i\mathbf{k} \cdot \mathbf{r}} | s_B \rangle$, $\langle z_A | e^{i\mathbf{k} \cdot \mathbf{r}} | z_B \rangle$, $\langle x_A | e^{i\mathbf{k} \cdot \mathbf{r}} | x_B \rangle$, $\langle y_A | e^{i\mathbf{k} \cdot \mathbf{r}} | y_B \rangle$, and permutations of these integrals. In the case of the x and y integrals it is easier to make the expansions if the linear combination $\langle x_A | e^{i\mathbf{k} \cdot \mathbf{r}} | x_B \rangle + \langle y_A | e^{i\mathbf{k} \cdot \mathbf{r}} | y_B \rangle$ is considered. Since we are dealing only

with cylindrical diatomics using $\phi_{\pi x}$ and $\phi_{\pi y}$ orbitals, this is the only way the x and y integrals appear in the final result. In the case of the integrals where the basis functions share the same center, the results from the two center calculations may be extended if the inter-nuclear distance R is set equal to zero and the argument q of the spherical bessel functions is changed from that in (9) to $-\kappa R/2$ when center A is shared, to $+\kappa R/2$ when center B is shared. Table 1 summarizes the results for the integrals considered in this work; the Jth coefficient is tabulated.

If the harmonic expansions just obtained for the integrals are denoted by

$$\langle B_i | e^{i\vec{\kappa} \cdot \vec{r}} | B_j \rangle = \sum_{J=0}^{\infty} D_{Jij}(\kappa) Y_{J,0}(\theta) ,$$

then from (6) and (2) we see that

$$a_J(\kappa) = \left(\frac{1}{\pi}\right)^{1/2} \sum_n \sum_{i,j} c_i^n c_j^n D_{Jij}(\kappa) . \quad (14)$$

(14) was used to calculate the MO scattering coefficients tabulated in the next section.

We now turn to the form of the molecular scattering factor obtained from the assumption of independent atom scatterers. The basic scattering equation is the familiar weighted sum over atomic scattering factors¹

$$a(\kappa, \Omega^{\kappa}) = \sum_j f_j(\kappa) e^{i\vec{\kappa} \cdot \vec{r}_j} \quad (15)$$

where j is the sum over atoms in the molecule, r_j is the vector distance of atom j from the origin of the system, and κ is the z -axis in the laboratory system. Expand the exponential to give

$$a(\kappa, \Omega^K) = \sum_j f_j(\kappa) \sum_{J=0}^{\infty} [(2J+1)4\pi]^{1/2} i^J j_J(\kappa r_j) Y_{J,0}(\theta_x^j \phi_x^j) \quad (16)$$

where x denotes the laboratory system. We want each atom expressed in molecular-fixed coordinates rather than laboratory coordinates. Hence we will use the identity¹²

$$D_{\kappa M}^J(\Omega_A) = \sum_R D_{\kappa, R}^J(\Omega_{AB}) D_{R, M}^J(\Omega_B) \left(\frac{8\pi^2}{2J+1} \right)^{1/2}, \quad (17)$$

where Ω_{AB} is the set of Euler angles rotating A into B, Ω_A is the set rotating A into C, and Ω_B is the set rotating B into C. Our D function normalization convention is that of Steele, Pecora⁹. From the general expression¹⁰ $D_{\kappa, 0}^J(\alpha\beta 0) = (2\pi)^{-1/2} Y_{J, \kappa}^*(\beta\alpha)$, we note that $D_{00}^J(\phi_x \theta_x) = (2\pi)^{-1/2} Y_{J, 0}(\theta_x \phi_x)$. Thus from this last equality and (17) we obtain the molecular fixed expression for $Y_{J, 0}(\theta_x \phi_x)$ and may substitute it into (16) to yield

$$a(\kappa, \Omega^K) = (8\pi^2)^{1/2} \sum_{J=0}^{\infty} \sum_{R=-J}^J \sum_j f_j(\kappa) i^J j_J(\kappa r_j) D_{R, 0}^{*J}(\phi_m^j \theta_m^j) (8\pi^2)^{1/2} D_{0, R}^{*J}(\Omega^K) \quad (18)$$

where Ω^K rotates the laboratory axes into the molecular fixed axes. If we now compare equations (1) and (18), we see that

$$a_{0M}^J(\kappa) = (4\pi)^{1/2} \sum_j f_j(\kappa) i^J j_J(\kappa r_j) Y_{J,M}(\theta_{jm}^j, \phi_{jm}^j) \quad (19)$$

This is the general equation for the harmonic expansion coefficients of the scattering factor for a rigid molecule of independent scatterers. In the case of heteronuclear diatomics, using the coordinate system in Figure 1, (19) reduces to

$$a_{00}^J(\kappa) \equiv a_J(\kappa) = (2J+1)^{1/2} i^J ((-)^J f_A(\kappa) + f_B(\kappa)) j_J(\kappa \frac{R}{2}) \quad (20)$$

If both (13) and (20) are expanded, it will be seen that the odd J terms drop out for homonuclear diatomics as symmetry tells us they should.

We note two other properties of the harmonic scattering factors. First are the values of the $a_J(\kappa)$ at $\kappa=0$. If an angular average is taken over the expression (3) we find

$$a_0(\kappa) = 4\pi \int \rho_0(x) \frac{\sin \kappa x}{\kappa x} x^2 dx ,$$

where $\rho_0(x)$ is the spherical average of the electron density. Hence $a_0(0)$ equals the number of electrons in the molecule, N. From a typical expansion such as (13) or (19), we see that all other $a_J(0)=0$ because $j_J(0)=0$. Secondly, we restate the expression for the scattering intensity from a single freely rotating molecule (gas scattering)⁹,

$$I(\kappa) = \sum_J \sum_{M=-J}^J |a_{0M}^J(\kappa)|^2 , \quad (21)$$

this being equivalent to the expression (9.41) given in James¹.

Results

We first note the source of the wavefunctions we have used to calculate the MO scattering factors. Except for nitrogen, we have begun with previously published wavefunctions, retained only the s and p basis functions, and reoptimized the coefficients using a version of POLYATOM¹³. The LiH, H₂, and HF wavefunctions were derived from references 14, 15, and 16 respectively. The LiH and H₂ functions were originally given in Slater-type orbitals which were converted to a Gaussian set using Huzinaga's results.¹⁷ The HF function was given as a Gaussian set originally but was not at the equilibrium distance of 1.7328 a.u. and was therefore reoptimized for this distance. In the case of nitrogen we have used the recent results of Dunning.¹⁸ The composition and the total energies of the final wavefunctions used were: H₂, 7s4p, -1.133055 a.u.; LiH, <5s5p/3s1p>, -7.98309 a.u.; N₂, <4s3p>, -108.88768 a.u.; HF, 9s5p/3s1p, -100.016386 a.u. The sets for LiH and N₂ employ contracted orbitals and if described by uncontracted orbitals are, respectively, 8s5p/6s1p and 9s5p.

The numerical accuracy of the program computing the MO scattering coefficients was checked by allowing κ to equal zero and then checking the resulting Gaussian overlap integrals for equality against those computed in an independent Hartree-Fock program; the behavior $a_J(0) = N\delta_{J,0}$ mentioned

above was also verified. Furthermore, the calculation for hydrogen allowed us to compare our results to those of Stewart.⁷ We did this by taking his results for the best H-atom spherical density scattering factors and substituting these into equation (20), using his value of $0.81 R_e$ ($R_e = 1.4009$ a.u.) for the internuclear distance. The a_0 coefficient and gas scattering values obtained in this way are very close to those obtained by us; the higher coefficients are less close. Exact duplication should not be expected since we have used Stewart's averaged values; after taking this into account, the agreement found was deemed to be a satisfactory check.

In Table 2 are found the first few MO scattering coefficients calculated from (14) for each of the molecules studied as well as the corresponding values for gas scattering from (21). κ is in reciprocal angstroms. The a_j and the gas scattering intensities, originally calculated in electrons and electrons squared, have been reduced by N (the number of electrons in the molecule) and N^2 respectively. Since total scattering amplitude is roughly proportional to the number of electrons in the molecule, these scaling factors allow for easy comparisons between molecules. a_1 values have been listed as real values and are to be multiplied by i before use. The gas scattering for HF has been obtained previously by Hake and Banyard;¹⁹ our results compare well with their one-center (OCE) result. We have

also obtained isolated atom (IA) scattering coefficients from (20) where we used the atomic scattering factors^{20,21} H^0 for H_2 , N^0 for N_2 , Li^+ , H^- and Li^0 , H^0 for LiH , F^- and H^0 , F^0 for HF . One should note that the higher $a_J(\kappa)$ coefficients for F^- are not zero since the center of the molecule does not lie at the F nucleus. The IA and MO $a_0(\kappa)$ coefficients differ by about 3% maximum up to $\kappa=5.5A^{-1}$; corresponding differences for each of $a_1(\kappa)$ and $a_2(\kappa)$ are about 5% maximum.

Some of the a_0 , a_1 , a_2 coefficients obtained by us are plotted in figures 2-4. We have plotted only those coefficients which differ to a significant degree from the curves obtained from the IA calculations. The a_4 coefficients for both H_2 and N_2 differ considerably from IA values but have not been plotted because of space.

The gas scattering curves from both the IA and MO calculations are shown in figure 5. The hydrogen values have not been plotted since they are available elsewhere⁷. In the case of LiH we have plotted the IA values from Li^+ , H^- as well as Li^0 , H^0 . While differences between these two are nearly too small to be seen in the graphs of the $a_J(\kappa)$, they do become apparent in the gas scattering. In general, the gas differences are greater in the case of Li^+ , H^- , although neither is very accurate. If in the case of HF one compares the MO gas scattering result to the IA result for F^- , it is found that the plots of the two gas curves are practically indistinguishable. The

zero valence state treatment leads to maximum gas scattering errors of 15.8% and 7.3% for LiH and HF respectively, whereas the ionic states lead to a 21.7% error for LiH and an error of less than 2.0% for HF. N_2 shows much the same behavior for MO and IA results.

Another result of importance is the determination of the convergence rate of the series for gas scattering, (21). In Table 3 we have recorded the largest J value in $a_J(\kappa)$ required to make $I(\kappa)$ convergent to four significant figures. As one progresses to higher κ values it can be seen that more coefficients are required. However, even in the worst case of LiH only thirteen coefficients are required at $\kappa=6.0$ a.u. In view of the fact that it does not take much time to calculate these coefficients (less than 1 min/molecule on the 360), we see that (21) is a rapidly converging series presenting no computational problem.

Discussion

One of the principal results of this work is the demonstration that the harmonic expansion of the molecular scattering factor is a truly practical technique. The convergence data in Table 3 indicate that great numbers of the $a_J(\kappa)$ coefficients do not have to be calculated for 10^{-4} convergence accuracy, even in the cases of LiH and HF where the center of the coordinate system is far from any point which might be taken as the center of

a spherical system where convergence rates would be expected to be rapid. When coupled with fast computation times for each $a_j(\kappa)$, the feasibility of the MO calculation becomes apparent. It is to be noted that much of the time for these two-center calculations goes into the evaluation of the spherical Bessel functions required in (19) and Table 1, and thus the more efficient this routine may be made, the more efficient is the entire calculation.

Perhaps the greatest advantage of having this harmonic expansion is that data covering the entire orientational range of the molecule can be easily tabulated, thereby replacing the long columns of $a(\kappa\Omega^K)$, Ω^K data which would be needed otherwise. It will be particularly useful for the case where one wishes to perform an orientational average of some sort over the scattering factor, as did Pecora and Steele.⁹ The expansion allows one to perform an analytical average over angles and thus avoid the interpolation of $a(\kappa\Omega^K)$ over Ω^K which would be required if one had only $a(\kappa\Omega^K)$, Ω^K tabulated data.

The differences between the MO calculations and the isolated atom results plotted in figures 2-4 are large enough to be significant (i.e. experimentally measurable), a conclusion reached earlier by McWeeny⁴ and Stewart⁸ in their work. It should be noted that the gas scattering

curves give a better impression of the errors involved here than do the individual $a_J(\kappa)$ curves. This is due to the fact that the experimental quantity measured is the intensity, which is proportional to squares or products of the $a_J(\kappa)$ rather than the $a_J(\kappa)$ alone.

One is tempted to look for smaller variations between the two approaches for calculating scattering factors in the case of N_2 and HF. Since these two molecules have relatively larger percentages of electrons in low lying orbitals, it might be expected that these electrons would be less effected by bonding and that the isolated atom results would be better than for H_2 or LiH. Since HF has the least number of its electrons in a primary bonding orbital, it would be expected to have the best isolated atom results. We have seen that in the case of nitrogen, good agreement is found between MO and IA results. In the case of HF we found relatively good agreement between MO and F^- results but poor agreement between MO and H^0 , F^0 results. This difference in agreement for HF implies that molecules composed of first row atoms do not have enough tightly bonded electrons to overshadow any scattering differences due to bonding distortions of the valence orbitals. If they did, both the H^0 , F^0 , and F^- results would be in close agreement with the MO data. Similar observations were made by McWeeny^{4,22} in the particular case of carbon compounds and he was led to stress the importance of choosing the correct

valence state of an atom if the IA approach were to be used. It thus appears as though one will have to proceed to second row atoms before bonding distortions can be ignored.

We note that the relative accuracy of the F^- calculation does not imply that the IA calculation will be reliable for calculations on other first row molecules. The IA approximation requires that one represent the atomic scattering by factors chosen from the commonly tabulated free and ionic valence state data. While electronegativity considerations may aid one in selecting the ionic data for the particular case of HF, generally they will not permit such a selection in the case of other first row molecules such as LiH. The use of Debye's equation would then be restricted to molecules containing predominantly second row or higher atoms.

Of significant consequence is the ability to obtain the harmonic expansion from two-center Gaussian wavefunctions. Gaussian wavefunctions are to be preferred over Slater wavefunctions if two-centers are employed since the corresponding Slater expansions for the scattering coefficients are quite lengthy and slow to compute.²³ Two-center functions are preferred over one²⁴⁻²⁶ because these give more accurate scattering results for fewer basis functions.⁶ This is especially likely to be true as one proceeds to multicenter non-hydride molecules.²⁷ The scattering factors for these molecules will be

expressed as sums over two-center scattering integrals and, with the addition of appropriate rotations, our method should be adaptable to these cases.

In the work of McWeeny,⁴ it was proposed that the anisotropic two-center integrals be expanded in principal factors, one corresponding to a parallel orientation between \tilde{R} and $\tilde{\kappa}$ and one to a perpendicular orientation, with the two weighted by $\cos^2\theta$ and $\sin^2\theta$ respectively. It was later concluded by Stewart⁸ that this approach would not work for all the integrals involved, especially $2p\sigma$ type orbital products. In the present work we have confirmed this conclusion and have shown that a full harmonic expansion of the integrals, a suggestion implicit in the principal factor approach, leads to accurate results for all types of orbital products.

We finally mention that these scattering factors may be used directly in interpreting scattered intensities from fluids. As noted previously, these results find direct application in the scattering equation of Pecora and Steele. While LiH and, to a great extent, H_2 do not form practical fluids for study, nitrogen and hydrogen fluoride do and thus, of the factors obtained here, those for these species are most applicable to experiment. In particular, the MO gas scattering curves are useful since scattering data are often normalized to this curve and slight errors in this normalization lead to inaccurate

distribution functions. An application of harmonically expanded scattering factors to Steele and Pecora's equation is presently underway.

Figure Captions

- Figure 1. Coordinate system employed. For heteronuclear diatomics, center A denotes the heaviest atom.
- Figure 2. $a_0(\kappa)/N$ coefficient. Curve 1, H_2 (MO). Curve 2, H_2 (IA). Curve 3, LiH(MO). Curve 4, LiH (IA using Li^+ , H^- factors). Curve 5, LiH (IA using Li^0 , H^0 factors).
- Figure 3. $a_1(\kappa)/N$ coefficient, real coefficient of i . Curve 1, LiH(MO). Curve 2, LiH (IA using Li^+ , H^- factors). Curve 3, LiH (IA using Li^0 , H^0 factors). Curve 4, HF (IA using H^0 , F^0 factors). Curve 5, HF(MO).
- Figure 4. $a_2(\kappa)/N$ coefficient. Curve 1, H_2 (MO). Curve 2, H_2 (IA). Curve 3, N_2 (IA). Curve 4, N_2 (MO).
- Figure 5. Reduced gas scattering intensity, $I(\kappa)/N^2$. Curve 1, HF(MO). Curve 2, HF (IA using H^0 , F^0 factors). Curve 3, N_2 (MO and IA). Curve 4, LiH(MO). Curve 5, LiH (IA using Li^0 , H^0 factors). Curve 6, LiH (IA using Li^+ , H^- factors).

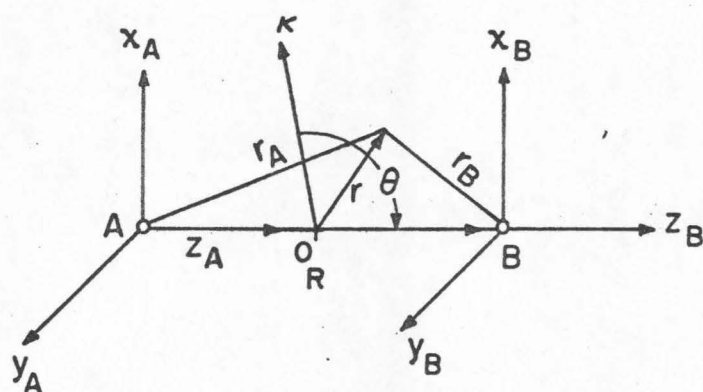


Figure 1.

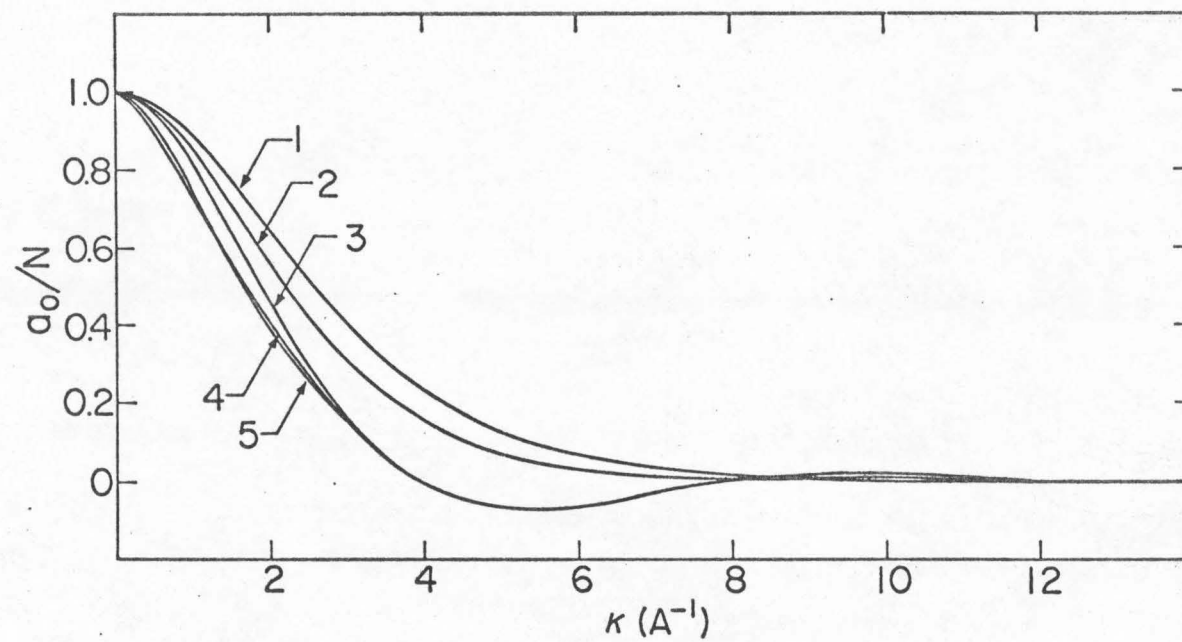


Figure 2.

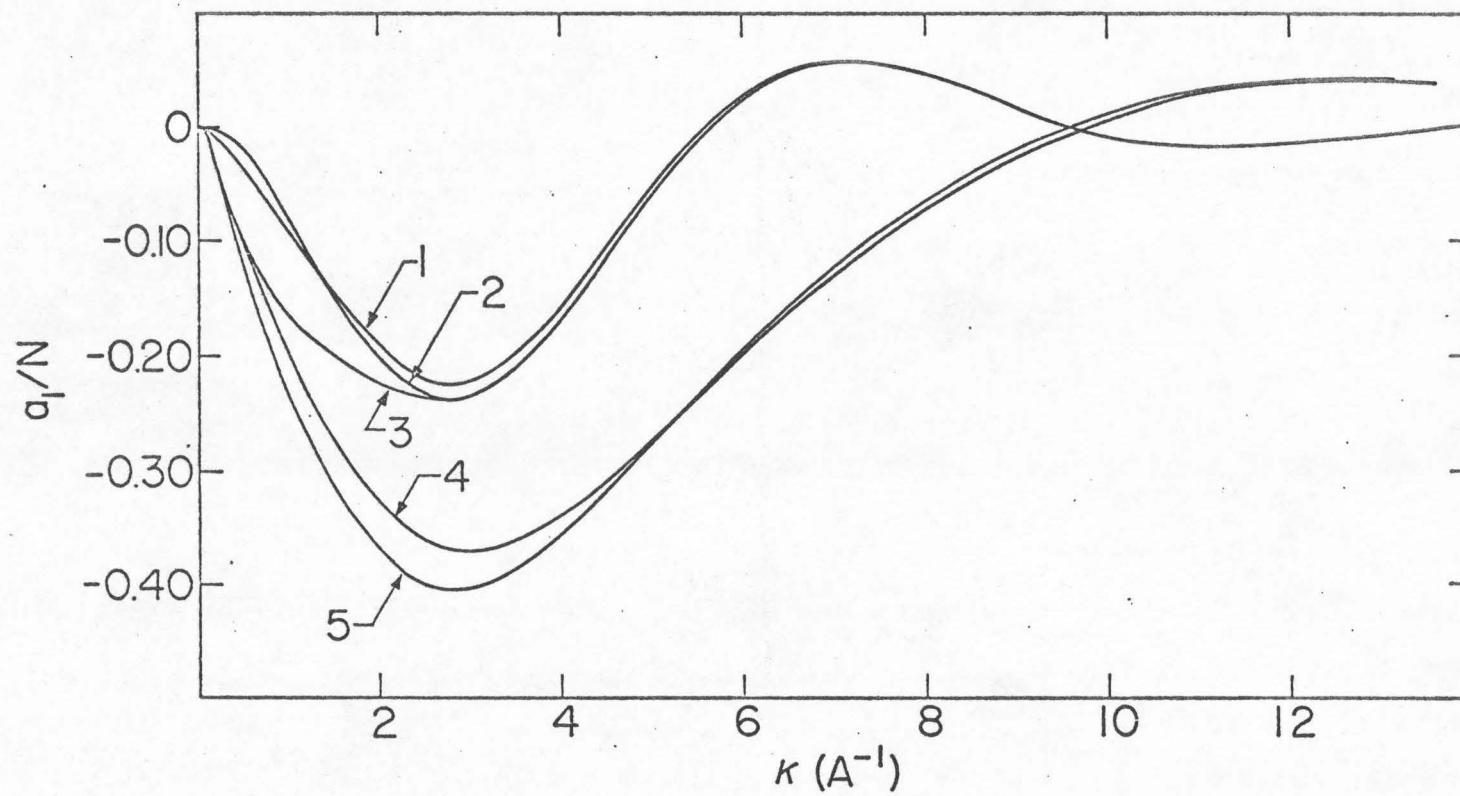


Figure 3.

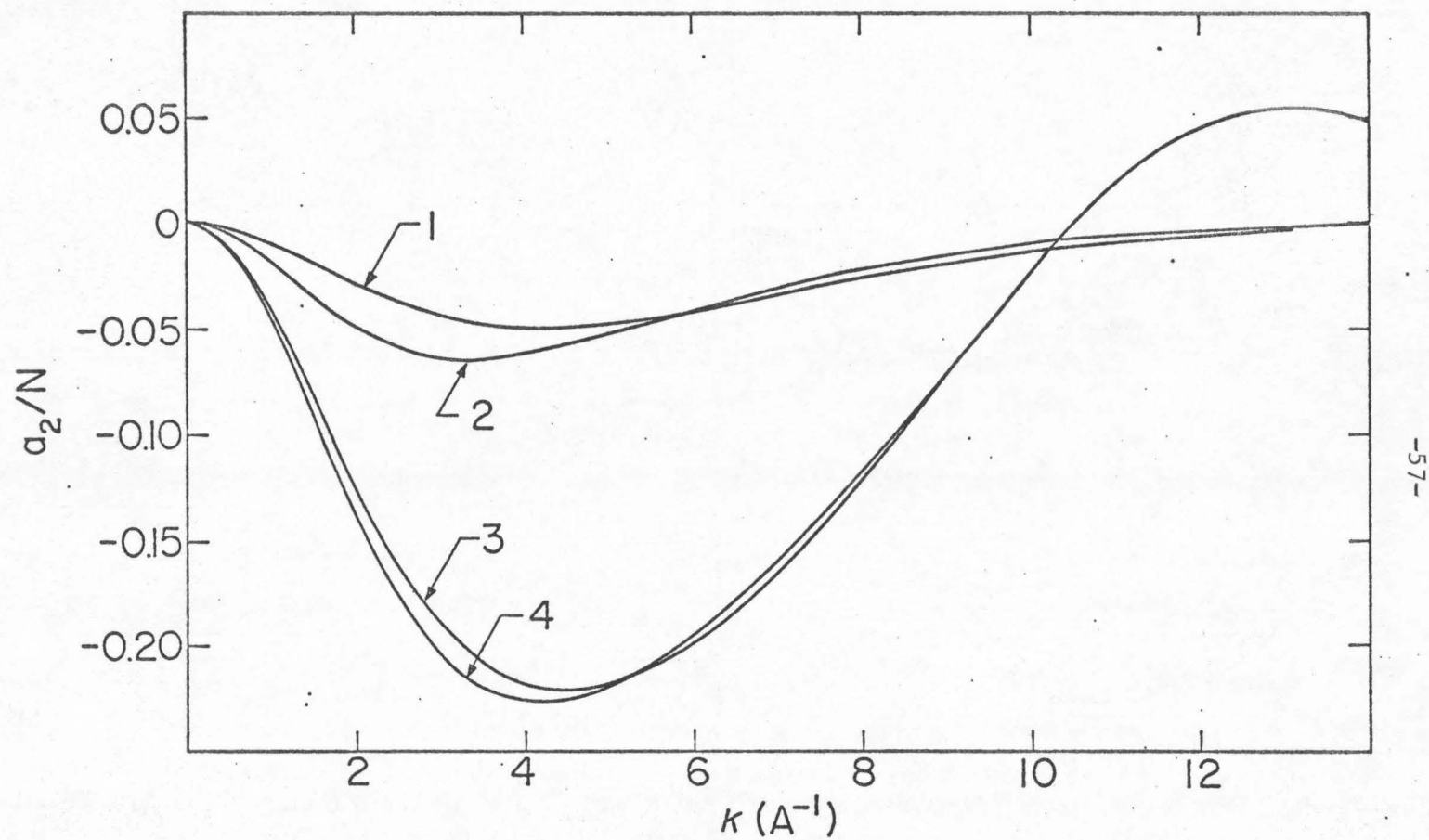


Figure 4.

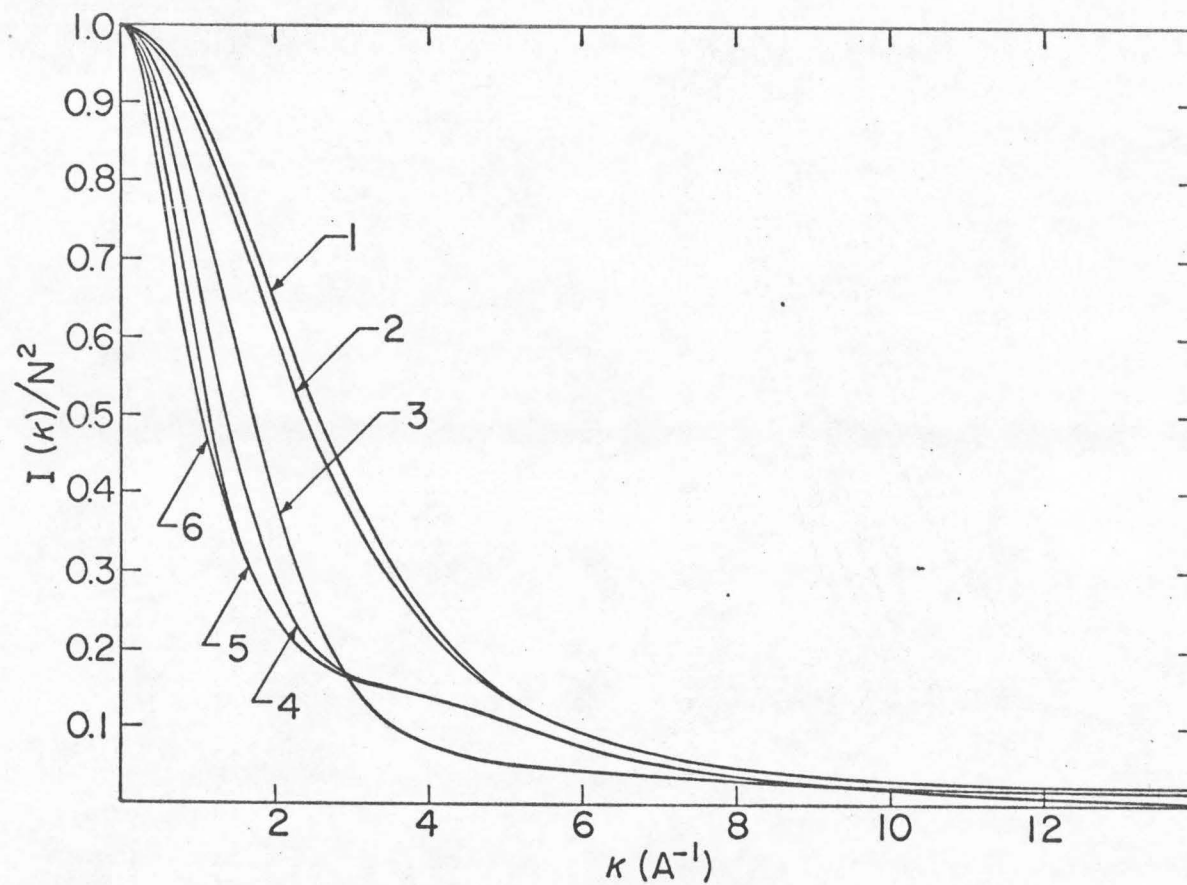


Figure 5.

TABLE 1. Harmonic Coefficients of Various Scattering Factor Integrals

$$\langle s_A | e | s_B \rangle_J = G(2J+1)^{1/2} (-)^{J/2} j_J(q)$$

$$\langle s_A | e | z_B \rangle_J = x_1 G(2J+1)^{1/2} \frac{x_2^R}{\alpha+\beta} (-)^{J/2} j_J(q) + \frac{\kappa G}{2(\alpha+\beta)} \sum_{L=J-1}^{J+1} \frac{(2L+1)}{(2J+1)^{1/2}} (-)^{(L+1)/2} j_L(q) C^2(L1J;00);$$

(2)

$$x_1 = -1, x_2 = \alpha$$

$$\langle s_B | e | z_A \rangle_J = \langle s_A | e | z_B \rangle_J ; x_1 = +1, x_2 = \beta$$

$$\langle z_A | e | z_B \rangle_J = \frac{1}{12(\alpha+\beta)^2} (-12\alpha\beta R^2 + 6(\alpha+\beta) - \kappa^2) G(2J+1)^{1/2} (-)^{J/2} j_J(q) + \frac{\kappa R}{2} \frac{(\beta-\alpha)}{(\alpha+\beta)^2} G \sum_{L=J-1}^{J+1} \frac{(2L+1)}{(2J+1)^{1/2}} (-)^{L/2} C^2(L1J;00) (-)^{(L+1)/2} j_L(q) - \frac{\kappa^2}{6(\alpha+\beta)^2} G \sum_{L=J-2}^{J+2} \frac{2L+1}{(2J+1)^{1/2}} (-)^{L/2} C^2(L2J;00) j_L(q)$$

-59-

$$\langle x_A | e | x_B \rangle_J + \langle y_A | e | y_B \rangle_J = \frac{G}{6(\alpha+\beta)^2} \left\{ (-\kappa^2 + 6(\alpha+\beta)) (2J+1)^{1/2} (-)^{J/2} j_J(q) + \kappa^2 \sum_{L=J-2}^{J+2} \frac{2L+1}{(2J+1)^{1/2}} (-)^{L/2} j_L(q) C^2(L2J;00) \right\}$$

(2)

$$G = \frac{2\pi^2}{(\alpha+\beta)^{3/2}} \exp \left[\frac{-4\alpha\beta R^2 - \kappa^2}{4(\alpha+\beta)} \right]$$

$$q = \frac{\kappa R}{2} \frac{(\beta-\alpha)}{(\alpha+\beta)}$$

$$e = \exp(i\vec{\kappa} \cdot \vec{r})$$

TABLE 1. (cont.)

Special Cases: $\sum_{L=J-1}^{J+1}$ is replaced by $L = 1$ if $J = 0$.
 (2)
 $\sum_{L=J-2}^{J+2}$ is replaced by $L = 2$ if $J = 0$; by $L = 1, 3$ if $J = 1$.
 (2)

If $A = B$ and both centers are at A , then $R = 0$ and q is replaced
 by $-\frac{\kappa R}{2}$.

If $A = B$ and both centers are at B , then $R = 0$ and q is replaced
 by $+\frac{\kappa R}{2}$.

TABLE 2. Scattering Factor Coefficients and Gas Scattering Intensities.
Units of Quantities are: κ , \AA^{-1} ; a_J , electrons/ Z ; $\sum |a_J|^2$,
electrons²/ Z^2 .

<u>Lithium Hydride</u>					<u>Hydrogen Fluoride</u>			
κ	a_0	a_1/i	a_2	$\sum a_J ^2$	a_0	a_1/i	a_2	$\sum a_J ^2$
0.0000	1.0000	0.0000	0.0000	1.0000	1.0000	0.0000	0.0000	1.0000
0.5669	0.9325	-0.0448	-0.0231	0.8725	0.9712	-0.1381	-0.0095	0.9632
1.1338	0.7638	-0.1022	-0.0830	0.6006	0.8904	-0.2569	-0.0355	0.8600
1.7008	0.5588	-0.1643	-0.1583	0.3644	0.7727	-0.3429	-0.0722	0.7199
2.2677	0.3653	-0.2100	-0.2287	0.2316	0.6371	-0.3910	-0.1121	0.5716
2.8346	0.2045	-0.2246	-0.2793	0.1766	0.5008	-0.4040	-0.1487	0.4371
3.4015	0.0829	-0.2056	-0.3018	0.1553	0.3761	-0.3896	-0.1778	0.3268
3.9685	0.0000	-0.1604	-0.2943	0.1401	0.2694	-0.3569	-0.1975	0.2424
4.5354	-0.0482	-0.1016	-0.2605	0.1219	0.1825	-0.3139	-0.2077	0.1805
5.1023	-0.0680	-0.0425	-0.2081	0.1018	0.1144	-0.2668	-0.2098	0.1361
5.6692	-0.0672	0.0068	-0.1464	0.0829	0.0628	-0.2199	-0.2052	0.1046
6.2361	-0.0535	0.0404	-0.0847	0.0672	0.0250	-0.1756	-0.1957	0.0824
6.8031	-0.0340	0.0569	-0.0306	0.0546	-0.0020	-0.1354	-0.1827	0.0666
7.3700	-0.0142	0.0583	0.0108	0.0446	-0.0204	-0.0995	-0.1672	0.0553
7.9369	-0.0021	0.0487	0.0375	0.0364	-0.0321	-0.0681	-0.1499	0.0470
8.5038	0.0130	0.0330	0.0497	0.0295	-0.0387	-0.0409	-0.1314	0.0408
9.0708	0.0182	0.0158	0.0498	0.0238	-0.0413	-0.0177	-0.1120	0.0361
9.6377	0.0184	0.0005	0.0414	0.0192	-0.0408	0.0016	-0.0922	0.0324
10.2046	0.0150	-0.0107	0.0282	0.0154	-0.0379	0.0171	-0.0722	0.0294
10.7715	0.0097	-0.0168	0.0138	0.0124	-0.0332	0.0291	-0.0527	0.0271
11.3384	0.0041	-0.0182	0.0009	0.0101	-0.0272	0.0375	-0.0340	0.0251

TABLE 2. (cont.)

<u>Hydrogen</u>					<u>Nitrogen</u>				
κ	a_0	a_2	a_4	$\sum a_J ^2$	κ	a_0	a_2	a_4	$\sum a_J ^2$
0.0000	1.0000	0.0000	0.0000	1.0000	0.0000	1.0000	0.0000	0.0000	1.0000
0.5669	0.9625	-0.0032	0.0000	0.9269	0.7559	0.9281	-0.0269	0.0001	0.8621
1.1338	0.8615	-0.0116	0.0000	0.7426	1.5118	0.7468	-0.0912	0.0017	0.5660
1.7008	0.7230	-0.0224	0.0001	0.5231	2.2677	0.5297	-0.1588	0.0067	0.3058
2.2677	0.5750	-0.0329	0.0003	0.3320	3.0236	0.3371	-0.2051	0.0158	0.1559
2.8346	0.4395	-0.0411	0.0007	0.1949	3.7795	0.1929	-0.2251	0.0280	0.0886
3.4015	0.3258	-0.0465	0.0011	0.1084	4.5354	0.0949	-0.2249	0.0420	0.0613
3.9685	0.2360	-0.0489	0.0017	0.0581	5.2913	0.0315	-0.2126	0.0569	0.0494
4.5354	0.1676	-0.0488	0.0022	0.0305	6.0472	-0.0084	-0.1929	0.0722	0.0426
5.1023	0.1169	-0.0468	0.0028	0.0159	6.8031	-0.0318	-0.1679	0.0875	0.0371
5.6692	0.0801	-0.0436	0.0033	0.0083	7.5590	-0.0431	-0.1379	0.1019	0.0317
6.2361	0.0537	-0.0396	0.0038	0.0045	8.3149	-0.0449	-0.1039	0.1139	0.0266
6.8031	0.0352	-0.0353	0.0042	0.0025	9.0708	-0.0394	-0.0677	0.1219	0.0225
7.3700	0.0223	-0.0309	0.0045	0.0015	9.8267	-0.0289	-0.0318	0.1244	0.0199
7.9369	0.0135	-0.0267	0.0048	0.0009	10.5826	-0.0159	0.0006	0.1202	0.0187
8.5038	0.0075	-0.0228	0.0050	0.0006	11.3384	-0.0027	0.0027	0.1091	0.0183
9.0708	0.0036	-0.0193	0.0051	0.0004					
9.6377	0.0011	-0.0161	0.0051	0.0003					
10.2046	-0.0004	-0.0133	0.0051	0.0002					
10.7715	-0.0013	-0.0109	0.0050	0.0001					
11.3384	-0.0017	-0.0087	0.0049	0.0001					

TABLE 3. Largest J Value Required for Convergence of Gas Scattering Intensity

<u>K</u>	<u>H₂</u>	<u>N₂</u>	<u>LiH</u>	<u>HF</u>
0.0	0	0	0	0
2.27	2	2	4	3
4.54	2	4	7	4
6.80	4	6	9	6
9.07	6	8	10	7
11.34	6	10	12	8

Bibliography

1. R. W. James, The Optical Principles of the Diffraction of X-Rays, Vol II (1965).
2. P. Debye, Phys. Zeits., 31, 419 (1930).
3. R. McWeeny, Acta. Cryst., 6, 631 (1953).
4. R. McWeeny, Acta. Cryst., 7, 180 (1954).
5. C. Tavard, M. Rouault, M. Roux, M. Cornille, J. Chim. Phys., 61, 1324 (1964).
6. C. Tavard, M. Rouault, M. Roux, M. Cornille, J. Chim. Phys., 61, 1330 (1964).
7. R. Stewart, JCP, 42, 3175 (1965).
8. R. Stewart, JCP, 51, 4569 (1969).
9. W. Steele, R. Pecora, JCP, 42, 1863 (1965).
10. M. Rose, Elementary Theory of Angular Momentum (1957).
11. E. Condon, G. Shortley, The Theory of Atomic Spectra (1967).
12. A. Edmonds, Angular Momentum in Quantum Mechanics (1957).
13. POLYATOM written by D. Neumann, H. Basch, C. Hornbeck, C. Hollister, J. W. Moskowitz.
14. B. Ransil, Revs. Mod. Phys., 32, 245 (1960).
15. B. Ransil, S. Fraga, JCP, 35, 1967 (1961).
16. M. Harrison, JCP, 41, 499 (1964).
17. S. Huzinaga, JCP, 42, 1293 (1965).
18. T. Dunning, JCP, to be published.
19. R. Hake, K. Banyard, JCP, 45, 3199 (1966).
20. D. Cromer, J. Mann, Los Alamos Scientific Laboratory LA-3816 (1968).
21. International Tables for X-Ray Crystallography, Vol. III, (1962).
22. R. McWeeny, Acta. Cryst., 4, 513 (1951).

23. This laboratory, unpublished results.
24. R. Hake, K. Banyard, JCP, 41, 3221 (1964), 43, 2684 (1965), 44, 3523 (1966).
25. R. Moccia, JCP, 40, 2164, 2176, 2186 (1964).
26. B. Joshi, JCP, 43, 540 (1965).
27. P. Olympia, B. Fung, JCP, 53, 1066 (1970).

PART III

PERCUS-YEVICK SOLUTIONS FOR THE TWO-CENTERED LENNARD-JONES POTENTIAL

Introduction

The Percus-Yevick theory has been established for some time as a means of obtaining fairly accurate dense fluid properties. Radial distribution functions seem to be described correctly as are certain thermodynamic quantities such as the internal energy. The theory provides less accurate results for the pressure, being in error by as much as orders of magnitude. It nevertheless does as well and usually better than other alternatives and thus retains considerable value.

It has been applied to a variety of potentials, mostly of spherical symmetry. It was applied to the hard-sphere potential by Wertheim¹ who was able to develop an analytical solution for this case. It has been applied to the physically more realistic Lennard-Jones potential by a variety of authors. A fairly extensive tabulation of radial distribution functions has been given by Throop and Bearman² and Mandel, Bearman, and Bearman³ covering most of the dense gas and liquid region. Watts⁴ has applied Baxter's⁵ treatment of the Percus-Yevick equation to the critical region using a spherical Lennard-Jones potential and has shown that it will predict the critical point, yielding values which compare well with the experimental values for argon.

Applications of the theory to nonspherical potentials are relatively recent and do not cover a great variety of potentials. The Percus-Yevick equation was solved for two tetrahedrally symmetric water potentials by Ben-Naim⁶. One of the most significant nonspherical applications was published by Chen and Steele^{7a}, who applied the Percus-Yevick theory to a system of diatomic hard-core molecules. Because the distribution functions for this system were angular dependent, the

methods of solving the Percus-Yevick equation used for spherical systems were no longer useful. In order to obtain a tractable form, they applied the D-orthonormal expansion method of Steele⁸ to the equation and were able to derive a system of equations which could be solved for the expansion coefficients of the angular dependent radial distribution function and direct correlation function. Most significantly, the method is quite general and may also be applied to other potentials.

This work is a direct extension of the technique developed by Chen and Steele to the two-centered Lennard-Jones potential and is primarily a derivation of the distribution functions determined by this potential. This choice of potential, of course, allows for attractive as well as repulsive forces in the intermolecular interaction, and leads to distribution functions that are temperature dependent. This introduces a variable not treated previously.

Because this laboratory is concerned with x-ray scattering from molecules, it became apparent that angular dependent distribution functions for a real system would eventually be required. Partly because of scattering properties and partly because heat capacities seem to indicate a large orientational effect, we have therefore solved the Percus-Yevick equation for parameters characteristic of chlorine.

We present below the simultaneous equations whose solution gives the desired Percus-Yevick results. We also show the equations required for high order evaluation of the pair correlation function and direct correlation function. The potential parameters for chlorine are then determined and finally the numerical results for the distribution functions are presented and discussed.

Theory

A. The Percus-Yevick Solution

We begin this section by reviewing the method used by Chen and Steele⁷ to solve the Percus-Yevick equation for a system of diatomic hard-core molecules. We first write the general expansion developed by Steele⁸ which expands any pair property in terms of spherical harmonics (D-function in the general case) whose arguments Ω_j are the Euler angles of orientation of the two molecules involved.

$$X(\underline{R}_1 \underline{R}_2) = 4\pi \sum_{\ell \ell', m} X_{\ell \ell', m}(r_{12}) Y_{\ell, m}(\Omega_1) Y_{\ell', -m}(\Omega_2), \quad \underline{R}_j = \{\underline{r}_j, \Omega_j\} \quad (1)$$

\underline{r}_j is the position vector of the center of molecule j . A function $H(\underline{R}_1 \underline{R}_2)$ may be defined in terms of the density dependent part of the pair correlation function

$$H(\underline{R}_1 \underline{R}_2) = g^0(\underline{R}_1 \underline{R}_2) - 1 \quad (2)$$

By generalization of the usual Percus-Yevick approximation

$c(r) = g(r)[1 - \exp(\beta u(r))]$, one may write

$$C(\underline{R}_1 \underline{R}_2) = f(\underline{R}_1 \underline{R}_2) [H(\underline{R}_1 \underline{R}_2) + 1] \quad (3)$$

The Ornstein-Zernike equation when combined with (3) gives

$$H(\underline{R}_1 \underline{R}_2) = \frac{\rho}{4\pi} \int C(\underline{R}_2 \underline{R}_3) [C(\underline{R}_1 \underline{R}_3) + H(\underline{R}_1 \underline{R}_3)] d\underline{r}_3 d\Omega_3 \quad (4)$$

This is the angular-dependent Percus-Yevick equation.

Equation (4) is solved by Fourier transforming both sides of the equation to yield

$$H_{12}(\underline{v}) = \frac{\rho}{4\pi} \int C_{23}(\underline{v}) [C_{13}(\underline{v}) + H_{13}(\underline{v})] d\Omega_3 \quad (5)$$

where $H_{12}(\underline{v}) = \int H(\underline{R}_1, \underline{R}_2) e^{i\underline{v} \cdot \underline{r}_{12}} d\underline{r}_{12}$. The $H(\underline{R}_1, \underline{R}_2)$ and $C(\underline{R}_1, \underline{R}_2)$ in each transform in (5) are then expanded according to (1), while each $\exp(i\underline{v} \cdot \underline{r}_{ij})$ is expanded into spherical waves according to

$$\exp(i\underline{v} \cdot \underline{r}_{ij}) = (4\pi)^{1/2} \sum_{s=0}^{\infty} (2s+1)^{1/2} i^s j_s(vr) Y_{s,0}(\Omega_v^{ij})$$

The various sets of Euler angles which result refer to a variety of relative coordinate systems and must therefore be rotated to a common laboratory coordinate system. The rotations are carried out by repeatedly applying Eq. (2-2) of Appendix 2 and making use of the orthonormality properties of D functions (see Ref. (7b) for details). The result of the expansions and rotations is for the left-hand side of (5):

$$H_{12}(\underline{v}) = (4\pi)^2 \sigma^3 \sum_{\ell, \ell', s=0}^{\infty} \sum_{v=-\ell}^{\ell} \sum_{v'=-\ell'}^{\ell'} \sum_{\underline{m} \in \underline{\ell}' \cap \underline{\ell}} i^s D_{v+v', 0}^s(\Omega_v) \quad (6)$$

$$\times Y_{\ell, v}(\Omega_1) Y_{\ell', v'}(\Omega_2) H(\ell \ell' ms) c(\ell \ell' s; v, v') c(\ell \ell' s; m, -m)$$

where Ω_v is the set of Euler angles describing the orientation of \underline{v} relative to a laboratory system, Ω_1 and Ω_2 give the orientations of molecules 1 and 2, $c(j_1 j_2 j_3; m_1 m_2)$ is a Clebsch-Gordan (CG) coefficient⁹, and $H(\ell \ell' ms)$ is a Hankel transform defined by

$$H(\ell \ell' ms) = \int_0^{\infty} H_{\ell \ell' m}(r^*) j_s(vr^*) r^{*2} dr^* \quad (7)$$

with inverse

$$H_{\ell\ell'm}(r^*) = \frac{2\sigma^3}{\pi} \int_0^\infty H(\ell\ell'ms) j_s(vr^*) v^2 dv \quad (8)$$

also $\underline{\ell} = \{-\ell, -(\ell-1), \dots, \ell-1, \ell\}$. Similarly the right-hand side of (5) becomes:

$$\begin{aligned} H_{12}(\underline{v}) = & (4\pi)^3 \sigma^6 \rho \sum_{\ell, \ell', \ell'', s, s'=0}^\infty \sum_{v=-\ell}^{\ell} \sum_{v'=-\ell'}^{\ell'} \sum_{v''=-\ell''}^{\ell''} \sum_{\underline{m} \subseteq \underline{\ell} \cap \underline{\ell}'} \sum_{\underline{m}' \subseteq \underline{\ell} \cap \underline{\ell}'} \\ & \times [C(\ell\ell'ms) + H(\ell\ell'ms)] C(\ell''\ell'm's') i^{s+s'} (-)^{v'} \\ & \times \sum_{j=|s-s'|}^{s+s'} c(ss'j; v+v', v''-v') c(ss'j; 00) D_{v+v'', 0}^j(\Omega_v) c(\ell\ell's; vv') \\ & \times c(\ell\ell's; m, -m) c(\ell''\ell's'; v'', -v') c(\ell''\ell's'; m', -m') Y_{\ell, v}(\Omega_1) Y_{\ell'', v''}(\Omega_2) \end{aligned} \quad (9)$$

If one notes the independent harmonics appearing in each of Eqs. (6) and (9), one may generate a series of equations by equating like coefficients according to (5). Simultaneous solution of these equations for the various $H(\ell\ell'ms)$ constitutes the Percus-Yevick solution.

Expressions for specific $H(\ell\ell'ms)$ may be derived by letting the desired Hankel transform subscripts define the spherical harmonic subscripts in (6) and thus the corresponding subscripts in (9) as well. It should be noticed, however, that if the transform is specified by ℓ, ℓ', m, s , then the v, v' subscripts in (6) are in general still left unspecified. If ℓ (or ℓ') is zero, then the range of v (or v') is restricted trivially to zero as well; but if ℓ (or ℓ') is greater than zero, several values for v (or v') are allowed. This non-specification

of v or v' appears to be no problem however, in that the same equations for $H(\ell\ell'ms)$ result for all choices of v or v' . This has been verified for $H(2002)$ and $H(2200)$.

While solutions for $H(0000)$ and $H(2002)$ were obtained by Chen for the diatomic hard-core model, it was indicated that errors in the final values for H_{000} and H_{200} , as well as the $g_{\ell\ell'm}$ terms derived from them, might arise from neglect of the higher coefficients H_{220} , H_{221} , H_{222} , H_{400} , etc. In order to see if these higher terms did give rise to an error, we have included two of them in our calculation, H_{220} and H_{400} , assuming the others to be negligibly small. Our Percus-Yevick solution thus involved the simultaneous solution of equations for $H(0000)$, $H(2002)$, $H(2200)$, $H(2202)$, $H(2204)$, and $H(4004)$. That these are the complete set of transform functions for H_{000} , H_{200} , H_{220} , and H_{400} is proven in Appendix 3.

We will now derive the equation for $H(2200)$ as an exemplary case. The equations for the other transforms will then merely be listed. For $H(2200)$ it can be seen that in (6) this requires that $\ell = 2$, $\ell' = 2$, $s = 0$, and $m = 0$; v and v' are not specified. Hence the coefficient of the harmonics, A , becomes

$$A = (4\pi)^2 \sigma^3 H(2200) c(220;v,v') c(220;00)$$

Using (4-6) of Appendix 4, the CG coefficients can be rearranged to give

$$A = (4\pi)^2 \sigma^3 H(2200) (-)^v \left(\frac{1}{5}\right) c(202;v,-v-v') c(202;00)$$

Equation (4-10) shows that these CG coefficients reduce to $\delta_{v,-v'}$

and 1 respectively so that

$$A = (4\pi)^2 \sigma^3 H(2200) (-)^v \left(\frac{1}{5}\right) \quad (10)$$

In (9), $H(2200)$ requires that $\ell = 2$, $\ell'' = 2$, and $j = 0$. Equality of harmonics requires the v, v' of (6) to equal the v, v'' of (9) respectively. Thus from (9) we obtain as coefficient of the harmonics

$$\begin{aligned} A = & (4\pi)^3 \sigma^6 \rho \sum_{\ell'} \sum_{m, m'} \sum_{ss'} [C(2\ell' ms) + H(2\ell' ms)] C(2\ell' m' s') i^{s+s'} \\ & \times \sum_{v'} (-)^{v'} c(ss'0; v+v', v''-v') c(2\ell' s; v, v') c(2\ell' s'; v'', -v') \\ & \times c(ss'0; 00) c(2\ell' s; m, -m) c(2\ell' s'; m', -m') \end{aligned} \quad (11)$$

By applying (4-6) and (4-10) again we obtain

$$\begin{aligned} c(ss'0; v+v', v''-v') &= (-)^{s-v-v'} \left(\frac{1}{2s+1}\right)^{1/2} c(s0s'; v+v', -v-v'') \\ &= (-)^{s-v-v'} \left(\frac{1}{2s+1}\right)^{1/2} \delta_{ss'} \delta_{v, -v''} \end{aligned} \quad (12)$$

and

$$c(ss'0; 00) = (-)^s \left(\frac{1}{2s+1}\right)^{1/2} \delta_{ss'}$$

Note that (12) results in $\delta_{v, -v''}$. This condition had to be present since a similar $\delta_{v, -v'}$ was obtained from (6). (11) now becomes:

$$\begin{aligned} A = & (4\pi)^3 \sigma^6 \rho \sum_{\ell'} \sum_{mm'} \sum_s [C(2\ell' ms) + H(2\ell' ms)] C(2\ell' m' s) i^{2s} \\ & \times (-)^s \left(\frac{1}{2s+1}\right) (-)^v c(2\ell' s; m, -m) c(2\ell' s; m', -m') \left[\sum_{v'} c(2\ell' s; v, v') \right. \\ & \left. \times c(2\ell' s; v'', -v') \right] \end{aligned} \quad (13)$$

The coefficients depending on v' have been grouped together in this last equation because this grouping nearly forms the orthogonality expression of Clebsch-Gordan coefficients. [Equation (4-2) of Appendix 4.] Substitution of $-v$ for v'' and application of (4-4) to the summation lead to a value for it of $(-)^{\ell'-s}$. Thus equating (10) and (13) and cancelling terms, one is led to

$$H(2200) = 20\pi\sigma^3\rho \sum_{\ell'} \sum_{mm'} \sum_s [C(2\ell'm's) + H(2\ell'm's)] C(2\ell'm's) \\ \times i^{2s} \left(\frac{1}{2s+1}\right) (-)^{\ell'-s} c(2\ell's;m,-m) c(2\ell's;m',-m') \quad (14)$$

Notice that (14) results with no specifications placed on the harmonic subscripts v, v', v'' .

Similar derivations may be performed to obtain the other transforms although the simplification introduced by the use of the orthogonality condition cannot be used in the derivation of $H(2202)$ and $H(2204)$. The results are as follows:

$$H(0000) = 4\pi\sigma^3\rho \sum_{\ell'} [C(0\ell'0\ell') + H(0\ell'0\ell')] C(0\ell'0\ell') \quad (15)$$

$$H(2002) = -4\pi\sigma^3\rho \sum_{\ell,m,s} [C(2\ell ms) + H(2\ell ms)] C(0\ell 0\ell) i^{\ell+s} (-)^s \\ \times \left(\frac{2s+1}{5}\right)^{1/2} c(s\ell 2;00) c(2\ell s;m,-m) \quad (16)$$

These two are the same as the two expressions used by Chen in the hard core work.

$$\begin{aligned}
 H(2202) = & -14\pi\sigma^3\rho \sum_{\ell'} \sum_{m,m'} \sum_{s,s'} [C(2\ell' ms) + H(2\ell' ms)] C(2\ell' m' s') \\
 & \times i^{s+s'} \left[\sum_{v'} (-)^{v'} c(ss'2; v', -v') c(2\ell' s; 0v') c(2\ell' s'; 0, -v') \right] \\
 & \times c(ss'2; 00) c(2\ell' s; m, -m) c(2\ell' s'; m', -m') \quad (17)
 \end{aligned}$$

$$\begin{aligned}
 H(2204) = & \frac{70}{9} \pi\sigma^3\rho \sum_{\ell'} \sum_{m,m'} \sum_{s,s'} [C(2\ell' ms) + H(2\ell' ms)] C(2\ell' m' s') \\
 & \times i^{s+s'} \left[\sum_{v'} (-)^{v'} c(ss'4; v', -v') c(2\ell' s; 0v') \right. \\
 & \times \left. c(2\ell' s'; 0, -v') \right] c(2\ell' s'; m', -m') c(ss'4; 00) c(2\ell' s; m, -m) \quad (18)
 \end{aligned}$$

$$\begin{aligned}
 H(4004) = & 4\pi\sigma^3\rho \sum_{\ell', m, s} [C(4\ell' ms) + H(4\ell' ms)] C(0\ell' 0\ell') i^{s+\ell'} (-)^s \\
 & \times \left(\frac{2s+1}{9} \right)^{1/2} c(s\ell'4; 00) c(4\ell' s; m, -m) \quad (19)
 \end{aligned}$$

Each of the equations (14) to (19) may now be expanded over ℓ, m, m', s, s' , retaining only those terms which include members of the transform set listed above. These expansions are straightforward but are quite long and tedious, and we will simply list the results. It is apparent that sums over a large number of CG coefficients will result. Those required for these expansions are summarized in Appendix 4. Using the same reducing parameters as Chen,

$$\rho^* = \rho v, \quad v = \frac{2\pi\sigma^3 x}{3}, \quad x = 1 + \frac{3}{2} R^* - \frac{1}{2} R^{*3},$$

and defining $K = \frac{6\rho^*}{x}$, we obtain from (15)

$$H(0000) = A H(2002) + B H(4004) + C$$

$$A = K C(2002)/Z$$

$$B = K C(4004)/Z$$

$$C = K (C^2(0000) + C^2(2002) + C^2(4004)) / Z \quad (20)$$

where $Z = 1 - K C(0000)$. From (19) we obtain

$$H(4004) = K C(4004) C(0000) / Z \quad (21)$$

The results of the expansions of Eqs. (14), (16)-(18) can be written in a common form:

$$A_{i1} H(2002) + A_{i2} H(2200) + A_{i3} H(2202) + A_{i4} H(2204) = B_i \quad (22)$$

where i is an index running from 1 to 4 denoting from which of the equations (14), (16)-(18) the coefficients were derived. Each coefficient is somewhat lengthy and they have therefore been collected in Table I. Equations (20), (21), and (22) along with (3) provide the Percus-Yevick solution.

We now present the methods by which the isothermal compressibility κ_T may be calculated. This is of importance in that the compressibility goes to infinity at the critical point of a fluid and hence may be used to locate it. Two methods of calculation exist. The first is that developed by Steele⁸, which is a straightforward extension of the usual pair distribution equation of spherical systems:

$$\kappa = \beta [\rho^{-1} + \int (g_{000}(r) - 1) 4\pi r^2 dr] = \frac{1}{\rho} \left(\frac{\partial \rho}{\partial P} \right)_T \quad (23)$$

The second method has been employed by several authors^{2,3,7} and for

angular systems takes the form

$$\kappa_T^{-1} = 1 - \frac{6\rho^*}{x} \int C_{000}(r^*) r^{*2} dr^* \quad (24)$$

where $\kappa_T = \rho k T \kappa$. We have used both methods in this work.

TABLE I

COEFFICIENTS OF SIMULTANEOUS EQUATIONS FOR H(2002), H(2200), H(2202), H(2204)

i^a	A_{i1}	A_{i2}	A_{i3}	A_{i4}
1(16)	$1 - K C(0000)$	$-\frac{K}{5} C(2002)$	$\frac{2}{7} K C(2002)$	$-\frac{18}{35} K C(2002)$
2(14)	$-K C(2002)$	$1 - K C(2200)$	$-\frac{2}{7} K C(2202)$	$-\frac{18}{63} K C(2204)$
3(17)	$K C(2002)$	$-\frac{K}{5} C(2202)$	$1 - \frac{K}{5} C(2200) - \frac{3}{49} K C(2202)$ $-\frac{36}{245} K C(2204)$	$-K \frac{36}{245} C(2202) + \frac{18}{49} K C(2204)$
4(18)	$-K C(2002)$	$-\frac{K}{5} C(2204)$	$-K \frac{4}{49} C(2202) + K \frac{10}{49} C(2204)$	$1 - \frac{K}{5} C(2200) + K \frac{10}{49} C(2202)$ $-K \frac{27}{245} C(2204)$

-78-

$$B_1 = K[C(2002) C(0000) + \frac{1}{5} C(2200) C(2002) - \frac{2}{7} C(2202) C(2002) + \frac{18}{35} C(2204) C(2002)]$$

$$B_2 = K[C^2(2002) + C^2(2200) + \frac{2}{7} C^2(2202) + \frac{18}{63} C^2(2204)]$$

$$B_3 = K[-C^2(2002) + \frac{2}{5} C(2200) C(2202) + \frac{3}{49} C^2(2202) + \frac{72}{245} C(2202) C(2204) - \frac{18}{49} C^2(2204)]$$

$$B_4 = K[C^2(2002) + \frac{2}{5} C(2200) C(2204) + \frac{4}{49} C^2(2202) - \frac{20}{49} C(2202) C(2204) + \frac{27}{245} C^2(2204)]$$

^aNumber in parentheses denotes the source equation in text.

B. Expansions for Pair and Direct Correlation Functions

In order to obtain the direct correlation function expansion coefficients which are required in Eqs. (20)-(22) above, an expansion of (3) must be made. While a partial expansion has been done previously by Chen⁷, several terms have been omitted. We present a more complete expansion here so that higher terms will be included in the expansion, thus reducing truncation error.

We note that the expression for the expansion of the product of $f(\underline{R}_1 \underline{R}_2)$ and $[1 + H(\underline{R}_1 \underline{R}_2)]$ gives the expansion for any product of two harmonically expanded series if the proper identification is made. Such products occur often in the orthonormal expansion approach to statistical mechanics, and the expression below is therefore of wide use. In this work, it is also used to expand the pair correlation function as a product of $[1 + f(\underline{R}_1 \underline{R}_2)] = g^0(\underline{R}_1 \underline{R}_2)$ and $[1 + H(\underline{R}_1 \underline{R}_2)]$. The $(^0)$ denotes the zero density limit of $g(\underline{R}_1 \underline{R}_2)$.

To evaluate (3), expand each function according to (1). Then,

$$\begin{aligned}
 C_{000} + 4\pi \sum_{\ell \ell' m} C_{\ell \ell' m} Y_{\ell m}(\Omega_1) Y_{\ell' -m}(\Omega_2) &= f_{000} [H_{000} + 1] \\
 + f_{000} 4\pi \sum_{\ell = \ell' \neq 0} H_{\ell \ell' m} Y_{\ell m}(\Omega_1) Y_{\ell' -m}(\Omega_2) \\
 + (H_{000} + 1) 4\pi \sum_{\ell = \ell' \neq 0} f_{\ell \ell' m} Y_{\ell m}(\Omega_1) Y_{\ell' -m}(\Omega_2) \\
 + (4\pi)^2 \sum_{\ell = \ell' \neq 0} f_{\ell \ell' m} Y_{\ell m}(\Omega_1) Y_{\ell' -m}(\Omega_2) \sum_{\ell = \ell' \neq 0} H_{\ell \ell' m} Y_{\ell m}(\Omega_1) Y_{\ell' -m}(\Omega_2)
 \end{aligned} \tag{25}$$

The last term, involving the product of two series was omitted entirely in earlier work. If it is denoted by S , and the harmonics are

combined by using the spherical harmonic coupling rule (Eq. (11), Part II), then

$$\begin{aligned}
 S = & (4\pi)^2 \sum_{\ell, \ell'}^{\infty} \sum_{\underline{m} \leq \underline{\ell}'}^{\infty} \sum_{\underline{n} \leq \underline{\ell}'}^{\infty} \sum_{\underline{v}, \underline{v}'}^{\infty} \sum_{\underline{n} \leq \underline{v}'}^{\infty} f_{\ell \ell' m} H_{v v' n} \sum_{j=|\ell-v|}^{\ell+v} \left[\frac{(2\ell+1)(2v+1)}{4\pi(2j+1)} \right]^{1/2} \\
 & \times c(\ell v j; m n) c(\ell v j; 00) Y_{j, m+n}(\Omega_1) \sum_{j'=|\ell'-v'|}^{\ell'+v'} \left[\frac{(2\ell'+1)(2v'+1)}{4\pi(2j'+1)} \right]^{1/2} \\
 & \times c(\ell' v' j'; -m, -n) c(\ell' v' j'; 00) Y_{j', -m-n}(\Omega_2)
 \end{aligned} \tag{26}$$

Equation (26) may be improved by recognizing that

$$\sum_{\ell=0}^{\infty} \sum_{v=0}^{\infty} \sum_{j=|\ell-v|}^{\ell+v} = \sum_{j=0}^{\infty} \sum_{\ell=0}^{\infty} \sum_{v=|j-\ell|}^{j+\ell} \tag{27}$$

If this is substituted into (26) and (26) in turn is substituted into (25), one then obtains an expression from which the coefficients of specific harmonics are easily identified.

Coefficients have been identified for the set H_{000} , H_{200} , H_{220} , H_{400} , all other $H_{\ell \ell' m} = 0$. Once again several CG coefficients are required, and these are given in Appendix 4. The results are:

$$C_{000} = f_{000}(H_{000} + 1) + 2f_{200}H_{200} + f_{220}H_{220} + 2f_{400}H_{400}$$

$$\begin{aligned}
 C_{200} = & f_{000}H_{200} + f_{200}[(H_{000} + 1) + H_{220} + \frac{2\sqrt{5}}{7}H_{200} + \frac{6}{7}H_{400}] \\
 & + f_{220}[H_{200} + \frac{2\sqrt{5}}{7}H_{220}] + f_{400}[\frac{6}{7}H_{200} + \frac{900}{693\sqrt{5}}H_{400}]
 \end{aligned}$$

$$\begin{aligned}
 C_{220} &= f_{000} H_{220} + f_{200} [2H_{200} + H_{220} \frac{4\sqrt{5}}{7}] + f_{220} [H_{000} + 1 \\
 &\quad + \frac{4\sqrt{5}}{7} H_{200} + \frac{20}{49} H_{220} + \frac{12}{7} H_{400}] + \frac{12}{7} f_{400} H_{220} \\
 C_{400} &= f_{000} H_{400} + f_{200} [\frac{18\sqrt{5}}{35} H_{200} + \frac{60}{77} H_{400}] + \frac{18\sqrt{5}}{35} f_{220} H_{220} \\
 &\quad + f_{400} [\frac{60}{77} H_{200} + \frac{1458}{1001\sqrt{5}} H_{400} + H_{000} + 1]
 \end{aligned} \tag{28}$$

As mentioned above, if $f_{\ell\ell',m}$ is identified with the zero density $g_{\ell\ell',m}^o$ coefficient and $C_{\ell\ell',m}$ is identified with $g_{\ell\ell',m}$, these equations give the expansion coefficients of the pair distribution function as well. For future work, we also desire to have the g_{221} and g_{222} coefficients derived from the $H_{\ell\ell',m}$ set above. These are:

$$\begin{aligned}
 g_{221} &= g_{221}^o [H_{000} + 1 + \frac{2\sqrt{5}}{7} H_{200} + \frac{5}{49} H_{220} - \frac{8}{7} H_{400}] \\
 g_{222} &= g_{222}^o [H_{000} + 1 - \frac{4\sqrt{5}}{7} H_{200} + \frac{20}{49} H_{220} + \frac{2}{7} H_{400}]
 \end{aligned} \tag{29}$$

C. Potential Parameters for Chlorine

The potential that has been employed in this work is the two-centered Lennard-Jones potential. It has been discussed in detail by Sweet and Steele¹⁰. We have applied it here to the diatomic chlorine, choosing this substance because it is nonspherical, nonparamagnetic, and composed of just two atoms which are likely centers for the Lennard-Jones functions. Furthermore, it apparently has a high configurational heat capacity¹¹ indicating strong orientational correlations in the fluid state.

Because we are dealing with a homonuclear diatomic, just one set of σ and ϵ values characterizes the molecule. A third parameter $R^* = R/\sigma$, where R is the distance between interaction centers, is also required. In solving the Percus-Yevick equation for a particular substance, the R^* (and hence σ) parameters are required as input. In this section values for σ , ϵ , and R^* for chlorine are derived.

The method of solution is that due to Sweet¹². In this method the parameters are determined from the second virial coefficient. Reduced virial coefficients and temperatures are written as

$$B^* = B/b_o, \quad b_o = \frac{2}{3} \pi \sigma^3 N \quad (30)$$

$$T^* = kT/\epsilon \quad (31)$$

or

$$\log |B^*| = \log |B| - \log b_o$$

$$\log |T^*| = \log |T| - \log (\epsilon/k)$$

If one then has a set of reduced (B^*, T^*) pairs from theory and a set of experimental (B, T) pairs, log plots of the two data sets will yield $\log b_0$ and $\log \epsilon/k$ as intercept values if the two curves are superimposed. However, unlike spherical systems, the B^* values are also a function of R^* and one must repeat this determination of intercept values from new B^* curves until a σ is found from b_0 that will give an R/σ that is self-consistent with the R^* on which that B^* curve depends.

Theoretical $B^*(T^*)$ values have been calculated from

$$B^*(T^*) = -3 \int_0^{\infty} (g_{000}^0(r^*) - 1) r^{*2} dr^*$$

by Sweet for $R^* = 0.1, 0.2, 0.3$, and 0.4 and are reproduced in Appendix 5. Using the same numerical methods, we have extended these calculations for $B^*(T^*)$ to $R^* = 0.50, 0.55$, and 0.70 for a temperature range of $T^* = 0.2$ to 1.8 . These values appear in Table II.

Very few experimental values of $B(T)$ exist. Gmelin¹³ gives several references to chlorine PVT data, but nearly all refer to A. Eucken's work¹⁴. These data are suspicious in that the second virial curves derived from it do not have the same shape as is found for nearly all other monatomics and diatomics, the Eucken curves being too steep in the low temperature region. In addition, later Eucken data on ethane and ethylene has been found in error by McGlashen and Potter¹⁵ and Sweet¹⁶ respectively.

We have therefore used the data of Kapoor and Martin¹⁷. They have fitted other earlier data and give the empirical equation of state

TABLE II

SECOND VIRIAL COEFFICIENTS FOR THE TWO-CENTERED L-J POTENTIAL

T^* \ R^*	0.50	0.55	0.70
0.2	-	-	-25.677538
0.4	-	-6.685302	- 5.742034
0.6	-3.294647	-3.078723	- 2.537592
0.8	-1.839501	-1.678720	- 1.259973
1.0	-1.076307	-0.941468	- 0.579727
1.2	-0.609611	-0.489253	- 0.160139
1.3	-	-	- 0.006307
1.4	-0.295928	-0.185074	+ 0.122153
1.6	-0.072185	+0.032303	0.324136
1.8	+0.095208	-	-

$$P = \frac{RT}{V-b} + \sum_{n=2}^5 [A_n + B_n T + C_n \exp(-\frac{kT}{T_c})] (\frac{1}{V-b})^n$$

T_c is the critical temperature and $V \gg b$. If the bracketed quantity is defined as β_n and the $(V-b)$ terms are binomially expanded, one obtains

$$\frac{PV}{RT} = 1 + \frac{b}{V} + \dots + \frac{1}{RT} \sum_{n=2}^5 \beta_n \frac{1}{V^{n-1}} (1 + n \frac{b}{V} + \frac{n(n-1)}{2} \frac{b^2}{V^2} + \dots)$$

from which the second virial may be obtained as the coefficient of the $1/\tilde{V}$ term.

$$B(T) = b + \frac{1}{RT} (A_2 + B_2 T + C_2 \exp(-kT/T_c)) \quad (32)$$

The constants of (32) are tabulated in Table III.

TABLE III

$A_2 = -0.46496772246$	$B_2 = 2.129865506 \cdot 10^{-4}$	$C_2 = -0.098636526$
$T_c = 751^\circ R (417^\circ K)$	$R = 0.010296$	$b = 0.00608353$
		$k = 2.3$
Units are atm - ft ³ - lb - °R		

A list of values of $B(T)$ and T derived from this expression appears in Table IV, and a plot of the data is found in Figure 1.

The theoretical and experimental curves were superimposed as discussed above for all the R^* and the b_0 and ϵ/k parameters were determined. Fits were closest in the region of $T = 273$ to

417°K, where much of the original experimental data was concentrated, and in the region of the "V" . The results are tabulated in Table V. Plots of σ vs. R^* and ϵ/k vs. R^* appear as Figures 2 and 3. The points in Figure 2 were fitted with a straight line by least squares with the result

$$\sigma = -1.9016R^* + 4.76107 \quad (33)$$

Since $R^* = R/\sigma$ this equation can be solved for σ once R is known.

Sweet and Steele used 0.577 times the internuclear distance as the the interaction separation R for diatomics. This resulted from other work where longer molecules were viewed as a continuum and the two LJ centers were Gaussian distributed to represent this continuum. While this seems reasonable for molecules such as propane or butane, it is not required for diatomics since the two nuclei themselves may serve as the centers. Recently Kong¹⁸ has applied the two-center Lennard-Jones potential plus dipole and induced dipole terms to the calculation of ordinary and dielectric second virial coefficients with some success. In his potential the separation R is the distance between the centers of gravity of the two LJ atomic groupings rather than 0.577 times that distance, encouraging us to use the internuclear distance for R . It must be added, however, that in light of little other theoretical justification for this choice of R , it is possible that the best value for representing the true potential may lie somewhere between the two extremes discussed here.

We have therefore solved (33) for σ with $R = 1.988\text{\AA}$ and have carried along the least square error. The result is

TABLE IV

SECOND VIRIAL DATA FOR CHLORINE (from KAPOOR, MARTIN¹⁷)

T(°K)	B(cc/mole)	log B	log T
244.0	-361.60	2.558	2.387
250.4	-348.50	2.542	2.399
273.2	-307.00	2.487	2.436
298.2	-269.00	2.430	2.475
323.2	-237.20	2.375	2.509
373.2	-187.00	2.272	2.572
423.2	-149.20	2.174	2.627
457.2	-128.50	2.109	2.660
550.0	- 85.40	1.931	2.740
650.0	- 53.30	1.727	2.813
750.0	- 30.10	1.479	2.875
850.0	- 12.40	1.093	2.929
860.0	- 10.87	1.036	2.934
870.0	- 9.37	.972	2.939
880.0	- 7.91	.898	2.945
890.0	- 6.48	.812	2.949
900.0	- 5.08	.706	2.954
910.0	- 3.71	.569	2.959
920.0	- 2.38	.377	2.964
930.0	- 1.07	.029	2.968
940.0	+ 0.21	- .678	2.973
950.0	1.46	+ .164	2.978

TABLE V

R^*	b_o	ϵ/k	σ
0.10	120.23	292.42	4.568
0.20	109.65	331.13	4.430
0.30	91.20	403.65	4.166
0.40	79.43	481.95	3.978
0.50	69.34	553.4	3.802
0.55	63.10	599.8	3.684
0.70	52.72	724.4	3.470

$$\sigma_{\text{cl}_2} = 3.754 \pm .05 \text{\AA}$$

$$R^* = 0.53 \pm .01$$

From a quartic fit to Figure 3 and the R^* just obtained,

$$\epsilon/k = 581.0^\circ\text{K}$$

Numerical Evaluation

The general method of numerical solution of the Percus-Yevick equations for the $H_{\ell\ell',m}$ is that of Chen and Steele⁷ with appropriate modifications having been made to handle the longer ranged two-centered Lennard-Jones potential and the larger number of $H_{\ell\ell',m}$ coefficients. This is an iterative method in which the Mayer f function coefficients $f_{\ell\ell',m}$ are known beforehand. In the first iteration, an initial guess is made for the $H_{\ell\ell',m}$. Direct correlation function coefficients are calculated from (28), are Hankel transformed by (7), and are used to obtain Hankel transforms of the $H_{\ell\ell',m}$ by solution of Eqs. (20) to (22). The $H_{\ell\ell',m}$ transforms are then back transformed to a new set of $H'_{\ell\ell',m}$ by (8). A new guess for $H_{\ell\ell',m}$ is fashioned from the new $H'_{\ell\ell',m}$ and old $H_{\ell\ell',m}$ and the process repeated until the difference $|r_i(H'_{\ell\ell',m} - H_{\ell\ell',m})|$ is less than some predetermined value. Once the $H_{\ell\ell',m}$ functions are known for a particular density, the pair correlation function coefficients can be calculated from (28) and (29).

In the earlier hard core work, the Mayer functions were quite short-ranged since the potential and thus $[\exp(-u(R_1R_2)) - 1]$ went to zero beyond the largest overlap distance between molecules. Those $f_{\ell\ell',m}$ were zero beyond about $r^* = 1.60$. When the two-centered Lennard-Jones potential is used, however, the $f_{\ell\ell',m}$ are non-zero as far out as $r^* = 4.00$ for the higher coefficients and as far out as 6.00 for f_{000} . We have therefore computed $f_{\ell\ell',m}$ from $r^* = 0.70$ to 4.00 numerically and for f_{000} have extended these data to $r^* = 6.00$ by using the asymptotic formula for it. The $f_{\ell\ell',m}$ calculation is based on Gaussian quadrature integration^{12,19} of the triple integral

$$f_{\ell\ell',m}(r) = 4 \int_0^\pi \int_0^1 \int_0^1 (e^{-\beta u(\underline{R}_1, \underline{R}_2)} - 1) P_{\ell,m}(\cos \theta_1) P_{\ell',-m}(\cos \theta_2) \cos m\phi \\ \times d \cos \theta_1 d \cos \theta_2 d\phi \quad (34)$$

which results from (1) if $f(\underline{R}_1, \underline{R}_2)$ is identified with $X(\underline{R}_1, \underline{R}_2)$ and both sides of the equation are multiplied by $Y_{\ell,m}^*(\Omega_1) Y_{\ell',-m}^*(\Omega_2)$ and integrated over angle space. The asymptotic formula for f_{000} is given by

$$\lim_{r \rightarrow \infty} f(\underline{R}_1, \underline{R}_2) = \lim_{r \rightarrow \infty} f_{000}(r) = \frac{4}{T^* r^{*6}} \quad (35)$$

where the last equality arises from noting that $u(\underline{R}_1, \underline{R}_2) \rightarrow u_{LJ}(r)$ as $r \rightarrow \infty$ and then retaining the first term of a Maclaurin expansion of $\exp[-\beta u_{LJ}(r)] - 1$.

The use of these Mayer f coefficients allowed us to calculate $H_{\ell\ell',m}$ and $g_{\ell\ell',m}$ functions out to $r^* = 6.00$ as well. With an eye toward obtaining thermodynamic properties from these functions, it was noted that in the case of spherical systems Bearman et al.^{2,20} have shown that truncation error in thermodynamic integrals over r^* is virtually eliminated if the upper limit of integration is 6.00 or greater. In particular, those authors showed that the $g(r)$ of spherical systems may be replaced by 1.00 beyond this value. We have found that $g_{000}(r)$ behaves similarly and thus it too has been set equal to 1.00 beyond $r^* = 6.00$.

The core of the Percus-Yevick solution is the solution of Eqs. (20)-(22). This was accomplished here by noting that the equations of (22) are linear, consisting of four equations in four unknowns.

It was found that the A_{ii} and B_i terms of Table I were the largest, thus indicating that the matrix is somewhat diagonal and not ill-conditioned. The equations were solved simultaneously using the C(ℓℓ'ms) calculated beforehand. Equation (21) was solved for $H(4004)$ directly. Equations (22) were then solved as a group. Next, $H(2002)$ from (22) and $H(4004)$ from (21) were substituted into (20) to obtain $H(0000)$. Hence all H transforms were determined. The simultaneous solution of Eqs. (22) was done by the standard method of Gaussian elimination²¹, this being chosen because it is straightforward and rapid. Furthermore the round-off errors in this method have been studied carefully and are known to be reduced greatly if the technique of pivotal condensation is included in the programming.

Hankel transforms were obtained by expanding the spherical Bessel functions in the standard trigonometric representations (see Appendix 6) and then evaluating the resulting Fourier integrals by standard techniques. Like Chen and Steele⁷ we have employed the Fast Fourier Transform²² (FFT) because of its great speed. Because we have included H_{220} and H_{400} terms, fourth order as well as zero and second order Hankel transforms are required. The evaluation of this fourth order transform requires the summation of five Fourier transforms, two cosine and three sine transforms. It seemed possible that Fourier transform errors over a sum this large might begin to build to the point of introducing significant error in the final result. To test this, calculations were performed on $x^4 e^{-x^2}$ and it was found that the Fourier summation approach was adequate. When fourth order numerical results were compared with analytical values, the FFT Hankel transforms

were accurate to six digits or better up to a transform value of 10^{-10} (peak value .24). Inverting the transform itself gave the original function back with negligible error. When applied to the $H_{\ell\ell'm}$ functions, it was verified that the transform functions were effectively zero at the maximum value of v for which the transform was evaluated. We note that a result of having this higher order transform included in the calculation of H_{220} and H_{400} was to slightly more than double the computation time than when it was omitted and just H_{000} and H_{200} were calculated.

It is now necessary to consider the extrapolation procedures used in this work. There are two extrapolations involved here. The first is to be able to find initial guesses for the $H_{\ell\ell'm}$ at one density from the results previously obtained at lower densities. The individual $H_{\ell\ell'm}$ data points form well-behaved and generally monotonic curves as a function of density, and are thus amenable to a polynomial fit. Accordingly we have employed a five-point Newton forward extrapolation procedure.

Since the Newton method requires at least five points, these first five were treated differently. The first density treated was $\rho^* = 0.1$ and was low enough so that all $H_{\ell\ell'm}$ input were taken as zero. This approach was followed quite successfully by Watts⁴. The final output for $H_{\ell\ell'm}$ at $\rho^* = 0.1$ became the input for $\rho^* = 0.2$ and so forth until the first five densities were evaluated.

The second extrapolation is to determine at fixed density the $H_{\ell\ell'm}$ required for a particular iteration based upon results from previous iterations. If this extrapolation is not done, convergence will

either not be obtained at all or else convergence will be attained so slowly it will not be acceptable. A variety of schemes are available for this extrapolation and we have investigated two of them.

The first scheme is a simple linear extrapolation and has been applied in different forms by Chen⁷ and Bearman³ in earlier studies. We denote the $H_{\ell\ell',m}(r_i)$ values obtained after the n th iteration by H_n . Straight linear extrapolation gives as a result for the $(n+1)$ th iteration,

$$H_{n+1} = H_n + (H_n - H_{n-1})$$

A modification includes a mixing parameter α and

$$H_{n+1} = H_n + \alpha(H_n - H_{n-1}) \quad 0 < \alpha < 1 \quad (36)$$

and is the form employed by Chen. If $\alpha = 0$, the new input H_{n+1} equals the last output H_n .

The second method is based upon the e_k -transformation described by Shanks²³ and Peterson and McKoy²⁴. It was found by these authors to be extremely efficient and, if allowed to extrapolate on five points, to be capable of handling oscillatory and divergent series. In this work, however, we have employed the three point (e_1) transformation, principally so that more extrapolations will be done for a given number of iterations (typically on the order of 6-9).

This technique views each H_n as the n th partial sum of a convergent series whose limit H is the actual value of $H_{\ell\ell',m}(r_i)$. For the three point extrapolation the transformation assumes that for any partial sum

$$H = H_n + \epsilon_n = H_n + Aq^n$$

where the truncation error ϵ_n is composed of an amplitude A and a ratio q , assumed less than one. Defining $\Delta H_i = H_{i+1} - H_i$ and forming the differences ΔH_{n-1} and ΔH_{n-2} by eliminating H from the above equation, one may solve for ϵ_n in terms of previous partial sums. The expression for H then becomes

$$H = H_{n-1} + [(1/\Delta H_{n-1}) - (1/\Delta H_{n-2})]^{-1} \quad (37)$$

A slightly modified form of this equation using the Wynn algorithm²⁴ was used in our program. If the assumed form for ϵ_n is close to the actual truncation error, then the H given by (37) is far better converged than the last iteration result H_n . It is apparent that if H is taken to be the first of a new series of H_n , then an extrapolation will be done after every two iterations until convergence is obtained.

All of our final results have used the e_k -transformation (37). It was preferred over linear extrapolation principally because for many choices of α it allowed convergence in fewer iterations. A sample hard core PY solution at $\rho^* = 0.1$, and $R^* = 0.2$ required one-third more iterations using (36) with $\alpha = 0.2$ than (37). The iterations required were nearly the same with $\alpha = 0.05$. Since it is known³ that α is generally a function of density, the e_k method thus offers a way of avoiding excessive iterations due to non-optimization of this parameter at each density.

As outlined above, these iterations and extrapolations continue until the difference between two successive iterations satisfies

$$|r_i[H'_{\ell\ell'm} - H_{\ell\ell'm}]| < \zeta$$

For H_{000} , ζ has been taken as 4×10^{-4} , and for other $H_{\ell\ell'm}$, ζ has been taken as 10^{-4} . This compares with 10^{-4} used by Mandel, Bearman, and Bearman³ and nearly identical values used by Chen.

Results

Using the numerical procedures just discussed, we have obtained the $H_{\ell\ell'm}$ and $g_{\ell\ell'm}$ solutions for the grid given by $\rho^* = 0.1$ to 1.2 ($\Delta\rho^* = 0.1$), $T^* = 0.75, 1.00, 1.30$ for the two separation distances $R^* = 0.53, 0.68$. Numerical results for the $H_{\ell\ell'm}$ at $\rho^* = 0.6, 1.2$ and $T^* = 0.75$ may be found in Tables VI and VII. The data for $(\rho^*, T^*) = (1.2, 0.75)$ are plotted in Figure 4. Obviously, the functions are oscillatory and are dominated by H_{000} and H_{200} in the r^* range above 0.90. Since, in order to calculate the $g_{\ell\ell'm}$, the $H_{\ell\ell'm}$ are always multiplied by $g_{\ell\ell'm}^0$ which are zero below $r^* = 0.90$, it is only the $r^* > .90$ range which is eventually important for pair distribution determination. Below $r^* = 0.90$, H_{220} is also quite significant, especially near $r^* = 0.0$. We note that the general curve shapes of these functions agree with those obtained from two-center hard core cluster results²⁵ when the appropriate sum over cluster diagrams is taken. Differences between the H_{000} curves and H_{200} curves when H_{220} and H_{400} are and are not included depend on the r^* range and (ρ^*, T^*) point under consideration. For H_{000} at $(\rho^*, T^*) = (0.7, 0.75)$ the differences in the range $r^* = 0.90$ to 2.50 are on the order of 1% or less, climbing to approximately 4% or less at 3.20. The corresponding differences for H_{200} are larger, about 6%.

The pair distribution coefficients for the grid $\rho^* = 0.4$ to 1.2 ($\Delta\rho^* = 0.2$), $T^* = 1.30, 1.00, 0.75$ and for $R^* = 0.53$ are tabulated in Tables VIII-XXII. The $g_{000}(r)$ coefficient has been plotted in Figure 5 for $\rho^* = 0.2$ to 1.2 ($\Delta\rho^* = 0.2$) at $T^* = 1.30$. The same densities are also plotted in Figure 6 for $T^* = 0.75$. It is apparent

TABLE VI
H(R) COEFFICIENTS OF 2 L-J POTENTIAL FROM PY EQUATION

RHU*=0.60 T*=0.75 K*=0.53

R	H000	H200	H220	H400
0.04	2.0777	0.0018	0.5371	-0.0000
0.08	2.0239	0.0071	0.5027	-0.0000
0.12	1.9455	0.0150	0.4515	-0.0001
0.16	1.8537	0.0248	0.3905	-0.0003
0.20	1.7569	0.0354	0.3268	-0.0007
0.24	1.6586	0.0458	0.2665	-0.0014
0.28	1.5593	0.0556	0.2134	-0.0023
0.32	1.4589	0.0642	0.1691	-0.0032
0.36	1.3577	0.0715	0.1337	-0.0040
0.40	1.2570	0.0774	0.1059	-0.0046
0.44	1.1585	0.0822	0.0842	-0.0050
0.48	1.0634	0.0859	0.0672	-0.0052
0.52	0.9726	0.0887	0.0537	-0.0052
0.56	0.8863	0.0907	0.0427	-0.0050
0.60	0.8046	0.0921	0.0336	-0.0047
0.64	0.7273	0.0931	0.0259	-0.0043
0.68	0.6543	0.0935	0.0194	-0.0039
0.72	0.5854	0.0937	0.0138	-0.0034
0.76	0.5204	0.0935	0.0090	-0.0029
0.80	0.4591	0.0931	0.0049	-0.0024
0.84	0.4014	0.0924	0.0014	-0.0019
0.88	0.3470	0.0915	-0.0016	-0.0015
0.92	0.2959	0.0904	-0.0041	-0.0011
0.96	0.2480	0.0892	-0.0062	-0.0007
1.00	0.2032	0.0878	-0.0079	-0.0003
1.04	0.1614	0.0862	-0.0094	-0.0000
1.08	0.1225	0.0845	-0.0105	0.0002
1.12	0.0866	0.0826	-0.0114	0.0004
1.16	0.0535	0.0804	-0.0121	0.0006
1.20	0.0233	0.0780	-0.0125	0.0006
1.24	-0.0042	0.0755	-0.0127	0.0007
1.28	-0.0289	0.0727	-0.0127	0.0007
1.32	-0.0509	0.0697	-0.0127	0.0006
1.36	-0.0703	0.0666	-0.0125	0.0005
1.40	-0.0872	0.0634	-0.0122	0.0005
1.44	-0.1016	0.0600	-0.0118	0.0004
1.48	-0.1137	0.0565	-0.0113	0.0003
1.52	-0.1235	0.0530	-0.0108	0.0002
1.56	-0.1311	0.0493	-0.0102	0.0001
1.60	-0.1366	0.0455	-0.0095	0.0000
1.64	-0.1402	0.0417	-0.0087	-0.0000

TABLE VI (cont'd)

1.68	-0.1419	0.0377	-0.0078	-0.0000
1.72	-0.1418	0.0336	-0.0068	-0.0000
1.76	-0.1400	0.0294	-0.0056	0.0000
1.80	-0.1365	0.0251	-0.0044	0.0001
1.84	-0.1314	0.0207	-0.0030	0.0002
1.88	-0.1249	0.0161	-0.0014	0.0004
1.92	-0.1169	0.0114	0.0003	0.0007
1.96	-0.1076	0.0067	0.0021	0.0009
2.00	-0.0972	0.0018	0.0040	0.0012
2.04	-0.0859	-0.0031	0.0058	0.0014
2.08	-0.0739	-0.0078	0.0073	0.0014
2.12	-0.0614	-0.0122	0.0085	0.0013
2.16	-0.0484	-0.0161	0.0088	0.0011
2.20	-0.0351	-0.0192	0.0085	0.0007
2.24	-0.0221	-0.0215	0.0077	0.0003
2.28	-0.0099	-0.0227	0.0065	-0.0001
2.32	0.0007	-0.0229	0.0053	-0.0005
2.36	0.0094	-0.0222	0.0042	-0.0007
2.40	0.0163	-0.0206	0.0035	-0.0008
2.44	0.0216	-0.0185	0.0030	-0.0009
2.48	0.0258	-0.0159	0.0026	-0.0008
2.52	0.0290	-0.0131	0.0023	-0.0006
2.56	0.0311	-0.0103	0.0017	-0.0005
2.60	0.0322	-0.0076	0.0010	-0.0003
2.64	0.0324	-0.0051	0.0002	-0.0002
2.68	0.0318	-0.0029	-0.0006	-0.0001
2.72	0.0307	-0.0010	-0.0013	-0.0000
2.76	0.0291	0.0005	-0.0018	0.0000
2.80	0.0274	0.0016	-0.0021	0.0000
2.84	0.0255	0.0024	-0.0021	0.0001
2.88	0.0235	0.0029	-0.0020	0.0001
2.92	0.0217	0.0032	-0.0017	0.0001
2.96	0.0199	0.0032	-0.0014	0.0001
3.00	0.0184	0.0030	-0.0011	0.0001
3.10	0.0154	0.0021	-0.0003	0.0001
3.20	0.0138	0.0010	0.0002	0.0001
3.30	0.0133	-0.0001	0.0004	0.0001
3.40	0.0134	-0.0008	0.0005	0.0000
3.50	0.0136	-0.0011	0.0004	0.0000
3.60	0.0136	-0.0012	0.0002	-0.0000
3.70	0.0134	-0.0010	0.0000	-0.0000
3.80	0.0129	-0.0006	-0.0001	-0.0000
3.90	0.0121	-0.0003	-0.0001	-0.0000
4.00	0.0113	-0.0001	-0.0001	-0.0000

TABLE VII
H(R) COEFFICIENTS OF 2 L-J POTENTIAL FROM PY EQUATION

RH0*=1.20 T*=0.75 R*=0.53

R	H000	H200	H220	H400
0.04	5.5424	0.0048	1.4533	-0.0000
0.08	5.3897	0.0185	1.3508	-0.0000
0.12	5.1711	0.0391	1.2004	-0.0002
0.16	4.9216	0.0641	1.0241	-0.0007
0.20	4.6658	0.0906	0.8430	-0.0021
0.24	4.4136	0.1164	0.6741	-0.0043
0.28	4.1644	0.1398	0.5280	-0.0073
0.32	3.9151	0.1600	0.4084	-0.0107
0.36	3.6648	0.1767	0.3143	-0.0137
0.40	3.4156	0.1900	0.2417	-0.0162
0.44	3.1708	0.2004	0.1860	-0.0179
0.48	2.9334	0.2083	0.1428	-0.0189
0.52	2.7051	0.2141	0.1086	-0.0192
0.56	2.4866	0.2181	0.0810	-0.0190
0.60	2.2779	0.2206	0.0584	-0.0184
0.64	2.0788	0.2220	0.0395	-0.0173
0.68	1.8889	0.2224	0.0237	-0.0160
0.72	1.7079	0.2220	0.0105	-0.0145
0.76	1.5354	0.2207	-0.0004	-0.0128
0.80	1.3713	0.2189	-0.0094	-0.0110
0.84	1.2152	0.2164	-0.0164	-0.0092
0.88	1.0671	0.2133	-0.0218	-0.0074
0.92	0.9269	0.2099	-0.0257	-0.0057
0.96	0.7944	0.2062	-0.0283	-0.0040
1.00	0.6698	0.2023	-0.0300	-0.0024
1.04	0.5531	0.1980	-0.0309	-0.0008
1.08	0.4443	0.1933	-0.0312	0.0007
1.12	0.3437	0.1879	-0.0309	0.0020
1.16	0.2512	0.1818	-0.0300	0.0030
1.20	0.1668	0.1748	-0.0286	0.0038
1.24	0.0907	0.1672	-0.0268	0.0042
1.28	0.0227	0.1591	-0.0248	0.0044
1.32	-0.0374	0.1506	-0.0227	0.0045
1.36	-0.0898	0.1418	-0.0207	0.0045
1.40	-0.1348	0.1328	-0.0188	0.0045
1.44	-0.1728	0.1237	-0.0169	0.0044
1.48	-0.2040	0.1144	-0.0151	0.0043
1.52	-0.2290	0.1050	-0.0134	0.0042
1.56	-0.2481	0.0956	-0.0117	0.0041
1.60	-0.2618	0.0860	-0.0100	0.0040
1.64	-0.2705	0.0764	-0.0083	0.0039

TABLE VII (cont'd)

1.68	-0.2745	0.0667	-0.0004	0.0039
1.72	-0.2742	0.0569	-0.0044	0.0040
1.76	-0.2700	0.0472	-0.0023	0.0041
1.80	-0.2622	0.0374	0.0001	0.0044
1.84	-0.2509	0.0275	0.0027	0.0047
1.88	-0.2366	0.0177	0.0056	0.0050
1.92	-0.2195	0.0079	0.0087	0.0055
1.96	-0.2001	-0.0020	0.0121	0.0059
2.00	-0.1791	-0.0117	0.0154	0.0063
2.04	-0.1571	-0.0211	0.0182	0.0062
2.08	-0.1347	-0.0297	0.0202	0.0057
2.12	-0.1117	-0.0373	0.0207	0.0047
2.16	-0.0882	-0.0431	0.0196	0.0032
2.20	-0.0645	-0.0468	0.0168	0.0014
2.24	-0.0418	-0.0482	0.0130	-0.0004
2.28	-0.0220	-0.0472	0.0090	-0.0020
2.32	-0.0066	-0.0439	0.0055	-0.0033
2.36	0.0039	-0.0389	0.0031	-0.0043
2.40	0.0103	-0.0325	0.0020	-0.0047
2.44	0.0137	-0.0254	0.0017	-0.0047
2.48	0.0153	-0.0181	0.0016	-0.0043
2.52	0.0155	-0.0110	0.0014	-0.0037
2.56	0.0145	-0.0046	0.0006	-0.0030
2.60	0.0123	0.0011	-0.0007	-0.0022
2.64	0.0090	0.0057	-0.0022	-0.0015
2.68	0.0050	0.0093	-0.0037	-0.0009
2.72	0.0007	0.0117	-0.0047	-0.0004
2.76	-0.0035	0.0132	-0.0052	0.0000
2.80	-0.0074	0.0138	-0.0051	0.0003
2.84	-0.0108	0.0136	-0.0045	0.0006
2.88	-0.0136	0.0127	-0.0036	0.0008
2.92	-0.0157	0.0113	-0.0025	0.0009
2.96	-0.0171	0.0096	-0.0013	0.0010
3.00	-0.0177	0.0077	-0.0003	0.0010
3.10	-0.0164	0.0026	0.0017	0.0010
3.20	-0.0122	-0.0016	0.0024	0.0008
3.30	-0.0068	-0.0041	0.0021	0.0004
3.40	-0.0019	-0.0048	0.0014	0.0001
3.50	0.0012	-0.0042	0.0004	-0.0002
3.60	0.0025	-0.0027	-0.0004	-0.0004
3.70	0.0023	-0.0010	-0.0010	-0.0004
3.80	0.0012	0.0004	-0.0012	-0.0003
3.90	-0.0001	0.0013	-0.0009	-0.0002
4.00	-0.0011	0.0015	-0.0005	-0.0000

TABLE VIII
PAIR DISTRIBUTION COEFFICIENTS FOR 2 L-J POTENTIAL
FROM PY EQUATION $\rho^*=0.40$ $T^*=1.30$ $R^*=0.53$

R	G000	G200	G220	G221	G222	G400
0.80	0.0000	-0.0000	0.0000	-0.0000	-0.0000	0.0000
0.84	0.0002	-0.0002	0.0003	-0.0000	-0.0003	0.0006
0.88	0.0042	-0.0043	0.0049	-0.0001	-0.0041	0.0106
0.92	0.0285	-0.0283	0.0310	-0.0018	-0.0159	0.0566
0.96	0.0967	-0.0925	0.0953	-0.0092	-0.0293	0.1384
1.00	0.2147	-0.1945	0.1839	-0.0260	-0.0354	0.1812
1.04	0.3687	-0.3097	0.2593	-0.0515	-0.0339	0.1125
1.08	0.5430	-0.4093	0.2845	-0.0801	-0.0287	-0.0584
1.12	0.7277	-0.4703	0.2359	-0.1049	-0.0224	-0.2207
1.16	0.9122	-0.4794	0.1156	-0.1184	-0.0164	-0.2481
1.20	1.0792	-0.4396	-0.0364	-0.1173	-0.0111	-0.1312
1.24	1.2119	-0.3662	-0.1664	-0.1027	-0.0069	0.0240
1.28	1.3038	-0.2760	-0.2408	-0.0800	-0.0038	0.1154
1.32	1.3570	-0.1827	-0.2523	-0.0553	-0.0017	0.1117
1.36	1.3772	-0.0966	-0.2146	-0.0335	-0.0004	0.0553
1.40	1.3707	-0.0263	-0.1533	-0.0174	0.0002	0.0074
1.44	1.3440	0.0220	-0.0947	-0.0072	0.0005	-0.0109
1.48	1.3050	0.0490	-0.0523	-0.0016	0.0006	-0.0117
1.52	1.2610	0.0603	-0.0265	0.0010	0.0005	-0.0078
1.56	1.2174	0.0621	-0.0123	0.0021	0.0005	-0.0043
1.60	1.1773	0.0591	-0.0051	0.0023	0.0004	-0.0021
1.64	1.1419	0.0540	-0.0017	0.0022	0.0003	-0.0010
1.68	1.1114	0.0482	-0.0003	0.0020	0.0003	-0.0004
1.72	1.0856	0.0425	0.0003	0.0017	0.0002	-0.0001
1.76	1.0640	0.0370	0.0005	0.0014	0.0002	-0.0000
1.80	1.0462	0.0320	0.0007	0.0012	0.0001	0.0000
1.84	1.0318	0.0274	0.0008	0.0010	0.0001	0.0000
1.88	1.0203	0.0231	0.0011	0.0008	0.0001	0.0001
1.92	1.0114	0.0191	0.0014	0.0006	0.0001	0.0001
1.96	1.0047	0.0154	0.0018	0.0005	0.0001	0.0001
2.00	0.9998	0.0119	0.0023	0.0004	0.0000	0.0002
2.04	0.9967	0.0087	0.0027	0.0004	0.0000	0.0002
2.08	0.9950	0.0057	0.0031	0.0003	0.0000	0.0002
2.12	0.9946	0.0030	0.0033	0.0002	0.0000	0.0001
2.16	0.9952	0.0006	0.0034	0.0002	0.0000	0.0000
2.20	0.9965	-0.0014	0.0033	0.0002	0.0000	-0.0000
2.24	0.9982	-0.0030	0.0031	0.0001	0.0000	-0.0001
2.28	1.0001	-0.0042	0.0028	0.0001	0.0000	-0.0002
2.32	1.0020	-0.0050	0.0026	0.0001	0.0000	-0.0002
2.36	1.0037	-0.0054	0.0023	0.0001	0.0000	-0.0002
2.40	1.0054	-0.0055	0.0021	0.0001	0.0000	-0.0002

TABLE VIII (cont'd)

2.44	1.0069	-0.0053	0.0019	0.0001	0.0000	-0.0001
2.48	1.0082	-0.0049	0.0017	0.0001	0.0000	-0.0001
2.52	1.0093	-0.0044	0.0014	0.0000	0.0000	-0.0000
2.56	1.0100	-0.0038	0.0011	0.0000	0.0000	-0.0000
2.60	1.0105	-0.0031	0.0007	0.0000	0.0000	0.0000
2.64	1.0107	-0.0025	0.0004	0.0000	0.0000	0.0000
2.68	1.0107	-0.0018	0.0000	0.0000	0.0000	0.0000
2.72	1.0104	-0.0013	-0.0002	0.0000	0.0000	0.0000
2.76	1.0101	-0.0008	-0.0004	0.0000	0.0000	0.0000
2.80	1.0096	-0.0004	-0.0005	0.0000	0.0000	0.0000
2.84	1.0090	-0.0000	-0.0005	0.0000	0.0000	0.0000
2.88	1.0083	0.0002	-0.0005	0.0000	0.0000	0.0000
2.92	1.0076	0.0004	-0.0005	0.0000	0.0000	0.0000
2.96	1.0069	0.0005	-0.0004	0.0000	0.0000	0.0000
3.00	1.0063	0.0006	-0.0003	0.0000	0.0000	0.0000
3.10	1.0048	0.0006	-0.0002	0.0000	0.0000	0.0000
3.20	1.0036	0.0005	-0.0001	0.0000	0.0000	0.0000
3.30	1.0028	0.0003	0.0000	0.0000	0.0000	0.0000
3.40	1.0022	0.0001	0.0001	0.0000	0.0000	-0.0000
3.50	1.0019	0.0000	0.0001	0.0000	0.0000	-0.0000
3.60	1.0017	-0.0001	0.0001	0.0000	0.0000	-0.0000
3.70	1.0016	-0.0001	0.0000	0.0000	0.0000	-0.0000
3.80	1.0015	-0.0001	0.0000	0.0000	0.0000	-0.0000
3.90	1.0013	-0.0001	0.0000	0.0000	0.0000	-0.0000
4.00	1.0012	-0.0000	-0.0000	0.0000	0.0000	0.0000
4.20	1.0009	-0.0000	-0.0000	0.0	0.0	0.0000
4.40	1.0007	-0.0000	-0.0000	0.0	0.0	0.0000
4.60	1.0005	0.0000	-0.0000	0.0	0.0	0.0000
4.80	1.0004	-0.0000	0.0000	0.0	0.0	-0.0000
5.00	1.0003	-0.0000	0.0000	0.0	0.0	0.0000
5.20	1.0003	-0.0000	0.0000	0.0	0.0	-0.0000
5.40	1.0002	-0.0000	0.0000	0.0	0.0	-0.0000
5.60	1.0002	-0.0000	-0.0000	0.0	0.0	0.0000
5.80	1.0001	-0.0000	-0.0000	0.0	0.0	0.0000
6.00	1.0001	-0.0000	-0.0000	0.0	0.0	0.0000

TABLE IX
PAIR DISTRIBUTION COEFFICIENTS FOR 2 L-J POTENTIAL
FROM PY EQUATION $\rho^*=0.60$ $T^*=1.30$ $R^*=0.53$

R	G000	G200	G220	G221	G222	G400
0.80	0.0000	-0.0000	0.0000	-0.0000	-0.0000	0.0000
0.84	0.0002	-0.0003	0.0003	-0.0000	-0.0004	0.0007
0.88	0.0046	-0.0046	0.0055	-0.0002	-0.0046	0.0120
0.92	0.0309	-0.0303	0.0344	-0.0021	-0.0175	0.0635
0.96	0.1039	-0.0985	0.1042	-0.0103	-0.0319	0.1533
1.00	0.2286	-0.2063	0.1986	-0.0289	-0.0381	0.1971
1.04	0.3894	-0.3271	0.2762	-0.0565	-0.0361	0.1170
1.08	0.5695	-0.4306	0.2980	-0.0872	-0.0302	-0.0727
1.12	0.7585	-0.4915	0.2404	-0.1130	-0.0233	-0.2487
1.16	0.9457	-0.4953	0.1077	-0.1264	-0.0169	-0.2758
1.20	1.1132	-0.4463	-0.0556	-0.1240	-0.0114	-0.1484
1.24	1.2438	-0.3629	-0.1919	-0.1077	-0.0070	0.0177
1.28	1.3311	-0.2647	-0.2664	-0.0832	-0.0038	0.1148
1.32	1.3780	-0.1662	-0.2736	-0.0570	-0.0017	0.1120
1.36	1.3911	-0.0773	-0.2297	-0.0342	-0.0004	0.0549
1.40	1.3771	-0.0059	-0.1628	-0.0176	0.0002	0.0069
1.44	1.3430	0.0424	-0.1004	-0.0073	0.0005	-0.0109
1.48	1.2971	0.0684	-0.0558	-0.0016	0.0005	-0.0112
1.52	1.2472	0.0782	-0.0289	0.0010	0.0005	-0.0071
1.56	1.1986	0.0784	-0.0143	0.0021	0.0004	-0.0036
1.60	1.1545	0.0737	-0.0069	0.0023	0.0004	-0.0015
1.64	1.1159	0.0670	-0.0033	0.0022	0.0003	-0.0004
1.68	1.0831	0.0597	-0.0016	0.0019	0.0002	0.0001
1.72	1.0557	0.0525	-0.0008	0.0016	0.0002	0.0003
1.76	1.0332	0.0456	-0.0003	0.0014	0.0002	0.0003
1.80	1.0151	0.0392	0.0001	0.0011	0.0001	0.0004
1.84	1.0009	0.0333	0.0006	0.0009	0.0001	0.0004
1.88	0.9901	0.0277	0.0013	0.0008	0.0001	0.0004
1.92	0.9823	0.0225	0.0020	0.0006	0.0001	0.0005
1.96	0.9770	0.0175	0.0028	0.0005	0.0001	0.0005
2.00	0.9741	0.0127	0.0037	0.0004	0.0000	0.0006
2.04	0.9731	0.0082	0.0045	0.0004	0.0000	0.0006
2.08	0.9739	0.0041	0.0050	0.0003	0.0000	0.0005
2.12	0.9761	0.0004	0.0054	0.0002	0.0000	0.0004
2.16	0.9794	-0.0028	0.0054	0.0002	0.0000	0.0002
2.20	0.9835	-0.0055	0.0051	0.0002	0.0000	0.0001
2.24	0.9879	-0.0075	0.0047	0.0001	0.0000	-0.0001
2.28	0.9921	-0.0089	0.0042	0.0001	0.0000	-0.0002
2.32	0.9960	-0.0096	0.0038	0.0001	0.0000	-0.0003
2.36	0.9996	-0.0098	0.0034	0.0001	0.0000	-0.0003
2.40	1.0027	-0.0095	0.0030	0.0001	0.0000	-0.0003

TABLE IX (cont'd)

2.44	1.0054	-0.0088	0.0027	0.0001	0.0000	-0.0003
2.48	1.0077	-0.0078	0.0023	0.0001	0.0000	-0.0002
2.52	1.0095	-0.0067	0.0018	0.0000	0.0000	-0.0002
2.56	1.0108	-0.0055	0.0013	0.0000	0.0000	-0.0001
2.60	1.0115	-0.0043	0.0007	0.0000	0.0000	-0.0000
2.64	1.0117	-0.0031	0.0002	0.0000	0.0000	-0.0000
2.68	1.0116	-0.0020	-0.0003	0.0000	0.0000	0.0000
2.72	1.0112	-0.0011	-0.0007	0.0000	0.0000	0.0000
2.76	1.0105	-0.0003	-0.0009	0.0000	0.0000	0.0000
2.80	1.0097	0.0003	-0.0010	0.0000	0.0000	0.0000
2.84	1.0087	0.0008	-0.0010	0.0000	0.0000	0.0000
2.88	1.0077	0.0012	-0.0010	0.0000	0.0000	0.0000
2.92	1.0066	0.0014	-0.0008	0.0000	0.0000	0.0000
2.96	1.0056	0.0015	-0.0007	0.0000	0.0000	0.0000
3.00	1.0047	0.0016	-0.0006	0.0000	0.0000	0.0000
3.10	1.0027	0.0013	-0.0003	0.0000	0.0000	0.0000
3.20	1.0015	0.0009	-0.0000	0.0000	0.0000	0.0000
3.30	1.0008	0.0005	0.0001	0.0000	0.0000	0.0000
3.40	1.0006	0.0001	0.0002	0.0000	0.0000	0.0000
3.50	1.0007	-0.0002	0.0002	0.0000	0.0000	-0.0000
3.60	1.0009	-0.0003	0.0001	0.0000	0.0000	-0.0000
3.70	1.0010	-0.0003	0.0001	0.0000	0.0000	-0.0000
3.80	1.0011	-0.0002	0.0000	0.0000	0.0000	-0.0000
3.90	1.0011	-0.0002	-0.0000	0.0000	0.0000	-0.0000
4.00	1.0010	-0.0001	-0.0000	0.0000	0.0000	-0.0000
4.20	1.0007	0.0000	-0.0000	0.0	0.0	0.0000
4.40	1.0005	0.0000	-0.0000	0.0	0.0	0.0000
4.60	1.0003	0.0000	0.0000	0.0	0.0	0.0000
4.80	1.0003	-0.0000	0.0000	0.0	0.0	-0.0000
5.00	1.0002	-0.0000	0.0000	0.0	0.0	-0.0000
5.20	1.0002	-0.0000	0.0000	0.0	0.0	-0.0000
5.40	1.0002	-0.0000	-0.0000	0.0	0.0	-0.0000
5.60	1.0001	-0.0000	-0.0000	0.0	0.0	0.0000
5.80	1.0001	-0.0000	0.0000	0.0	0.0	0.0000
6.00	1.0001	-0.0000	0.0000	0.0	0.0	0.0000

TABLE X
PAIR DISTRIBUTION COEFFICIENTS FOR 2 L-J POTENTIAL
FROM PY EQUATION $\rho^*=0.80$ $T^*=1.30$ $R^*=0.53$

R	G000	G200	G220	G221	G222	G400
0.80	0.0000	-0.0000	0.0000	-0.0000	-0.0000	0.0000
0.84	0.0003	-0.0003	0.0004	-0.0000	-0.0004	0.0009
0.88	0.0052	-0.0051	0.0063	-0.0002	-0.0052	0.0139
0.92	0.0342	-0.0331	0.0387	-0.0024	-0.0196	0.0727
0.96	0.1138	-0.1069	0.1160	-0.0117	-0.0354	0.1731
1.00	0.2477	-0.2226	0.2182	-0.0327	-0.0418	0.2183
1.04	0.4181	-0.3513	0.2991	-0.0633	-0.0391	0.1233
1.08	0.6063	-0.4600	0.3169	-0.0565	-0.0323	-0.0910
1.12	0.8017	-0.5209	0.2478	-0.1238	-0.0246	-0.2849
1.16	0.9932	-0.5180	0.0987	-0.1370	-0.0176	-0.3116
1.20	1.1619	-0.4573	-0.0794	-0.1331	-0.0117	-0.1703
1.24	1.2900	-0.3612	-0.2239	-0.1144	-0.0072	0.0104
1.28	1.3716	-0.2527	-0.2987	-0.0875	-0.0039	0.1149
1.32	1.4107	-0.1474	-0.3004	-0.0593	-0.0017	0.1131
1.36	1.4147	-0.0550	-0.2486	-0.0353	-0.0004	0.0548
1.40	1.3912	0.0179	-0.1744	-0.0180	0.0002	0.0065
1.44	1.3479	0.0661	-0.1070	-0.0074	0.0005	-0.0108
1.48	1.2935	0.0909	-0.0597	-0.0016	0.0005	-0.0106
1.52	1.2362	0.0988	-0.0314	0.0010	0.0005	-0.0062
1.56	1.1817	0.0968	-0.0161	0.0021	0.0004	-0.0026
1.60	1.1328	0.0899	-0.0083	0.0023	0.0004	-0.0006
1.64	1.0906	0.0811	-0.0044	0.0021	0.0003	0.0004
1.68	1.0552	0.0719	-0.0025	0.0019	0.0002	0.0009
1.72	1.0261	0.0628	-0.0014	0.0016	0.0002	0.0010
1.76	1.0028	0.0543	-0.0006	0.0013	0.0002	0.0010
1.80	0.9845	0.0462	0.0002	0.0011	0.0001	0.0010
1.84	0.9708	0.0387	0.0011	0.0009	0.0001	0.0011
1.88	0.9611	0.0315	0.0022	0.0007	0.0001	0.0011
1.92	0.9549	0.0247	0.0034	0.0006	0.0001	0.0012
1.96	0.9517	0.0182	0.0046	0.0005	0.0001	0.0013
2.00	0.9511	0.0120	0.0059	0.0004	0.0000	0.0013
2.04	0.9528	0.0061	0.0070	0.0003	0.0000	0.0013
2.08	0.9565	0.0008	0.0077	0.0003	0.0000	0.0011
2.12	0.9618	-0.0040	0.0080	0.0002	0.0000	0.0008
2.16	0.9683	-0.0080	0.0079	0.0002	0.0000	0.0005
2.20	0.9754	-0.0112	0.0074	0.0002	0.0000	0.0002
2.24	0.9826	-0.0134	0.0066	0.0001	0.0000	-0.0001
2.28	0.9893	-0.0147	0.0057	0.0001	0.0000	-0.0004
2.32	0.9951	-0.0152	0.0050	0.0001	0.0000	-0.0006
2.36	1.0002	-0.0148	0.0044	0.0001	0.0000	-0.0007
2.40	1.0045	-0.0138	0.0039	0.0001	0.0000	-0.0007

TABLE X (cont'd)

2.44	1.0080	-0.0124	0.0033	0.0001	0.0000	-0.0006
2.48	1.0109	-0.0106	0.0028	0.0001	0.0000	-0.0005
2.52	1.0129	-0.0086	0.0021	0.0000	0.0000	-0.0004
2.56	1.0142	-0.0066	0.0013	0.0000	0.0000	-0.0003
2.60	1.0146	-0.0047	0.0005	0.0000	0.0000	-0.0002
2.64	1.0145	-0.0029	-0.0003	0.0000	0.0000	-0.0001
2.68	1.0138	-0.0013	-0.0010	0.0000	0.0000	-0.0001
2.72	1.0127	0.0001	-0.0014	0.0000	0.0000	-0.0000
2.76	1.0113	0.0011	-0.0017	0.0000	0.0000	-0.0000
2.80	1.0098	0.0020	-0.0018	0.0000	0.0000	-0.0000
2.84	1.0082	0.0026	-0.0017	0.0000	0.0000	0.0000
2.88	1.0066	0.0029	-0.0015	0.0000	0.0000	0.0000
2.92	1.0050	0.0031	-0.0013	0.0000	0.0000	0.0000
2.96	1.0036	0.0031	-0.0010	0.0000	0.0000	0.0000
3.00	1.0023	0.0029	-0.0008	0.0000	0.0000	0.0001
3.10	0.9999	0.0022	-0.0002	0.0000	0.0000	0.0001
3.20	0.9988	0.0012	0.0002	0.0000	0.0000	0.0001
3.30	0.9986	0.0004	0.0003	0.0000	0.0000	0.0000
3.40	0.9991	-0.0003	0.0004	0.0000	0.0000	0.0000
3.50	0.9997	-0.0006	0.0003	0.0000	0.0000	0.0000
3.60	1.0004	-0.0007	0.0002	0.0000	0.0000	-0.0000
3.70	1.0008	-0.0006	0.0000	0.0000	0.0000	-0.0000
3.80	1.0010	-0.0004	-0.0000	0.0000	0.0000	-0.0000
3.90	1.0010	-0.0002	-0.0001	0.0000	0.0000	-0.0000
4.00	1.0009	0.0000	-0.0001	0.0000	0.0000	-0.0000
4.20	1.0004	0.0001	-0.0001	0.0	0.0	0.0000
4.40	1.0002	0.0001	-0.0000	0.0	0.0	0.0000
4.60	1.0001	0.0000	0.0000	0.0	0.0	0.0000
4.80	1.0001	-0.0000	0.0000	0.0	0.0	-0.0000
5.00	1.0001	-0.0000	0.0000	0.0	0.0	-0.0000
5.20	1.0001	-0.0000	-0.0000	0.0	0.0	-0.0000
5.40	1.0001	0.0000	-0.0000	0.0	0.0	-0.0000
5.60	1.0001	0.0000	-0.0000	0.0	0.0	0.0000
5.80	1.0001	0.0000	0.0000	0.0	0.0	0.0000
6.00	1.0001	-0.0000	0.0000	0.0	0.0	0.0000

TABLE XI
PAIR DISTRIBUTION COEFFICIENTS FOR 2 L-J POTENTIAL
FROM PY EQUATION $\rho^*=1.00$ $T^*=1.30$ $R^*=0.53$

R	G000	G200	G220	G221	G222	G400
0.80	0.0000	-0.0000	0.0000	-0.0000	-0.0000	0.0000
0.84	0.0003	-0.0003	0.0004	-0.0000	-0.0005	0.0010
0.88	0.0059	-0.0058	0.0074	-0.0002	-0.0061	0.0165
0.92	0.0387	-0.0370	0.0446	-0.0028	-0.0226	0.0852
0.96	0.1271	-0.1184	0.1320	-0.0137	-0.0401	0.2000
1.00	0.2738	-0.2450	0.2447	-0.0378	-0.0467	0.2471
1.04	0.4572	-0.3843	0.3302	-0.0723	-0.0432	0.1319
1.08	0.6565	-0.5001	0.3428	-0.1091	-0.0352	-0.1156
1.12	0.8605	-0.5608	0.2582	-0.1383	-0.0264	-0.3333
1.16	1.0576	-0.5489	0.0874	-0.1512	-0.0187	-0.3591
1.20	1.2278	-0.4727	-0.1105	-0.1451	-0.0123	-0.1989
1.24	1.3526	-0.3600	-0.2656	-0.1232	-0.0074	0.0011
1.28	1.4265	-0.2381	-0.3404	-0.0931	-0.0039	0.1156
1.32	1.4550	-0.1242	-0.3346	-0.0625	-0.0017	0.1149
1.36	1.4470	-0.0273	-0.2722	-0.0368	-0.0004	0.0551
1.40	1.4112	0.0473	-0.1886	-0.0186	0.0002	0.0064
1.44	1.3561	0.0952	-0.1146	-0.0075	0.0005	-0.0103
1.48	1.2910	0.1182	-0.0636	-0.0017	0.0005	-0.0093
1.52	1.2247	0.1234	-0.0335	0.0010	0.0005	-0.0046
1.56	1.1629	0.1185	-0.0174	0.0020	0.0004	-0.0010
1.60	1.1085	0.1087	-0.0091	0.0023	0.0003	0.0010
1.64	1.0623	0.0972	-0.0049	0.0021	0.0003	0.0019
1.68	1.0242	0.0853	-0.0027	0.0018	0.0002	0.0022
1.72	0.9937	0.0739	-0.0013	0.0016	0.0002	0.0023
1.76	0.9699	0.0630	-0.0001	0.0013	0.0001	0.0023
1.80	0.9521	0.0528	0.0011	0.0011	0.0001	0.0023
1.84	0.9397	0.0432	0.0025	0.0009	0.0001	0.0023
1.88	0.9319	0.0340	0.0041	0.0007	0.0001	0.0024
1.92	0.9281	0.0253	0.0058	0.0006	0.0001	0.0025
1.96	0.9279	0.0169	0.0076	0.0005	0.0001	0.0025
2.00	0.9305	0.0089	0.0093	0.0004	0.0000	0.0025
2.04	0.9357	0.0015	0.0106	0.0003	0.0000	0.0023
2.08	0.9431	-0.0052	0.0114	0.0003	0.0000	0.0020
2.12	0.9522	-0.0111	0.0116	0.0002	0.0000	0.0015
2.16	0.9625	-0.0158	0.0110	0.0002	0.0000	0.0009
2.20	0.9733	-0.0193	0.0099	0.0002	0.0000	0.0003
2.24	0.9836	-0.0215	0.0086	0.0001	0.0000	-0.0003
2.28	0.9927	-0.0223	0.0072	0.0001	0.0000	-0.0008
2.32	1.0003	-0.0220	0.0060	0.0001	0.0000	-0.0011
2.36	1.0065	-0.0207	0.0051	0.0001	0.0000	-0.0013
2.40	1.0114	-0.0185	0.0044	0.0001	0.0000	-0.0013

TABLE XI (cont'd)

2.44	1.0153	-0.0158	0.0037	0.0001	0.0000	-0.0012
2.48	1.0180	-0.0128	0.0029	0.0001	0.0000	-0.0011
2.52	1.0197	-0.0097	0.0020	0.0000	0.0000	-0.0009
2.56	1.0202	-0.0066	0.0009	0.0000	0.0000	-0.0007
2.60	1.0197	-0.0038	-0.0002	0.0000	0.0000	-0.0005
2.64	1.0185	-0.0012	-0.0012	0.0000	0.0000	-0.0004
2.68	1.0166	0.0009	-0.0020	0.0000	0.0000	-0.0002
2.72	1.0144	0.0026	-0.0025	0.0000	0.0000	-0.0002
2.76	1.0119	0.0039	-0.0028	0.0000	0.0000	-0.0001
2.80	1.0093	0.0048	-0.0027	0.0000	0.0000	-0.0000
2.84	1.0068	0.0054	-0.0025	0.0000	0.0000	0.0000
2.88	1.0044	0.0055	-0.0021	0.0000	0.0000	0.0001
2.92	1.0022	0.0054	-0.0017	0.0000	0.0000	0.0001
2.96	1.0003	0.0051	-0.0013	0.0000	0.0000	0.0002
3.00	0.9987	0.0046	-0.0008	0.0000	0.0000	0.0002
3.10	0.9963	0.0030	0.0001	0.0000	0.0000	0.0002
3.20	0.9958	0.0012	0.0006	0.0000	0.0000	0.0002
3.30	0.9967	-0.0002	0.0008	0.0000	0.0000	0.0001
3.40	0.9982	-0.0011	0.0007	0.0000	0.0000	0.0001
3.50	0.9997	-0.0014	0.0004	0.0000	0.0000	-0.0000
3.60	1.0008	-0.0013	0.0002	0.0000	0.0000	-0.0001
3.70	1.0014	-0.0009	-0.0001	0.0000	0.0000	-0.0001
3.80	1.0015	-0.0004	-0.0002	0.0000	0.0000	-0.0001
3.90	1.0012	-0.0000	-0.0002	0.0000	0.0000	-0.0000
4.00	1.0008	0.0003	-0.0002	0.0000	0.0000	-0.0000
4.20	1.0001	0.0003	-0.0001	0.0	0.0	0.0000
4.40	0.9998	0.0001	0.0000	0.0	0.0	0.0000
4.60	0.9999	-0.0001	0.0001	0.0	0.0	0.0000
4.80	1.0001	-0.0001	0.0000	0.0	0.0	-0.0000
5.00	1.0001	-0.0000	-0.0000	0.0	0.0	-0.0000
5.20	1.0001	0.0000	-0.0000	0.0	0.0	-0.0000
5.40	1.0000	0.0000	-0.0000	0.0	0.0	0.0000
5.60	1.0000	0.0000	0.0000	0.0	0.0	0.0000
5.80	1.0000	-0.0000	0.0000	0.0	0.0	0.0000
6.00	1.0000	-0.0000	0.0000	0.0	0.0	-0.0000

TABLE XII
PAIR DISTRIBUTION COEFFICIENTS FOR 2 L-J POTENTIAL
FROM PY EQUATION $\rho^*=1.20$ $T^*=1.30$ $R^*=0.53$

R	G000	G200	G220	G221	G222	G400
0.80	0.0000	-0.0000	0.0000	-0.0000	-0.0000	0.0000
0.84	0.0004	-0.0004	0.0005	-0.0000	-0.0006	0.0013
0.88	0.0069	-0.0066	0.0087	-0.0003	-0.0072	0.0199
0.92	0.0445	-0.0420	0.0522	-0.0034	-0.0264	0.1016
0.96	0.1444	-0.1333	0.1525	-0.0163	-0.0463	0.2352
1.00	0.3073	-0.2737	0.2787	-0.0444	-0.0532	0.2844
1.04	0.5069	-0.4265	0.3700	-0.0841	-0.0484	0.1425
1.08	0.7198	-0.5508	0.3756	-0.1252	-0.0388	-0.1479
1.12	0.9338	-0.6110	0.2708	-0.1567	-0.0287	-0.3957
1.16	1.1370	-0.5872	0.0721	-0.1691	-0.0199	-0.4197
1.20	1.3081	-0.4910	-0.1505	-0.1601	-0.0129	-0.2350
1.24	1.4277	-0.3572	-0.3183	-0.1340	-0.0076	-0.0104
1.28	1.4911	-0.2187	-0.3923	-0.0999	-0.0040	0.1164
1.32	1.5058	-0.0946	-0.3761	-0.0661	-0.0017	0.1174
1.36	1.4824	0.0073	-0.3002	-0.0384	-0.0004	0.0559
1.40	1.4312	0.0834	-0.2045	-0.0192	0.0002	0.0069
1.44	1.3618	0.1303	-0.1225	-0.0077	0.0004	-0.0089
1.48	1.2842	0.1506	-0.0670	-0.0017	0.0005	-0.0071
1.52	1.2076	0.1522	-0.0347	0.0010	0.0005	-0.0020
1.56	1.1379	0.1434	-0.0175	0.0020	0.0004	0.0017
1.60	1.0777	0.1298	-0.0088	0.0022	0.0003	0.0036
1.64	1.0278	0.1146	-0.0042	0.0021	0.0003	0.0043
1.68	0.9876	0.0995	-0.0017	0.0018	0.0002	0.0045
1.72	0.9565	0.0849	0.0001	0.0015	0.0002	0.0045
1.76	0.9332	0.0712	0.0017	0.0013	0.0001	0.0044
1.80	0.9170	0.0582	0.0033	0.0010	0.0001	0.0043
1.84	0.9070	0.0460	0.0052	0.0009	0.0001	0.0043
1.88	0.9025	0.0344	0.0073	0.0007	0.0001	0.0044
1.92	0.9025	0.0233	0.0096	0.0006	0.0001	0.0044
1.96	0.9064	0.0127	0.0119	0.0005	0.0001	0.0044
2.00	0.9134	0.0027	0.0140	0.0004	0.0000	0.0043
2.04	0.9232	-0.0065	0.0155	0.0003	0.0000	0.0038
2.08	0.9351	-0.0147	0.0162	0.0003	0.0000	0.0031
2.12	0.9489	-0.0215	0.0159	0.0002	0.0000	0.0022
2.16	0.9638	-0.0267	0.0146	0.0002	0.0000	0.0012
2.20	0.9786	-0.0302	0.0126	0.0002	0.0000	0.0001
2.24	0.9921	-0.0317	0.0104	0.0001	0.0000	-0.0009
2.28	1.0034	-0.0316	0.0082	0.0001	0.0000	-0.0017
2.32	1.0122	-0.0298	0.0065	0.0001	0.0000	-0.0022
2.36	1.0188	-0.0268	0.0053	0.0001	0.0000	-0.0025
2.40	1.0234	-0.0229	0.0044	0.0001	0.0000	-0.0025

TABLE XII (cont'd)

2.44	1.0266	-0.0184	0.0035	0.0001	0.0000	-0.0024
2.48	1.0283	-0.0136	0.0026	0.0001	0.0000	-0.0021
2.52	1.0286	-0.0090	0.0013	0.0000	0.0000	-0.0017
2.56	1.0275	-0.0046	-0.0000	0.0000	0.0000	-0.0014
2.60	1.0252	-0.0008	-0.0014	0.0000	0.0000	-0.0010
2.64	1.0221	0.0025	-0.0027	0.0000	0.0000	-0.0007
2.68	1.0184	0.0052	-0.0036	0.0000	0.0000	-0.0005
2.72	1.0145	0.0071	-0.0040	0.0000	0.0000	-0.0002
2.76	1.0105	0.0084	-0.0041	0.0000	0.0000	-0.0001
2.80	1.0066	0.0091	-0.0038	0.0000	0.0000	0.0001
2.84	1.0030	0.0093	-0.0033	0.0000	0.0000	0.0002
2.88	0.9999	0.0090	-0.0026	0.0000	0.0000	0.0003
2.92	0.9972	0.0083	-0.0019	0.0000	0.0000	0.0004
2.96	0.9950	0.0074	-0.0012	0.0000	0.0000	0.0004
3.00	0.9935	0.0063	-0.0005	0.0000	0.0000	0.0005
3.10	0.9919	0.0031	0.0008	0.0000	0.0000	0.0005
3.20	0.9931	0.0003	0.0013	0.0000	0.0000	0.0004
3.30	0.9958	-0.0017	0.0014	0.0000	0.0000	0.0002
3.40	0.9987	-0.0026	0.0010	0.0000	0.0000	0.0001
3.50	1.0010	-0.0026	0.0005	0.0000	0.0000	-0.0001
3.60	1.0023	-0.0020	-0.0000	0.0000	0.0000	-0.0002
3.70	1.0026	-0.0010	-0.0004	0.0000	0.0000	-0.0002
3.80	1.0021	-0.0001	-0.0006	0.0000	0.0000	-0.0001
3.90	1.0013	0.0005	-0.0005	0.0000	0.0000	-0.0001
4.00	1.0005	0.0008	-0.0003	0.0000	0.0000	-0.0000
4.20	0.9994	0.0006	0.0000	0.0	0.0	0.0001
4.40	0.9994	0.0000	0.0002	0.0	0.0	0.0000
4.60	0.9999	-0.0003	0.0001	0.0	0.0	0.0000
4.80	1.0002	-0.0002	0.0000	0.0	0.0	-0.0000
5.00	1.0002	-0.0000	-0.0000	0.0	0.0	-0.0000
5.20	1.0000	0.0001	-0.0000	0.0	0.0	-0.0000
5.40	0.9999	0.0001	0.0000	0.0	0.0	0.0000
5.60	1.0000	0.0000	0.0000	0.0	0.0	0.0000
5.80	1.0000	-0.0000	0.0000	0.0	0.0	0.0000
6.00	1.0001	-0.0000	-0.0000	0.0	0.0	-0.0000

TABLE XIII
PAIR DISTRIBUTION COEFFICIENTS FOR 2 L-J POTENTIAL
FROM PY EQUATION $\rho^*=0.40$ $T^*=1.00$ $R^*=0.53$

R	G000	G200	G220	G221	G222	G400
0.80	0.0000	-0.0000	0.0000	-0.0000	-0.0000	0.0000
0.84	0.0001	-0.0001	0.0001	-0.0000	-0.0001	0.0002
0.88	0.0020	-0.0020	0.0024	-0.0000	-0.0023	0.0054
0.92	0.0191	-0.0190	0.0218	-0.0010	-0.0134	0.0432
0.96	0.0812	-0.0786	0.0848	-0.0068	-0.0311	0.1387
1.00	0.2040	-0.1890	0.1881	-0.0230	-0.0419	0.2255
1.04	0.3736	-0.3249	0.2894	-0.0505	-0.0420	0.1930
1.08	0.5672	-0.4495	0.3404	-0.0839	-0.0358	0.0133
1.12	0.7702	-0.5330	0.3088	-0.1149	-0.0278	-0.2139
1.16	0.9731	-0.5561	0.1866	-0.1349	-0.0203	-0.3184
1.20	1.1598	-0.5175	0.0085	-0.1382	-0.0138	-0.2282
1.24	1.3098	-0.4343	-0.1601	-0.1248	-0.0086	-0.0387
1.28	1.4124	-0.3289	-0.2691	-0.0999	-0.0048	0.1083
1.32	1.4688	-0.2191	-0.3022	-0.0710	-0.0021	0.1436
1.36	1.4864	-0.1172	-0.2706	-0.0441	-0.0005	0.0910
1.40	1.4733	-0.0322	-0.2017	-0.0234	0.0003	0.0253
1.44	1.4373	0.0288	-0.1282	-0.0098	0.0007	-0.0081
1.48	1.3866	0.0639	-0.0714	-0.0023	0.0008	-0.0141
1.52	1.3300	0.0787	-0.0357	0.0014	0.0007	-0.0103
1.56	1.2743	0.0807	-0.0160	0.0028	0.0006	-0.0058
1.60	1.2233	0.0763	-0.0062	0.0032	0.0005	-0.0028
1.64	1.1786	0.0690	-0.0016	0.0030	0.0004	-0.0012
1.68	1.1406	0.0610	0.0003	0.0026	0.0003	-0.0005
1.72	1.1087	0.0532	0.0009	0.0022	0.0003	-0.0001
1.76	1.0824	0.0459	0.0011	0.0019	0.0002	-0.0000
1.80	1.0610	0.0392	0.0012	0.0015	0.0002	0.0000
1.84	1.0439	0.0332	0.0013	0.0013	0.0001	0.0000
1.88	1.0304	0.0277	0.0015	0.0010	0.0001	0.0001
1.92	1.0201	0.0226	0.0019	0.0008	0.0001	0.0001
1.96	1.0125	0.0179	0.0024	0.0007	0.0001	0.0002
2.00	1.0073	0.0135	0.0030	0.0006	0.0001	0.0003
2.04	1.0040	0.0095	0.0036	0.0005	0.0001	0.0003
2.08	1.0024	0.0057	0.0041	0.0004	0.0000	0.0003
2.12	1.0023	0.0023	0.0045	0.0003	0.0000	0.0003
2.16	1.0034	-0.0007	0.0046	0.0003	0.0000	0.0002
2.20	1.0054	-0.0032	0.0044	0.0002	0.0000	0.0000
2.24	1.0079	-0.0052	0.0041	0.0002	0.0000	-0.0001
2.28	1.0105	-0.0067	0.0037	0.0002	0.0000	-0.0002
2.32	1.0130	-0.0076	0.0033	0.0001	0.0000	-0.0002
2.36	1.0151	-0.0080	0.0029	0.0001	0.0000	-0.0003
2.40	1.0170	-0.0079	0.0026	0.0001	0.0000	-0.0003

TABLE XIII (cont'd)

2.44	1.0185	-0.0075	0.0023	0.0001	0.0000	-0.0002
2.48	1.0198	-0.0069	0.0020	0.0001	0.0000	-0.0002
2.52	1.0207	-0.0060	0.0017	0.0001	0.0000	-0.0001
2.56	1.0212	-0.0051	0.0014	0.0001	0.0000	-0.0000
2.60	1.0213	-0.0041	0.0009	0.0000	0.0000	-0.0000
2.64	1.0211	-0.0032	0.0005	0.0000	0.0000	0.0000
2.68	1.0206	-0.0023	0.0001	0.0000	0.0000	0.0000
2.72	1.0198	-0.0015	-0.0003	0.0000	0.0000	0.0001
2.76	1.0188	-0.0008	-0.0005	0.0000	0.0000	0.0000
2.80	1.0178	-0.0002	-0.0007	0.0000	0.0000	0.0000
2.84	1.0166	0.0002	-0.0007	0.0000	0.0000	0.0000
2.88	1.0154	0.0006	-0.0007	0.0000	0.0000	0.0000
2.92	1.0142	0.0008	-0.0007	0.0000	0.0000	0.0000
2.96	1.0130	0.0009	-0.0006	0.0000	0.0000	0.0000
3.00	1.0119	0.0010	-0.0005	0.0000	0.0000	0.0000
3.10	1.0094	0.0009	-0.0002	0.0000	0.0000	0.0000
3.20	1.0076	0.0007	-0.0001	0.0000	0.0000	0.0000
3.30	1.0063	0.0004	0.0000	0.0000	0.0000	0.0000
3.40	1.0054	0.0001	0.0001	0.0000	0.0000	0.0000
3.50	1.0048	-0.0001	0.0001	0.0000	0.0000	-0.0000
3.60	1.0044	-0.0002	0.0001	0.0000	0.0000	-0.0000
3.70	1.0041	-0.0002	0.0000	0.0000	0.0000	-0.0000
3.80	1.0037	-0.0002	0.0000	0.0000	0.0000	-0.0000
3.90	1.0034	-0.0001	-0.0000	0.0000	0.0000	-0.0000
4.00	1.0031	-0.0001	-0.0000	0.0000	0.0000	-0.0000
4.20	1.0024	-0.0000	-0.0000	0.0	0.0	0.0000
4.40	1.0019	0.0000	-0.0000	0.0	0.0	0.0000
4.60	1.0015	-0.0000	-0.0000	0.0	0.0	0.0000
4.80	1.0012	-0.0000	0.0000	0.0	0.0	-0.0000
5.00	1.0010	-0.0000	0.0000	0.0	0.0	0.0000
5.20	1.0008	-0.0000	0.0000	0.0	0.0	-0.0000
5.40	1.0006	-0.0000	-0.0000	0.0	0.0	0.0000
5.60	1.0005	-0.0000	-0.0000	0.0	0.0	0.0000
5.80	1.0004	-0.0000	-0.0000	0.0	0.0	0.0000
6.00	1.0004	-0.0000	0.0000	0.0	0.0	0.0000

TABLE XIV
PAIR DISTRIBUTION COEFFICIENTS FOR 2 L-J POTENTIAL
FROM PY EQUATION $\rho^*=0.60$ $T^*=1.00$ $R^*=0.53$

R	G000	G200	G220	G221	G222	G400
0.80	0.0000	-0.0000	0.0000	-0.0000	-0.0000	0.0000
0.84	0.0001	-0.0001	0.0001	-0.0000	-0.0001	0.0002
0.88	0.0021	-0.0021	0.0026	-0.0000	-0.0025	0.0061
0.92	0.0204	-0.0199	0.0237	-0.0011	-0.0145	0.0479
0.96	0.0857	-0.0819	0.0913	-0.0075	-0.0333	0.1520
1.00	0.2131	-0.1960	0.1999	-0.0252	-0.0444	0.2429
1.04	0.3869	-0.3358	0.3034	-0.0548	-0.0439	0.2016
1.08	0.5829	-0.4633	0.3513	-0.0901	-0.0370	0.0029
1.12	0.7866	-0.5467	0.3112	-0.1222	-0.0285	-0.2414
1.16	0.9889	-0.5650	0.1769	-0.1421	-0.0205	-0.3499
1.20	1.1734	-0.5172	-0.0125	-0.1442	-0.0138	-0.2512
1.24	1.3194	-0.4235	-0.1876	-0.1290	-0.0086	-0.0502
1.28	1.4161	-0.3099	-0.2966	-0.1024	-0.0047	0.1040
1.32	1.4656	-0.1955	-0.3248	-0.0721	-0.0021	0.1417
1.36	1.4760	-0.0922	-0.2863	-0.0445	-0.0005	0.0895
1.40	1.4560	-0.0075	-0.2112	-0.0234	0.0003	0.0246
1.44	1.4135	0.0521	-0.1335	-0.0098	0.0006	-0.0078
1.48	1.3571	0.0854	-0.0746	-0.0022	0.0007	-0.0131
1.52	1.2959	0.0980	-0.0379	0.0014	0.0007	-0.0091
1.56	1.2366	0.0979	-0.0179	0.0028	0.0006	-0.0047
1.60	1.1829	0.0914	-0.0078	0.0031	0.0005	-0.0019
1.64	1.1365	0.0823	-0.0031	0.0029	0.0004	-0.0004
1.68	1.0975	0.0726	-0.0010	0.0026	0.0003	0.0002
1.72	1.0653	0.0631	-0.0001	0.0022	0.0003	0.0005
1.76	1.0393	0.0543	0.0003	0.0018	0.0002	0.0005
1.80	1.0186	0.0462	0.0007	0.0015	0.0002	0.0005
1.84	1.0027	0.0387	0.0012	0.0012	0.0001	0.0005
1.88	0.9909	0.0318	0.0018	0.0010	0.0001	0.0006
1.92	0.9827	0.0254	0.0027	0.0008	0.0001	0.0006
1.96	0.9776	0.0193	0.0036	0.0007	0.0001	0.0007
2.00	0.9750	0.0136	0.0047	0.0006	0.0001	0.0008
2.04	0.9746	0.0082	0.0057	0.0005	0.0001	0.0009
2.08	0.9761	0.0033	0.0065	0.0004	0.0000	0.0008
2.12	0.9793	-0.0012	0.0069	0.0003	0.0000	0.0007
2.16	0.9837	-0.0051	0.0070	0.0003	0.0000	0.0005
2.20	0.9891	-0.0083	0.0067	0.0002	0.0000	0.0002
2.24	0.9948	-0.0107	0.0061	0.0002	0.0000	-0.0000
2.28	1.0002	-0.0123	0.0053	0.0002	0.0000	-0.0002
2.32	1.0051	-0.0130	0.0046	0.0001	0.0000	-0.0004
2.36	1.0093	-0.0131	0.0039	0.0001	0.0000	-0.0005
2.40	1.0127	-0.0126	0.0034	0.0001	0.0000	-0.0005

TABLE XIV (cont'd)

2.44	1.0155	-0.0115	0.0030	0.0001	0.0000	-0.0005
2.48	1.0178	-0.0101	0.0026	0.0001	0.0000	-0.0004
2.52	1.0194	-0.0085	0.0022	0.0001	0.0000	-0.0003
2.56	1.0204	-0.0068	0.0016	0.0001	0.0000	-0.0002
2.60	1.0207	-0.0052	0.0009	0.0000	0.0000	-0.0001
2.64	1.0205	-0.0036	0.0003	0.0000	0.0000	-0.0001
2.68	1.0198	-0.0022	-0.0003	0.0000	0.0000	-0.0000
2.72	1.0187	-0.0009	-0.0008	0.0000	0.0000	0.0000
2.76	1.0174	0.0001	-0.0012	0.0000	0.0000	0.0000
2.80	1.0159	0.0009	-0.0013	0.0000	0.0000	0.0000
2.84	1.0144	0.0015	-0.0014	0.0000	0.0000	0.0000
2.88	1.0128	0.0019	-0.0013	0.0000	0.0000	0.0000
2.92	1.0112	0.0022	-0.0011	0.0000	0.0000	0.0000
2.96	1.0097	0.0023	-0.0010	0.0000	0.0000	0.0000
3.00	1.0084	0.0022	-0.0008	0.0000	0.0000	0.0000
3.10	1.0057	0.0018	-0.0003	0.0000	0.0000	0.0000
3.20	1.0039	0.0011	0.0000	0.0000	0.0000	0.0000
3.30	1.0031	0.0004	0.0002	0.0000	0.0000	0.0000
3.40	1.0029	-0.0001	0.0003	0.0000	0.0000	0.0000
3.50	1.0029	-0.0004	0.0002	0.0000	0.0000	0.0000
3.60	1.0030	-0.0005	0.0002	0.0000	0.0000	-0.0000
3.70	1.0031	-0.0005	0.0001	0.0000	0.0000	-0.0000
3.80	1.0030	-0.0004	-0.0000	0.0000	0.0000	-0.0000
3.90	1.0028	-0.0002	-0.0001	0.0000	0.0000	-0.0000
4.00	1.0026	-0.0001	-0.0001	0.0000	0.0000	-0.0000
4.20	1.0019	0.0000	-0.0000	0.0	0.0	0.0000
4.40	1.0014	0.0000	-0.0000	0.0	0.0	0.0000
4.60	1.0011	-0.0000	0.0000	0.0	0.0	0.0000
4.80	1.0009	-0.0000	0.0000	0.0	0.0	-0.0000
5.00	1.0008	-0.0000	0.0000	0.0	0.0	-0.0000
5.20	1.0006	-0.0000	-0.0000	0.0	0.0	-0.0000
5.40	1.0005	-0.0000	-0.0000	0.0	0.0	-0.0000
5.60	1.0004	-0.0000	-0.0000	0.0	0.0	0.0000
5.80	1.0004	-0.0000	0.0000	0.0	0.0	0.0000
6.00	1.0003	-0.0000	0.0000	0.0	0.0	0.0000

TABLE XV
PAIR DISTRIBUTION COEFFICIENTS FOR 2 L-J POTENTIAL
FROM PY EQUATION $\rho^*=0.80$ $T^*=1.00$ $R^*=0.53$

R	G000	G200	G220	G221	G222	G400
0.80	0.0000	-0.0000	0.0000	-0.0000	-0.0000	0.0000
0.84	0.0001	-0.0001	0.0001	-0.0000	-0.0001	0.0002
0.88	0.0023	-0.0023	0.0030	-0.0001	-0.0028	0.0070
0.92	0.0222	-0.0214	0.0264	-0.0013	-0.0161	0.0543
0.96	0.0924	-0.0873	0.1004	-0.0085	-0.0365	0.1702
1.00	0.2274	-0.2077	0.2170	-0.0282	-0.0481	0.2674
1.04	0.4087	-0.3543	0.3247	-0.0607	-0.0469	0.2148
1.08	0.6105	-0.4867	0.3696	-0.0987	-0.0390	-0.0092
1.12	0.8177	-0.5708	0.3188	-0.1325	-0.0297	-0.2770
1.16	1.0214	-0.5833	0.1685	-0.1523	-0.0211	-0.3912
1.20	1.2050	-0.5238	-0.0367	-0.1529	-0.0141	-0.2808
1.24	1.3472	-0.4168	-0.2212	-0.1354	-0.0086	-0.0638
1.28	1.4373	-0.2922	-0.3312	-0.1064	-0.0047	0.1005
1.32	1.4784	-0.1713	-0.3536	-0.0742	-0.0021	0.1412
1.36	1.4797	-0.0653	-0.3064	-0.0453	-0.0005	0.0890
1.40	1.4505	0.0196	-0.2233	-0.0237	0.0003	0.0243
1.44	1.3996	0.0780	-0.1399	-0.0098	0.0006	-0.0072
1.48	1.3358	0.1094	-0.0779	-0.0022	0.0007	-0.0119
1.52	1.2684	0.1195	-0.0398	0.0014	0.0006	-0.0076
1.56	1.2043	0.1168	-0.0191	0.0027	0.0006	-0.0032
1.60	1.1471	0.1078	-0.0088	0.0030	0.0005	-0.0005
1.64	1.0983	0.0964	-0.0039	0.0028	0.0004	0.0008
1.68	1.0579	0.0845	-0.0017	0.0025	0.0003	0.0013
1.72	1.0252	0.0731	-0.0005	0.0021	0.0002	0.0014
1.76	0.9994	0.0624	0.0002	0.0017	0.0002	0.0014
1.80	0.9797	0.0526	0.0010	0.0014	0.0002	0.0014
1.84	0.9652	0.0435	0.0019	0.0012	0.0001	0.0014
1.88	0.9553	0.0350	0.0029	0.0010	0.0001	0.0014
1.92	0.9494	0.0269	0.0042	0.0008	0.0001	0.0015
1.96	0.9470	0.0193	0.0057	0.0007	0.0001	0.0017
2.00	0.9474	0.0121	0.0072	0.0005	0.0001	0.0017
2.04	0.9502	0.0054	0.0085	0.0004	0.0001	0.0017
2.08	0.9550	-0.0009	0.0095	0.0004	0.0000	0.0016
2.12	0.9616	-0.0064	0.0100	0.0003	0.0000	0.0013
2.16	0.9695	-0.0111	0.0099	0.0003	0.0000	0.0009
2.20	0.9783	-0.0148	0.0092	0.0002	0.0000	0.0004
2.24	0.9872	-0.0174	0.0081	0.0002	0.0000	-0.0000
2.28	0.9954	-0.0189	0.0069	0.0002	0.0000	-0.0004
2.32	1.0024	-0.0192	0.0057	0.0001	0.0000	-0.0007
2.36	1.0081	-0.0186	0.0048	0.0001	0.0000	-0.0009
2.40	1.0126	-0.0172	0.0041	0.0001	0.0000	-0.0010

TABLE XV (cont'd)

2.44	1.0162	-0.0152	0.0036	0.0001	0.0000	-0.0010
2.48	1.0188	-0.0128	0.0030	0.0001	0.0000	-0.0008
2.52	1.0206	-0.0103	0.0024	0.0001	0.0000	-0.0007
2.56	1.0215	-0.0076	0.0016	0.0001	0.0000	-0.0005
2.60	1.0215	-0.0051	0.0007	0.0000	0.0000	-0.0004
2.64	1.0207	-0.0029	-0.0002	0.0000	0.0000	-0.0003
2.68	1.0193	-0.0009	-0.0011	0.0000	0.0000	-0.0002
2.72	1.0176	0.0008	-0.0017	0.0000	0.0000	-0.0001
2.76	1.0155	0.0021	-0.0021	0.0000	0.0000	-0.0000
2.80	1.0133	0.0031	-0.0022	0.0000	0.0000	0.0000
2.84	1.0111	0.0037	-0.0021	0.0000	0.0000	0.0000
2.88	1.0090	0.0041	-0.0019	0.0000	0.0000	0.0001
2.92	1.0069	0.0042	-0.0016	0.0000	0.0000	0.0001
2.96	1.0051	0.0041	-0.0013	0.0000	0.0000	0.0001
3.00	1.0035	0.0038	-0.0009	0.0000	0.0000	0.0001
3.10	1.0007	0.0027	-0.0002	0.0000	0.0000	0.0001
3.20	0.9995	0.0013	0.0003	0.0000	0.0000	0.0001
3.30	0.9995	0.0002	0.0005	0.0000	0.0000	0.0001
3.40	1.0002	-0.0006	0.0005	0.0000	0.0000	0.0000
3.50	1.0011	-0.0010	0.0004	0.0000	0.0000	0.0000
3.60	1.0018	-0.0010	0.0002	0.0000	0.0000	-0.0000
3.70	1.0022	-0.0008	0.0000	0.0000	0.0000	-0.0000
3.80	1.0023	-0.0005	-0.0001	0.0000	0.0000	-0.0000
3.90	1.0021	-0.0002	-0.0002	0.0000	0.0000	-0.0000
4.00	1.0018	0.0001	-0.0001	0.0000	0.0000	-0.0000
4.20	1.0010	0.0002	-0.0001	0.0	0.0	0.0000
4.40	1.0006	0.0001	0.0000	0.0	0.0	0.0000
4.60	1.0005	-0.0000	0.0000	0.0	0.0	0.0000
4.80	1.0005	-0.0001	0.0000	0.0	0.0	-0.0000
5.00	1.0005	-0.0000	-0.0000	0.0	0.0	-0.0000
5.20	1.0004	-0.0000	-0.0000	0.0	0.0	-0.0000
5.40	1.0003	0.0000	-0.0000	0.0	0.0	-0.0000
5.60	1.0002	0.0000	0.0000	0.0	0.0	0.0000
5.80	1.0002	-0.0000	0.0000	0.0	0.0	0.0000
6.00	1.0002	-0.0000	0.0000	0.0	0.0	0.0000

TABLE XVI
PAIR DISTRIBUTION COEFFICIENTS FOR 2 L-J POTENTIAL
FROM PY EQUATION $\rho^*=1.00$ $T^*=1.00$ $R^*=0.53$

R	G000	G200	G220	G221	G222	G400
0.80	0.0000	-0.0000	0.0000	-0.0000	-0.0000	0.0000
0.84	0.0001	-0.0001	0.0001	-0.0000	-0.0001	0.0003
0.88	0.0026	-0.0025	0.0034	-0.0001	-0.0033	0.0082
0.92	0.0249	-0.0236	0.0302	-0.0015	-0.0184	0.0634
0.96	0.1022	-0.0954	0.1132	-0.0099	-0.0411	0.1957
1.00	0.2486	-0.2255	0.2414	-0.0324	-0.0534	0.3019
1.04	0.4419	-0.3824	0.3558	-0.0689	-0.0514	0.2342
1.08	0.6531	-0.5225	0.3974	-0.1108	-0.0421	-0.0247
1.12	0.8667	-0.6082	0.3326	-0.1469	-0.0315	-0.3250
1.16	1.0739	-0.6132	0.1602	-0.1669	-0.0221	-0.4472
1.20	1.2577	-0.5382	-0.0670	-0.1654	-0.0145	-0.3204
1.24	1.3957	-0.4132	-0.2649	-0.1446	-0.0088	-0.0809
1.28	1.4776	-0.2738	-0.3765	-0.1123	-0.0047	0.0976
1.32	1.5079	-0.1438	-0.3914	-0.0774	-0.0020	0.1424
1.36	1.4971	-0.0338	-0.3327	-0.0468	-0.0005	0.0896
1.40	1.4559	0.0518	-0.2387	-0.0241	0.0003	0.0246
1.44	1.3938	0.1092	-0.1477	-0.0099	0.0006	-0.0062
1.48	1.3203	0.1381	-0.0813	-0.0022	0.0007	-0.0100
1.52	1.2449	0.1451	-0.0412	0.0014	0.0006	-0.0054
1.56	1.1746	0.1390	-0.0197	0.0027	0.0005	-0.0009
1.60	1.1130	0.1267	-0.0090	0.0030	0.0004	0.0016
1.64	1.0614	0.1122	-0.0038	0.0028	0.0004	0.0027
1.68	1.0194	0.0976	-0.0013	0.0024	0.0003	0.0031
1.72	0.9863	0.0836	0.0001	0.0020	0.0002	0.0031
1.76	0.9610	0.0706	0.0011	0.0017	0.0002	0.0030
1.80	0.9425	0.0585	0.0022	0.0014	0.0002	0.0029
1.84	0.9300	0.0473	0.0035	0.0011	0.0001	0.0028
1.88	0.9227	0.0368	0.0051	0.0009	0.0001	0.0029
1.92	0.9199	0.0268	0.0069	0.0008	0.0001	0.0030
1.96	0.9208	0.0174	0.0089	0.0006	0.0001	0.0031
2.00	0.9249	0.0084	0.0108	0.0005	0.0001	0.0032
2.04	0.9314	0.0001	0.0125	0.0004	0.0001	0.0031
2.08	0.9401	-0.0076	0.0136	0.0004	0.0000	0.0027
2.12	0.9506	-0.0142	0.0140	0.0003	0.0000	0.0022
2.16	0.9626	-0.0157	0.0134	0.0003	0.0000	0.0014
2.20	0.9751	-0.0237	0.0120	0.0002	0.0000	0.0006
2.24	0.9874	-0.0262	0.0102	0.0002	0.0000	-0.0002
2.28	0.9982	-0.0271	0.0082	0.0002	0.0000	-0.0009
2.32	1.0070	-0.0266	0.0065	0.0001	0.0000	-0.0014
2.36	1.0137	-0.0248	0.0052	0.0001	0.0000	-0.0018
2.40	1.0185	-0.0220	0.0043	0.0001	0.0000	-0.0019

TABLE XVI (cont'd)

2.44	1.0220	-0.0186	0.0037	0.0001	0.0000	-0.0018
2.48	1.0243	-0.0148	0.0030	0.0001	0.0000	-0.0016
2.52	1.0255	-0.0109	0.0022	0.0001	0.0000	-0.0014
2.56	1.0255	-0.0071	0.0012	0.0001	0.0000	-0.0011
2.60	1.0244	-0.0036	0.0000	0.0000	0.0000	-0.0008
2.64	1.0225	-0.0006	-0.0012	0.0000	0.0000	-0.0006
2.68	1.0198	0.0020	-0.0022	0.0000	0.0000	-0.0004
2.72	1.0168	0.0040	-0.0029	0.0000	0.0000	-0.0002
2.76	1.0137	0.0055	-0.0032	0.0000	0.0000	-0.0001
2.80	1.0104	0.0065	-0.0033	0.0000	0.0000	0.0000
2.84	1.0074	0.0070	-0.0030	0.0000	0.0000	0.0001
2.88	1.0045	0.0071	-0.0026	0.0000	0.0000	0.0002
2.92	1.0019	0.0068	-0.0021	0.0000	0.0000	0.0002
2.96	0.9998	0.0063	-0.0015	0.0000	0.0000	0.0002
3.00	0.9980	0.0056	-0.0009	0.0000	0.0000	0.0003
3.10	0.9956	0.0034	0.0002	0.0000	0.0000	0.0003
3.20	0.9955	0.0011	0.0008	0.0000	0.0000	0.0003
3.30	0.9969	-0.0007	0.0010	0.0000	0.0000	0.0002
3.40	0.9988	-0.0017	0.0009	0.0000	0.0000	0.0001
3.50	1.0006	-0.0020	0.0005	0.0000	0.0000	-0.0000
3.60	1.0018	-0.0017	0.0001	0.0000	0.0000	-0.0001
3.70	1.0023	-0.0011	-0.0002	0.0000	0.0000	-0.0001
3.80	1.0022	-0.0004	-0.0003	0.0000	0.0000	-0.0001
3.90	1.0017	0.0001	-0.0004	0.0000	0.0000	-0.0001
4.00	1.0011	0.0004	-0.0003	0.0000	0.0000	-0.0000
4.20	1.0001	0.0005	-0.0001	0.0	0.0	0.0000
4.40	0.9999	0.0001	0.0001	0.0	0.0	0.0000
4.60	1.0001	-0.0001	0.0001	0.0	0.0	0.0000
4.80	1.0003	-0.0002	0.0000	0.0	0.0	-0.0000
5.00	1.0003	-0.0000	-0.0000	0.0	0.0	-0.0000
5.20	1.0002	0.0000	-0.0000	0.0	0.0	-0.0000
5.40	1.0001	0.0000	-0.0000	0.0	0.0	0.0000
5.60	1.0001	0.0000	0.0000	0.0	0.0	0.0000
5.80	1.0001	-0.0000	0.0000	0.0	0.0	0.0000
6.00	1.0001	-0.0000	0.0000	0.0	0.0	-0.0000

TABLE XVII
PAIR DISTRIBUTION COEFFICIENTS FOR 2 L-J POTENTIAL
FROM PY EQUATION $RHC^*=1.20$ $T^*=1.00$ $R^*=0.53$

R	G000	G200	G220	G221	G222	G400
0.80	0.0000	-0.0000	0.0000	-0.0000	-0.0000	0.0000
0.84	0.0001	-0.0001	0.0001	-0.0000	-0.0002	0.0003
0.88	0.0031	-0.0029	0.0041	-0.0001	-0.0039	0.0100
0.92	0.0286	-0.0268	0.0354	-0.0018	-0.0216	0.0759
0.96	0.1160	-0.1071	0.1310	-0.0118	-0.0476	0.2312
1.00	0.2786	-0.2508	0.2753	-0.0383	-0.0608	0.3501
1.04	0.4888	-0.4224	0.3993	-0.0804	-0.0576	0.2615
1.08	0.7134	-0.5731	0.4368	-0.1275	-0.0464	-0.0456
1.12	0.9357	-0.6610	0.3527	-0.1668	-0.0341	-0.3901
1.16	1.1478	-0.6558	0.1502	-0.1867	-0.0235	-0.5228
1.20	1.3319	-0.5598	-0.1070	-0.1824	-0.0152	-0.3732
1.24	1.4642	-0.4107	-0.3226	-0.1572	-0.0090	-0.1029
1.28	1.5351	-0.2517	-0.4358	-0.1202	-0.0047	0.0948
1.32	1.5506	-0.1096	-0.4403	-0.0816	-0.0020	0.1451
1.36	1.5237	0.0056	-0.3660	-0.0487	-0.0005	0.0914
1.40	1.4668	0.0922	-0.2574	-0.0248	0.0003	0.0258
1.44	1.3903	0.1479	-0.1562	-0.0101	0.0006	-0.0040
1.48	1.3045	0.1735	-0.0841	-0.0022	0.0006	-0.0068
1.52	1.2193	0.1762	-0.0413	0.0013	0.0006	-0.0017
1.56	1.1418	0.1655	-0.0187	0.0026	0.0005	0.0027
1.60	1.0753	0.1488	-0.0076	0.0029	0.0004	0.0050
1.64	1.0207	0.1303	-0.0023	0.0027	0.0003	0.0058
1.68	0.9776	0.1119	0.0004	0.0023	0.0003	0.0059
1.72	0.9446	0.0946	0.0020	0.0020	0.0002	0.0057
1.76	0.9207	0.0784	0.0033	0.0016	0.0002	0.0054
1.80	0.9046	0.0635	0.0048	0.0013	0.0001	0.0053
1.84	0.8952	0.0496	0.0066	0.0011	0.0001	0.0052
1.88	0.8917	0.0365	0.0087	0.0009	0.0001	0.0052
1.92	0.8932	0.0241	0.0110	0.0007	0.0001	0.0053
1.96	0.8988	0.0124	0.0136	0.0006	0.0001	0.0054
2.00	0.9076	0.0014	0.0160	0.0005	0.0001	0.0053
2.04	0.9189	-0.0089	0.0179	0.0004	0.0001	0.0050
2.08	0.9323	-0.0181	0.0190	0.0004	0.0000	0.0043
2.12	0.9475	-0.0258	0.0189	0.0003	0.0000	0.0032
2.16	0.9640	-0.0318	0.0174	0.0003	0.0000	0.0019
2.20	0.9808	-0.0357	0.0150	0.0002	0.0000	0.0005
2.24	0.9965	-0.0375	0.0120	0.0002	0.0000	-0.0008
2.28	1.0097	-0.0372	0.0090	0.0002	0.0000	-0.0019
2.32	1.0197	-0.0350	0.0065	0.0001	0.0000	-0.0028
2.36	1.0264	-0.0313	0.0049	0.0001	0.0000	-0.0033
2.40	1.0306	-0.0264	0.0038	0.0001	0.0000	-0.0035

TABLE XVII (cont'd)

2.44	1.0329	-0.0210	0.0032	0.0001	0.0000	-0.0033
2.48	1.0337	-0.0152	0.0025	0.0001	0.0000	-0.0030
2.52	1.0331	-0.0096	0.0016	0.0001	0.0000	-0.0025
2.56	1.0313	-0.0044	0.0003	0.0001	0.0000	-0.0020
2.60	1.0282	0.0002	-0.0011	0.0000	0.0000	-0.0015
2.64	1.0243	0.0041	-0.0026	0.0000	0.0000	-0.0010
2.68	1.0197	0.0072	-0.0037	0.0000	0.0000	-0.0006
2.72	1.0150	0.0094	-0.0045	0.0000	0.0000	-0.0003
2.76	1.0103	0.0108	-0.0047	0.0000	0.0000	-0.0000
2.80	1.0058	0.0114	-0.0045	0.0000	0.0000	0.0002
2.84	1.0018	0.0114	-0.0039	0.0000	0.0000	0.0003
2.88	0.9983	0.0109	-0.0031	0.0000	0.0000	0.0005
2.92	0.9954	0.0100	-0.0022	0.0000	0.0000	0.0006
2.96	0.9932	0.0087	-0.0013	0.0000	0.0000	0.0006
3.00	0.9916	0.0072	-0.0004	0.0000	0.0000	0.0007
3.10	0.9906	0.0032	0.0011	0.0000	0.0000	0.0007
3.20	0.9925	-0.0002	0.0018	0.0000	0.0000	0.0005
3.30	0.9960	-0.0025	0.0017	0.0000	0.0000	0.0003
3.40	0.9995	-0.0035	0.0012	0.0000	0.0000	0.0001
3.50	1.0021	-0.0033	0.0005	0.0000	0.0000	-0.0001
3.60	1.0033	-0.0023	-0.0002	0.0000	0.0000	-0.0003
3.70	1.0033	-0.0011	-0.0006	0.0000	0.0000	-0.0003
3.80	1.0025	0.0001	-0.0008	0.0000	0.0000	-0.0002
3.90	1.0014	0.0008	-0.0007	0.0000	0.0000	-0.0001
4.00	1.0003	0.0011	-0.0004	0.0000	0.0000	-0.0000
4.20	0.9992	0.0007	0.0001	0.0	0.0	0.0001
4.40	0.9994	-0.0001	0.0002	0.0	0.0	0.0001
4.60	1.0001	-0.0004	0.0001	0.0	0.0	0.0000
4.80	1.0004	-0.0002	-0.0000	0.0	0.0	-0.0000
5.00	1.0002	0.0000	-0.0001	0.0	0.0	-0.0000
5.20	1.0000	0.0001	-0.0000	0.0	0.0	-0.0000
5.40	0.9999	0.0001	0.0000	0.0	0.0	0.0000
5.60	1.0000	-0.0000	0.0000	0.0	0.0	0.0000
5.80	1.0001	-0.0000	0.0000	0.0	0.0	0.0000
6.00	1.0001	-0.0000	-0.0000	0.0	0.0	-0.0000

TABLE XVIII
PAIR DISTRIBUTION COEFFICIENTS FOR 2 L-J POTENTIAL
FROM PY EQUATION $\rho^*=0.40$ $T^*=0.75$ $R^*=0.53$

R	G000	G200	G220	G221	G222	G400
0.80	0.0000	-0.0000	0.0000	-0.0000	-0.0000	0.0000
0.84	0.0000	-0.0000	0.0000	-0.0000	-0.0000	0.0000
0.88	0.0008	-0.0008	0.0010	-0.0000	-0.0011	0.0023
0.92	0.0120	-0.0118	0.0145	-0.0005	-0.0108	0.0314
0.96	0.0691	-0.0669	0.0770	-0.0050	-0.0344	0.1417
1.00	0.2050	-0.1924	0.2047	-0.0212	-0.0544	0.2939
1.04	0.4080	-0.3649	0.3490	-0.0533	-0.0578	0.3213
1.08	0.6421	-0.5333	0.4399	-0.0957	-0.0496	0.1332
1.12	0.8825	-0.6538	0.4288	-0.1374	-0.0381	-0.1883
1.16	1.1184	-0.6976	0.2980	-0.1674	-0.0273	-0.4193
1.20	1.3370	-0.6567	0.0753	-0.1769	-0.0184	-0.3892
1.24	1.5144	-0.5507	-0.1588	-0.1643	-0.0115	-0.1577
1.28	1.6327	-0.4132	-0.3259	-0.1349	-0.0063	0.0776
1.32	1.6913	-0.2714	-0.3930	-0.0981	-0.0028	0.1827
1.36	1.7004	-0.1415	-0.3690	-0.0625	-0.0007	0.1488
1.40	1.6722	-0.0330	-0.2867	-0.0339	0.0005	0.0610
1.44	1.6170	0.0470	-0.1878	-0.0145	0.0010	0.0011
1.48	1.5446	0.0945	-0.1058	-0.0033	0.0011	-0.0165
1.52	1.4655	0.1143	-0.0524	0.0021	0.0010	-0.0141
1.56	1.3882	0.1159	-0.0227	0.0041	0.0009	-0.0082
1.60	1.3183	0.1081	-0.0080	0.0046	0.0007	-0.0038
1.64	1.2578	0.0965	-0.0014	0.0043	0.0006	-0.0015
1.68	1.2070	0.0841	0.0011	0.0038	0.0005	-0.0004
1.72	1.1652	0.0722	0.0019	0.0032	0.0004	-0.0000
1.76	1.1312	0.0614	0.0020	0.0026	0.0003	0.0001
1.80	1.1040	0.0516	0.0020	0.0021	0.0002	0.0001
1.84	1.0826	0.0429	0.0020	0.0018	0.0002	0.0001
1.88	1.0662	0.0351	0.0023	0.0014	0.0002	0.0001
1.92	1.0540	0.0279	0.0029	0.0012	0.0001	0.0002
1.96	1.0454	0.0214	0.0036	0.0010	0.0001	0.0003
2.00	1.0399	0.0153	0.0045	0.0008	0.0001	0.0005
2.04	1.0368	0.0096	0.0055	0.0007	0.0001	0.0006
2.08	1.0357	0.0044	0.0063	0.0005	0.0001	0.0007
2.12	1.0364	-0.0003	0.0069	0.0004	0.0001	0.0006
2.16	1.0385	-0.0044	0.0071	0.0004	0.0000	0.0005
2.20	1.0417	-0.0079	0.0069	0.0003	0.0000	0.0003
2.24	1.0455	-0.0105	0.0063	0.0003	0.0000	0.0001
2.28	1.0494	-0.0123	0.0055	0.0002	0.0000	-0.0002
2.32	1.0528	-0.0133	0.0046	0.0002	0.0000	-0.0003
2.36	1.0555	-0.0135	0.0038	0.0002	0.0000	-0.0004
2.40	1.0573	-0.0131	0.0033	0.0001	0.0000	-0.0005

TABLE XVIII (cont'd)

2.44	1.0583	-0.0121	0.0028	0.0001	0.0000	-0.0004
2.48	1.0589	-0.0108	0.0025	0.0001	0.0000	-0.0004
2.52	1.0589	-0.0092	0.0022	0.0001	0.0000	-0.0003
2.56	1.0584	-0.0075	0.0018	0.0001	0.0000	-0.0002
2.60	1.0574	-0.0058	0.0012	0.0001	0.0000	-0.0001
2.64	1.0558	-0.0042	0.0006	0.0001	0.0000	-0.0000
2.68	1.0539	-0.0028	0.0000	0.0000	0.0000	0.0000
2.72	1.0516	-0.0015	-0.0005	0.0000	0.0000	0.0001
2.76	1.0491	-0.0004	-0.0009	0.0000	0.0000	0.0001
2.80	1.0465	0.0004	-0.0011	0.0000	0.0000	0.0001
2.84	1.0438	0.0010	-0.0012	0.0000	0.0000	0.0001
2.88	1.0412	0.0015	-0.0012	0.0000	0.0000	0.0000
2.92	1.0387	0.0017	-0.0011	0.0000	0.0000	0.0000
2.96	1.0363	0.0019	-0.0009	0.0000	0.0000	0.0000
3.00	1.0341	0.0019	-0.0008	0.0000	0.0000	0.0000
3.10	1.0292	0.0015	-0.0003	0.0000	0.0000	0.0000
3.20	1.0256	0.0009	-0.0000	0.0000	0.0000	0.0000
3.30	1.0229	0.0003	0.0002	0.0000	0.0000	0.0000
3.40	1.0210	-0.0001	0.0002	0.0000	0.0000	0.0000
3.50	1.0195	-0.0004	0.0002	0.0000	0.0000	-0.0000
3.60	1.0182	-0.0005	0.0001	0.0000	0.0000	-0.0000
3.70	1.0169	-0.0005	0.0001	0.0000	0.0000	-0.0000
3.80	1.0157	-0.0004	0.0000	0.0000	0.0000	-0.0000
3.90	1.0145	-0.0003	-0.0000	0.0000	0.0000	-0.0000
4.00	1.0133	-0.0001	-0.0000	0.0000	0.0000	-0.0000
4.20	1.0110	-0.0000	-0.0000	0.0	0.0	0.0000
4.40	1.0092	-0.0000	-0.0000	0.0	0.0	0.0000
4.60	1.0078	-0.0000	0.0000	0.0	0.0	0.0000
4.80	1.0066	-0.0001	0.0000	0.0	0.0	-0.0000
5.00	1.0056	-0.0001	0.0000	0.0	0.0	-0.0000
5.20	1.0048	-0.0000	-0.0000	0.0	0.0	-0.0000
5.40	1.0041	-0.0000	-0.0000	0.0	0.0	-0.0000
5.60	1.0035	-0.0000	-0.0000	0.0	0.0	0.0000
5.80	1.0030	-0.0000	0.0000	0.0	0.0	0.0000
6.00	1.0026	-0.0000	0.0000	0.0	0.0	0.0000

TABLE XIX
PAIR DISTRIBUTION COEFFICIENTS FOR 2 L-J POTENTIAL
FROM PY EQUATION $\rho\sigma^*=0.60$ $T^*=0.75$ $R^*=0.53$

R	G000	G200	G220	G221	G222	G400
0.80	0.0000	-0.0000	0.0000	-0.0000	-0.0000	0.0000
0.84	0.0000	-0.0000	0.0000	-0.0000	-0.0000	0.0000
0.88	0.0008	-0.0008	0.0010	-0.0000	-0.0011	0.0026
0.92	0.0124	-0.0120	0.0154	-0.0005	-0.0114	0.0343
0.96	0.0707	-0.0672	0.0808	-0.0054	-0.0360	0.1523
1.00	0.2074	-0.1924	0.2120	-0.0228	-0.0561	0.3108
1.04	0.4090	-0.3640	0.3564	-0.0567	-0.0588	0.3312
1.08	0.6385	-0.5312	0.4421	-0.1006	-0.0499	0.1240
1.12	0.8718	-0.6496	0.4216	-0.1430	-0.0379	-0.2164
1.16	1.0956	-0.6884	0.2793	-0.1723	-0.0268	-0.4538
1.20	1.3098	-0.6382	0.0468	-0.1803	-0.0179	-0.4169
1.24	1.4785	-0.5218	-0.1916	-0.1657	-0.0110	-0.1749
1.28	1.5882	-0.3767	-0.3559	-0.1348	-0.0060	0.0669
1.32	1.6386	-0.2323	-0.4155	-0.0972	-0.0027	0.1748
1.36	1.6407	-0.1043	-0.3827	-0.0614	-0.0006	0.1434
1.40	1.6068	0.0000	-0.2932	-0.0331	0.0005	0.0588
1.44	1.5474	0.0755	-0.1903	-0.0140	0.0009	0.0018
1.48	1.4722	0.1189	-0.1068	-0.0032	0.0010	-0.0144
1.52	1.3915	0.1352	-0.0531	0.0020	0.0009	-0.0118
1.56	1.3139	0.1337	-0.0236	0.0040	0.0008	-0.0061
1.60	1.2445	0.1233	-0.0090	0.0044	0.0007	-0.0021
1.64	1.1852	0.1094	-0.0025	0.0041	0.0005	-0.0001
1.68	1.1362	0.0950	0.0001	0.0036	0.0004	0.0007
1.72	1.0965	0.0814	0.0011	0.0030	0.0004	0.0010
1.76	1.0651	0.0689	0.0015	0.0025	0.0003	0.0010
1.80	1.0409	0.0575	0.0018	0.0020	0.0002	0.0009
1.84	1.0227	0.0473	0.0023	0.0017	0.0002	0.0009
1.88	1.0098	0.0380	0.0031	0.0014	0.0002	0.0009
1.92	1.0013	0.0294	0.0041	0.0011	0.0001	0.0010
1.96	0.9967	0.0214	0.0054	0.0009	0.0001	0.0012
2.00	0.9952	0.0139	0.0068	0.0008	0.0001	0.0014
2.04	0.9963	0.0068	0.0082	0.0006	0.0001	0.0015
2.08	0.9995	0.0003	0.0094	0.0005	0.0001	0.0015
2.12	1.0043	-0.0055	0.0102	0.0004	0.0000	0.0013
2.16	1.0107	-0.0106	0.0103	0.0004	0.0000	0.0010
2.20	1.0181	-0.0147	0.0097	0.0003	0.0000	0.0006
2.24	1.0260	-0.0176	0.0087	0.0003	0.0000	0.0002
2.28	1.0336	-0.0194	0.0073	0.0002	0.0000	-0.0003
2.32	1.0400	-0.0201	0.0059	0.0002	0.0000	-0.0006
2.36	1.0450	-0.0197	0.0047	0.0002	0.0000	-0.0008
2.40	1.0486	-0.0185	0.0039	0.0001	0.0000	-0.0009

TABLE XIX (cont'd)

2.44	1.0509	-0.0165	0.0034	0.0001	0.0000	-0.0009
2.48	1.0524	-0.0141	0.0030	0.0001	0.0000	-0.0008
2.52	1.0531	-0.0115	0.0025	0.0001	0.0000	-0.0007
2.56	1.0530	-0.0088	0.0020	0.0001	0.0000	-0.0005
2.60	1.0521	-0.0062	0.0012	0.0001	0.0000	-0.0004
2.64	1.0505	-0.0039	0.0004	0.0001	0.0000	-0.0002
2.68	1.0483	-0.0018	-0.0005	0.0000	0.0000	-0.0001
2.72	1.0457	-0.0000	-0.0012	0.0000	0.0000	-0.0000
2.76	1.0428	0.0014	-0.0017	0.0000	0.0000	0.0000
2.80	1.0399	0.0024	-0.0020	0.0000	0.0000	0.0000
2.84	1.0369	0.0032	-0.0021	0.0000	0.0000	0.0001
2.88	1.0340	0.0036	-0.0019	0.0000	0.0000	0.0001
2.92	1.0313	0.0038	-0.0017	0.0000	0.0000	0.0001
2.96	1.0287	0.0037	-0.0014	0.0000	0.0000	0.0001
3.00	1.0264	0.0035	-0.0010	0.0000	0.0000	0.0001
3.10	1.0220	0.0025	-0.0003	0.0000	0.0000	0.0001
3.20	1.0192	0.0012	0.0002	0.0000	0.0000	0.0001
3.30	1.0177	0.0001	0.0005	0.0000	0.0000	0.0001
3.40	1.0171	-0.0006	0.0005	0.0000	0.0000	0.0000
3.50	1.0167	-0.0010	0.0004	0.0000	0.0000	0.0000
3.60	1.0163	-0.0011	0.0002	0.0000	0.0000	-0.0000
3.70	1.0156	-0.0009	0.0000	0.0000	0.0000	-0.0000
3.80	1.0148	-0.0006	-0.0001	0.0000	0.0000	-0.0000
3.90	1.0138	-0.0003	-0.0001	0.0000	0.0000	-0.0000
4.00	1.0127	-0.0001	-0.0001	0.0000	0.0000	-0.0000
4.20	1.0106	0.0001	-0.0001	0.0	0.0	0.0000
4.40	1.0090	0.0000	0.0000	0.0	0.0	0.0000
4.60	1.0078	-0.0001	0.0000	0.0	0.0	0.0000
4.80	1.0069	-0.0001	0.0000	0.0	0.0	-0.0000
5.00	1.0060	-0.0001	0.0000	0.0	0.0	-0.0000
5.20	1.0052	-0.0000	-0.0000	0.0	0.0	-0.0000
5.40	1.0046	-0.0000	-0.0000	0.0	0.0	-0.0000
5.60	1.0040	-0.0000	-0.0000	0.0	0.0	0.0000
5.80	1.0035	-0.0000	0.0000	0.0	0.0	0.0000
6.00	1.0031	-0.0000	0.0000	0.0	0.0	0.0000

TABLE XX
PAIR DISTRIBUTION COEFFICIENTS FOR 2 L-J POTENTIAL
FROM PY EQUATION $\rho^*=0.80$ $T^*=0.75$ $R^*=0.53$

R	G000	G200	G220	G221	G222	G400
0.80	0.0000	-0.0000	0.0000	-0.0000	-0.0000	0.0000
0.84	0.0000	-0.0000	0.0000	-0.0000	-0.0000	0.0000
0.88	0.0008	-0.0008	0.0011	-0.0000	-0.0012	0.0029
0.92	0.0131	-0.0124	0.0166	-0.0006	-0.0123	0.0378
0.96	0.0736	-0.0689	0.0860	-0.0060	-0.0383	0.1657
1.00	0.2136	-0.1960	0.2228	-0.0248	-0.0589	0.3330
1.04	0.4168	-0.3694	0.3695	-0.0610	-0.0609	0.3464
1.08	0.6448	-0.5374	0.4512	-0.1071	-0.0510	0.1166
1.12	0.8736	-0.6548	0.4207	-0.1505	-0.0382	-0.2474
1.16	1.0950	-0.6881	0.2646	-0.1794	-0.0267	-0.4937
1.20	1.2979	-0.6275	0.0192	-0.1856	-0.0176	-0.4488
1.24	1.4582	-0.4989	-0.2257	-0.1688	-0.0107	-0.1934
1.28	1.5585	-0.3444	-0.3882	-0.1359	-0.0058	0.0573
1.32	1.5996	-0.1961	-0.4401	-0.0970	-0.0025	0.1688
1.36	1.5930	-0.0692	-0.3977	-0.0608	-0.0006	0.1393
1.40	1.5519	0.0317	-0.3002	-0.0324	0.0004	0.0574
1.44	1.4868	0.1029	-0.1925	-0.0137	0.0008	0.0029
1.48	1.4075	0.1425	-0.1070	-0.0031	0.0009	-0.0120
1.52	1.3242	0.1551	-0.0528	0.0019	0.0009	-0.0091
1.56	1.2453	0.1504	-0.0233	0.0038	0.0007	-0.0036
1.60	1.1758	0.1372	-0.0089	0.0042	0.0006	0.0000
1.64	1.1172	0.1209	-0.0025	0.0039	0.0005	0.0017
1.68	1.0696	0.1045	0.0002	0.0034	0.0004	0.0023
1.72	1.0319	0.0889	0.0013	0.0028	0.0003	0.0024
1.76	1.0029	0.0747	0.0020	0.0023	0.0003	0.0022
1.80	0.9814	0.0618	0.0026	0.0019	0.0002	0.0021
1.84	0.9663	0.0500	0.0035	0.0016	0.0002	0.0020
1.88	0.9568	0.0392	0.0046	0.0013	0.0001	0.0021
1.92	0.9519	0.0292	0.0061	0.0011	0.0001	0.0022
1.96	0.9510	0.0198	0.0078	0.0009	0.0001	0.0024
2.00	0.9534	0.0110	0.0097	0.0007	0.0001	0.0026
2.04	0.9583	0.0027	0.0115	0.0006	0.0001	0.0027
2.08	0.9653	-0.0050	0.0129	0.0005	0.0001	0.0026
2.12	0.9739	-0.0118	0.0136	0.0004	0.0000	0.0022
2.16	0.9840	-0.0176	0.0135	0.0004	0.0000	0.0017
2.20	0.9952	-0.0220	0.0124	0.0003	0.0000	0.0009
2.24	1.0066	-0.0250	0.0107	0.0003	0.0000	0.0002
2.28	1.0171	-0.0265	0.0086	0.0002	0.0000	-0.0005
2.32	1.0259	-0.0265	0.0067	0.0002	0.0000	-0.0011
2.36	1.0324	-0.0252	0.0051	0.0002	0.0000	-0.0015
2.40	1.0368	-0.0228	0.0040	0.0001	0.0000	-0.0017

TABLE XX (cont'd)

2.44	1.0397	-0.0197	0.0034	0.0001	0.0000	-0.0017
2.48	1.0413	-0.0161	0.0030	0.0001	0.0000	-0.0015
2.52	1.0420	-0.0124	0.0025	0.0001	0.0000	-0.0013
2.56	1.0417	-0.0087	0.0019	0.0001	0.0000	-0.0010
2.60	1.0405	-0.0052	0.0009	0.0001	0.0000	-0.0008
2.64	1.0384	-0.0021	-0.0002	0.0001	0.0000	-0.0005
2.68	1.0357	0.0005	-0.0012	0.0000	0.0000	-0.0003
2.72	1.0325	0.0026	-0.0021	0.0000	0.0000	-0.0002
2.76	1.0291	0.0042	-0.0027	0.0000	0.0000	-0.0001
2.80	1.0256	0.0053	-0.0029	0.0000	0.0000	0.0000
2.84	1.0223	0.0060	-0.0029	0.0000	0.0000	0.0001
2.88	1.0191	0.0062	-0.0026	0.0000	0.0000	0.0001
2.92	1.0162	0.0061	-0.0021	0.0000	0.0000	0.0002
2.96	1.0137	0.0058	-0.0016	0.0000	0.0000	0.0002
3.00	1.0116	0.0052	-0.0011	0.0000	0.0000	0.0002
3.10	1.0080	0.0033	-0.0000	0.0000	0.0000	0.0002
3.20	1.0067	0.0012	0.0006	0.0000	0.0000	0.0002
3.30	1.0070	-0.0004	0.0009	0.0000	0.0000	0.0001
3.40	1.0079	-0.0014	0.0008	0.0000	0.0000	0.0001
3.50	1.0088	-0.0018	0.0005	0.0000	0.0000	-0.0000
3.60	1.0093	-0.0016	0.0002	0.0000	0.0000	-0.0001
3.70	1.0093	-0.0012	-0.0001	0.0000	0.0000	-0.0001
3.80	1.0088	-0.0006	-0.0003	0.0000	0.0000	-0.0001
3.90	1.0079	-0.0001	-0.0003	0.0000	0.0000	-0.0000
4.00	1.0070	0.0002	-0.0003	0.0000	0.0000	-0.0000
4.20	1.0053	0.0003	-0.0001	0.0	0.0	0.0000
4.40	1.0044	0.0001	0.0001	0.0	0.0	0.0000
4.60	1.0039	-0.0001	0.0001	0.0	0.0	0.0000
4.80	1.0036	-0.0002	0.0000	0.0	0.0	-0.0000
5.00	1.0032	-0.0001	-0.0000	0.0	0.0	-0.0000
5.20	1.0027	-0.0000	-0.0000	0.0	0.0	-0.0000
5.40	1.0023	0.0000	-0.0000	0.0	0.0	0.0000
5.60	1.0020	-0.0000	0.0000	0.0	0.0	0.0000
5.80	1.0018	-0.0000	0.0000	0.0	0.0	0.0000
6.00	1.0016	-0.0000	0.0000	0.0	0.0	-0.0000

TABLE XXI
PAIR DISTRIBUTION COEFFICIENTS FOR 2 L-J POTENTIAL
FROM PY EQUATION $\rho^*=1.00$ $T^*=0.75$ $R^*=0.53$

R	G000	G200	G220	G221	G222	G400
0.80	0.0000	-0.0000	0.0000	-0.0000	-0.0000	0.0000
0.84	0.0000	-0.0000	0.0000	-0.0000	-0.0000	0.0000
0.88	0.0009	-0.0009	0.0013	-0.0000	-0.0014	0.0033
0.92	0.0143	-0.0133	0.0185	-0.0007	-0.0137	0.0431
0.96	0.0794	-0.0732	0.0946	-0.0068	-0.0422	0.1866
1.00	0.2275	-0.2066	0.2419	-0.0279	-0.0639	0.3691
1.04	0.4389	-0.3872	0.3957	-0.0678	-0.0652	0.3744
1.08	0.6714	-0.5608	0.4751	-0.1177	-0.0537	0.1116
1.12	0.9005	-0.6795	0.4318	-0.1633	-0.0396	-0.2897
1.16	1.1194	-0.7068	0.2554	-0.1922	-0.0272	-0.5522
1.20	1.3176	-0.6320	-0.0114	-0.1564	-0.0177	-0.4962
1.24	1.4707	-0.4856	-0.2696	-0.1764	-0.0106	-0.2186
1.28	1.5612	-0.3167	-0.4331	-0.1402	-0.0056	0.0483
1.32	1.5909	-0.1604	-0.4765	-0.0989	-0.0024	0.1662
1.36	1.5728	-0.0318	-0.4216	-0.0612	-0.0006	0.1382
1.40	1.5211	0.0670	-0.3127	-0.0323	0.0004	0.0575
1.44	1.4472	0.1349	-0.1972	-0.0135	0.0008	0.0048
1.48	1.3610	0.1705	-0.1077	-0.0031	0.0009	-0.0089
1.52	1.2728	0.1790	-0.0519	0.0018	0.0008	-0.0056
1.56	1.1908	0.1705	-0.0220	0.0037	0.0007	-0.0003
1.60	1.1196	0.1537	-0.0077	0.0040	0.0006	0.0030
1.64	1.0608	0.1344	-0.0013	0.0037	0.0005	0.0043
1.68	1.0139	0.1151	0.0014	0.0032	0.0004	0.0046
1.72	0.9778	0.0971	0.0027	0.0027	0.0003	0.0044
1.76	0.9510	0.0806	0.0035	0.0022	0.0002	0.0041
1.80	0.9323	0.0657	0.0044	0.0018	0.0002	0.0039
1.84	0.9204	0.0520	0.0056	0.0015	0.0002	0.0038
1.88	0.9144	0.0394	0.0071	0.0012	0.0001	0.0038
1.92	0.9135	0.0276	0.0091	0.0010	0.0001	0.0040
1.96	0.9167	0.0165	0.0113	0.0008	0.0001	0.0042
2.00	0.9232	0.0061	0.0136	0.0007	0.0001	0.0044
2.04	0.9321	-0.0037	0.0157	0.0006	0.0001	0.0043
2.08	0.9430	-0.0126	0.0172	0.0005	0.0001	0.0040
2.12	0.9554	-0.0204	0.0178	0.0004	0.0000	0.0034
2.16	0.9693	-0.0267	0.0171	0.0003	0.0000	0.0024
2.20	0.9842	-0.0314	0.0153	0.0003	0.0000	0.0012
2.24	0.9989	-0.0341	0.0126	0.0002	0.0000	0.0000
2.28	1.0122	-0.0348	0.0095	0.0002	0.0000	-0.0011
2.32	1.0227	-0.0336	0.0068	0.0002	0.0000	-0.0020
2.36	1.0299	-0.0309	0.0048	0.0002	0.0000	-0.0026
2.40	1.0343	-0.0270	0.0036	0.0001	0.0000	-0.0029

TABLE XXI (cont'd)

2.44	1.0366	-0.0223	0.0030	0.0001	0.0000	-0.0029
2.48	1.0375	-0.0171	0.0027	0.0001	0.0000	-0.0027
2.52	1.0373	-0.0120	0.0023	0.0001	0.0000	-0.0023
2.56	1.0361	-0.0070	0.0015	0.0001	0.0000	-0.0018
2.60	1.0338	-0.0026	0.0004	0.0001	0.0000	-0.0014
2.64	1.0306	0.0013	-0.0010	0.0001	0.0000	-0.0010
2.68	1.0267	0.0044	-0.0022	0.0000	0.0000	-0.0006
2.72	1.0225	0.0067	-0.0032	0.0000	0.0000	-0.0003
2.76	1.0181	0.0084	-0.0038	0.0000	0.0000	-0.0001
2.80	1.0139	0.0093	-0.0040	0.0000	0.0000	0.0001
2.84	1.0100	0.0097	-0.0037	0.0000	0.0000	0.0002
2.88	1.0066	0.0095	-0.0032	0.0000	0.0000	0.0003
2.92	1.0036	0.0089	-0.0025	0.0000	0.0000	0.0004
2.96	1.0011	0.0080	-0.0017	0.0000	0.0000	0.0004
3.00	0.9992	0.0069	-0.0009	0.0000	0.0000	0.0005
3.10	0.9970	0.0036	0.0006	0.0000	0.0000	0.0005
3.20	0.9975	0.0005	0.0013	0.0000	0.0000	0.0004
3.30	0.9997	-0.0016	0.0014	0.0000	0.0000	0.0003
3.40	1.0023	-0.0027	0.0011	0.0000	0.0000	0.0001
3.50	1.0043	-0.0028	0.0006	0.0000	0.0000	-0.0001
3.60	1.0053	-0.0022	0.0001	0.0000	0.0000	-0.0002
3.70	1.0054	-0.0013	-0.0004	0.0000	0.0000	-0.0002
3.80	1.0047	-0.0003	-0.0006	0.0000	0.0000	-0.0002
3.90	1.0037	0.0004	-0.0006	0.0000	0.0000	-0.0001
4.00	1.0027	0.0008	-0.0004	0.0000	0.0000	-0.0000
4.20	1.0013	0.0006	-0.0000	0.0	0.0	0.0000
4.40	1.0011	0.0000	0.0002	0.0	0.0	0.0000
4.60	1.0013	-0.0003	0.0001	0.0	0.0	0.0000
4.80	1.0014	-0.0002	0.0000	0.0	0.0	-0.0000
5.00	1.0011	-0.0000	-0.0000	0.0	0.0	-0.0000
5.20	1.0008	0.0001	-0.0000	0.0	0.0	-0.0000
5.40	1.0006	0.0000	-0.0000	0.0	0.0	0.0000
5.60	1.0006	-0.0000	0.0000	0.0	0.0	0.0000
5.80	1.0006	-0.0000	0.0000	0.0	0.0	0.0000
6.00	1.0005	-0.0000	-0.0000	0.0	0.0	-0.0000

TABLE XXII
PAIR DISTRIBUTION COEFFICIENTS FOR 2 L-J POTENTIAL
FROM PY EQUATION $\rho^*=1.20$ $T^*=0.75$ $R^*=0.53$

R	G000	G200	G220	G221	G222	G400
0.80	0.0000	-0.0000	0.0000	-0.0000	-0.0000	0.0000
0.84	0.0000	-0.0000	0.0000	-0.0000	-0.0000	0.0001
0.88	0.0011	-0.0010	0.0015	-0.0000	-0.0016	0.0039
0.92	0.0162	-0.0148	0.0213	-0.0008	-0.0159	0.0511
0.96	0.0890	-0.0809	0.1079	-0.0080	-0.0483	0.2184
1.00	0.2517	-0.2260	0.2725	-0.0326	-0.0722	0.4249
1.04	0.4788	-0.4203	0.4393	-0.0783	-0.0723	0.4197
1.08	0.7224	-0.6049	0.5177	-0.1339	-0.0585	0.1082
1.12	0.9563	-0.7276	0.4571	-0.1832	-0.0423	-0.3498
1.16	1.1755	-0.7474	0.2502	-0.2126	-0.0286	-0.6381
1.20	1.3708	-0.6525	-0.0497	-0.2140	-0.0182	-0.5658
1.24	1.5168	-0.4803	-0.3296	-0.1893	-0.0107	-0.2537
1.28	1.5955	-0.2894	-0.4968	-0.1483	-0.0056	0.0391
1.32	1.6102	-0.1202	-0.5293	-0.1030	-0.0024	0.1672
1.36	1.5762	0.0128	-0.4570	-0.0629	-0.0005	0.1403
1.40	1.5097	0.1108	-0.3315	-0.0328	0.0004	0.0596
1.44	1.4231	0.1754	-0.2042	-0.0135	0.0007	0.0082
1.48	1.3268	0.2066	-0.1081	-0.0030	0.0008	-0.0042
1.52	1.2311	0.2100	-0.0496	0.0018	0.0007	-0.0005
1.56	1.1441	0.1963	-0.0189	0.0036	0.0006	0.0046
1.60	1.0702	0.1747	-0.0045	0.0039	0.0005	0.0074
1.64	1.0105	0.1510	0.0017	0.0036	0.0004	0.0082
1.68	0.9642	0.1278	0.0043	0.0031	0.0003	0.0080
1.72	0.9298	0.1064	0.0055	0.0026	0.0003	0.0075
1.76	0.9057	0.0868	0.0064	0.0021	0.0002	0.0070
1.80	0.8904	0.0690	0.0075	0.0018	0.0002	0.0066
1.84	0.8826	0.0527	0.0090	0.0014	0.0002	0.0064
1.88	0.8811	0.0377	0.0110	0.0012	0.0001	0.0064
1.92	0.8849	0.0236	0.0134	0.0010	0.0001	0.0065
1.96	0.8931	0.0104	0.0162	0.0008	0.0001	0.0067
2.00	0.9046	-0.0020	0.0190	0.0007	0.0001	0.0069
2.04	0.9182	-0.0135	0.0214	0.0006	0.0001	0.0067
2.08	0.9335	-0.0239	0.0230	0.0005	0.0001	0.0060
2.12	0.9500	-0.0328	0.0230	0.0004	0.0000	0.0047
2.16	0.9680	-0.0396	0.0214	0.0003	0.0000	0.0031
2.20	0.9868	-0.0440	0.0182	0.0003	0.0000	0.0012
2.24	1.0050	-0.0459	0.0140	0.0002	0.0000	-0.0006
2.28	1.0207	-0.0451	0.0096	0.0002	0.0000	-0.0023
2.32	1.0323	-0.0420	0.0060	0.0002	0.0000	-0.0037
2.36	1.0393	-0.0371	0.0035	0.0002	0.0000	-0.0046
2.40	1.0423	-0.0307	0.0022	0.0001	0.0000	-0.0050

TABLE XXII (cont'd)

2.44	1.0427	-0.0237	0.0019	0.0001	0.0000	-0.0049
2.48	1.0416	-0.0164	0.0019	0.0001	0.0000	-0.0045
2.52	1.0393	-0.0094	0.0016	0.0001	0.0000	-0.0038
2.56	1.0361	-0.0030	0.0008	0.0001	0.0000	-0.0031
2.60	1.0318	0.0026	-0.0005	0.0001	0.0000	-0.0023
2.64	1.0267	0.0071	-0.0021	0.0001	0.0000	-0.0015
2.68	1.0211	0.0105	-0.0036	0.0000	0.0000	-0.0009
2.72	1.0153	0.0129	-0.0047	0.0000	0.0000	-0.0004
2.76	1.0098	0.0143	-0.0052	0.0000	0.0000	0.0000
2.80	1.0047	0.0148	-0.0051	0.0000	0.0000	0.0004
2.84	1.0002	0.0144	-0.0045	0.0000	0.0000	0.0006
2.88	0.9965	0.0135	-0.0035	0.0000	0.0000	0.0008
2.92	0.9935	0.0120	-0.0024	0.0000	0.0000	0.0009
2.96	0.9914	0.0102	-0.0013	0.0000	0.0000	0.0010
3.00	0.9901	0.0082	-0.0002	0.0000	0.0000	0.0010
3.10	0.9900	0.0030	0.0017	0.0000	0.0000	0.0010
3.20	0.9931	-0.0013	0.0024	0.0000	0.0000	0.0008
3.30	0.9976	-0.0039	0.0022	0.0000	0.0000	0.0004
3.40	1.0017	-0.0047	0.0014	0.0000	0.0000	0.0001
3.50	1.0043	-0.0041	0.0004	0.0000	0.0000	-0.0002
3.60	1.0051	-0.0026	-0.0004	0.0000	0.0000	-0.0004
3.70	1.0045	-0.0010	-0.0010	0.0000	0.0000	-0.0004
3.80	1.0031	0.0005	-0.0012	0.0000	0.0000	-0.0003
3.90	1.0015	0.0013	-0.0009	0.0000	0.0000	-0.0002
4.00	1.0002	0.0016	-0.0005	0.0000	0.0000	-0.0000
4.20	0.9992	0.0007	0.0002	0.0	0.0	0.0001
4.40	0.9998	-0.0003	0.0003	0.0	0.0	0.0001
4.60	1.0007	-0.0005	0.0001	0.0	0.0	0.0000
4.80	1.0008	-0.0002	-0.0001	0.0	0.0	-0.0001
5.00	1.0004	0.0001	-0.0001	0.0	0.0	-0.0000
5.20	1.0001	0.0002	-0.0000	0.0	0.0	-0.0000
5.40	1.0000	0.0001	0.0000	0.0	0.0	0.0000
5.60	1.0001	-0.0000	0.0000	0.0	0.0	0.0000
5.80	1.0002	-0.0001	0.0000	0.0	0.0	0.0000
6.00	1.0002	-0.0000	-0.0000	0.0	0.0	-0.0000

that these functions show much the same variation with density as do spherical radial distribution functions. The differences resulting from changing the nonsphericity of the molecule are demonstrated in Figure 7 where we have compared the g_{000} curves for R^* values of 0.53 and 0.68 at the same T^* and ρ^* . The peaks are smaller and are shifted to higher r^* for the larger R^* value.

The main peak heights of the g_{000} , as well as of the higher $g_{\ell\ell'm}$ are recorded in Table XXIII. The g_{000} peak heights follow much the same pattern as is found in spherical PY results. At the isotherm closest to our critical temperature (approx. PY critical point for $R^* = 0.53$ is $\rho_c^* = 0.65$, $T_c^* = 0.70$), the main peak heights decrease with increasing density up to about $\rho^* = 0.90$ and then increase. At $T^* = 1.00$ the minimum peak height occurs lower near $\rho^* = 0.60$, and is barely observed at $T^* = 1.30$. Throop and Bearman's² spherical results for their $T^* = 1.40$ isotherm show behavior similar to our 0.75 isotherm in that a peak minimum occurs above the critical density at about $1.3\rho_c^*$. In Figure 8 one may see the temperature effect on $g_{000}(r)$ at the constant density of $\rho^* = 1.00$. The results are representative of the increase in peak height which is found at all densities as the temperature decreases.

The angular correlation functions have been plotted in Figures 9, 10, and 11. In each of these, $g_{222}(r)$ has been neglected because of its small value. Figure 9 shows curves for the constant temperature states $(\rho^*, T^*) = (0.6, 1.3), (1.2, 1.3)$. The positions of the peaks in these curves are not affected greatly by density, nor is the general curve shape. Figure 10 shows the effect of temperature

TABLE XXIII

MAIN PEAK HEIGHTS OF THE $g_{\ell\ell'm}$ FOR $R^* = 0.53$

T^*	$\frac{\rho^*}{\ell\ell'm}$	0.0	0.2	0.4	0.6	0.8	1.0	1.2
0.75	000	1.792	1.752	1.701	1.645	1.601	1.591	1.610
	200	- .716	- .707	- .697	- .688	- .688	- .706	- .752
	220	.455	.451	.448	.446	.451	.475	.517
		- .340	- .367	- .393	- .415	- .440	- .476	- .529
	400	.303	.317	.332	.348	.369	.404	.461
		- .366	- .403	- .438	- .471	- .508	- .564	- .646
1.00	000	1.534	1.507	1.486	1.476	1.483	1.508	1.551
	200	- .556	- .554	- .556	- .565	- .587	- .622	- .671
	220	.334	.335	.340	.351	.370	.397	.437
		- .265	- .283	- .302	- .324	- .354	- .395	- .450
	400	.210	.218	.229	.243	.267	.302	.350
		- .270	- .292	- .318	- .349	- .391	- .447	- .522
1.30	000	1.383	1.376	1.377	1.391	1.417	1.455	1.506
	200	- .465	- .470	- .481	- .501	- .528	- .564	- .611
	220	.270	.276	.284	.298	.318	.348	.386
		- .221	- .235	- .254	- .278	- .308	- .346	- .394
	400	.161	.169	.181	.197	.218	.247	.284
		- .214	- .232	- .255	- .285	- .324	- .375	- .440

and indicates that temperature variation has its primary effect on curve amplitudes. If the peak heights of the higher $g_{\ell\ell'm}$ tabulated in Table XXIII are studied as a function of density, one can see that g_{200} shows an absolute peak minimum near $\rho^* = 0.70$ at $T^* = 0.75$. Similarly g_{220} shows a peak minimum for its positive peak only near $\rho^* = 0.6$ at $T^* = 0.75$. At our higher isotherms, these functions effectively show no absolute minima and the other $g_{\ell\ell'm}$ show no absolute peak minima at any of our isotherms. It is thus possible to generalize and state that the angular correlations merely gain size as the density increases, with the exception of isotherms near the critical point. A further examination of Table XXIII shows that without exception, a decrease of temperature causes an increase in absolute peak height.

Because the shapes of the angular correlation functions change so little with increasing density, it is found that, as in the diatomic hard core system, the zero density limit of $g(\underline{R}_1, \underline{R}_2)$ determines the general shape for all densities up to 1.2, even for the lowest isotherm. Plots of angular $g_{\ell\ell'm}$ for $R^* = 0.53$ and 0.68 at $\rho^* = 1.2$, $T^* = 1.00$ in Figure 11 show the result of changing molecular shape, and indicate that the principal peaks are shifted to larger r^* as R^* increases.

The $g_{\ell\ell'm}$ coefficients have been calculated from the pair H_{000} , H_{200} as well as the longer H_{000} , H_{200} , H_{220} , H_{400} set over the density range of this work. The g_{000} values differ by no more than 0.4% and g_{200} by no more than 0.5%. The biggest differences occur in g_{220} and g_{400} and range around 1 to 3%. Thus we see that H_{220} and

H_{400} are minor contributions in the calculation of the pair distribution functions for the density and temperature range studied in this work.

We have also checked on the changes brought about in the distribution function coefficients when calculated from the $g_{\ell\ell'm}$ expansion of (25) or the shorter expansions of Chen^{7c}. We used Chen's hard core results for H_{000} and H_{200} (neglecting H_{220} and H_{400}) at $\rho^* = 1.0$, $R^* = 0.2$ as input. The two calculations yield g_{000} functions differing by about 3% up to $r^* = 2.00$ and slightly more at higher r^* . Main peak heights of g_{200} and g_{220} differ by 4-10% with some relative shifting of small-valued sections of the functions at large r^* . Similar percentages are obtained for the two-centered Lennard-Jones case. These are significant percentages, particularly in the case of $g_{000}(r)$. If one compares these percentages with those in the last paragraph, it is apparent that these errors exceed those arising from neglect of the H_{220} and H_{400} functions. It is felt therefore that these errors should be reduced by using the longer expansion of (25) especially since its employment produces an insignificant increase in computation time.

Using (23) and Simpson's rule we have calculated κ_T , the isothermal compressibility, for $R^* = 0.53$. The results are tabulated in Table XXIV. These values have been compared at certain states to those obtained from (24) using values of $1-K C(000)$ extrapolated to $v = 0$, and the results agree well enough to allow us to search for a critical point. It is apparent that at the lowest isotherm, $T^* = 0.75$, a strong maximum is occurring near $\rho^* = 0.55$. This is indicative of

a proximate critical point where κ_T becomes infinite. While our data do not accurately locate the critical point, it does show that one exists and an estimate may be made that it lies in the vicinity of $T^* = 0.70$, $\rho^* = 0.65$. We may compare these values with the experimental values for chlorine of $T^* = 0.72$, $\rho^* = 0.93$ ($T_c = 417^\circ\text{K}$, $\rho_c = 0.573 \text{ g/cc}$). It appears that our estimate of the critical temperature is fairly close to the experimental value, but our estimate of the critical density is far too low.

Watts⁴ has shown for the case of spherical systems near the critical point that two solutions may exist for the distribution function for certain densities. Because our lowest isotherm was close to critical, we have checked to make sure that our results do not involve such multiple solutions of the Percus-Yevick equation. One check we performed was to solve the Percus-Yevick equation for two paths to the $\rho^* = 1.2$, $T^* = 0.75$ state, one from $\rho^* = 0.0$ to 1.2 along $T^* = 1.00$ and then down to $T^* = 0.75$ along the constant $\rho^* = 1.2$ isochore, and the other from $\rho^* = 0.0$ to 1.2 along $T^* = 0.75$. The results agreed, indicating that we had not jumped to another solution along the lower isotherm. A second check was to verify that the $g_{000}(r)$ curves approached 1.0 asymptotically. In the spherical case one of the multiple solutions is unphysical in that its $g(r)$ is characterized by values much greater than 1.0 at values of r^* near 2.5 or 3.0. No such behavior was found in this work.

TABLE XXIV

ISOTHERMAL COMPRESSIBILITY VALUES ($R^* = 0.53$)

ρ^*	T^*	0.75	1.00	1.30
0.1		1.2683	1.1106	1.0307
0.2		1.6215	1.2067	1.0376
0.3		2.0443	1.2699	1.0163
0.4		2.4596	1.2833	0.9667
0.5		2.7250	1.2381	0.8923
0.6		2.7102	1.1401	0.8004
0.7		2.4211	1.0059	0.6997
0.8		1.9737	0.8531	0.5984
0.9		1.5063	0.7024	0.5022
1.0		1.1082	0.5654	0.4158
1.1		0.8038	0.4483	0.3405
1.2		0.5790	0.3529	0.2764

Discussion

One of the primary conclusions to be drawn from the previous section is that the higher $H_{\ell\ell'm}$ that we have included in the PY solution are indeed quite small contributions to the distribution function even at high densities and moderately low temperatures where they might be expected to be appreciable. We have thus confirmed the choice of Chen and Steele to use just H_{000} and H_{200} to describe the fluid in this temperature-density range. For future studies using this technique and covering the same range of states, it appears as though an adequate description may be obtained for temperature dependent systems if just these two are employed along with the extended series product of (25) and the calculations are carried out to $r^* = 6.00$.

While it is felt that the H_{220} and H_{400} functions are sufficiently accurate to judge the size of their contributions to the distribution functions, it must be added that they are not known to a high degree of accuracy. This is evident when the H_{220} obtained from $H(2200)$ is transformed to second and fourth orders and compared to the $H(2202)$ and $H(2204)$ values computed from Eqs. (22). The curves are of the same order of magnitude but show only marginal qualitative agreement.

Several effects contribute to this error, including truncation errors, transform errors, and incomplete convergence of the iterative PY solution. Truncation errors have little effect on the determination of $H(0000)$ and $H(2002)$ since these depend heavily on the very large $C(0000)$ transform. For the higher $H(\ell\ell'ms)$ transforms, however,

truncation is probably the greatest error. Three series, the $H(\underline{R}_1 \underline{R}_2)$, $C(\underline{R}_1 \underline{R}_2)$, and $f(\underline{R}_1 \underline{R}_2)$ series, have all had X_{221} and X_{222} omitted and have been truncated after the general term X_{400} , thus omitting contributions from the terms X_{440} , X_{420} , etc. X_{222} is most likely a small contribution, but the others may be of significance in computing X_{220} and X_{400} . The $C_{\ell\ell'm}$ terms where $\ell = \ell'$ may be particularly significant, since the zero order Hankel transform of these functions will be larger than the $C(2002)$ transform, the dominant member of the B_i terms of Table I, in the region near $v = 0$. Including these higher terms, however, is difficult. The expansions required to generate each member of a new set of simultaneous equations corresponding to Eqs. (14)-(18) are extremely lengthy. Furthermore, the number of simultaneous equations themselves will increase rapidly and require a large increase in computing time. If very many coefficients are included, this results in a prohibitive increase of time.

Our estimate of the critical point location allows us to draw some tentative conclusions about the choice of potential used to describe chlorine. Provided the Percus-Yevick theory remains a good physical representation in the critical region for nonspherical molecules, our estimate of the critical density implies that the potential is inadequate either in functional form or in choice of parameters. R^* is the principal variable parameter since it is the most arbitrary. σ and ϵ , once R^* is chosen, become fixed and are as accurate as the PVT data from which they are derived. A comparison of ρ_c values calculated from the ρ_c^* and σ values for $R^* = 0.0$ and $R^* = 0.53$ show little difference between one another ($R^* = 0.0$, $\rho_c^* = 0.59$,

↓
2.5 (Wat's value)
reduced our way instead of by
just 3.0 = ρ_c^* critical = 0.28

$\sigma = 4.7$; $R^* = 0.53$, $\rho_c^* = 0.65$, $\sigma = 3.75$); both are only about 70% of the actual experimental value of 0.573 g/cc . It appears, therefore, that if R^* were decreased to a lower value, such as by using the Gaussian weighting of Sweet¹², no improvement would be found in the ability to predict the critical density. A larger value of R^* would seem too large physically. Thus varying R^* holds little hope for improving the prediction of the experimental critical density value and, within our limited accuracy, one is led to the conclusion that the functional form of the two-centered Lennard-Jones potential is only marginally correct. Whether this is true for the calculation of all thermodynamic properties is yet to be proven and awaits further study.

The fact that results for the $H_{\ell\ell'm}$ and $g_{\ell\ell'm}$ have been obtained from the Percus-Yevick equations developed by Chen and Steele for hard core potentials shows that their procedure is equally applicable to the temperature dependent two-centered Lennard-Jones potentials. For similar convergence criteria, solutions were obtained in about the same number of iterations. Certain restrictions on this type of solution are apparent, however. One is that the required number of iterations increases rapidly in the vicinity of the critical point, implying that this may prohibit investigation of states very close to critical. Extension of the solution to states with densities greater than 1.2 is also restricted because of the large number of iterations required, a result noted by Chen in his hard core work as well. The effects of very low temperature are still unknown; we merely note that the temperature values covered in this work have only

a slight effect on the number of iterations (other than critical point increases), generally requiring more iterations as the temperature gets lower. Increasing the accuracy of the results by including a much larger number of $X_{\ell\ell',m}$ terms is, as we have seen, also restricted due to the greatly increased length of the expressions to be solved.

In conclusion, therefore, it is seen that the method employed here has allowed us to determine pair distribution coefficients accurate to first order for a given temperature dependent potential. These may find use in calculating thermodynamic properties. Evaluation of constant volume heat capacities may be interesting in that it has been reported¹¹ that chlorine shows a strong orientational contribution. Application of the coefficients to x-ray scattering from chlorine is presented in the next section.

Figure Captions

- Figure 1. Chlorine second virial data of Kapoor and Martin.
B is in units of cc/mole. T has units of $^{\circ}\text{K}$.
- Figure 2. Reduced internuclear distance versus σ as
determined from second virial data. \bullet denotes
 $R^* = 0.53$.
- Figure 3. Reduced internuclear distance versus ϵ/k as
determined from second virial data. \bullet denotes
 $R^* = 0.53$.
- Figure 4. $H_{ll'm}(r)$ functions for moderately high density
of $\rho^* = 1.20$, $T^* = 0.75$, $R^* = 0.53$.
- Figure 5. $g_{000}(r)$ as a function of density at $T^* = 1.30$.
- Figure 6. $g_{000}(r)$ as a function of density at $T^* = 0.75$.
- Figure 7. $g_{000}(r)$ showing curve shape dependence on R^* .
- Figure 8. $g_{000}(r)$ showing dependence on temperature. Curve 1
is for $T^* = 0.75$, curve 2 is for $T^* = 1.00$, and
curve 3 is for $T^* = 1.30$.
- Figure 9. $g_{ll'm}(r)$ functions showing dependence on density.
Curves 1 are for $\rho^* = 0.6$; curves 2 are for
 $\rho^* = 1.20$.
- Figure 10. $g_{ll'm}(r)$ functions showing dependence on temperature.
Curves 1 are for $T^* = 1.30$; curves 2 are for $T^* = 0.75$.

Figure 11. $g_{\ell\ell_m}(r)$ functions showing curve shape dependence on R^* . Curves 1 are for $R^* = 0.68$; curves 2 are for $R^* = 0.53$.

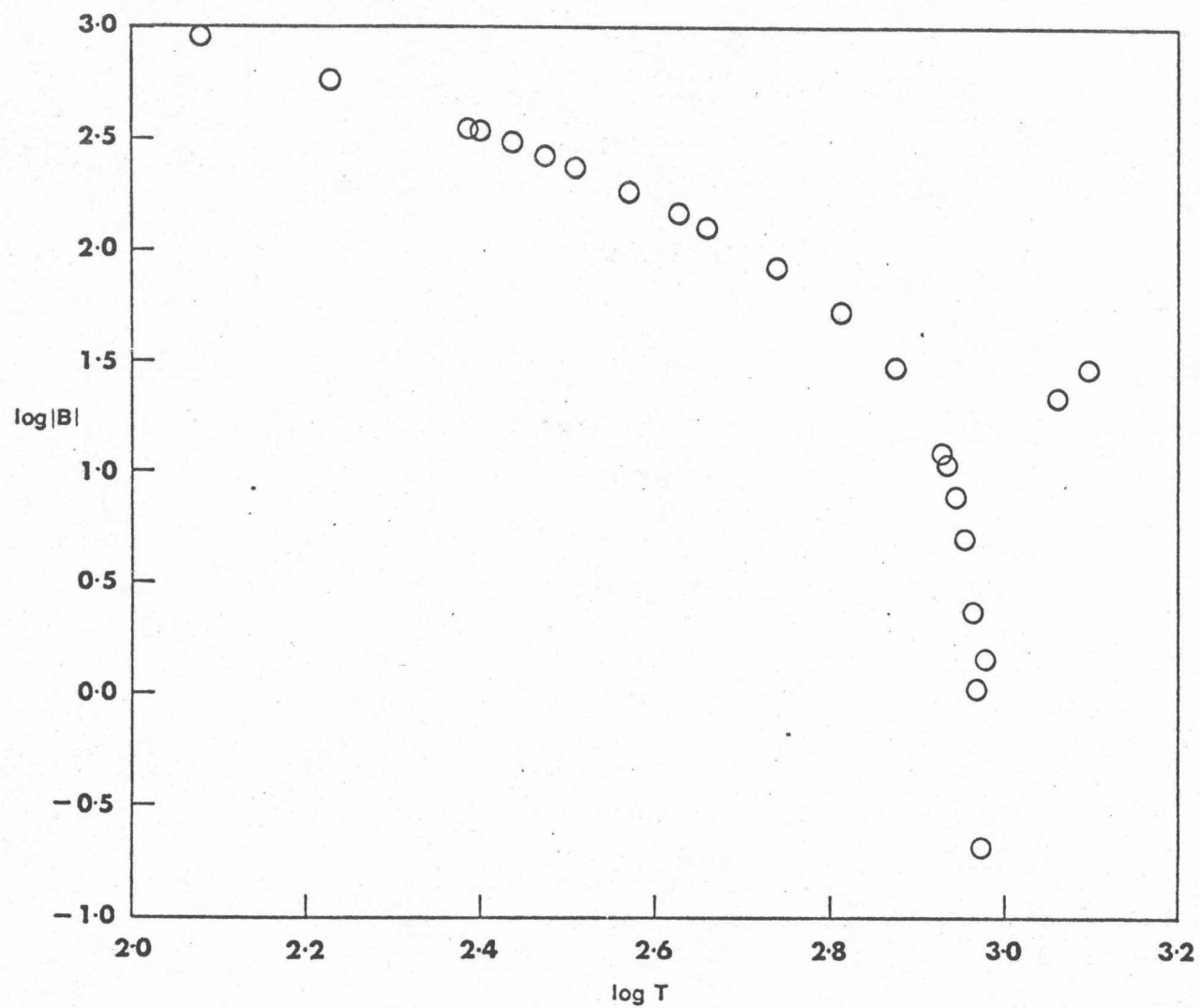


Figure 1.

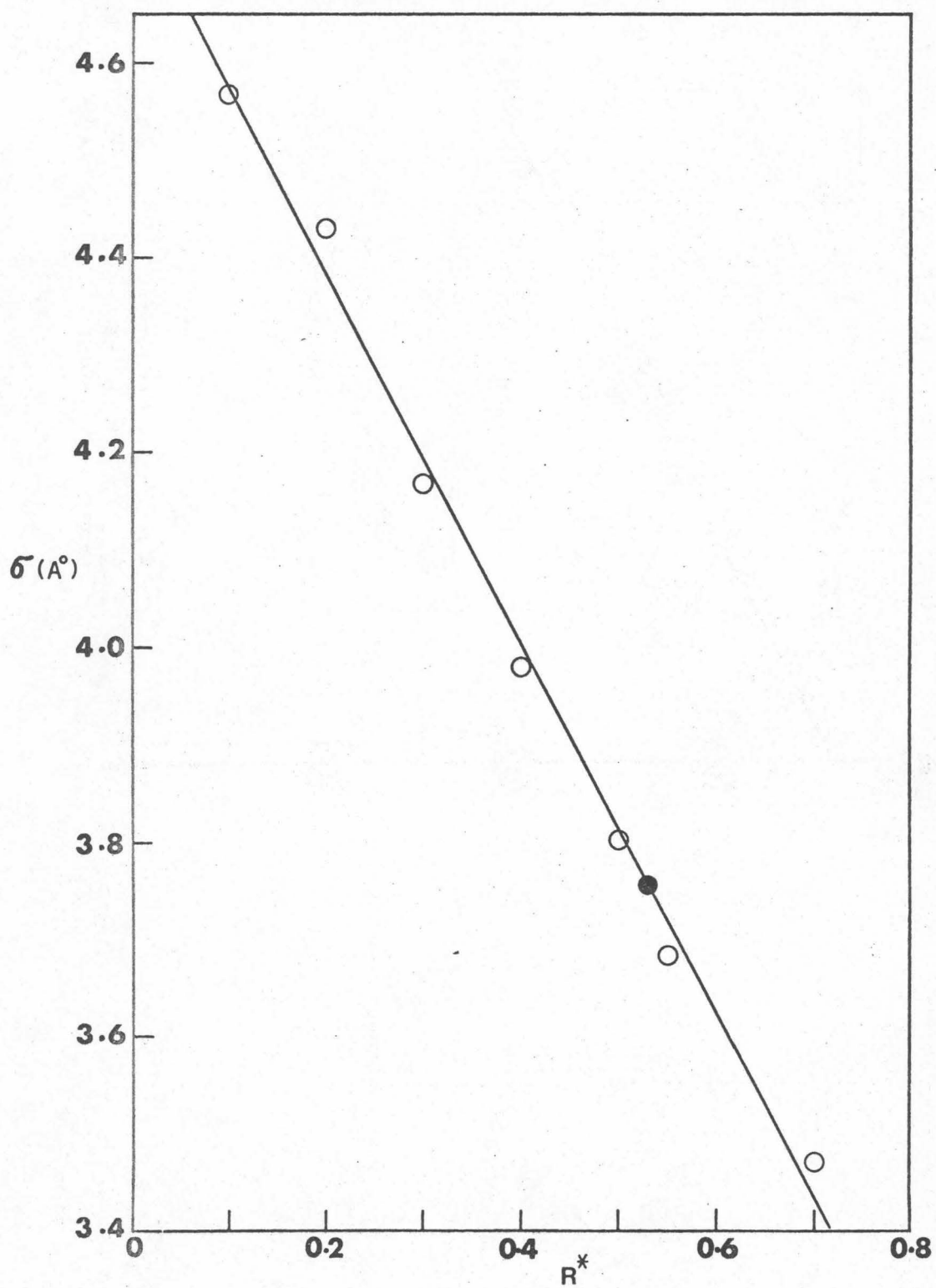


Figure 2.

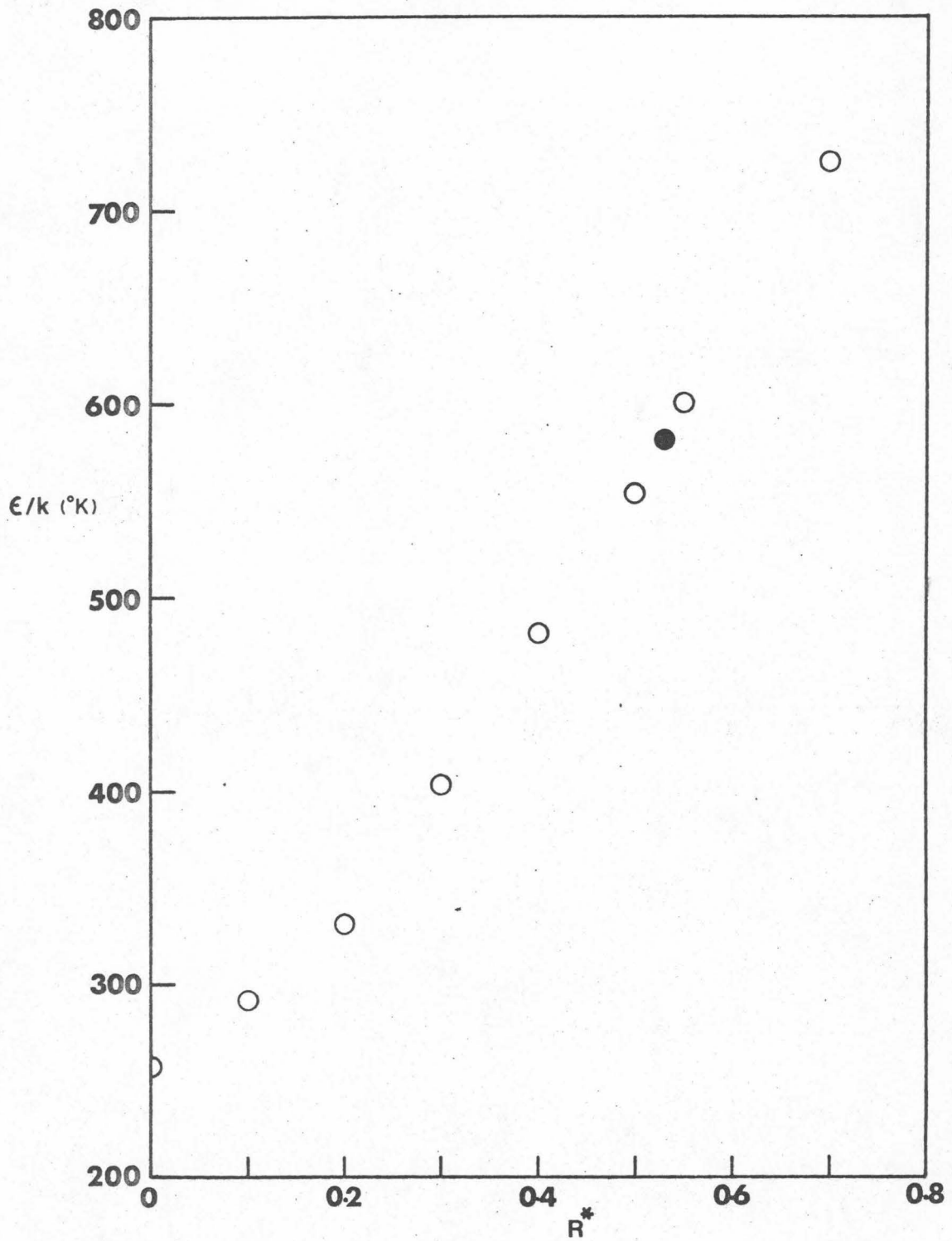


Figure 3.

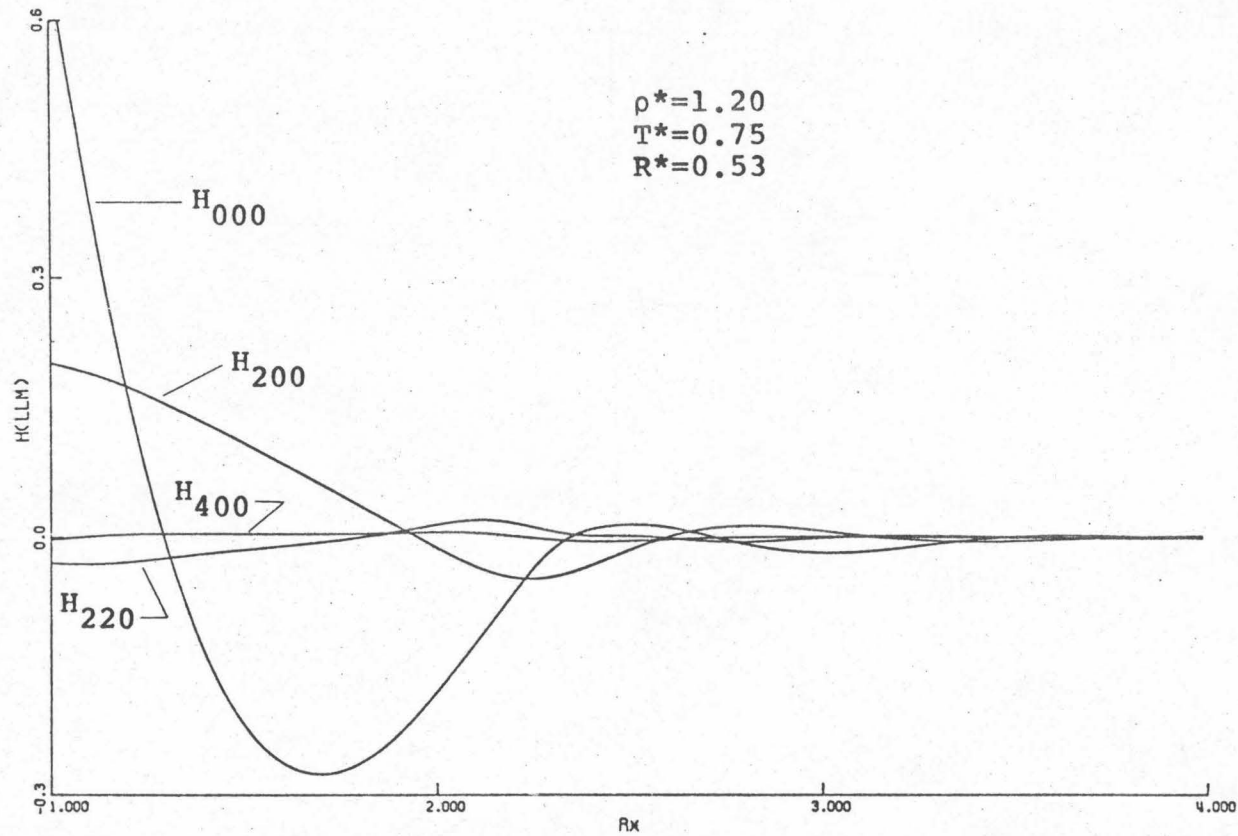


Figure 4.

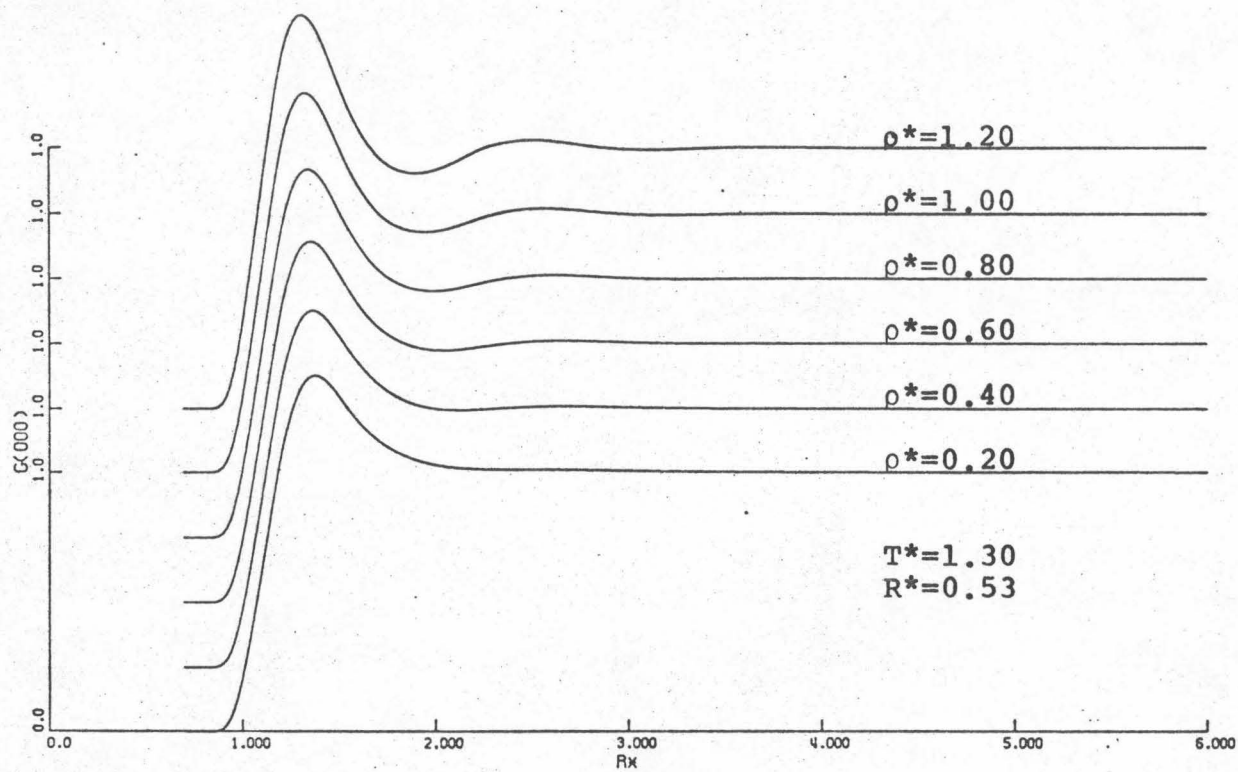


Figure 5.

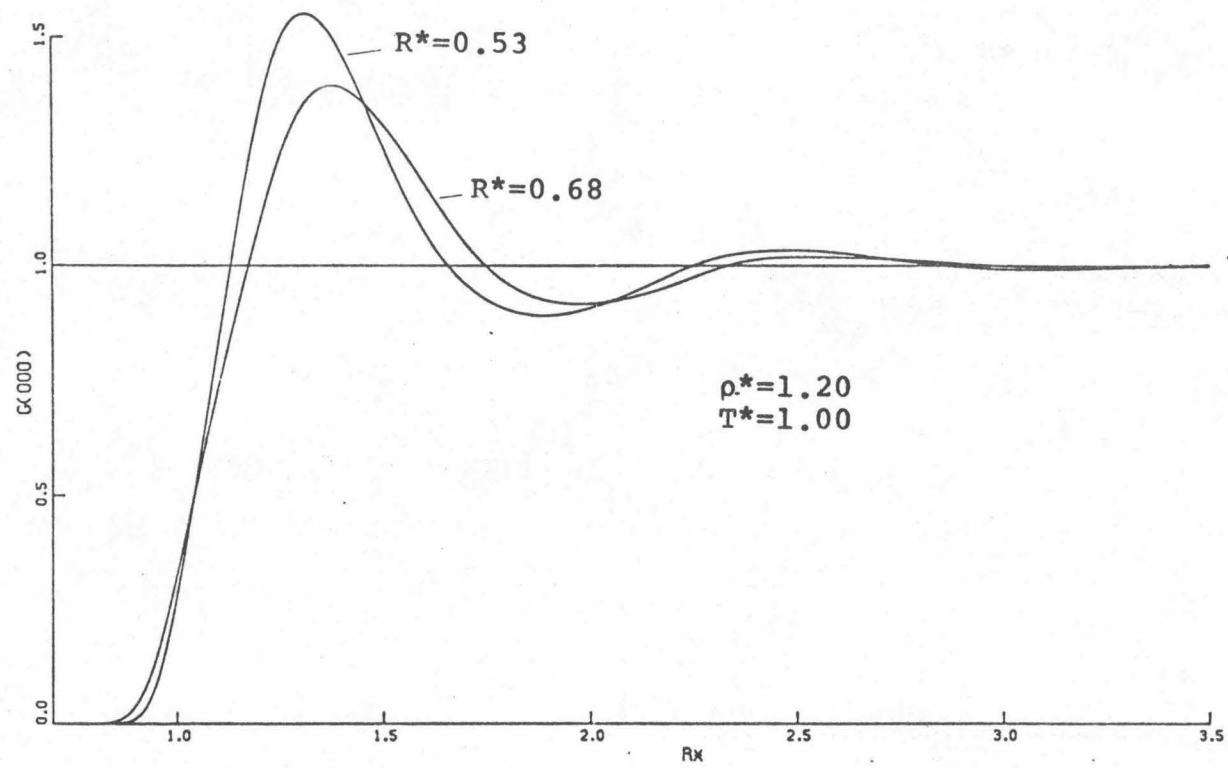


Figure 7.

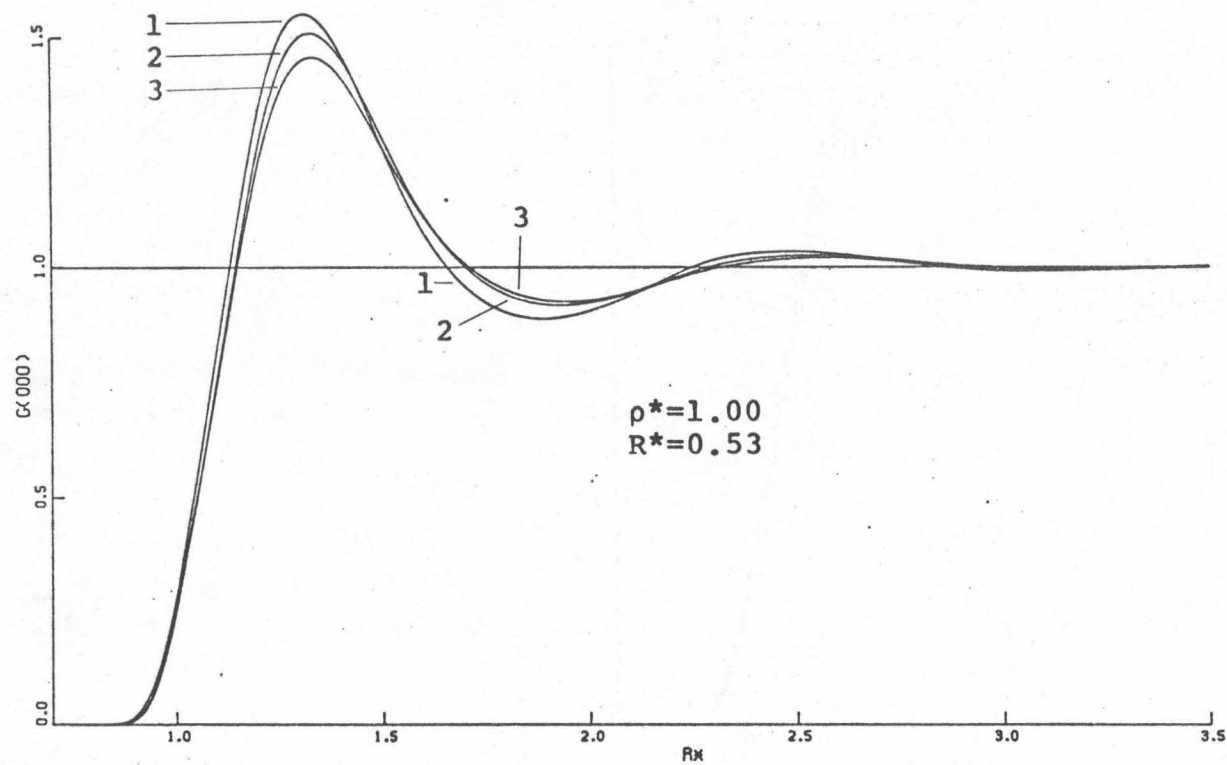


Figure 8.

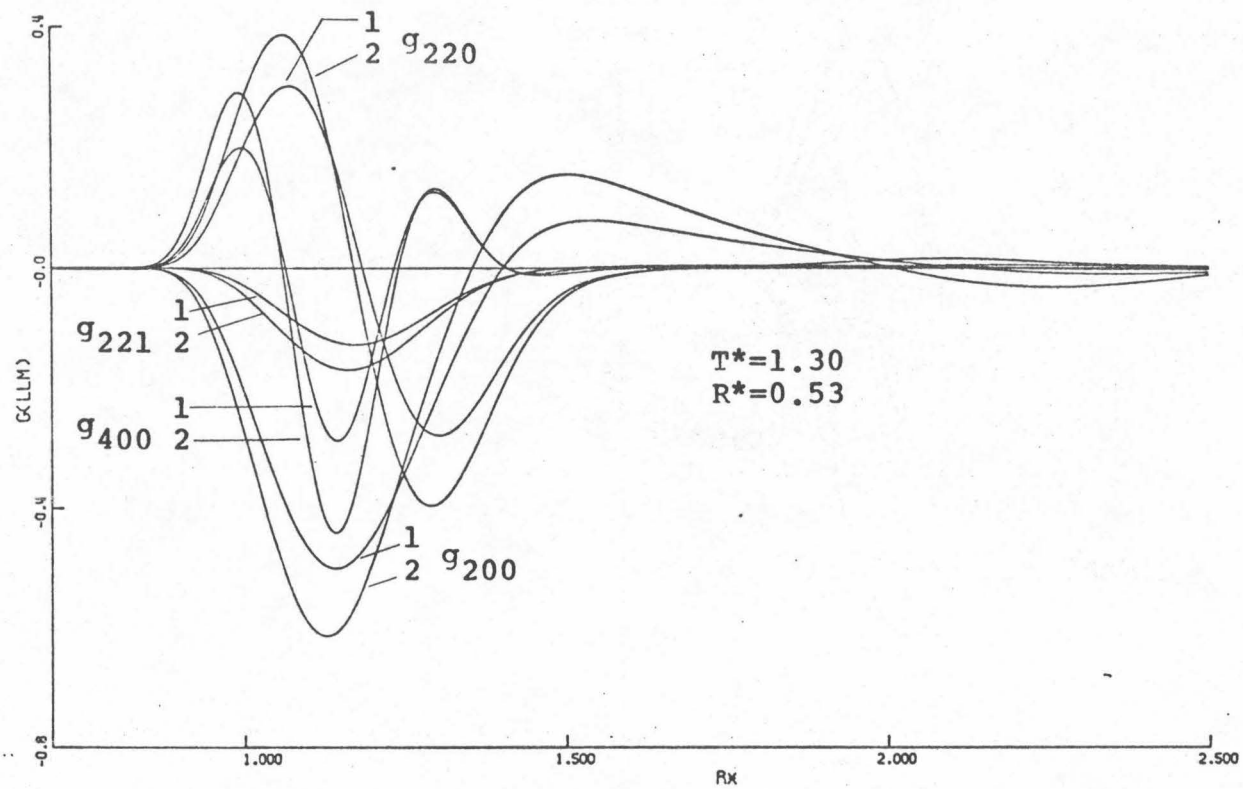


Figure 9.

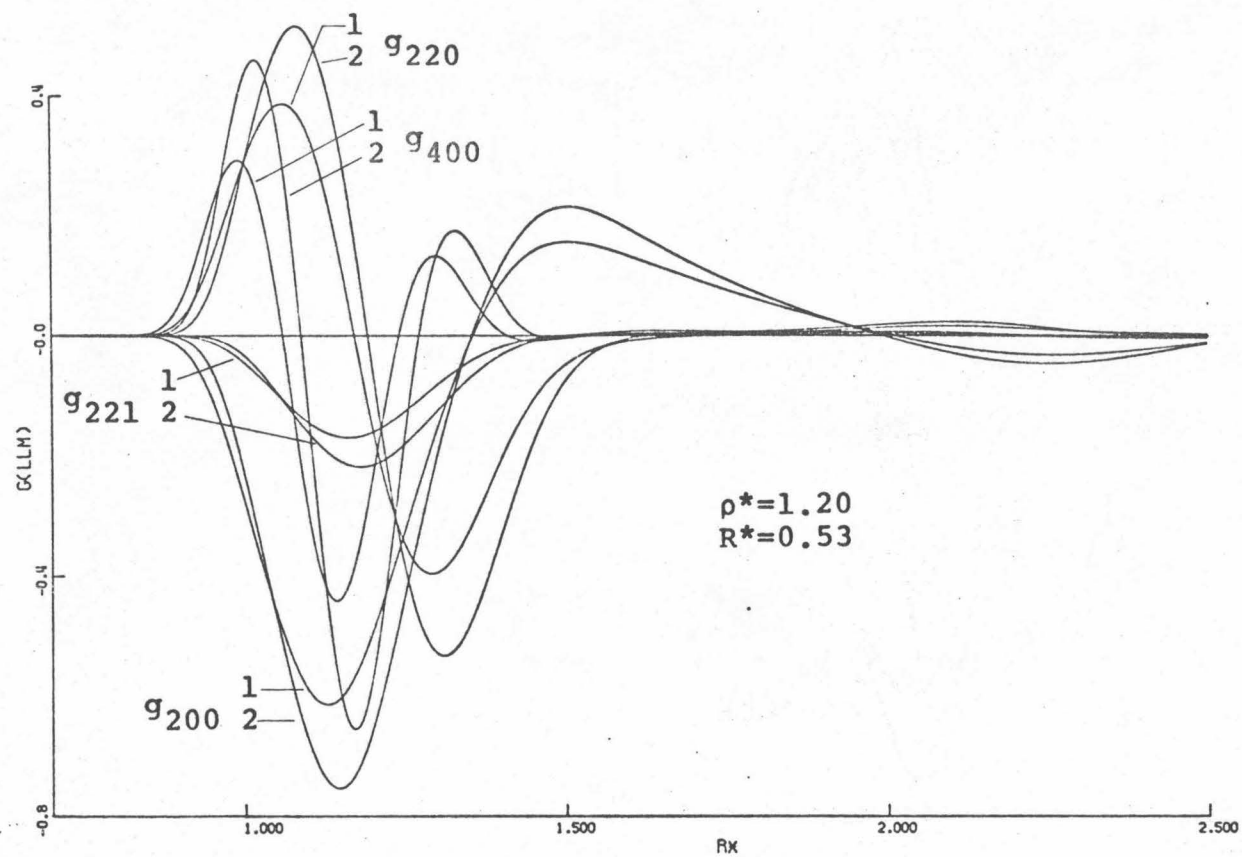


Figure 10.

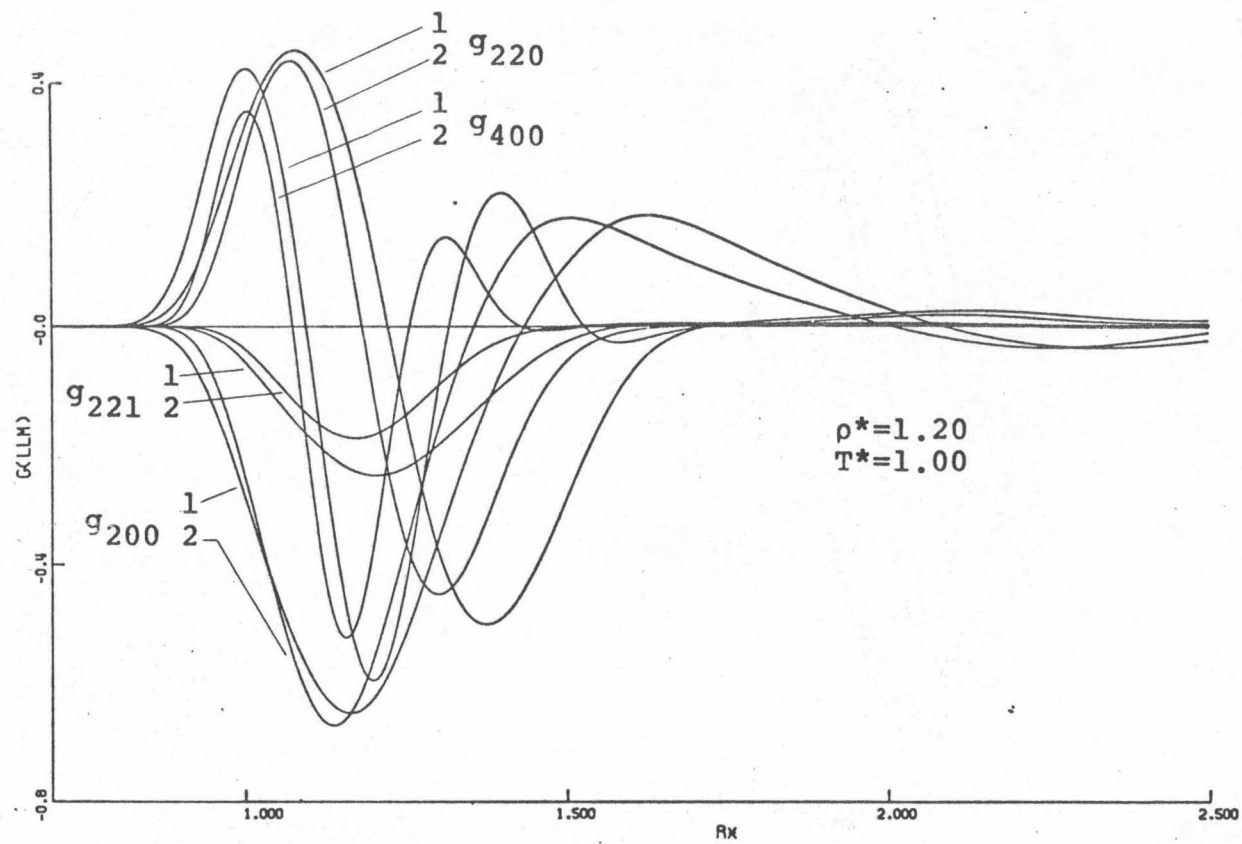


Figure 11.

Bibliography

1. M. S. Wertheim, Phys. Rev. Lett. 10, 321 (1963)
2. G. J. Throop, R. J. Bearman, Physica 32, 1298 (1966)
3. F. Mandel, R. J. Bearman, M. Y. Bearman, J. Chem. Phys. 52, 3315 (1970)
4. R. O. Watts, J. Chem. Phys. 48, 50 (1968)
5. R. J. Baxter, Phys. Rev. 154, 170 (1967)
6. A. Ben-Naim, J. Chem. Phys. 52, 5531 (1970); 54, 3682 (1971)
7. (a) Y. D. Chen, W. A. Steele, J. Chem. Phys. 54, 703 (1971);
(b) Y. D. Chen, Ph.D. Thesis, The Statistical Mechanics of Nonspherical Molecules, Penn State Univ., 1970; (c) *ibid.*, Eqs. 110.
8. W. A. Steele, J. Chem. Phys. 39, 3197 (1963)
9. M. E. Rose, Elementary Theory of Angular Momentum, J. Wiley, New York, 1957
10. J. R. Sweet, W. A. Steele, J. Chem. Phys. 47, 3022 (1967)
11. J. A. Pople, Disc. Far. Soc. 15, 35 (1953)
12. J. R. Sweet, W. A. Steele, J. Chem. Phys. 47, 3029 (1967)
13. Gmelin, Handbuch der anorganischen Chemie, 8A, 1968, p. 189
14. A. Eucken, G. Hoffmann, Z. Physik. Chem. B5, 442 (1929)
15. M. L. McGlashen, D. J. Potter, Proc. Roy. Soc. A267, 478 (1962)
16. J. R. Sweet, Ph.D. Thesis, The Statistical Mechanics of Simple Linear Molecules, Penn State Univ., 1966
17. J. J. Martin, A. Kapoor, Thermodynamic Properties of Chlorine, U. of Michigan Press, Ann Arbor, 1955
18. C. L. Kong, J. Chem. Phys. 53, 1516, 1522 (1970)
19. Z. Kopal, Numerical Analysis, J. Wiley, New York, 1955

20. R. J. Bearman, F. Mandel, J. Chem. Phys. 50, 4121 (1969);
R. O. Watts, J. Chem. Phys. 50, 4122 (1969)
21. D. D. McCracken, W. S. Dorn, Introduction to Fortran Programming,
J. Wiley, New York, 1964
22. IBM System/360 Scientific Subroutine Package, Version III
Programmers' Manual, IBM Publications Dept., New York, 1968
23. D. Shanks, J. Math. Phys. 34, 1 (1955)
24. G. A. Peterson, V. McKoy, J. Chem. Phys. 46, 4362 (1967)
25. Y. D. Chen, W. A. Steele, J. Chem. Phys. 50, 1428 (1969)

PART IV

X-RAY SCATTERING FROM DIATOMICS

Introduction

This paper presents the theoretical x-ray intensity curves for a single component molecular liquid, taking into account angular correlations in the liquid. The principal basis for this work is the Steele and Pecora treatment of scattering from nonspherical molecules¹. The manner of appearance of angular effects is investigated, as is the relative size of such effects. Although other systems are occasionally referred to, the great majority of the work deals with the fluid chlorine system.

Other methods of calculating the x-ray intensity for molecules depend on the early work of Menke² and Zachariasen³, or on the later work of Waser and Schomaker⁴. Menke's equation for the intensity $I(\kappa)$ is

$$I(\kappa) = i_g(\kappa) + 4\pi\rho F_e(\kappa) \int_0^\infty [g(r) - 1] j_0(\kappa r) r^2 dr \quad (1)$$

where

$$F_e(\kappa) = \sum_p \sum_q f_p(\kappa) f_q(\kappa) j_0(\kappa b_q) j_0(\kappa b_p) \quad (2)$$

$i_g(\kappa)$ is the usual gas scattering, $g(r)$ is the molecular distribution function with center c , $f_p(\kappa)$ is the atomic scattering factor of atom p , and b_p is the distance to atom p from center c ⁵.

Equation (1) does not include any angles of orientation of the molecules because orientation has been assumed to be random. DeVries⁶ has shown that this assumption leads to a dependence of $I(\kappa)$ on the coordinate system chosen, i.e., on the location of c . He showed that $E_q(1)$ is approximately true only if the center of the coordinate

system lies near the center of symmetry of a nearly spherical particle. DeVries presented no equations able to handle more nonspherical molecules.

Steele and Pecora¹ (henceforth SP) employed the method of orthonormal D expansion originally developed by Steele⁷ and obtained an expression for the total scattered intensity in terms of harmonically expanded scattering factors and expansion coefficients of an angular dependent molecular distribution function, $g(\underline{R}_1, \underline{R}_2)$. Because angular correlations between molecules are explicitly handled in the SP approach, the center of symmetry restriction discussed by DeVries has been removed as a problem in the treatment of complex molecules. We may therefore replace Eq.(1) with the result obtained by Steele and Pecora and consider the SP result to be currently the best method for dealing with nonspherical molecules.

We add that the molecular method based on the work of Waser and Schomaker, and applied by several authors^{8,9,10,11} is subject to objections on grounds different from the Menke approach, the principal difficulty being that it in general changes the scattering problem into that of multicomponent (mixture) atomic scattering. It gives a radial function which is complexly related through a convolution to a sum over spherical atomic pair distributions rather than a single molecular distribution. Angular information does not appear explicitly, and the study of the effects of angular correlations therefore becomes much more difficult than in the SP approach.

However, several questions remain unanswered in the SP approach, and this paper attempts to answer some of them. Steele and Pecora did

not evaluate their expression for any particular system and so the relative contribution of the angular dependency of $g(\underline{R}_1 \underline{R}_2)$ was quantitatively unknown. In the first two sections below, we have adapted their equation for use with diatomics and have specifically evaluated it for chlorine. Recent work by Sweet and Steele^{11,12}, Chen and Steele¹³, and Morrison and Pings^{14,15} provided the means by which the quantities required for the SP evaluation could be obtained. The diatomic was described by the two-centered Lennard-Jones potential¹¹ and Percus-Yevick results¹⁵ for $g(\underline{R}_1 \underline{R}_2)$ were used to evaluate the SP equation. The location and magnitude of the angular contributions as a function of both density and temperature are presented below. The significance of these contributions in future x-ray work is discussed.

In still another section below, we discuss the problem of inverting molecular x-ray data. Several authors^{6,16} have stated that it is difficult or impossible to invert $E_q(l)$ if $F_e(\kappa)$ has zeros. This problem carries over to the SP equation since a function nearly identical to $F_e(\kappa)$ occurs there as well. We show that these zeros represent no theoretical problem but are quite bothersome in an experimental situation.

Theory

We begin our treatment by recalling that the total scattered intensity of x-rays from a fluid may be written in terms of the pair distribution function. In general this distribution depends on the distances between molecules and their orientation angles. Using orthonormal D function expansions⁷, this distribution may be written

$$g(\underline{R}_1, \underline{R}_2) = 8\pi^2 \sum_{\underline{N}_1} \sum_{\underline{N}_2} g_{\underline{N}_1 \underline{N}_2}(r) D_{\underline{N}_1}(\Omega_1) D_{\underline{N}_2}(\Omega_2) \quad (3)$$

where $\underline{R}_j = (\underline{r}_j, \Omega_j)$ denotes the molecular position of molecule j by vector \underline{r}_j and Ω_j are the Euler angles of orientation.

$\underline{N}_1 = \{J_1, K_1, M_1\}$. Applying Eq.(3) to the usual elastic scattering theory, Steele and Pecora¹ obtained the following expression for the scattering cross section $I(\kappa)$:

$$\begin{aligned} I(\kappa) = & \sum_{M,J} |a_{0,M}^J|^2 + \rho |a_0|^2 \int [g_{\underline{0}\underline{0}}(r) - 1] j_0(\kappa r) 4\pi r^2 dr \\ & + \rho \sum_{\underline{N}_1} \sum_{\underline{N}_2} (-)^{K_1-M_1} a_{0,-M_1}^{*J_1} a_{0,M_2}^{J_2} \sum_J i^J \frac{2J+1}{2J_2+1} c(J, J_1, J_2; 0, 0) \\ & \times c(J, J_1, J_2; 0, K_2) \int g_{-K_2, M_1, K_2, M_2}(r) j_J(\kappa r) 4\pi r^2 dr \end{aligned} \quad (4)$$

The notation used here is the same as that of SP. $a_{0,M}$ denotes a coefficient of the D function expansion of the molecular scattering factor and $c(j_1 j_2 j_3; m_1 m_2)$ denotes a Clebsch-Gordan coefficient¹⁷.

$\kappa = 4\pi \sin \theta / \lambda$. We note that Eq.(4) differs somewhat from that published by SP since we have corrected some index and omission errors. The most important difference is that the factor $(2J+1)/(2J_2+1)$ was not

present in the original paper. Eq.(4) is useful for nonspherical molecules under the assumption that the molecules are rigid; otherwise the Euler angles of orientation lose their meaning. It is apparent therefore, that this equation is useful only for small molecules where the overall length is somewhere on the order of six atoms or less, where bending is negligible¹⁸.

If Eq.(4) is examined, it can be seen that the first summation gives the independent molecule or gas scattering. The second term gives the usual Fourier integral over the (here averaged) pair distribution function. This will be termed the spherical intensity. These two terms correspond to the Menke equation if $|a_0|^2$ is identified with the molecular scattering factor $F_e(\kappa)$. The remainder of the terms give the contribution to the intensity from the angular correlations, henceforth collectively termed angular intensity. It is convenient to rewrite Eq.(4) showing these three parts explicitly.

$$I(\kappa) = i_g(\kappa) + i_s(\kappa) + i_{ang}(\kappa) \quad (5)$$

In this work we wish to evaluate Eq.(4) for a specific system. We have chosen to carry out this evaluation for a diatomic and must therefore adapt Eq.(4) to this system. Following Sweet¹¹ we recognize that, for diatomics, Eq.(3) becomes a sum over spherical harmonics, the indices $M_1, M_2 = 0$, and $K_1 = -K_2$. Thus the summations over N_1 and N_2 in both Eq.(3) and Eq.(4) are restricted to just three indices: J_1, J_2, K_2 . Replacing these with ℓ, ℓ', m respectively, Eq.(4) becomes

$$\begin{aligned}
 I(\kappa) = & \sum_J |a_J|^2 + \rho |a_0|^2 \int [g_{000}(r) - 1] j_0(\kappa r) 4\pi r^2 dr \\
 & + \rho \sum_{\ell}^{\infty} \sum_{\ell'}^{\infty} \sum_{m \atop \ell=\ell' \neq 0} (-)^m a_{\ell}^*(\kappa) a_{\ell'}(\kappa) \sum_{J \atop \Delta\ell, \ell'} \left(\frac{2J+1}{2\ell'+1} \right) (-)^{J/2} c(J, \ell, \ell'; 00) \\
 & \times c(J, \ell, \ell'; 0m) \int g_{\ell\ell'm}(r) j_J(\kappa r) 4\pi r^2 dr
 \end{aligned} \tag{6}$$

where $\Delta\ell, \ell'$ denotes the range $|\ell - \ell'| \leq J \leq \ell + \ell'$ and m takes on the values $-\ell$ to $+\ell$ or $-\ell'$ to $+\ell'$, whichever is the smaller range.

As Eq. (6) stands, it is applicable to both homonuclear and heteronuclear diatomics. For homonuclears ℓ and ℓ' must be even integers and for heteronuclears $\ell + \ell'$ must be even. Since $c(J, \ell, \ell'; 00) = 0$ unless $J + \ell + \ell'$ is even¹⁷, J must also be even for all diatomics. Making use of the symmetry relation $c(j_1 j_2 j_3; m_1 m_2 m_3) = (-)^{j_1 + j_2 - j_3} c(j_1 j_2 j_3; -m_1 -m_2 -m_3)$ we see that even J also requires that

$$c(J\ell\ell'; 0m) = c(J\ell\ell'; 0-m) \tag{7}$$

From these restrictions on ℓ and ℓ' , one may write the first few $g_{\ell\ell'm}(r)$ coefficients. For homonuclear diatomics the first six coefficients are those with the indices 000, 200, 220, 221, 222, 400. Higher coefficients include those with indices in the 400, 600, ... series. For heteronuclear diatomics one also has the 110 and 111 coefficients, as well as higher coefficients in the 300, 500, ... series. Since Eq. (6) contains an infinite number of terms, some truncation must be made and we have therefore included only those terms up through $g_{400}(r)$ in the remainder of this work.

Expanding Eq.(6) up through g_{400} and including only the homonuclear terms, one obtains for the angular intensity:

$$\begin{aligned}
 \rho^{-1} i_{\text{ang}}^{\text{homo}}(\kappa) = & -a_0(\kappa)a_2(\kappa)[c^2(202;00)\langle 020;2\rangle + 5c^2(220;00)\langle 200;2\rangle] \\
 & + a_2^2(\kappa)\left[\frac{1}{5}c^2(022;00)\langle 220;0\rangle - c^2(222;00)\langle 220;2\rangle + \frac{9}{5}c^2(422;00)\langle 220;4\rangle\right. \\
 & - 2\left(\frac{1}{5}\right)c(022;00)c(022;01)\langle 221;0\rangle + 2c(222;00)c(222;01)\langle 221;2\rangle \\
 & - 2\left(\frac{9}{5}\right)c(422;00)c(422;01)\langle 221;4\rangle + 2\left(\frac{1}{5}\right)c(022;00)c(022;02)\langle 222;0\rangle \\
 & - 2c(222;00)c(222;02)\langle 222;2\rangle + 2\left(\frac{9}{5}\right)c(442;00)c(442;02)\langle 222;4\rangle] \\
 & + a_0(\kappa)a_4(\kappa)[9c^2(440;00)\langle 400;4\rangle + c^2(404;00)\langle 040;4\rangle] \quad (8)
 \end{aligned}$$

where $\langle \ell\ell'm;J \rangle = \int g_{\ell\ell'm}(r) j_J(\kappa r) dr$. The factors of two which appear in front of several terms result from the inclusion of two values of $m, \pm m$, for each set of ℓ and ℓ' . Using the identity $g_{\ell\ell'm} = g_{\ell\ell',-m}$ and Eq. (7), it is apparent that the plus and minus terms are equal. All the Clebsch-Gordan coefficients¹⁹ required in Eq.(8) are tabulated in Appendix 4.

Next it is to be noted that the $j_J(\kappa r)$ can be expanded in trigonometric functions. (See Appendix 5 for standard formulas.) Since substitution of these expansions into each Bessel integral above causes each one to be expressed as a sum of sine and cosine Fourier transforms, it is possible to numerically evaluate Eq.(8) at this stage of development. However, if all the sine transform integrands are grouped

together as well as all the cosine integrands, then Eq.(7) may be expressed as a function of just two integrals. This results in the following. Define

$$W_1 = g_{220} - g_{221} - 2g_{222}$$

$$W_2 = \frac{1}{7} g_{220} + \frac{4}{21} g_{221} + \frac{1}{21} g_{222}$$

Then

$$\begin{aligned} \rho^{-1} i_{ang}^{homo}(\kappa) = & 4\pi \int_0^\infty \sin \kappa r \left[\frac{r a_2^2(\kappa)}{5\kappa} (g_{220} - 2g_{221} + 2g_{222}) \right. \\ & + \left(\frac{r}{\kappa} - \frac{3}{\kappa^3 r} \right) (2a_0(\kappa)a_2(\kappa)g_{200} + \frac{2}{7} a_2^2(\kappa)W_1) + \left(\frac{105}{\kappa^5 r^3} - \frac{45}{\kappa^3 r} + \frac{r}{\kappa} \right) \\ & \times \left(\frac{18}{5} a_2^2(\kappa)W_2 + 2a_0(\kappa)a_4(\kappa)g_{400} \right) \Big] dr + 4\pi \int_0^\infty \cos \kappa r \\ & \times \left[\frac{3}{\kappa^2} (2a_0(\kappa)a_2(\kappa)g_{200} + \frac{2}{7} a_2^2(\kappa)W_1) + \left(\frac{10}{\kappa^2} - \frac{105}{\kappa^4 r^2} \right) \right. \\ & \times \left. \left(\frac{18}{5} a_2^2(\kappa)W_2 + 2a_0(\kappa)a_4(\kappa)g_{400} \right) \right] dr \end{aligned}$$

Equation (9) is the result for the homonuclear case. If one wishes to consider the heteronuclear case, then the g_{110} and g_{111} terms must be included as well. Proceeding as before, the following expression for the angular intensity of heteronuclear diatomics may be derived:

$$\begin{aligned} i_{ang}^{hetero}(\kappa) = & 4\pi\rho a_1^2(\kappa) \left\{ \int \left[\frac{r}{\kappa} g_{110} - \frac{2}{\kappa^3 r} (g_{111} + g_{110}) \right] \sin \kappa r dr \right. \\ & \left. + \int \frac{2}{\kappa^2} (g_{111} + g_{110}) \cos \kappa r dr \right\} + i_{ang}^{homo}(\kappa) \end{aligned} \quad (10)$$

The two new integrals in Eq.(10) may be combined with the two in

$i_{\text{ang}}^{\text{homo}}(\kappa)$ to give a final expression involving only two transforms.

It is appropriate at this point to discuss the asymptotic behavior of Eq.(6) as $\kappa \rightarrow 0$ and $\kappa \rightarrow \infty$. In earlier work¹⁴ it was shown that the $a_J(\kappa)$, $J \neq 0$ go to zero as $\kappa \rightarrow 0$. One therefore can see that Eq.(6) reduces to

$$I(0) = |a_0|^2 \left[1 + \rho \int (g_{00}(r) - 1) 4\pi r^2 dr \right] \quad (11)$$

where we have used $j_0(\kappa r) = 1$ at $\kappa = 0$. Steele⁷ has shown that the isothermal compressibility κ_T depends only on the average value of $g(\underline{R}_1 \underline{R}_2)$, i.e., $g_{000}(r)$, and that $\rho k T \kappa_T$ is equal to the bracketed expression above. Thus

$$I(0) = \rho k T \kappa_T N^2 \quad (12)$$

where N is the number of electrons in the molecule. In the case of the region where $\kappa \rightarrow \infty$ one obtains the usual result that the total scattering approaches the gas scattering curve. This results from the fact that for all J , $j_J(\kappa r) \rightarrow 0$ as $\kappa \rightarrow \infty$ and thus all the integrals of Eq.(6) go to zero in this limit.

Numerical Evaluation and Results

It was decided to evaluate Eq.(5) and Eq.(9) for the chlorine molecule. This required a knowledge of the molecular scattering factor coefficients for chlorine and a knowledge of the various $g_{\ell\ell'm}(r)$ as a function of density and temperature. The $a_J(\kappa)$ can be obtained either by MO methods or by the Debye method employing the assumption of independent atomic (IA) scatterers¹⁴. Because of the large atomic number of the chlorine atom and the small percentage of bonding electrons in the molecule, the Debye method was used. As further assurance of the IA assumption, one may note that the gas scattering calculated from the IA approach agrees well with experimental values²⁰. The first three coefficients, $a_0(\kappa)$, $a_2(\kappa)$, and $a_4(\kappa)$, and the gas scattering $i_g(\kappa)$, were calculated; numerical values of these functions are tabulated in Table I and the coefficients have been plotted in Figure 1. It is to be noted that $a_2(\kappa)$ and $a_4(\kappa)$ are both much greater than $a_0(\kappa)$ at the higher scattering angles.

The $g_{\ell\ell'm}(r)$ have been obtained from earlier work¹⁵ where Percus-Yevick solutions were obtained for a two-centered Lennard-Jones potential appropriate to chlorine. The density and temperature ranges covered by that data define the ranges of the x-ray data in this paper. They are: $\rho^* = 0.1$ to 1.2 ; $T^* = 0.75, 1.00, 1.30$. The potential parameters are $\sigma = 3.754\text{\AA}$, $\epsilon = 581.0^\circ\text{K}$ and $R^* = 0.53$. The reduced density and temperature are those defined by Chen and Steele²¹:

$$\rho^* = \frac{2}{3} \pi \sigma^3 \rho \left(1 + \frac{3}{2} R^* - \frac{1}{2} R^{*3}\right)$$

$$T^* = kT/\epsilon \quad (13)$$

TABLE I
Cl₂ Molecular Scattering Factor Coefficients
(IA approximation)

κ	$a_0(\kappa)$	$a_2(\kappa)$	$a_4(\kappa)$	$i_g(\kappa)$
0.0	34.0000	0.0	0.0	1156.0000
0.189	33.7166	-0.1779	0.0001	1136.8400
0.378	32.8813	-0.7012	0.0021	1081.6700
0.567	31.5309	-1.5392	0.0105	996.5640
0.756	29.7195	-2.6436	0.0323	890.2390
0.945	27.5219	-3.9525	0.0760	773.0810
1.134	25.0255	-5.3954	0.1509	655.4080
1.323	22.3219	-6.8988	0.2660	545.9320
1.512	19.5036	-8.3906	0.4288	450.9750
1.701	16.6593	-9.8059	0.6451	374.1040
1.890	13.8686	-11.0904	0.9183	316.1790
2.079	11.1980	-12.2017	1.2496	275.8390
2.268	8.6977	-13.1076	1.6376	250.1470
2.457	6.4055	-13.7881	2.0785	235.4740
2.646	4.3468	-14.2347	2.5670	228.1370
2.835	2.5354	-14.4474	3.0963	224.7940
3.024	0.9753	-14.4332	3.6584	222.7490
3.213	-0.3368	-14.2061	4.2449	220.1190
3.402	-1.4102	-13.7828	4.8467	215.7390
3.591	-2.2582	-13.1799	5.4537	209.0340
3.779	-2.8960	-12.4164	6.0548	199.9780
3.968	-3.3404	-11.5128	6.6391	188.9480
4.157	-3.6091	-10.4900	7.1949	176.5710
4.346	-3.7202	-9.3700	7.7103	163.6040
4.535	-3.6922	-8.1752	8.1735	150.8340
4.724	-3.5435	-6.9286	8.5724	138.9710
4.913	-3.2926	-5.6534	8.8954	128.5840
5.102	-2.9579	-4.3732	9.1313	120.0620
5.291	-2.5579	-3.1119	9.2706	113.5930
5.480	-2.1110	-1.8933	9.3059	109.1660
5.669	-1.6351	-0.7396	9.2317	106.5700
5.858	-1.1473	0.3283	9.0446	105.4330
6.047	-0.6637	1.2917	8.7438	105.2740
6.236	-0.1991	2.1346	8.3312	105.5650
6.425	0.2332	2.8437	7.8115	105.7970
6.614	0.6216	3.4097	7.1929	105.5460
6.803	0.9570	3.8273	6.4869	104.5180
6.992	1.2323	4.0952	5.7073	102.5580

The transform integrals in Eq.(9) and Eq.(5) have been evaluated by both Filon's method²² and the Fast Fourier Transform²³ with equivalent results. Because of the grouping of many terms in the integrand of each transform, it appeared possible that functions might occur which would be difficult to transform. In the case of chlorine, however, we obtained smoothly oscillating integrands which dropped off to less than 1% of their maximum peak value by $r^* = 3.00$ and which became effectively zero by our upper integration limit of $r^* = 6.00$. The transforms were done piecewise, having broken the integrals into the ranges 0 to x_0 and x_0 to 6.00. For most calculations x_0 was equal to 0.70. In the $0 \rightarrow x_0$ range, $g_{000}(r^*) - 1$ was taken as just -1.0 and the integral $\int_0^{x_0} [g_{000}(r^*) - 1] j_0(\kappa r^*) r^{*2} dr^*$ was done analytically. The integrals over the angular correlation functions in the range of 0 to x_0 were identically zero, since the $g_{\ell\ell'm}(\ell, \ell' \neq 0)$ were zero in this range. When $\kappa = 0$, the intensity was calculated by making use of Eq.(12) and substituting values of κ_T from the Percus-Yevick results.

The final intensity data are collected in Tables II-VII. All the tables contain the functions of Eq. (5) as well as the ratio of the angular intensity to the total intensity. Tables II-V summarize the results for four densities at constant temperature. Tables IV, VI, VII summarize the results for three different temperatures at constant density.

Plots of $I(\kappa)$ and $i_g(\kappa) + i(\kappa)$ may be found in Figure 2 for four different densities at $T^* = 0.75$. It is apparent that the angular correlation functions contribute strongly in the region of

TABLE II
X-ray Scattering Functions
 $\rho^*=0.50$ $T^*=0.75$ $R^*=0.53$

κ	$i_g(\kappa)$	$i(\kappa)$	$i_{ang}(\kappa)$	$I(\kappa)$	$\kappa i(\kappa)/a_0^2(\kappa)$	$i_{ang}(\kappa)/I(\kappa)$
0.0	1156.00	1994.06	0.0	3150.06	0.0	0.0
0.189	1136.84	512.79	-0.13	1649.50	0.085	-0.000
0.378	1081.67	-272.44	-1.40	807.83	-0.095	-0.002
0.567	996.56	-400.36	-5.59	590.62	-0.228	-0.009
0.756	890.24	-321.94	-13.86	554.45	-0.276	-0.025
0.945	773.08	-174.78	-23.46	574.84	-0.218	-0.041
1.134	655.41	-24.08	-23.98	607.35	-0.044	-0.039
1.323	545.93	58.43	-6.15	598.22	0.155	-0.010
1.512	450.98	50.64	16.29	517.91	0.201	0.031
1.701	374.10	14.57	22.79	411.46	0.089	0.055
1.890	316.18	-4.10	14.66	326.74	-0.040	0.045
2.079	275.84	-6.18	2.71	272.37	-0.102	0.010
2.268	250.15	-2.92	-6.07	241.15	-0.088	-0.025
2.457	235.47	-0.44	-9.10	225.93	-0.026	-0.040
2.646	228.14	0.22	-7.21	221.15	0.031	-0.033
2.835	224.79	0.12	-3.03	221.88	0.051	-0.014
3.024	222.75	0.01	1.01	223.77	0.037	0.005
3.213	220.12	0.00	3.31	223.43	0.007	0.015
3.402	215.74	-0.01	3.21	218.94	-0.016	0.015
3.591	209.03	-0.03	1.37	210.38	-0.022	0.007
3.779	199.98	-0.03	-0.57	199.38	-0.013	-0.003
3.968	188.95	-0.01	-1.36	187.57	-0.004	-0.007
4.157	176.57	0.01	-0.88	175.70	0.004	-0.005
4.346	163.60	0.02	0.09	163.72	0.007	0.001
4.535	150.83	0.02	0.66	151.51	0.006	0.004
4.724	138.97	0.01	0.52	139.49	0.003	0.004
4.913	128.58	0.00	-0.01	128.58	0.001	-0.000
5.102	120.06	-0.00	-0.38	119.68	-0.001	-0.003
5.291	113.59	-0.00	-0.37	113.22	-0.002	-0.003
5.480	109.17	-0.00	-0.14	109.03	-0.002	-0.001
5.669	106.57	-0.00	0.07	106.64	-0.002	0.001
5.858	105.43	-0.00	0.13	105.56	-0.001	0.001
6.047	105.27	0.00	0.07	105.34	0.001	0.001
6.236	105.57	0.00	0.01	105.58	0.001	0.000
6.425	105.80	0.00	0.01	105.81	0.001	0.000
6.614	105.55	0.00	0.04	105.58	0.002	0.000
6.803	104.52	0.00	0.04	104.56	0.001	0.000
6.992	102.56	-0.00	0.01	102.57	-0.000	0.000

TABLE III
X-ray Scattering Functions
 $\rho^*=0.80$ $T^*=0.75$ $R^*=0.53$

κ	$i_g(\kappa)$	$i(\kappa)$	$i_{ang}(\kappa)$	$I(\kappa)$	$\kappa i(\kappa)/a_0^2(\kappa)$	$i_{ang}(\kappa)/I(\kappa)$
0.0	1155.00	1125.57	0.0	2281.57	0.0	0.0
0.189	1136.84	29.44	-0.16	1166.12	0.005	-0.000
0.378	1081.67	-509.21	-1.65	570.81	-0.178	-0.003
0.567	996.56	-561.26	-6.74	428.56	-0.320	-0.016
0.756	890.24	-449.71	-17.75	422.78	-0.385	-0.042
0.945	773.08	-266.82	-33.41	472.85	-0.333	-0.071
1.134	655.41	-59.12	-40.29	555.99	-0.107	-0.072
1.323	545.93	81.09	-16.07	610.95	0.215	-0.026
1.512	450.98	82.54	24.25	557.76	0.328	0.043
1.701	374.10	25.39	37.48	436.97	0.156	0.086
1.890	316.18	-5.79	24.73	335.11	-0.057	0.074
2.079	275.84	-9.61	5.89	272.12	-0.159	0.022
2.268	250.15	-4.65	-8.59	236.91	-0.139	-0.036
2.457	235.47	-0.78	-14.52	220.17	-0.047	-0.066
2.646	228.14	0.31	-12.24	216.21	0.044	-0.057
2.835	224.79	0.18	-5.67	219.31	0.081	-0.026
3.024	222.75	0.02	1.11	223.88	0.061	0.005
3.213	220.12	0.00	5.29	225.41	0.014	0.023
3.402	215.74	-0.01	5.42	221.14	-0.024	0.025
3.591	209.03	-0.05	2.46	211.44	-0.034	0.012
3.779	199.98	-0.05	-0.80	199.13	-0.022	-0.004
3.968	188.95	-0.02	-2.19	186.74	-0.007	-0.012
4.157	176.57	0.02	-1.46	175.12	0.005	-0.008
4.346	163.60	0.04	0.12	163.76	0.011	0.001
4.535	150.83	0.03	1.08	151.94	0.010	0.007
4.724	138.97	0.01	0.86	139.85	0.005	0.006
4.913	128.58	0.00	-0.00	128.58	0.001	-0.000
5.102	120.06	-0.00	-0.63	119.43	-0.001	-0.005
5.291	113.59	-0.00	-0.64	112.95	-0.003	-0.006
5.480	109.17	-0.00	-0.24	108.92	-0.004	-0.002
5.669	106.57	-0.00	0.12	106.69	-0.003	0.001
5.858	105.43	-0.00	0.21	105.64	-0.002	0.002
6.047	105.27	0.00	0.12	105.39	0.000	0.001
6.236	105.57	0.00	0.02	105.59	0.001	0.000
6.425	105.80	0.00	0.02	105.82	0.002	0.000
6.614	105.55	0.00	0.06	105.61	0.003	0.001
6.803	104.52	0.00	0.07	104.59	0.002	0.001
6.992	102.56	-0.00	0.02	102.57	-0.000	0.000

TABLE IV
X-ray Scattering Functions
 $\rho^*=1.20$ $T^*=0.75$ $R^*=0.53$

κ	$i_g(\kappa)$	$i(\kappa)$	$i_{ang}(\kappa)$	$I(\kappa)$	$\kappa i(\kappa)/a_0^2(\kappa)$	$i_{ang}(\kappa)/I(\kappa)$
0.0	1156.00	-486.67	0.0	669.33	0.0	0.0
0.189	1136.84	-669.84	-0.14	466.86	-0.111	-0.000
0.378	1081.67	-773.99	-1.66	306.02	-0.271	-0.005
0.567	996.56	-727.80	-7.29	261.47	-0.415	-0.028
0.756	890.24	-594.22	-20.88	275.13	-0.509	-0.076
0.945	773.08	-392.21	-44.59	336.28	-0.489	-0.133
1.134	655.41	-137.74	-66.08	451.59	-0.249	-0.146
1.323	545.93	88.11	-42.48	591.57	0.234	-0.072
1.512	450.98	135.61	32.44	619.03	0.539	0.052
1.701	374.10	49.07	64.69	487.87	0.301	0.133
1.890	316.18	-6.41	44.12	353.89	-0.063	0.125
2.079	275.84	-14.72	13.46	274.58	-0.244	0.049
2.268	250.15	-7.60	-11.14	231.41	-0.228	-0.048
2.457	235.47	-1.58	-23.45	210.44	-0.095	-0.111
2.646	228.14	0.35	-21.75	206.74	0.049	-0.105
2.835	224.79	0.28	-11.45	213.63	0.125	-0.054
3.024	222.75	0.03	0.36	223.15	0.109	0.002
3.213	220.12	0.00	8.50	228.62	0.034	0.037
3.402	215.74	-0.02	9.61	225.33	-0.034	0.043
3.591	209.03	-0.08	4.73	213.69	-0.053	0.022
3.779	199.98	-0.08	-1.00	198.90	-0.038	-0.005
3.968	188.95	-0.04	-3.55	185.36	-0.015	-0.019
4.157	176.57	0.01	-2.50	174.08	0.004	-0.014
4.346	163.60	0.05	0.10	163.76	0.016	0.001
4.535	150.83	0.05	1.80	152.69	0.018	0.012
4.724	138.97	0.02	1.50	140.49	0.009	0.011
4.913	128.58	0.00	0.02	128.61	0.002	0.000
5.102	120.06	-0.00	-1.11	118.95	-0.000	-0.009
5.291	113.59	-0.00	-1.15	112.44	-0.003	-0.010
5.480	109.17	-0.01	-0.46	108.70	-0.007	-0.004
5.669	106.57	-0.00	0.19	106.75	-0.007	0.002
5.858	105.43	-0.00	0.37	105.80	-0.003	0.004
6.047	105.27	-0.00	0.22	105.49	-0.000	0.002
6.236	105.57	0.00	0.05	105.61	0.001	0.000
6.425	105.80	0.00	0.04	105.84	0.004	0.000
6.614	105.55	0.00	0.12	105.67	0.006	0.001
6.803	104.52	0.00	0.13	104.65	0.005	0.001
6.992	102.56	0.00	0.04	102.60	0.001	0.000

TABLE V
X-ray Scattering Functions
 $\rho^*=1.50$ $T^*=0.75$ $R^*=0.53$

κ	$i_g(\kappa)$	$i(\kappa)$	$i_{ang}(\kappa)$	$I(\kappa)$	$\kappa i(\kappa)/a_0^2(\kappa)$	$i_{ang}(\kappa)/I(\kappa)$
0.0	1156.00	-890.63	0.0	265.37	0.0	0.0
0.189	1136.84	-923.66	-0.12	213.06	-0.154	-0.001
0.378	1081.67	-905.89	-1.52	174.27	-0.317	-0.009
0.567	996.56	-824.12	-7.15	165.29	-0.470	-0.043
0.756	890.24	-684.47	-21.98	183.79	-0.586	-0.120
0.945	773.08	-484.96	-51.52	236.60	-0.605	-0.218
1.134	655.41	-223.63	-88.86	342.92	-0.405	-0.259
1.323	545.93	55.04	-79.91	521.07	0.146	-0.153
1.512	450.98	181.94	30.11	663.02	0.723	0.045
1.701	374.10	83.21	98.57	555.88	0.510	0.177
1.890	316.18	-3.67	68.79	381.30	-0.036	0.180
2.079	275.84	-19.19	23.94	280.59	-0.318	0.085
2.268	250.15	-10.73	-12.02	227.41	-0.322	-0.053
2.457	235.47	-2.69	-32.68	200.10	-0.161	-0.163
2.646	228.14	0.24	-33.12	195.25	0.033	-0.170
2.835	224.79	0.37	-19.36	205.80	0.162	-0.094
3.024	222.75	0.05	-1.77	221.03	0.167	-0.008
3.213	220.12	0.00	11.66	231.79	0.067	0.050
3.402	215.74	-0.02	14.76	230.48	-0.036	0.064
3.591	209.03	-0.10	7.83	216.76	-0.072	0.036
3.779	199.98	-0.12	-0.95	198.91	-0.056	-0.005
3.968	188.95	-0.08	-4.98	183.88	-0.030	-0.027
4.157	176.57	-0.01	-3.69	172.87	-0.003	-0.021
4.346	163.60	0.07	0.02	163.69	0.021	0.000
4.535	150.83	0.08	2.59	153.51	0.028	0.017
4.724	138.97	0.04	2.25	141.26	0.015	0.016
4.913	128.58	0.01	0.06	128.65	0.004	0.000
5.102	120.06	0.00	-1.68	118.38	0.003	-0.014
5.291	113.59	-0.00	-1.79	111.80	-0.001	-0.016
5.480	109.17	-0.01	-0.76	108.40	-0.010	-0.007
5.669	106.57	-0.01	0.25	106.82	-0.013	0.002
5.858	105.43	-0.00	0.57	106.00	-0.007	0.005
6.047	105.27	-0.00	0.34	105.62	-0.002	0.003
6.236	105.57	0.00	0.08	105.65	0.001	0.001
6.425	105.80	0.00	0.07	105.86	0.006	0.001
6.614	105.55	0.00	0.19	105.74	0.011	0.002
6.803	104.52	0.00	0.22	104.74	0.009	0.002
6.992	102.56	0.00	0.08	102.64	0.002	0.001

TABLE VI
X-ray Scattering Functions
 $\rho^*=1.20$ $T^*=1.00$ $R^*=0.53$

κ	$i_g(\kappa)$	$i(\kappa)$	$i_{ang}(\kappa)$	$I(\kappa)$	$\kappa i(\kappa)/a_0^2(\kappa)$	$i_{ang}(\kappa)/I(\kappa)$
0.0	1156.00	-748.10	0.0	407.90	0.0	0.0
0.189	1136.84	-795.73	-0.12	340.99	-0.132	-0.000
0.378	1081.67	-806.97	-1.56	273.14	-0.282	-0.006
0.567	996.56	-733.27	-7.05	256.24	-0.418	-0.028
0.756	890.24	-589.12	-20.18	280.95	-0.504	-0.072
0.945	773.08	-380.95	-42.37	349.76	-0.475	-0.121
1.134	655.41	-125.21	-60.82	469.38	-0.227	-0.130
1.323	545.93	90.61	-36.84	599.70	0.241	-0.061
1.512	450.98	126.20	29.00	606.17	0.502	0.048
1.701	374.10	44.76	56.30	475.17	0.274	0.118
1.890	316.18	-5.52	39.14	349.80	-0.054	0.112
2.079	275.84	-13.37	12.79	275.26	-0.222	0.046
2.268	250.15	-7.02	-8.45	234.68	-0.211	-0.036
2.457	235.47	-1.52	-19.32	214.64	-0.091	-0.090
2.646	228.14	0.29	-18.57	209.85	0.041	-0.089
2.835	224.79	0.25	-10.52	214.53	0.111	-0.049
3.024	222.75	0.03	-0.87	221.91	0.099	-0.004
3.213	220.12	0.00	6.22	226.34	0.035	0.027
3.402	215.74	-0.01	7.99	223.71	-0.026	0.036
3.591	209.03	-0.07	4.68	213.65	-0.047	0.022
3.779	199.98	-0.08	-0.07	199.83	-0.036	-0.000
3.968	188.95	-0.04	-2.74	186.17	-0.014	-0.015
4.157	176.57	0.01	-2.41	174.17	0.003	-0.014
4.346	163.60	0.04	-0.39	163.25	0.013	-0.002
4.535	150.83	0.04	1.27	152.15	0.015	0.008
4.724	138.97	0.02	1.41	140.40	0.009	0.010
4.913	128.58	0.01	0.38	128.97	0.002	0.003
5.102	120.06	-0.00	-0.65	119.41	-0.001	-0.005
5.291	113.59	-0.00	-0.93	112.66	-0.002	-0.008
5.480	109.17	-0.00	-0.53	108.63	-0.004	-0.005
5.669	106.57	-0.00	-0.01	106.56	-0.005	-0.000
5.858	105.43	-0.00	0.23	105.67	-0.003	0.002
6.047	105.27	-0.00	0.18	105.45	-0.001	0.002
6.236	105.57	0.00	0.05	105.61	0.001	0.000
6.425	105.80	0.00	0.02	105.82	0.002	0.000
6.614	105.55	0.00	0.08	105.63	0.004	0.001
6.803	104.52	0.00	0.12	104.63	0.004	0.001
6.992	102.56	0.00	0.07	102.63	0.002	0.001

TABLE VII
X-ray Scattering Functions
 $\rho^*=1.20$ $T^*=1.30$ $R^*=0.53$

κ	$i_g(\kappa)$	$i(\kappa)$	$i_{ang}(\kappa)$	$I(\kappa)$	$\kappa i(\kappa)/a_0^2(\kappa)$	$i_{ang}(\kappa)/I(\kappa)$
0.0	1156.00	-836.47	0.0	319.53	0.0	0.0
0.189	1136.84	-848.96	-0.10	287.78	-0.141	-0.000
0.378	1081.67	-826.07	-1.49	254.11	-0.289	-0.006
0.567	996.56	-737.16	-6.83	252.58	-0.420	-0.027
0.756	890.24	-584.96	-19.51	285.77	-0.501	-0.068
0.945	773.08	-371.90	-40.48	360.70	-0.464	-0.112
1.134	655.41	-116.26	-56.82	482.33	-0.210	-0.118
1.323	545.93	90.00	-33.42	602.51	0.239	-0.055
1.512	450.98	118.24	25.53	594.74	0.470	0.043
1.701	374.10	42.18	50.19	466.48	0.259	0.108
1.890	316.18	-4.37	35.93	347.74	-0.043	0.103
2.079	275.84	-12.18	12.75	276.41	-0.202	0.046
2.268	250.15	-6.59	-6.19	237.37	-0.197	-0.026
2.457	235.47	-1.51	-16.23	217.73	-0.090	-0.075
2.646	228.14	0.22	-16.35	212.01	0.031	-0.077
2.835	224.79	0.22	-10.00	215.02	0.099	-0.046
3.024	222.75	0.03	-1.88	220.90	0.092	-0.009
3.213	220.12	0.00	4.52	224.64	0.037	0.020
3.402	215.74	-0.01	6.78	222.51	-0.018	0.030
3.591	209.03	-0.06	4.62	213.59	-0.042	0.022
3.779	199.98	-0.08	0.63	200.54	-0.034	0.003
3.968	188.95	-0.04	-2.07	186.84	-0.015	-0.011
4.157	176.57	0.00	-2.26	174.31	0.001	-0.013
4.346	163.60	0.03	-0.74	162.90	0.010	-0.005
4.535	150.83	0.04	0.83	151.71	0.013	0.005
4.724	138.97	0.02	1.27	140.27	0.009	0.009
4.913	128.58	0.01	0.60	129.19	0.003	0.005
5.102	120.06	-0.00	-0.31	119.75	-0.000	-0.003
5.291	113.59	-0.00	-0.73	112.86	-0.002	-0.006
5.480	109.17	-0.00	-0.54	108.62	-0.003	-0.005
5.669	106.57	-0.00	-0.13	106.44	-0.004	-0.001
5.858	105.43	-0.00	0.13	105.56	-0.003	0.001
6.047	105.27	-0.00	0.14	105.41	-0.001	0.001
6.236	105.57	0.00	0.05	105.61	0.000	0.000
6.425	105.80	0.00	0.01	105.81	0.001	0.000
6.614	105.55	0.00	0.05	105.60	0.002	0.000
6.803	104.52	0.00	0.10	104.61	0.003	0.001
6.992	102.56	0.00	0.08	102.64	0.002	0.001

$\kappa = 1.0$ to 3.5 . Shifts of the main peak as $i_{\text{ang}}(\kappa)$ is included are noticeable at all densities and always seem to be in the direction of higher κ . The main peak height of the $i_g(\kappa) + i(\kappa)$ curve is decreased at lower densities by $i_{\text{ang}}(\kappa)$ and is increased at higher densities. To show the differences between intensities including and excluding $i_{\text{ang}}(\kappa)$ more clearly, $\kappa i(\kappa)$ vs. $\kappa[i(\kappa) + i_{\text{ang}}(\kappa)]$ for $\rho^* = 1.2$, $T^* = 0.75$ has been plotted in Figure 3. It is clear that the spherical intensity contribution occurs only in the region of the first $I(\kappa)$ peak and the valley which follows. The angular intensity, however, is a significant contribution out to a small third peak.

Other density effects on the total scattering curve can also be seen in Figure 2. As expected, the curves show a strong increase in structure with density. The main peak shifts to higher κ with increasing density, reflecting closer packing of the molecules. It may also be seen that the $I(0)$ values given by Eq(12) decrease with increasing density over the range covered by these graphs, reflecting the trend to lower compressibilities of increasingly dense fluids. Although not shown here, it was also found that decreasing the density below $\rho^* = 0.5$ produces a decrease in these intercept values, finally approaching N^2 at zero density. The fact that a maximum occurs in the intercept values merely reflects a density region where critical behavior is becoming observable.

For all states covered in this work, the percentage contribution of the angular intensity to the total scattered intensity has been determined. Experimental errors in liquid diffraction work are in the range of ± 2 to 5% and these percentages must be surpassed if angular

contributions are to be experimentally measurable. From Tables II-V it can be seen that at $T^* = 0.75$ the angular contributions amount to 4 to 5% maximum at $\rho^* = 0.5$, 7 to 8% at $\rho^* = 0.8$, 13 to 14% at $\rho^* = 1.2$, and 17 to 20% at $\rho^* = 1.5$. These percentages occur primarily on the main peak. The contributions in the region of the second minima run 2 to 3% less than these figures. It is clear that these percentages, particularly at higher densities, exceed experimental error.

In Figure 4 one can observe the effect of temperature on total intensity. Data have been plotted for $\rho^* = 1.2$ and $T^* = 0.75, 1.30$, and the low κ part of $T^* = 1.00$. Only the lower section of the $T^* = 1.00$ curve was plotted since this is the only region where the curve does not fit closely between the other two temperatures. The small differences that do occur beyond $\kappa = 2.2$ are primarily due to changes in the angular intensity since the spherical contribution is practically zero in this range. Because temperature differences are relatively small at higher κ , it was concluded that over our range of states temperature is a weak variable.

We have selectively included the various angular $g_{\ell\ell'm}(r)$ in the intensity calculations in order to find which ones are most significant. The state chosen was $\rho^* = 1.2$, $T^* = 0.75$, and the results are plotted in Figures 5 and 6. Figure 5 shows the fluid intensity function $\kappa[i(\kappa) + i_{\text{ang}}(\kappa)]$ as a function of the $g_{\ell\ell'm}$. Figure 6 shows the dependence of the total intensity on the $g_{\ell\ell'm}$. It is found that if just g_{400} is set equal to zero, the $\kappa[i(\kappa) + i_{\text{ang}}(\kappa)]$ curve differs only slightly from the case where all the $g_{\ell\ell'm}$ are

included. Compare curves 3 and 4 of Figure 5. The total intensity curve changed by an amount too small to be seen on the scale of Figure 6. Differences in $I(\kappa)$ were limited to less than 0.6% in the range below 4.0\AA^{-1} ; the greatest differences occurred between 4.0 and 6.0\AA^{-1} but at no time exceeded 1%. In the case of $i_{\text{ang}}(\kappa)$, it was apparent that large changes occurred beyond 4.0\AA^{-1} when g_{400} was set equal to zero. These changes, however, did not show up in the total intensity for our $\rho^* = 1.2$ state, since beyond 4.0\AA^{-1} the entire $i_{\text{ang}}(\kappa)$ accounted for only 1% or less of the total scattered radiation. At still higher densities than studied here, it is expected that the contribution of $i_{\text{ang}}(\kappa)$ will increase and errors in it due to the omission of $g_{400}(r)$ will become more important.

The 200 series $g_{\ell\ell'm}(r)$ contributes most heavily to the intensity curves in the range $\kappa = 0.9$ to 3.8\AA^{-1} . Differences in total intensity between the curves when all the $g_{\ell\ell'm}$ are included and when g_{221} , g_{222} are zero are quite small, amounting to no more than 1% and typically being lower at about 0.5%. When g_{220} is also zero (Figure 6, curve 3), differences reach as high as 8% and typically run about 4 or 5% in the region of $\kappa = 2.0$ to 3.0 . Finally when g_{200} is set equal to zero as well (Figure 6, curve 1), the full difference between $I(\kappa)$ and $i_g(\kappa) + i(\kappa)$ is obtained (except for a negligible g_{400} contribution). Note the large effect of g_{200} on the main peak. One may therefore view the dense fluid contribution to the chlorine intensity as being determined to first order by just g_{000} , g_{200} , and g_{220} .

Comparison of our intensity curves with presently available experimental data is quite limited. The only data known to us is the

work of Gamertsfelder²⁴. Only one state was studied and that was the liquid along the coexistence curve at 25°C, a state with a much higher density and lower temperature than any of our states. Nevertheless a comparison was made in which it was found that our state of $\rho^* = 1.5$, $T^* = 0.75$ had peak locations of 1.53, 3.32 whereas Gamertsfelder's state had locations of 1.53, 3.58 . The agreement of first peak locations is encouraging, but since extrapolation of either set of data to a common density is not possible, little more than a generally correct range is indicated. Furthermore, there are probably significant errors in the experimental data due to the outdated techniques.

The program we have used was checked in part by calculating the total intensity curve from a $g(r)$ for one of the thermodynamic states of argon and comparing it with the results of an earlier calculation²⁵. The two calculations were in agreement, indicating that the spherical intensity terms $i_g(\kappa)$ and $i(\kappa)$ were being computed properly. The mere existence of our $I(\kappa)$ second peak in the same general area as the experimental second peak provides confidence in the angular section of the program. From Figure 2 one can see that the spherical intensity does not account for this peak at all and shows little tendency to do so even at the highest density. Since the spherical intensity looks so little like the experimental data and yet the total curve does, it would appear that the angular contributions are qualitatively correct.

Inversion of Data

If one attempts to obtain a single function of all the $g_{\ell\ell'm}(r)$ from Eq.(4) by the usual method of Fourier transformation, it is found that this equation does not easily lend itself to such an approach. The principal problem is that the trigonometric expansions of the $j_J(\kappa r)$ which appear in the angular intensity integrals lead to sums of terms involving $1/\kappa^n \sin \kappa r$ or $1/\kappa^n \cos \kappa r$, where n takes on various values. The equation may not then be separated with κ dependence on one side and a typical Fourier integral over an r dependent function on the other, thereby allowing the Fourier transform to be taken, since there is no single κ^n multiplier which will lead to this form.

Instead an alternative approach may be taken. It is workable from a purely theoretical standpoint but will prove difficult to use in experimental situations. We first describe the approach and then turn to the practical difficulties of applying it.

The approach is to calculate the higher $g_{\ell\ell'm}(r)$ and $i_{ang}(\kappa)$ from theory and then to determine $g_{000}(r)$ by Fourier transformation of the equation

$$\kappa[I(\kappa) - i_g(\kappa) - i_{ang}(\kappa)] = 4\pi\rho|a_0|^2 \int_0^{\infty} r[g_{000}(r) - 1]\sin \kappa r dr \quad (14)$$

It is known that an x-ray experiment will determine only one function uniquely²⁶, and hence we have written an equation which will yield just one particular $g_{\ell\ell'm}(r)$. We single out $g_{000}(r)$ for Fourier determination (rather than direct theoretical evaluation) because it is the

largest contributor of all the $g_{\ell\ell'm}$ to the total scattered intensity.

Setting $\kappa i(\kappa)$ equal to the left hand side of Eq(14), Fourier inversion will lead to

$$r[g_{000}(r) - 1] = \frac{1}{2\pi^2 \rho} \int_0^\infty \frac{\kappa i(\kappa)}{|a_0|^2} \sin \kappa r \, d\kappa \quad (15)$$

which is the form of the transformation equation used in spherical systems. The calculation of $g_{000}(r)$ is possible if Eq(15) can be evaluated. Certainly if $a_0(\kappa)$ has no zeros, as in the case of H_2O with molecular center at the oxygen atom²⁷, the integral can be evaluated by standard Fourier techniques. In general, however, $a_0(\kappa)$ does have zeros¹⁴ and it must be shown that they do not mathematically prevent the inversion.

Rao¹⁶ has stated that zeros in the $F_e(\kappa)$ of the Menke equation lead to singularities in the Fourier kernel and prevent the inversion of the intensity data. Theoretically, however, such singularities never occur. From Eq(14) it can be seen that $\kappa i(\kappa)$ must be zero whenever $a_0(\kappa)$ is zero. The ratio $\kappa i(\kappa)/|a_0|^2$ is therefore of the form "0/0" and is indeterminate, not singular. The form of this ratio at the n^{th} root of $a_0(\kappa)$, κ_n , is determined by recognizing that the ratio is given by the integral on the right hand side of Eq(14). If the integral is Taylor expanded about the root κ_n , then to first order the integral is given by $c_{1n}\kappa + c_{2n}$.

If one has extremely accurate data for $\kappa i(\kappa)$ and $|a_0|^2$, c_{1n} and c_{2n} may be determined numerically from curve fitting the data in the region of the zero. $\kappa i(\kappa)$ may be fitted by $A_{1n}(\kappa - \kappa_n)^3 +$

$A_{2n}(\kappa - \kappa_n)^2$ and $|a_0(\kappa)|^2$ may be fitted by $A_{3n}(\kappa - \kappa_n)^2$. Note that both curves have zero slope at the root point as is required by the derivative of $|a_0(\kappa)|^2 = F(\kappa)$, $F'(\kappa) = 2|a_0(\kappa)||a_0(\kappa)|'$. Taking the ratio of these curves and rearranging, one obtains

$$c_{1n} = \frac{A_{1n}}{A_{3n}}, \quad c_{2n} = \frac{A_{2n}}{A_{3n}} - \frac{A_{1n}}{A_{3n}} \kappa_n.$$

Eq(15) may then be evaluated by breaking the integral into sections, splitting out the regions around the zeros of $a_0(\kappa)$ and representing them by $c_{1n}\kappa + c_{2n}$. The result is

$$\begin{aligned} 2\pi^2 \text{pr}[g_{000}(r) - 1] &= \sum_{n=0}^{n_u} \int_{\kappa_n - \epsilon}^{\kappa_{n+1} - \epsilon} \frac{\kappa i(\kappa)}{|a_0|^2} \sin \kappa r \, d\kappa \\ &+ \sum_{n=1}^{n_u} \left\{ \frac{2c_{1n}}{r} (\kappa_n r \sin \kappa_n r \sin \epsilon r - \epsilon r \cos \kappa_n r \cos \epsilon r + \cos \kappa_n r \sin \epsilon r) \right. \\ &\quad \left. + \frac{2c_{2n}}{r} \sin \kappa_n r \sin \epsilon r \right\} \end{aligned} \quad (16)$$

where the interval about each zero is $\kappa_n - \epsilon$ to $\kappa_n + \epsilon$, $\kappa_0 \equiv -\epsilon$, n_u denotes the upper root considered, and $\kappa_{n_u+1} - \epsilon$ has been chosen as the truncation value of the integral.

While formulas of the type of Eq(16) may be derived to handle the Fourier inversion, they are difficult to apply to real experimental data. The difficulty arises when one realizes that the quantity

$$i^{\text{exptl}}(\kappa) = I^{\text{exptl}}(\kappa) - i_g(\kappa) - i_{\text{ang}}(\kappa)$$

will seldom give zeros at the root points of $a_0(\kappa)$, yet this condition must be met if inversion is to be accurate. The combination of experimental and normalization error in $I^{\text{exptl}}(\kappa)$ and the error due

to an incorrect theoretical potential in the calculation of $i_{\text{ang}}(\kappa)$ are the principal sources of trouble.

In the case of chlorine the situation is quite bad. The quantity $\kappa i(\kappa)$ is given by the dotted line of Figure 3 and clearly becomes a very small number after $\kappa = 2.7\text{\AA}^{-1}$. However, $|a_0(\kappa)|^2$ also becomes quite small beyond this value of κ and the ratio $\kappa i(\kappa) / |a_0|^2$ is considerably longer ranged, as may be seen in Figure 7. Even a slight error in the calculation of $i^{\text{exptl}}(\kappa)$ will therefore lead to great errors in the transform function beyond $\kappa = 2.7\text{\AA}^{-1}$. Since $i_{\text{ang}}(\kappa)$ accounts for nearly all of the chlorine intensity in this high κ region, accurate inversion would require us to calculate $i_{\text{ang}}(\kappa)$ for chlorine to a very high degree of accuracy and with our present knowledge of angular potentials and fluid equations of state, this is virtually impossible. We must therefore conclude that while inversion of Eq(19) is possible, experimental inversion is not in general practical.

Discussion

It has been seen that angular correlations play a significant role in determining the x-ray scattering pattern of chlorine. The fact that these correlations become apparent in the case of chlorine is traceable to the relatively large length to width ratio of the molecule and an increased likelihood of a rodlike packing arrangement. It is also related to the forms of the scattering factor coefficients. As seen in Figure 1, $a_0(\kappa)$ drops off rapidly at higher κ while $a_2(\kappa)$ and $a_4(\kappa)$ are quite large. From Eq.(6) it can be seen that this causes the spherical intensity to drop off at high κ while the angular intensity increases as its $a_2(\kappa)$ and $a_4(\kappa)$ factors increase.

In the region of $\kappa = 3.2\text{\AA}^{-1}$, where the second peak appears in the total intensity spectrum, chlorine is a somewhat special diatomic in that the $a_2(\kappa)$ term is much larger, by nearly an order of magnitude, than the $a_0(\kappa)$. Even $a_4(\kappa)$ is larger than $a_0(\kappa)$ in this range. Other molecules, such as nitrogen¹⁴, do not show this $a_2(\kappa)$ dominance until well beyond the second peak where fluid structure contributions are diminishing²⁸. A short bond length in nitrogen is responsible for this occurrence.

Because angular correlations do contribute noticeably to the spectrum of chlorine, it is to be expected that they will play important roles in determining the scattering behavior of certain other polyatomic molecules. In the case of molecules of more extreme length, the higher $a_j(\kappa)$ will dominate the $a_0(\kappa)$ coefficient in even lower regions of space provided atoms of great scattering power are not located near the center of the molecule. Also, the higher order

$g_{\ell\ell'm}$ should be larger due to increased repulsive overlap in certain orientations. Polar molecules will have the added contributions to the angular intensity from $g_{110}(r)$ and $g_{111}(r)$ type terms as indicated in Eq(10). Applying the modified Stockmayer potential to a moderate length and moderate strength molecule ($t^* = 1.0$, $R^* = 0.4$), Sweet²⁹ showed that it would yield $g_{110}(r)$ and $g_{111}(r)$ functions which are greater in magnitude than the g_{200} term. These should therefore be strong contributors to the scattering expression, and preliminary calculations in this laboratory on methyl fluoride show this to be true.

The angular intensity results for chlorine show that, in general, one must interpret the total intensity spectra for molecules in terms of both spherical and angular contributions. In particular they indicate that one must be quite careful in applying the Menke and Zachariasen theory since the total intensity expression of that theory only includes spherical terms. Furthermore the chlorine results show that the total intensity curve will not necessarily contain features that will immediately suggest whether or not angular correlation effects should be taken into account since the total intensity curves obtained are qualitatively quite similar to those obtained for spherical systems³⁰.

The various sources of error in this calculation must now be considered. One such source is the original choice of potential. This choice has been discussed previously¹⁵, but it should be stressed again that the particular choice of R (the interaction separation distance) may be critical. If a much shorter potential separation

distance such as that used by Sweet¹² had been chosen for chlorine, the percentage contribution of the angular intensity would have been decreased, possibly down to the region of experimental error. The shorter separation distance would then have required one to proceed to longer molecules, particularly those with strong scattering centers near the ends, in order to find a system from which one could obtain a percentage contribution of the size found in this work.

Another possible source of error is the basic Percus-Yevick approximation, but the past agreement between the Fourier transforms of Percus-Yevick spherical distribution functions and the corresponding molecular dynamics transforms^{25,31} implies that the error is small for our nonspherical case. A more likely source of error for the present work is the inaccuracy of the computed $g_{\ell\ell'm}$ resulting from truncation of the $H(\underline{R}_1\underline{R}_2)$ series in numerically solving the Percus-Yevick integral equations¹⁵. To determine the size of such truncation errors in our intensity results, $g_{\ell\ell'm}$ functions obtained from two different $H(\underline{R}_1\underline{R}_2)$ truncations were used to calculate the total intensity at $\rho^* = 1.0$, $T^* = 0.75$. The two functions differed by less than 2% up to $\kappa = 0.35 \text{ \AA}^{-1}$ and by less than 1% above this κ value.

It is possible that the SP equation might be useful in future research for examining the accuracy of diatomic potentials. One route of investigation would be to see how well a given potential, assumed not vastly different from the one used here, would predict the form of the intensity curve in regions of high angular contribution when combined with a suitable equation of state such as the Percus-Yevick theory. However, if the intensity for nonspherical molecules shows as

weak a dependence on the detailed form of the intermolecular potential as the intensity for argon shows²⁵, useful information about the potential may be obtained only with great difficulty. The fact that the total intensity for chlorine appears qualitatively similar to that for argon suggests that a potential possessing no angular dependence at all may be found which will account for the intensity, thus indicating that a weak intensity-potential dependence may indeed be the case. The alternative route of obtaining $g_{000}(r)$ from $i^{\text{exptl}}(\kappa)$ and Eq(15) and comparing it with a theoretical $g_{000}(r)$ will also be very difficult due to the inversion difficulties.

In summary, we have shown that angular correlations can play a role in the molecular scattering of x-rays and have indicated some of the conditions required for this effect to be large. We have also shown that, presently, the Steele-Pecora equation has the only hope of treating this scattering, and we have presented the rather stringent condition for Fourier inversion of the molecular scattering data.

Figure Captions

- Figure 1. Chlorine molecular scattering factor coefficients. Curves 1, 2, and 3 refer to $a_0(\kappa)$, $a_2(\kappa)$, and $a_4(\kappa)$ respectively. Ordinate units are electrons.
- Figure 2. Total scattered intensity for four states at constant temperature. The broken curve is $i_g(\kappa) + i(\kappa)$. The solid curve is $I(\kappa)$. Intensity units are square electrons.
- Figure 3. Fluid intensity curves for $\rho^* = 1.2$, $T^* = 0.75$. The spherical contribution $\kappa i(\kappa)$ is given by the broken curve and the total fluid contribution $\kappa[i(\kappa) + i_{\text{ang}}(\kappa)]$ is given by the solid curve. Ordinate units are square electrons/A.
- Figure 4. Total scattered intensity for varying temperature at $\rho^* = 1.2$. Curve 1: $T^* = 0.75$; Curve 2: $T^* = 1.30$. The dashed curve is the initial part of the $T^* = 1.00$ isotherm. Intensity is in square electrons.
- Figure 5. Fluid intensity curves $\kappa[i(\kappa) + i_{\text{ang}}(\kappa)]$ showing various contributions of the $g_{\ell\ell'm}$. The state is $\rho^* = 1.2$, $T^* = 0.75$. Curve 1: g_{000} only; Curve 2: g_{000} , g_{200} , g_{400} included; Curve 3: all $g_{\ell\ell'm}$ included (it is nearly unchanged if g_{221} , $g_{222} = 0$). Curve 4 is identical to Curve 3 except in the dotted region which shows the area of g_{400} contribution. Ordinate units are square electrons/A.

Figure 6. Total intensity showing various contributions of the $g_{\ell\ell'm}$. Curve 1: g_{000} only; Curve 2: all $g_{\ell\ell'm}$ included. Curve 3: g_{000} , g_{200} , g_{400} included. Intensity units are square electrons.

Figure 7. The Fourier transform function $\kappa i(\kappa) / a_0(\kappa)^2$. Units are \AA^{-1} .

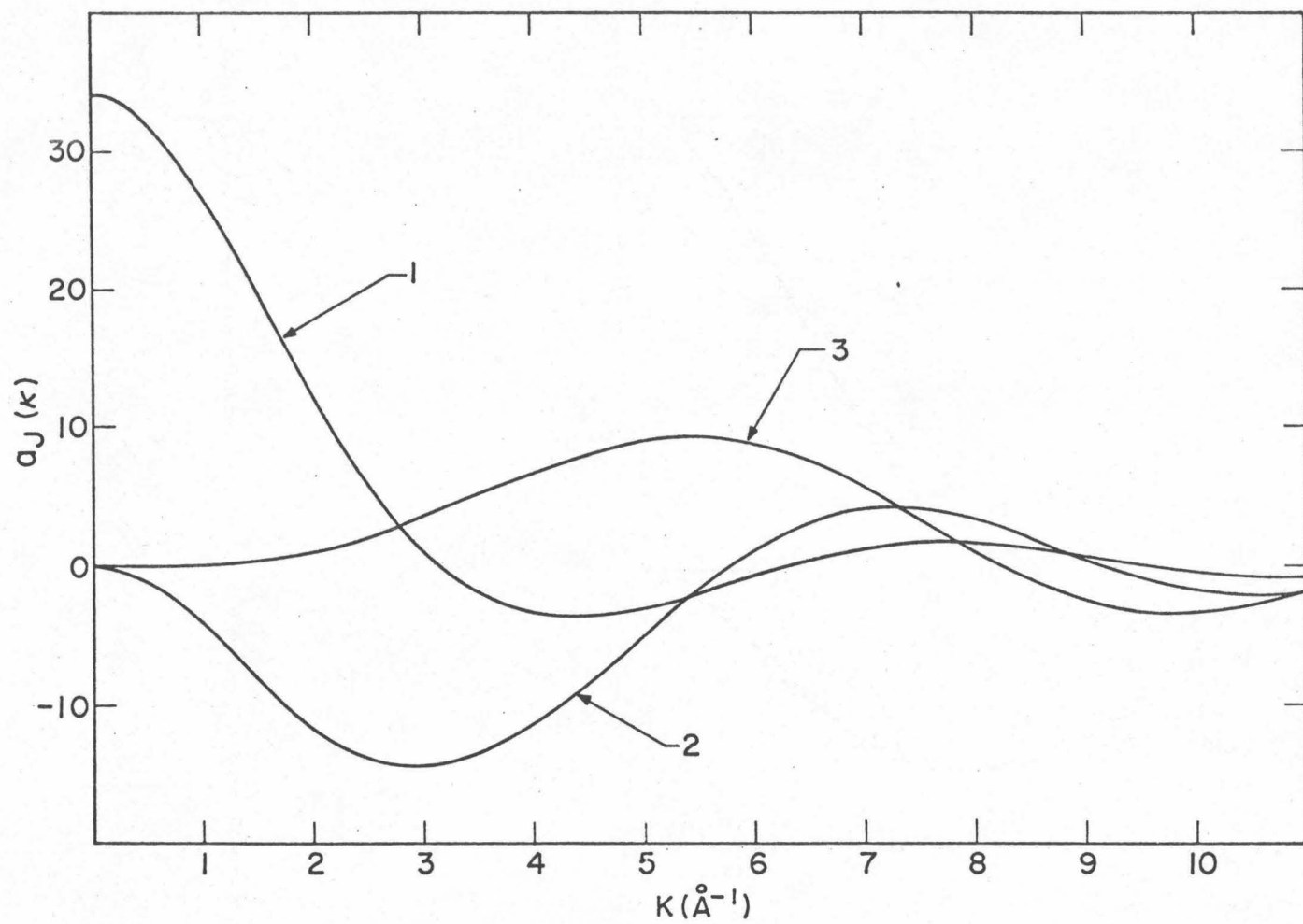


Figure 1.

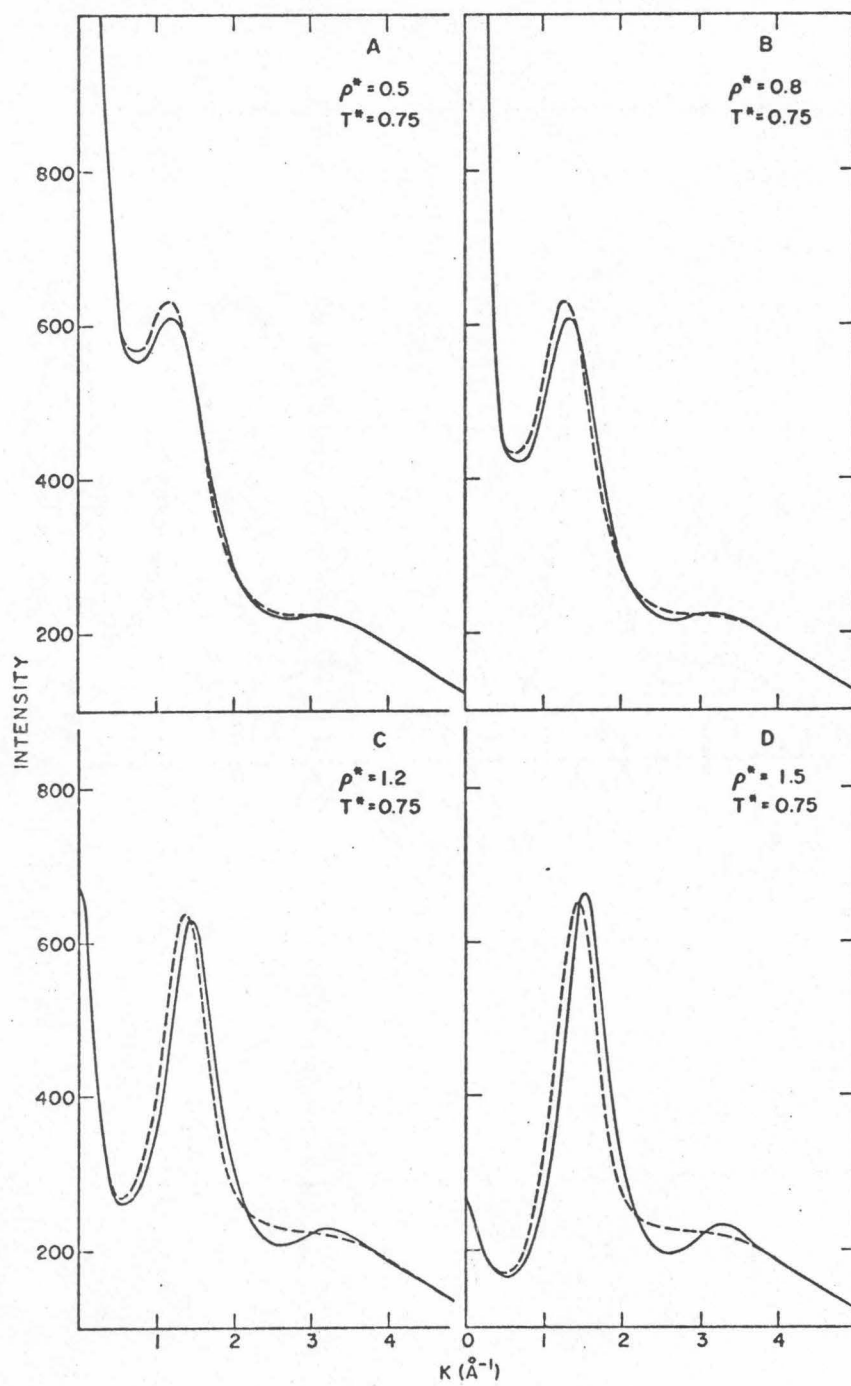


Figure 2.

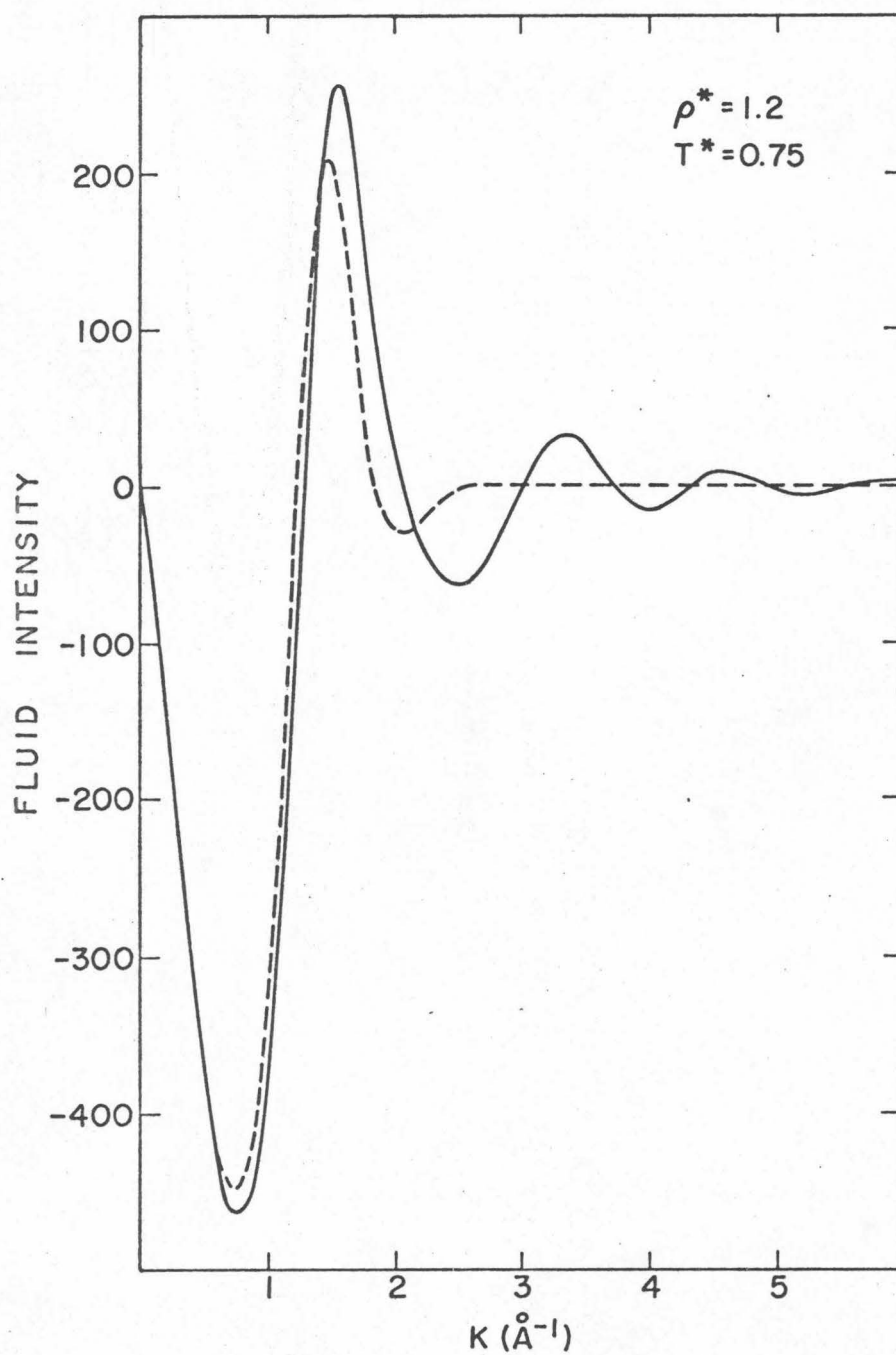


Figure 3.

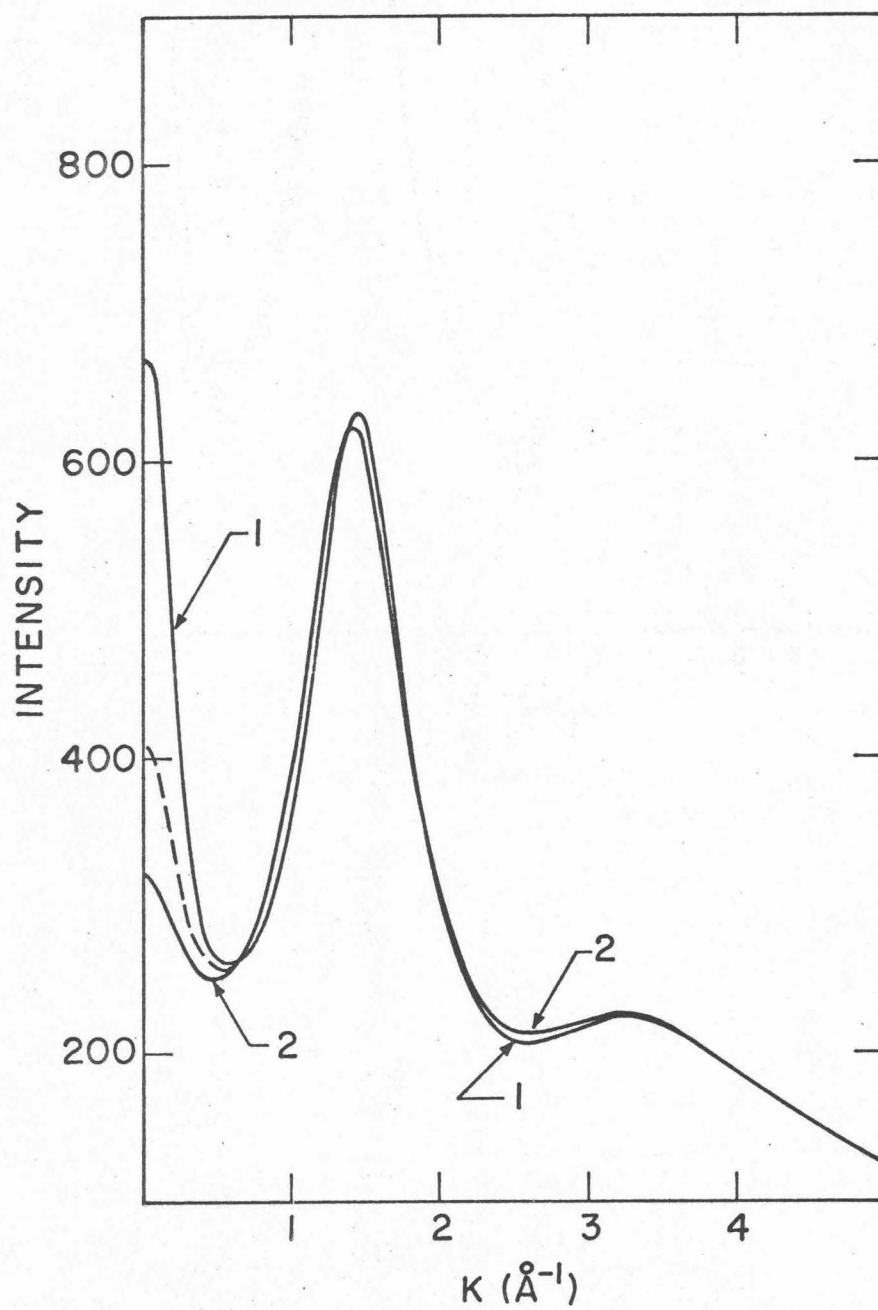


Figure 4.

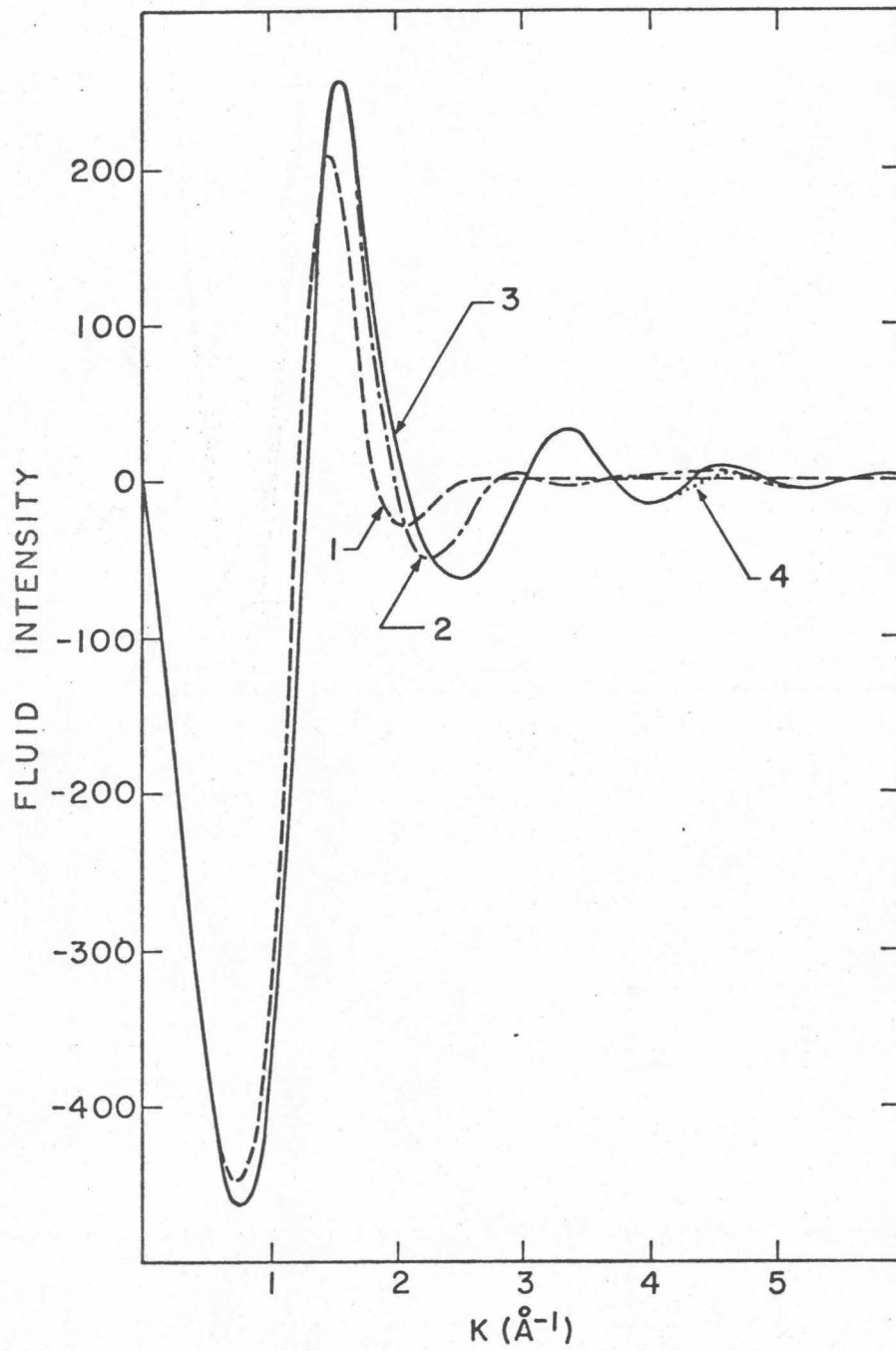


Figure 5.

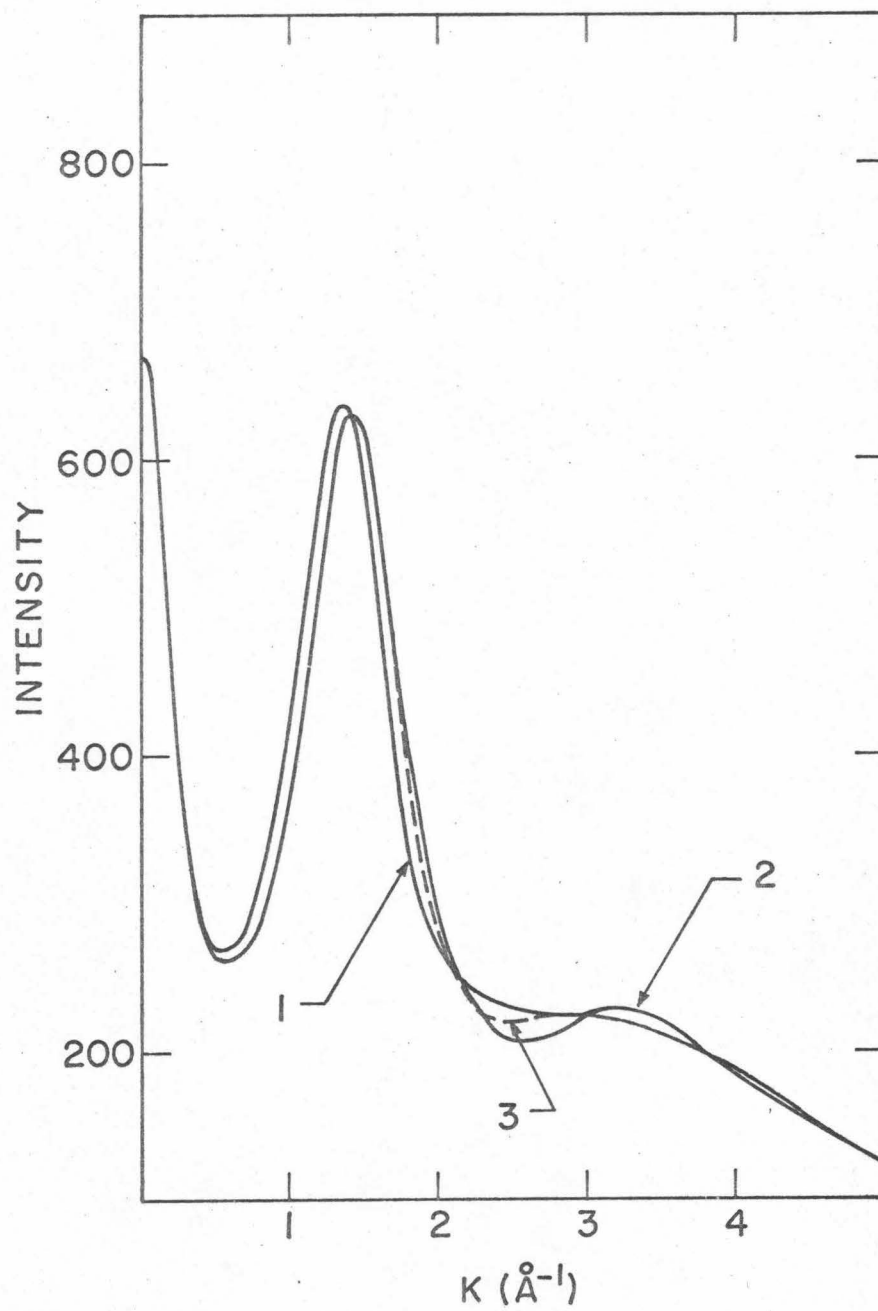


Figure 6.

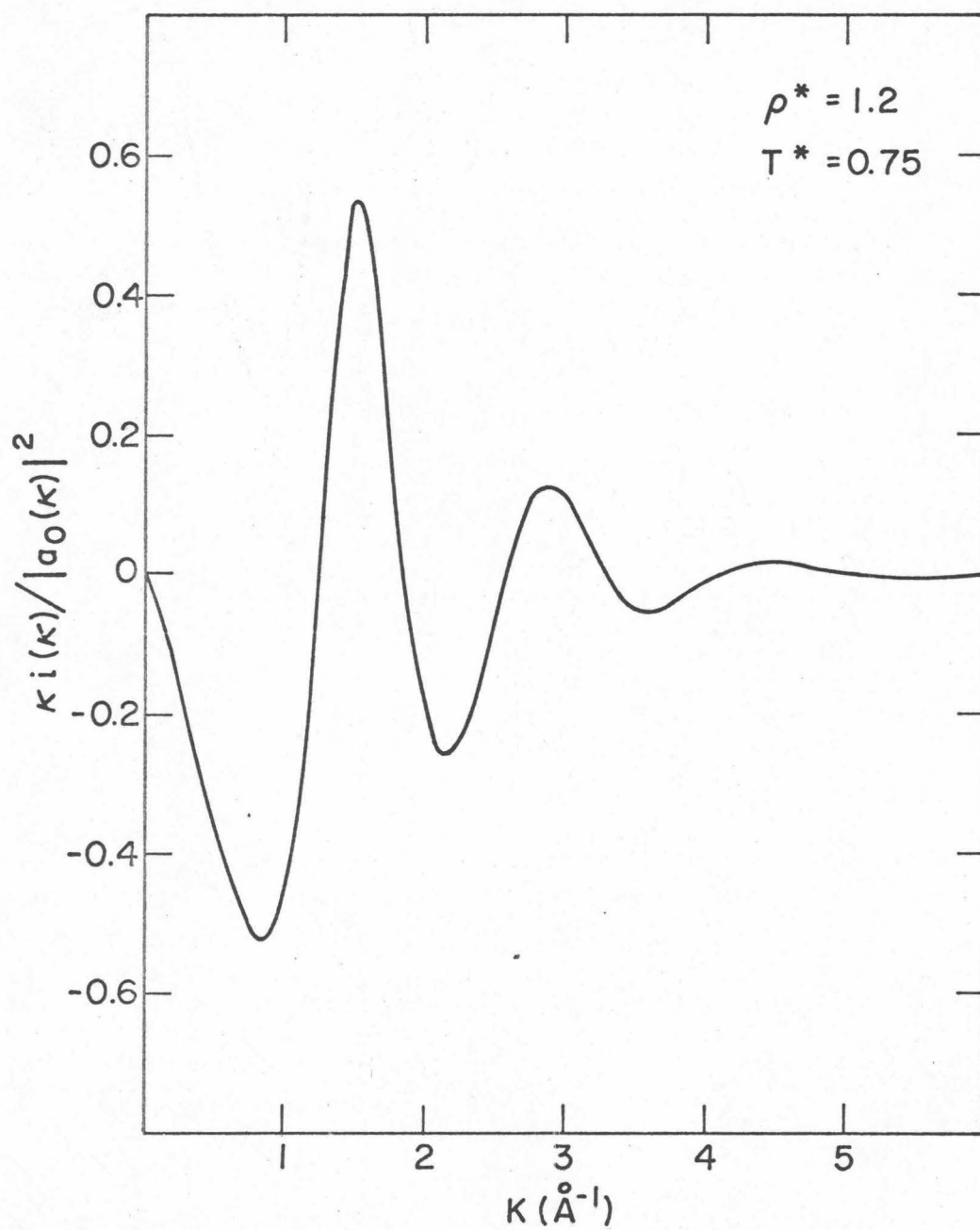


Figure 7.

Bibliography

1. W. Steele, R. Pecora, J. Chem. Phys. 42, 1863 (1965)
2. H. Menke, Physik. Z. 33, 593 (1932)
3. W. H. Zachariasen, Phys. Rev. 47, 277 (1935)
4. J. Waser, V. Schomaker, Rev. Mod. Phys. 25, 671 (1953)
5. R. W. James, The Optical Principles of the Diffraction of X-rays Cornell Univ. Press, 1965
6. A. DeVries, J. Chem. Phys. 46, 1610 (1967)
7. W. Steele, J. Chem. Phys. 39, 3197 (1963)
8. A. H. Narten, J. Chem. Phys. 48, 1630 (1968)
9. R. W. Harris, G. T. Clayton, J. Chem. Phys. 45, 2681 (1966)
10. R. W. Gruebel, G. T. Clayton, J. Chem. Phys. 47, 175 (1967)
11. J. R. Sweet, W. Steele, J. Chem. Phys. 47, 3022 (1967)
12. J. R. Sweet, W. Steele, J. Chem. Phys. 47, 3029 (1967)
13. Y. D. Chen, W. Steele, J. Chem. Phys. 54, 703 (1971)
14. P. Morrison, C. J. Pings, J. Chem. Phys. 56, 280 (1972)
15. P. Morrison, C. J. Pings, in preparation.
16. K. R. Rao, J. Chem. Phys. 48, 2395 (1968)
17. M. E. Rose, Elementary Theory of Angular Momentum, J. Wiley and Sons, N.Y., 1957
18. F. H. Eirich, Rheology Vol. IV, Academic Press, N.Y., 1967, p.52
19. E. U. Condon, G. H. Shortley, The Theory of Atomic Spectra, Cambridge Univ. Press, 1967
20. Reference 5, p. 485; Physik. Z. 33, 587 (1932)
21. Y. D. Chen, W. Steele, J. Chem. Phys. 50, 1428 (1969)
22. Z. Kopal, Numerical Analysis, J. Wiley and Sons, N.Y., 1955

23. System/360 Scientific Subroutine Package, Version III Programmers' Manual, I.B.M., N.Y., 1968
24. C. Gamertsfelder, J. Chem. Phys. 9, 450 (1941)
25. B. Kirstein, C. J. Pings, unpublished data
26. C. J. Pings, J. Waser, J. Chem. Phys. 48, 3016 (1968)
27. A. H. Narten, J. Chem. Phys. 55, 2263 (1971)
28. C. J. Pings, H. H. Paalman, Mol. Phys. 5, 531 (1962);
P. C. Sharrah, J. Chem. Phys. 11, 435 (1943)
29. J. R. Sweet, W. Steele, J. Chem. Phys. 50, 668 (1969)
30. P. G. Mikolaj, C. J. Pings, J. Chem. Phys. 46, 1401 (1967)
31. L. Verlet, Phys. Rev. 165, 201 (1968)

APPENDICES

Appendix 1

SCATTERING INTEGRAL EXPANSIONS

In this appendix details of the harmonic expansions of the scattering integrals given in Part II are given. In that section the derivation of the expansion for $\langle s_A | \exp(i\mathbf{k} \cdot \mathbf{r}) | z_B \rangle$ was presented but only the results were given for the other integrals. Thus, the expansions for $\langle s_A | \exp(i\mathbf{k} \cdot \mathbf{r}) | s_B \rangle$, $\langle z_A | \exp(i\mathbf{k} \cdot \mathbf{r}) | z_B \rangle$, $\langle x_A | \exp(i\mathbf{k} \cdot \mathbf{r}) | x_B \rangle + \langle y_A | \exp(i\mathbf{k} \cdot \mathbf{r}) | y_B \rangle$ and those where center A = center B will be given here. Some equations and tables in Part II are used here and are referred to by number only. $e \equiv \exp(i\mathbf{k} \cdot \mathbf{r})$, α is the Gaussian exponent on center A, and β is the exponent on center B.

$$\underline{\langle s_A | e | s_B \rangle}$$

This integral is the $(ls, a | f | ls, b)$ integral of McWeeny. Allowing for our coordinate system and using the definitions of G and q in Table I, this integral becomes

$$\begin{aligned} I_1 &= (4\pi)^{-1/2} G \exp \left[\frac{i\mathbf{k}(\beta-\alpha)\mathbf{R}/2 \cdot \hat{\mathbf{k}}}{(\alpha+\beta)} \right] \\ &= (4\pi)^{-1/2} G \exp(iq \cos \theta) \end{aligned} \quad (1-1)$$

Spherical wave expand the exponential to give

$$I_1 = G \sum_{J=0}^{\infty} (2J+1)^{1/2} i^J j_J(q) Y_{J,0}(\theta, \phi)$$

The coefficient of each harmonic is therefore

$$\langle s_A | e | s_B \rangle_J = G(2J+1)^{1/2} (-)^{J/2} j_J(q) \quad (1-2)$$

$$\langle s_A | e | s_A \rangle, \langle s_B | e | s_B \rangle$$

These integrals are the same as the last one except that both Gaussians are now on a common center. The differences between $\langle s_A | e | s_B \rangle$ and $\langle s_A | e | s_A \rangle$ or $\langle s_B | e | s_B \rangle$ are general and hold for all the integral types treated here.

We first adapt McWeeny's results, given with the Gaussians on different centers, to the case where they are on the same center, A . In his notation \underline{A} and \underline{B} are the vectors from the origin to each of the two Gaussians. Since we are taking the origin to be at the mid-point of the internuclear axis (see Fig. 1, Section II), $\underline{A} = -\underline{R}/2$, $\underline{B} = \underline{R}/2$, and McWeeny's result becomes

$$\begin{aligned} I_A &= \left(\frac{\pi}{\alpha+\beta} \right)^{3/2} \exp \left[\frac{-4\alpha\beta(\underline{A}-\underline{B})^2 - \kappa^2 + 4i\kappa(\alpha\underline{A} + \beta\underline{B}) \cdot \hat{\underline{K}}}{4(\alpha+\beta)} \right] \\ &= \left(\frac{\pi}{\alpha+\beta} \right)^{3/2} \exp\left(\frac{-\kappa^2}{4(\alpha+\beta)}\right) \exp\left(-i\kappa \frac{\underline{R}}{2} \cdot \hat{\underline{K}}\right) \end{aligned} \quad (1-3)$$

Denote by G_o , G when $R = 0$. Thus

$$I_A = (4\pi)^{-1/2} G_o \exp\left(-i\kappa \frac{\underline{R}}{2} \cdot \hat{\underline{K}}\right)$$

As before, if the exponential is spherical wave expanded, the desired coefficient may be obtained as

$$\langle s_A | e | s_A \rangle_J = G_o (2J+1)^{1/2} (-)^{J/2} j_J\left(-\frac{\kappa R}{2}\right) \quad (1-4)$$

The $\langle s_B | e | s_B \rangle_J$ coefficient is obtained in the same manner except that $\underline{A} = \underline{R}/2$ and $\underline{B} = \underline{R}/2$. Hence

$$\langle s_B | e | s_B \rangle_J = G_0 (2J+1)^{1/2} (-)^{J/2} j_J(\frac{\kappa R}{2}) \quad (1-5)$$

We have the rules therefore, that for integrals whose Gaussians share a common center, $R=0$ except in q , q being replaced by $-\kappa R/2$ if the common center is A and by $\kappa R/2$ if the common center is B .

$$\underline{\langle z_A | e | s_B \rangle}$$

This integral is the same as that derived in Section II except that A and B have been reversed. This is the $(1s, b | f | 2p, a)$ integral of McWeeny and is equal to

$$I_3 = \frac{\beta}{\alpha} A(2\alpha\beta R \cdot \hat{k} + i\kappa\alpha\hat{\kappa} \cdot \hat{k}) \exp(i\hat{\kappa} \cdot \hat{R}q) / (\alpha + \beta)$$

this equation being the counterpart of Eq. (7). An inspection of the constants between the two equations followed by investigation of their behavior through Eqs. (10-13) easily shows that the final result for the I_3 coefficient is

$$\begin{aligned} \langle z_A | e | s_B \rangle_J &= G(2J+1)^{1/2} \frac{\beta R}{\alpha + \beta} (-)^{J/2} j_J(q) \\ &+ \frac{\kappa G}{2(\alpha + \beta)} \sum_{L=J-1}^{J+1} \frac{(2L+1)}{(2J+1)^{1/2}} (-)^{\frac{L+1}{2}} j_L(q) c^2(L1J; 00) \end{aligned} \quad (1-6)$$

$L = 1$ only if $J = 0$

$$\underline{\langle z_A | e | z_B \rangle}$$

This is the $(2p, a | f | 2p, b)$ integral of McWeeny and is given by

$$I_4 = \int z_A z_B \exp(-\alpha r_A^2) \exp(-\beta r_B^2) \exp(i\hat{\kappa} \cdot \underline{r}) \underline{dr} =$$

$$= \frac{1}{4\alpha\beta} (4\pi)^{-1/2} G \exp(iq\hat{\underline{k}} \cdot \hat{\underline{R}}) \left\{ \left(\frac{2\alpha\beta\hat{\underline{R}} \cdot \hat{\underline{k}} + i\kappa\alpha\hat{\underline{\kappa}} \cdot \hat{\underline{k}}}{\alpha + \beta} \right) \right. \\ \left. \times \left(\frac{-2\alpha\beta\hat{\underline{R}} \cdot \hat{\underline{k}} + i\kappa\beta\hat{\underline{\kappa}} \cdot \hat{\underline{k}}}{\alpha + \beta} \right) + \frac{2\alpha\beta\hat{\underline{k}} \cdot \hat{\underline{k}}}{\alpha + \beta} \right\}$$

Note that $\hat{\underline{k}} \cdot \hat{\underline{R}}$ and $\hat{\underline{k}} \cdot \hat{\underline{k}} = \cos \theta$. If the exponential is now expanded and the bracketed expression is expanded as well, one obtains

$$I_4 = \left[\frac{-\alpha\beta R^2}{(\alpha + \beta)^2} G + \frac{G}{2(\alpha + \beta)} \right] \sum_{J=0}^{\infty} (2J+1)^{1/2} i^J j_J(q) Y_{J,0}(\theta, \phi) \\ + \frac{\kappa(\beta - \alpha)R}{2(\alpha + \beta)^2} G \sum_{\ell=0}^{\infty} (2\ell+1)^{1/2} i^{\ell+1} j_{\ell}(q) \cos \theta Y_{\ell,0}(\theta, \phi) \\ - \frac{\kappa^2 G}{4(\alpha + \beta)^2} \sum_{\ell=0}^{\infty} (2\ell+1)^{1/2} i^{\ell} j_{\ell}(q) \cos^2 \theta Y_{\ell,0}(\theta, \phi) \quad (1-7)$$

The latter two series each contain a $\cos^n(\theta) Y_{\ell,0}(\theta, \phi)$ type term. If the cosine terms are expressed as spherical harmonics, then the harmonic product may be coupled to give a single harmonic expansion by using Eq. (11). Now

$$Y_{2,0} = \sqrt{\frac{5}{16\pi}} (3 \cos^2 \theta - 1)$$

or

$$\cos^2 \theta = \frac{1}{3} + \frac{1}{3} \sqrt{\frac{16\pi}{5}} Y_{2,0}$$

Also

$$\cos \theta = \sqrt{\frac{4\pi}{3}} Y_{1,0}$$

So from Eq. (11)

$$\cos^2 \theta Y_{\ell,0}(\theta, \phi) = \frac{1}{3} Y_{\ell,0}(\theta, \phi) + \frac{2}{3} \sum_{\lambda=|\ell-2|}^{\ell+2} \left[\frac{(2\ell+1)}{(2\lambda+1)} \right]^{\frac{1}{2}} c^2(\ell 2 \lambda; 00) Y_{\lambda,0}(\theta, \phi) \quad (1-8)$$

$$\cos \theta Y_{\ell,0}(\theta, \phi) = \sum_{\lambda=|\ell-1|}^{\ell+1} \left(\frac{2\ell+1}{2\lambda+1} \right)^{1/2} c^2(\ell 1 \lambda; 00) Y_{\lambda,0}(\theta, \phi) \quad (1-9)$$

Substituting these equations into (1-7) yields

$$\begin{aligned} I_4 = & \left[\frac{-\alpha\beta R^2}{(\alpha+\beta)^2} G + \frac{G}{2(\alpha+\beta)} - \frac{\kappa^2 G}{12(\alpha+\beta)^2} \right] \sum_{J=0}^{\infty} (2J+1)^{1/2} i^J j_J(q) Y_{J,0}(\theta, \phi) \\ & + \frac{\kappa(\beta-\alpha)RG}{2(\alpha+\beta)^2} \sum_{\ell=0}^{\infty} \sum_{\lambda=|\ell-1|}^{\ell+1} \frac{2\ell+1}{(2\lambda+1)^{1/2}} c^2(\ell 1 \lambda; 00) i^{\ell+1} j_{\ell}(q) Y_{\lambda,0}(\theta, \phi) \\ & - \frac{\kappa^2 G}{6(\alpha+\beta)^2} \sum_{\ell=0}^{\infty} \sum_{\lambda=|\ell-2|}^{\ell+2} \frac{2\ell+1}{(2\lambda+1)^{1/2}} i^{\ell} j_{\ell}(q) c^2(\ell 2 \lambda; 00) Y_{\lambda,0}(\theta, \phi) \end{aligned}$$

The last two series are not arranged so as to immediately yield an expression for the Jth harmonic coefficient. A study of the summation indices indicates that a rearrangement is possible however. λ and ℓ in the summation indices (only) may be interchanged. After interchange it is to be noted that when $\lambda = 0$, $\ell = 1$ only in the $\sum_{\ell=|\lambda-1|}^{\lambda+1}$ series; when $\lambda = 0$ in the $\sum_{\ell=|\lambda-2|}^{\lambda+2}$ series, $\ell = 2$ only and when $\lambda = 1$, $\ell = 1$ and 3 only.

Identifying λ with J ,

$$\langle z_A | e | z_B \rangle_J = \left[\frac{-\alpha\beta R^2}{(\alpha+\beta)^2} G + \frac{G}{2(\alpha+\beta)} - \frac{\kappa^2 G}{12(\alpha+\beta)^2} \right] (2J+1)^{1/2} (-)^{J/2} j_J(q) +$$

$$\begin{aligned}
 & + \frac{\kappa(\beta-\alpha)RG}{2(\alpha+\beta)^2} \sum_{L=|J-1|}^{J+1} \frac{2L+1}{(2J+1)^{1/2}} c^2(L1J;00)(-)^{\frac{L+1}{2}} j_L(q) \\
 & - \frac{\kappa^2 G}{6(\alpha+\beta)^2} \sum_{L=|J-2|}^{J+2} \frac{2L+1}{(2J+1)^{1/2}} (-)^{L/2} j_L(q) c^2(L2J;00)
 \end{aligned} \quad (1-10)$$

$$\underline{\langle x_A | e | x_B \rangle + \langle y_A | e | y_B \rangle}$$

$\langle x_A | e | x_B \rangle$ and $\langle y_A | e | y_B \rangle$ may be calculated independently if so desired. However, this work is restricted to a study of linear molecules, and hence cylindrical symmetry must apply to the expression Eq. (6). This in turn requires that the coefficients of each of these integrals must be equal and hence one may deal exclusively with the sum of these two integrals.

These integrals are also given by the $(2p,a|f|2p,b)$ results of McWeeny but with different projection vectors $\underline{\delta}_B, \underline{\delta}_A$. Hence,

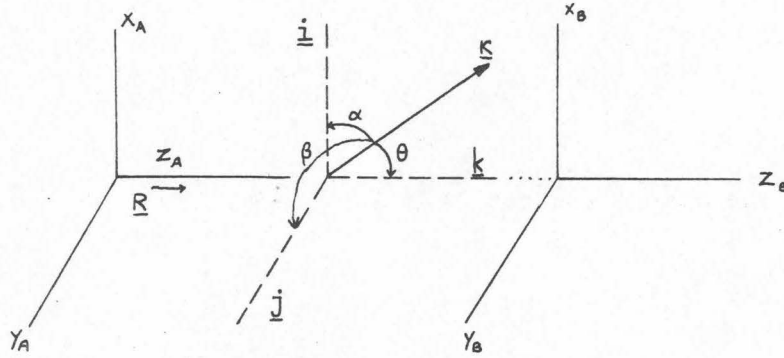
$$\begin{aligned}
 I_x + \langle x_A | e | x_B \rangle &= \frac{1}{4\alpha\beta} (4\pi)^{-1/2} G \exp(iq\underline{\kappa} \cdot \underline{\hat{R}}) \left\{ \left(\frac{2\alpha\beta \underline{R} \cdot \underline{\hat{i}} + i\kappa\alpha\underline{\kappa} \cdot \underline{\hat{i}}}{\alpha+\beta} \right) \right. \\
 &\quad \times \left(\frac{-2\alpha\beta \underline{R} \cdot \underline{\hat{i}} + i\kappa\beta\underline{\kappa} \cdot \underline{\hat{i}}}{\alpha+\beta} \right) + \frac{2\alpha\beta \underline{\hat{i}} \cdot \underline{\hat{i}}}{\alpha+\beta} \left. \right\}
 \end{aligned}$$

where $\underline{\hat{i}}, \underline{\hat{j}}, \underline{\hat{k}}$ denote unit vectors along the x,y,z axes respectively.

Now $\underline{R} \cdot \underline{\hat{i}} (= \underline{R} \cdot \underline{\hat{j}}) = 0$, $\underline{\hat{i}} \cdot \underline{\hat{i}} (= \underline{\hat{j}} \cdot \underline{\hat{j}}) = 1$. If these values are substituted in I_x and the exponential is expanded

$$I_x = \frac{G}{4\alpha\beta} \left(\frac{-\kappa^2 \alpha\beta (\underline{\kappa} \cdot \underline{\hat{i}})^2}{(\alpha+\beta)^2} + \frac{2\alpha\beta}{\alpha+\beta} \right) \sum_{\ell=0}^{\infty} (2\ell+1)^{1/2} i^\ell j_\ell(q) Y_{\ell,0}(\theta, \phi)$$

A similar expression may be written for I_y with $(\hat{\underline{\kappa}} \cdot \hat{\underline{i}})^2$ replaced by $(\hat{\underline{\kappa}} \cdot \hat{\underline{j}})^2$. Noting that $\hat{\underline{\kappa}} \cdot \hat{\underline{i}}$ and $\hat{\underline{\kappa}} \cdot \hat{\underline{j}}$ are two of the direction cosines of $\hat{\underline{\kappa}}$ (see figure below),



one may make use of the identity

$$\cos^2 \alpha + \cos^2 \beta + \cos^2 \theta = 1$$

to write

$$(\hat{\underline{\kappa}} \cdot \hat{\underline{i}})^2 + (\hat{\underline{\kappa}} \cdot \hat{\underline{j}})^2 = 1 - \cos^2 \theta$$

The sum $I_x + I_y$ contains this last expression and one may write

$$\begin{aligned} I_x + I_y &= \frac{-G\kappa^2 \alpha\beta}{4\alpha\beta(\alpha+\beta)^2} (1 - \cos^2 \theta) \sum_{\ell=0}^{\infty} (2\ell+1)^{1/2} i^{\ell} j_{\ell}(q) Y_{\ell,0}(\theta, \phi) \\ &+ \frac{G}{(\alpha+\beta)} \sum_{\ell=0}^{\infty} (2\ell+1)^{1/2} i^{\ell} j_{\ell}(q) Y_{\ell,0}(\theta, \phi) \end{aligned}$$

The term involving $\cos^2 \theta Y_{\ell,0}(\theta, \phi)$ may be expanded by Eq. (1-8), λ and ℓ in the summation indices may be interchanged as in $\langle z_A | e | z_B \rangle$, and one has

$$I_x + I_y = G \left(\frac{-\kappa^2}{6(\alpha+\beta)^2} + \frac{1}{(\alpha+\beta)} \right) \sum_{J=0}^{\infty} (2J+1)^{1/2} i^J j_J(q) Y_{J,0}(\theta, \phi) +$$

$$+ \frac{G_K^2}{6(\alpha+\beta)^2} \sum_{J=0}^{\infty} \sum_{L=|J-2|}^{J+2} \frac{2L+1}{(2J+1)^{1/2}} i^L j_L(q) c^2(L2J;00) Y_{J,0}(\theta, \phi) \quad (1-11)$$

The $\langle x_A | e | x_B \rangle_J + \langle y_A | e | y_B \rangle_J$ coefficient of Table I follows directly from this expression.

Other Integrals with Common Gaussian Centers

The integrals $\langle s_A | e | z_A \rangle$, $\langle z_A | e | z_A \rangle$, $\langle x_A | e | x_A \rangle + \langle y_A | e | y_A \rangle$ and the corresponding ones on center B are evaluated in this part. The mechanics of the derivations are the same as those used above, but the beginning expressions are different. The adaptation of McWeeny's results for each integral above follows.

By definition

$$I_A = \langle s_A | e | s_A \rangle = \int \exp(-(\alpha+\beta)r_A^2) \exp i\mathbf{k} \cdot \mathbf{r} \, d\mathbf{r}$$

A corresponding expression for I_B may be similarly defined. If center A is shifted along a vector $\underline{\delta}_A$ (commonly in \hat{i} , \hat{j} , or \hat{k} direction), \underline{r}_A may be replaced by $\underline{r}_A - \underline{\delta}_A$. If the shifted expression for I_A is differentiated with respect to $\underline{\delta}_A$ one obtains

$$\frac{\partial I_A}{\partial \underline{\delta}_A} = \int (\alpha+\beta)(2\underline{r}_A \cdot \hat{\underline{\delta}}_A + 2\delta_A) \exp[-(\alpha+\beta)(\underline{r}_A^2 - 2\underline{r}_A \cdot \underline{\delta}_A + \delta_A^2)] \times \exp(i\mathbf{k} \cdot \mathbf{r}) \, d\mathbf{r} \quad (1-12)$$

Hence

$$\langle s_A | e | z_A \rangle = \frac{1}{2(\alpha+\beta)} \lim_{\delta_A \rightarrow 0} \frac{\delta I_A}{\partial \delta_A}, \text{ if } \hat{\underline{\delta}}_A = \hat{k} \quad (1-13)$$

If Eq. (1-12) is differentiated again wrt. δ_A , one finds

$$\lim_{\delta_A \rightarrow 0} \frac{\partial^2 I_A}{\partial \delta_A^2} = -2(\alpha+\beta) I_A + 4(\alpha+\beta)^2 \int (\underline{r}_A \cdot \hat{\delta}_A)^2 \exp[-(\alpha+\beta)r_A^2] \times \exp(i\underline{k} \cdot \underline{r}) d\underline{r}$$

Thus

$$\begin{pmatrix} x_A & x_A \\ y_A & |e| & y_A \\ z_A & z_A \end{pmatrix} = \frac{1}{4(\alpha+\beta)^2} \lim_{\delta_A \rightarrow 0} \frac{\partial^2 I_A}{\partial \delta_A^2} + \frac{1}{2(\alpha+\beta)} I_A \quad \text{if } \hat{\delta}_A = \begin{pmatrix} \hat{i} \\ \hat{j} \\ \hat{k} \end{pmatrix} \quad (1-14)$$

If the Gaussians share center B, identical expressions may be written in which A is merely replaced by B.

The scattering integrals may be further evaluated by carrying out the operations of Eq. (1-13) and (1-14) on the I_A expression given by Eq. (1-3); \underline{A} and \underline{B} are replaced by $\underline{A} + \underline{\delta}_A$. There results

$$\begin{aligned} \langle s_A | e | z_A \rangle &= \frac{1}{2(\alpha+\beta)} I_A i \underline{k} \cdot \hat{\underline{k}} , \\ \langle z_A | e | z_A \rangle &= \frac{-I_A}{4(\alpha+\beta)^2} \kappa^2 (\hat{\underline{k}} \cdot \hat{\underline{k}})^2 + \frac{I_A}{2(\alpha+\beta)} , \\ \langle x_A | e | x_A \rangle + \langle y_A | e | y_A \rangle &= \frac{I_A}{(\alpha+\beta)} - \frac{I_A \kappa^2}{4(\alpha+\beta)^2} [(\hat{\underline{k}} \cdot \hat{\underline{j}})^2 + (\hat{\underline{k}} \cdot \hat{\underline{i}})^2] \quad (1-15) \end{aligned}$$

with similar expressions for the B center integrals. Each of these may be evaluated by proceeding through expansions of the same type as used above for the two center cases. Thus the harmonic coefficients obtained from Eqs. (1-2), (1-4), (1-5), (1-6), (1-10), (1-11) and (1-15) complete the set of coefficients summarized in Table I of Part II.

Appendix 2

REDERIVATION OF THE STEELE-PECORA X-RAY SCATTERING EQUATION

Because of the central importance of the Steele and Pecora molecular x-ray scattering equation¹ to this work, the derivation is presented here. The original derivation contained several algebraic errors which have been noted and corrected in this presentation.

The D functions used in this appendix are those of Steele² and not those of Rose³ as is more common. They are related to the spherical harmonics by

$$D_{M,0}^J(\phi, \theta, 0) = (2\pi)^{-1/2} Y_{J,M}^*(\theta, \phi) \quad (2-1)$$

The D functions in one coordinate system (system A) are related to those in another coordinate system (system B) by the Euler angles that rotate system A into system B by

$$D_{M,\kappa}^J(\Omega_A) = \left[\frac{8\pi^2}{2J+1} \right]^{1/2} \sum_{R=-J}^J D_{M,R}^J(\Omega_{AB}) D_{R,\kappa}^J(\Omega_B) \quad (2-2)$$

Three properties of D functions required below are:

$$\int D_{M_1,\kappa_1}^{*J_1}(\Omega) D_{M_2,\kappa_2}^{J_2}(\Omega) d\Omega = \delta_{M_1,M_2} \delta_{\kappa_1,\kappa_2} \delta_{J_1,J_2} \quad (2-3)$$

$$\begin{aligned}
 & \int D_{M_3, \kappa_3}^{*J_3}(\Omega) D_{M_2, \kappa_2}^{J_2}(\Omega) D_{M_1, \kappa_1}^{J_1}(\Omega) d\Omega \\
 & = c(J_1 J_2 J_3; M_1 M_2) c(J_1 J_2 J_3; \kappa_1 \kappa_2) \\
 & \times \delta_{M_1+M_2, M_3} \delta_{\kappa_1+\kappa_2, \kappa_3} \left[\frac{(2J_1+1)(2J_2+1)}{(2J_3+1) 8\pi^2} \right]^{1/2}
 \end{aligned} \tag{2-4}$$

$$D_{\kappa, M}^J(\Omega) = D_{\kappa, M}^J(\alpha, \beta, \gamma) = D_{M, \kappa}^{*J}(-\gamma, -\beta, -\alpha) = D_{M, \kappa}^{*J}(-\Omega) \tag{2-5}$$

The SP equation is derived in two parts. The first is the scattering factor and the second is the sum over scattering factors for total intensity.

Scattering Factor

The molecular scattering factor is defined as

$$a(\kappa, \Omega^K) = \int \rho(\underline{r}) \exp(i\kappa \cdot \underline{x}) d\underline{x} \tag{2-6}$$

where Ω^K are the Euler angles giving the molecular orientation relative to a laboratory coordinate system and where $\rho(\underline{r})$ is the electronic density within a molecule and is expressible as

$$\rho(\underline{r}) = \sum_{J, M} (4\pi)^{1/2} \rho_{J, M}(\underline{r}) Y_{J, M}^*(\theta_m \phi_m) \tag{2.7}$$

r, θ_m and ϕ_m give the positions of the electrons relative to a molecular fixed coordinate system (m), and \underline{x} is the same position vector as \underline{r} expressed in a laboratory frame where $\underline{\kappa}$ ($\kappa = 4\pi \sin \theta/\lambda$)

is the z-axis (see Fig. 1).

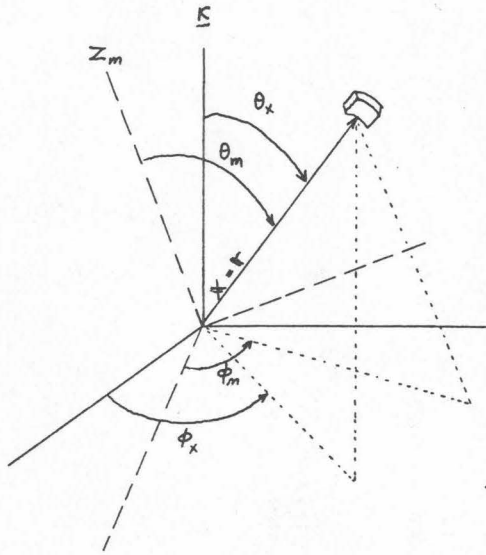


Fig. 1

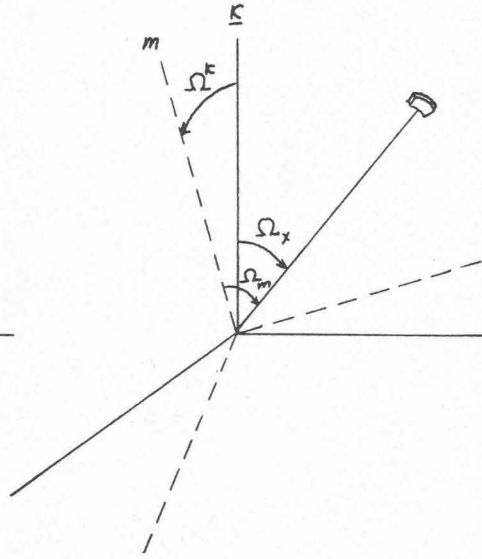


Fig. 2

In Fig. 2 the polar angles of location of \underline{r} in different coordinate systems are rewritten in terms of Euler angles. Ω^K rotates the laboratory system into the molecular fixed system. From Fig. 2 and Eq. (2-2) and (2-5), one has the relation

$$D_{K,M}^J(-\Omega_m) = \left(\frac{8\pi^2}{2J+1}\right)^{1/2} \sum_R D_{K,R}^J(-\Omega_x) D_{R,M}^J(\Omega^K)$$

$$D_{M,K}^J(\Omega_m) = \left(\frac{8\pi^2}{2J+1}\right)^{1/2} \sum_R D_{R,K}^J(\Omega_x) D_{R,M}^{*J}(\Omega^K)$$

$$\Omega_m = \{\phi_m, \theta_m, 0\}, \quad \Omega_x = \{\phi_x, \theta_x, 0\} \quad (2-8)$$

The exponential of Eq. (2-6) may be spherical wave expanded using Eq. (2-1) to give

$$\exp(i\mathbf{K} \cdot \underline{r}) = (8\pi^2)^{1/2} \sum_J i^J (2J+1)^{1/2} j_J(Kx) D_{0,0}^J(\Omega_x) \quad (2-9)$$

Substituting Eqs. (2-7) and (2-9) into (2-6), one obtains

$$a(\kappa, \Omega^K) = \sum_{J,M} \sum_{J'} 8\pi^2 i^{J'} (2J'+1)^{1/2} \int \rho_{J,M}(x) D_{M,0}^J(\Omega_m) D_{00}^{J'}(\Omega_x) j_{J'}(\kappa x) dx \quad (2-10)$$

where Eq. (2-1) was used to express the harmonic of Eq. (2-7) as a D function. Setting $\kappa = 0$ in Eq. (2-8) and substituting in (2-10) yields

$$a(\kappa, \Omega^K) = \sum_{J,M} \sum_{J'} (8\pi^2)^{3/2} i^{J'} \left(\frac{2J'+1}{2J+1} \right)^{1/2} \int \rho_{J,M}(x) \sum_R D_{R,M}^{*J}(\Omega^K) \times D_{R,0}^J(\Omega_x) D_{00}^{J'}(\Omega_x) j_{J'}(\kappa x) dx \quad (2-11)$$

The integral in Eq. (2-11) may be evaluated as follows:

$$\begin{aligned} \int &= \sum_R D_{R,M}^{*J}(\Omega^K) \int \rho_{J,M}(x) j_{J'}(\kappa x) x^2 dx \iint D_{R,0}^J(\Omega_x) D_{00}^{J'}(\Omega_x) \sin \theta_x d\theta_x d\phi_x \\ &= \sum_R D_{R,M}^{*J}(\Omega^K) \int \rho_{J,M}(x) j_{J'}(\kappa x) x^2 dx \frac{1}{2\pi} \int D_{R,0}^J(\Omega_x) D_{00}^{J'}(\Omega_x) d\Omega_x \end{aligned}$$

From Eq. (2-3) the last integral gives $J = J'$, $R = 0$ and

$$\int = \frac{1}{2\pi} D_{0,M}^{*J}(\Omega^K) \int \rho_{J,M}(x) j_J(\kappa x) x^2 dx \quad (2-12)$$

Substituting Eq. (2-12) into Eq. (2-11)

$$a(\kappa, \Omega^K) = \sum_{J,M} (8\pi^2)^{1/2} a_{0,M}^J D_{0,M}^{*J}(\Omega^K) \quad (2-13)$$

where

$$a_{0,M}^J = i^J \int \rho_{J,M}(\kappa) j_J(\kappa x) 4\pi x^2 dx \quad (2-14)$$

Note that both of these equations differ from those published by Steele and Pecora. Equation (2-13) differs by the complex conjugate and Eq. (2-14) differs by a factor of $(2J+1)^{1/2}$. We also note that Eq. (2-1) differs from the corresponding expression in the original work, the original expression being subject to a typographical mistake.

Elastic Scattering

The derivation of the scattering intensity begins with Eq. (27) in the Introduction. Several coordinate systems are involved in this expression and they are diagramed in Fig. 3.

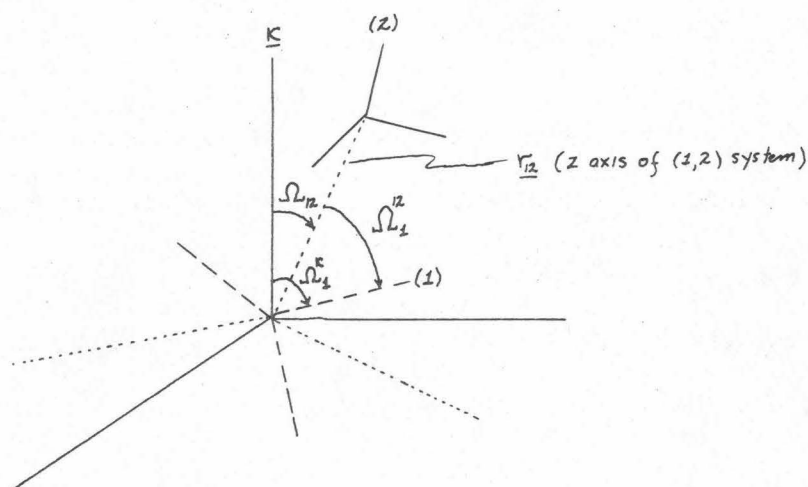


Fig. 3

Molecule 1 is at the origin and has a molecular coordinate system denoted by (1) (dashed lines). Molecule 2 is at the end of the $\underline{r} = \underline{r}_{12}$ vector and has a molecular coordinate system denoted by (2). A molecular-pair (1,2) coordinate system is defined with \underline{r}_{12} as its z-axis, and the pair distribution function has angles expressed in this system rather than a laboratory system. Ω_1^κ are the orientation angles of molecule 1 relative to the laboratory (κ) system, and Ω_{12}

is the set of angles which will rotate the laboratory system into the (1,2) system. Note that the polar coordinates of \underline{r} are two of the three Euler angles denoted by Ω_{12} and that

$$d\underline{r} = \frac{1}{2\pi} r^2 dr d\Omega_{12}$$

The beginning equation may thus be written

$$\begin{aligned} V^{-1} I(\kappa) &= \frac{\rho}{8\pi^2} \int a_1^*(\Omega_1^K) a_1(\Omega_1^K) d\Omega_1^K \\ &+ \frac{1}{2\pi} \int a_1^*(\Omega_1^K) a_2(\Omega_2^K) \exp(i\underline{\kappa} \cdot \underline{r}) \rho^{(2)}(\underline{R}_1, \underline{R}_2) d\Omega_1^{12} d\Omega_2^{12} d\Omega_{12} r^2 dr \quad (2-15) \end{aligned}$$

The first term of Eq. (2-15) is easily evaluated by substituting Eq. (2-13) into the integral twice and applying the orthogonality condition of Eq. (2-3). One obtains

$$V^{-1} I(\kappa) = \rho \sum_{M,J} |a_{O,M}^J|^2 + I_2 \quad (2-16)$$

where I_2 is the second integral of Eq. (2-15).

I_2 is more difficult to evaluate. The $a(\kappa, \Omega^K)$ factors are expressed relative to a laboratory coordinate system and must be re-expressed in the (1,2) frame. From Fig. 3 and Eq. (2-2), the $D_{O,M}^{*J}(\Omega^K)$ of Eq. (2-13) may be rotated to the (1,2) system and

$$a_1^*(\kappa, \Omega_1^K) = \sum_{R_1, M_1, J_1} \frac{8\pi^2}{(2J_1+1)^{1/2}} a_{O,M_1}^{*J_1} D_{O,R_1}^{J_1}(\Omega_{12}) D_{R_1,M_1}^{J_1}(\Omega_1^{12}) \quad (2-17)$$

If Eq. (5) of the Introduction for $g^{(2)}(\underline{R}_1, \underline{R}_2)$ and Eq. (2-17) are substituted into the expression for I_2 , one obtains

$$\begin{aligned}
 I_2 = & \frac{1}{2\pi} \frac{\rho^2}{8\pi^2} \sum_{R1, M1, J1} \sum_{R2, M2, J2} \frac{(8\pi^2)^2}{[(2J2+1)(2J1+1)]^{1/2}} \\
 & \times a_{0, M1}^{*J1} a_{0, M2}^{J2} \sum_{\underline{N1}} \sum_{\underline{N2}} \int D_{R1, M1}^{J1}(\Omega_1^{12}) D_{\underline{N1}}(\Omega_1^{12}) d\Omega_1^{12} \\
 & \times \int D_{R2, M2}^{*J2}(\Omega_2^{12}) D_{\underline{N2}}(\Omega_2^{12}) d\Omega_2^{12} \int D_{0, R1}^{J1}(\Omega_{12}) D_{0, R2}^{*J2}(\Omega_{12}) \exp(i\mathbf{\underline{\kappa}} \cdot \mathbf{\underline{r}}) g_{\underline{N1} \underline{N2}}(r) \\
 & \times d\Omega_{12} r^2 dr \quad (2-18)
 \end{aligned}$$

where $\underline{N1} = \{\kappa1, M1', J1'\}$ and where the terms have been grouped according to their variables. The first integral must be changed to contain a complex conjugate by employing the identity

$$D_{\kappa, M}^{*J}(\Omega) = (-)^{\kappa-M} D_{-\kappa, -M}^J(\Omega) \quad (2-19)$$

Once this change has been made, the first two integrals may be evaluated by using Eq. (2-3). Orthogonality requires $J1 = J1'$, $R1 = -\kappa1$, $M1 = -M1'$, $J2 = J2'$, $R2 = \kappa2$, and $M2 = M2'$. Many of the summations in Eq. (2-18) thus become redundant and may be dropped. Substitution of the orthogonality relations into Eq. (2-18) and dropping primes leads to

$$\begin{aligned}
 I_2 = & \sum_{\underline{N1}, \underline{N2}} \frac{4\pi\rho^2}{[(2J1+1)(2J2+1)]^{1/2}} a_0^{*J1} a_{0, M2}^{J2} (-)^{\kappa1-M1} \\
 & \times \iint D_{0, -\kappa1}^{J1}(\Omega_{12}) D_{0, \kappa2}^{*J2}(\Omega_{12}) \exp(i\mathbf{\underline{\kappa}} \cdot \mathbf{\underline{r}}) g_{\underline{N1} \underline{N2}}(r) d\Omega_{12} r^2 dr \quad (2-20)
 \end{aligned}$$

The Ω_{12} integration in (2-20) may be carried out by spherical wave expanding the exponential and then employing Eq. (2-4). Thus,

$$\exp(i\mathbf{\underline{\kappa}} \cdot \mathbf{\underline{r}}) = (8\pi^2)^{1/2} \sum_J i^J (2J+1)^{1/2} j_J(\kappa r) D_{00}^J(\Omega_{12}) \quad (2-21)$$

The integral in Eq. (2-20) becomes

$$\begin{aligned}
 & (8\pi^2)^{1/2} \sum_J i^J (2J+1)^{1/2} \int j_J(\kappa r) \left[\int D_{0,-\kappa 1}^{J1}(\Omega_{12}) D_{0,\kappa 2}^{*J2}(\Omega_{12}) D_{00}^J(\Omega_{12}) d\Omega_{12} \right] \\
 & \quad \times g_{\underline{N1} \underline{N2}}(r) r^2 dr \\
 & = (8\pi^2)^{1/2} \sum_J i^J (2J+1)^{1/2} c(J, J1, J2; 00) c(J, J1, J2; 0, -\kappa 1) \\
 & \quad \delta_{\kappa 1, -\kappa 2} \left[\frac{(2J+1)(2J1+1)}{8\pi^2(2J2+1)} \right]^{1/2} \int j_J(\kappa r) g_{\underline{N1} \underline{N2}}(r) r^2 dr \quad (2-22)
 \end{aligned}$$

Substituting Eq. (2-22) into Eq. (2-20) gives

$$\begin{aligned}
 I_2 = & \sum_{\underline{N1} \underline{N2}} \rho^2 a_{0,-M1}^{*J1} a_{0,M2}^{J2} (-)^{\kappa 1 - M1} \sum_J i^J \frac{(2J+1)}{(2J2+1)} \\
 & \times c(J, J1, J2; 00) c(J, J1, J2; 0, \kappa 2) \int j_J(\kappa r) g_{\underline{N1} \underline{N2}}(r) 4\pi r^2 dr, \kappa 1 = -\kappa 2
 \end{aligned}$$

The term where $\underline{N1}, \underline{N2} = \underline{0}$ may be split out from I_2 and written separately. Since this is the spherical average term, the $g_{\underline{00}}(r)$ function is replaced by $g_{\underline{00}}(r) - 1$ so that convergence of the integral is maintained. Thus this two part expression for I_2 can be combined with Eq. (2-16) to give the total scattered intensity

$$\begin{aligned}
 V^{-1} I(\kappa) = & \rho \sum_{M,J} |a_{0,M}^J|^2 + \rho^2 |a_{\underline{0}}|^2 \int [g_{\underline{00}}(r) - 1] j_0(\kappa r) 4\pi r^2 dr \\
 & + \rho^2 \sum_{\substack{\underline{N1} \underline{N2} \\ \neq 0}} a_{0,-M1}^{*J1} a_{0,M2}^{J2} (-)^{\kappa 1 - M1} \sum_{J=|J1-J2|}^{J1+J2} i^J \frac{(2J+1)}{(2J2+1)} \\
 & \times c(J, J1, J2; 00) c(J, J1, J2; 0, \kappa 2) \int g_{\underline{N1} \underline{N2}}(r) j_J(\kappa r) 4\pi r^2 dr, \kappa 1 = -\kappa 2 \quad (2-23)
 \end{aligned}$$

If this equation is compared to the published Steele-Pecora results, certain differences are apparent. The principal difference is the appearance of the $(2J+1)/(2J_2+1)$ term. Other versions are possible by applying the symmetry properties of Clebsch-Gordan coefficients to those written here, but they do not agree with the incorrect SP equation.

Bibliography

1. W. A. Steele, R. Pecora, JCP 42, 1863 (1965)
2. W. A. Steele, JCP 39, 3197 (1963)
3. M. E. Rose, Elementary Theory of Angular Momentum, J. Wiley & Sons, New York, 1957

Appendix 3

RESTRICTIONS ON THE PERCUS-YEVICK HANKEL TRANSFORMS

The solution of the Percus-Yevick equation leads to a series of simultaneous equations involving the Hankel (spherical Bessel) transforms of the coefficients of the spherical harmonic expansion of the direct correlation function $c(\underline{R}_1, \underline{R}_2)$ and the density dependent part of the pair distribution function $H(\underline{R}_1, \underline{R}_2)$. The allowed transforms constitute a finite set of even order transforms, and it is the purpose of this appendix to derive these latter two restrictions.

We begin by noting that equation (6) is a general expression for the Fourier transform of any pair property. Hence the conclusions we can draw from it about $H(\ell\ell'ms)$ will also apply to $C(\ell\ell'ms)$.

In Eq. (6) we may split out the terms depending on m to give

$$\sum_m \overline{H}(\ell\ell'ms) c(\ell\ell's; m, -m) \quad (3-1)$$

Now the m values occur in plus and minus pairs and they take on the values $-\ell, -(\ell-1) \dots (\ell-1), \ell$ except for zero which occurs once. The terms in (3-1) with $m \neq 0$ therefore occur in pairs given by

$$\overline{H}(\ell\ell'ms) c(\ell\ell's; m, -m) + \overline{H}(\ell\ell' -ms) c(\ell\ell's; -m, m) \quad (3-2)$$

From (4-4), Appendix 4, we may rewrite the second Clebsch-Gordan coefficient according to

$$c(\ell\ell's; -m, m) = (-)^{\ell+\ell'-s} c(\ell\ell's; m, -m)$$

and (3-2) becomes

$$\overline{H}(\ell\ell'ms) c(\ell\ell's;m-m) + (-)^{\ell+\ell'-s} \overline{H}(\ell\ell'ms) c(\ell\ell's;-mm) \quad (3-3)$$

where we have used the identity $H_{\ell\ell'm} = H_{\ell\ell',-m}$. From symmetry studies of pair property expansions, it can be shown that $\ell+\ell'$ must be even. Thus it is apparent that unless s is also even the terms of (3-3) will cancel. The form in (3-1) which has $m=0$ occurs by itself and includes the Clebsch-Gordan coefficient $c(\ell\ell's;00)$. From (4-9) we have

$$c(\ell\ell's;00) = 0 \quad \text{unless} \quad \ell+\ell'+s \quad \text{is even}$$

Since $\ell+\ell'$ is even, s must be even here too. Thus in order for the entire sum (3-1) to be non-zero, s must be even.

A further restriction on s is also obtained from the Clebsch-Gordan coefficient in (3-1). The leading three parameters, i.e., ℓ , ℓ' and s of any Clebsch-Gordan coefficient must satisfy the triangle rule (4-7). This requires that s must have a value between $|\ell-\ell'|$ and $\ell+\ell'$, and so the allowed s values clearly form a bounded set. The properties of finiteness and evenness have thus been proven.

It is important to note that (6) is applied repeatedly in obtaining equation (10). Therefore, the same restrictions as just derived for (6) apply to (10) as well. It follows that in equating coefficients of (6) and (10), the only transforms allowed in either equation are H_{0000} , H_{2002} , H_{2200} , H_{2202} , H_{2204} , H_{4004} , and the corresponding ones for the direct correlation transforms if the $H_{\ell\ell'm}$ set is restricted to H_{000} , H_{200} , H_{220} , and H_{400} .

Appendix 4

CLEBSCH-GORDAN COEFFICIENTS

In both the Percus Yevick equations (Section III, equations (15)-(20)) and in the x-ray scattering equations (Section IV, equation (4)), Clebsch-Gordan coefficients appear. The properties of these coefficients are well known and are discussed in detail by Rose, reference(9) of Section III. For convenience we tabulate here the properties which have been used in this work.

An analytical form due to Wigner (Rose, 3.18) exists for the Clebsch-Gordan coefficients and is given by

$$\begin{aligned}
 c(j_1 j_2 j_3 m_1 m_2 m_3) &= \delta_{m_3, m_1+m_2} [(2j_3+1) \\
 &\times \left[\frac{(j_3+j_1-j_2)! (j_3-j_1+j_2)! (j_1+j_2-j_3)! (j_3+m_3)! (j_3-m_3)!}{(j_1+j_2+j_3+1)! (j_1-m_1)! (j_1+m_1)! (j_2-m_2)! (j_2+m_2)!} \right]^{1/2} \\
 &\times \sum_v \frac{(-)^{v+j_2+m_2} (j_2+j_3+m_1-v)! (j_1-m_1+v)!}{v! (j_3-j_1+j_2-v)! (j_3+m_3-v)! (v+j_1-j_2-m_3)!} \quad (4-1)
 \end{aligned}$$

v assumes all integral values such that none of the factorial arguments are negative. Still another expression exists due to Racah (Rose, 3.19). Both of these expressions however are quite tedious to use for evaluation and one therefore performs as much analysis as possible by using the orthogonality and symmetry relations of these coefficients. When actual evaluation is required, the tables of Condon and Shortley (reference 11, Section II) are useful, provided at

least one of the $j_i \leq 2$.

The orthogonality properties are:

$$\sum_{m_1} c(j_1 j_2 j; m_1, m-m_1) c(j_1 j_2 j'; m_1, m-m_1) = \delta_{jj'}, \quad (4-2)$$

$$\sum_j c(j_1 j_2 j; m_1, m-m_1) c(j_1 j_2 j; m'_1, m'-m'_1) = \delta_{m, m'_1} \delta_{m, m'} \quad (4-3)$$

The symmetry properties are:

$$c(j_1 j_2 j_3; m_1 m_2 m_3) = (-)^{j_1+j_2-j_3} c(j_1 j_2 j_3; -m_1, -m_2, -m_3) \quad (4-4)$$

$$= (-)^{j_1+j_2-j_3} c(j_2 j_1 j_3; m_2 m_1 m_3) \quad (4-5)$$

$$= (-)^{j_1-m_1} \left(\frac{2j_3+1}{2j_2+1} \right)^{1/2} c(j_1 j_3 j_2; m_1, -m_3, -m_2) \quad (4-6)$$

The triangle rule for the numbers j, j_1, j_2 is

$$j = j_1 + j_2, j_1 + j_2 - 1, \dots, |j_1 - j_2| \quad (4-7)$$

or, more simply, just $\Delta(j_1 j_2 j)$. Using this definition we note that

$$c(j_1 j_2 j; m_1, m-m_1) = 0 \text{ unless } \Delta(j_1 j_2 j). \quad (4-8)$$

Also

$$|m_1| \leq j_1, \quad |m| \leq j, \quad |m-m_1| \leq j_2.$$

The parity c-coefficient is

$$c(j_1 j_2 j_3; 000) = 0 \text{ unless } j_1 + j_2 + j_3 \text{ is even.} \quad (4-9)$$

We now tabulate the Clebsch-Gordan coefficients required in this work.

- A. Those with at least one j_i equal to zero. By using equations (4-4), (4-5), and (4-6) along with (4-10),

$$c(j_1 0 j_3; m_1 0 m_3) = \delta_{j_1 j_3} \delta_{m_1 m_3}, \quad (4-10)$$

all coefficients with at least one zero j may be evaluated.

- B. Those with $j_i \geq 2$. These are derived from the Condon and Shortley tables.

<u>Clebsch-Gordan Index Numbers</u>	<u>Value of Coefficient</u>
21100	$-\sqrt{2/5}$
21101	$\sqrt{1/10}$
22200	$-\sqrt{2/7}$
22201, 2220-1	$-\sqrt{1/14}$
22202, 2220-2, 222-22	$\sqrt{2/7}$
222-11	$\sqrt{1/14}$
42200, 24200	$\sqrt{2/7}$
42201, 24210	$-\sqrt{8/63}$
42202	$\sqrt{1/126}$
22400	$\sqrt{18/35}$
4222-2, 242-22	$\sqrt{5/42}$
22402, 2240-2	$\sqrt{3/14}$
242-11, 422-11	$-\sqrt{5/21}$
22401	$\sqrt{3/7}$
2242-2	$\sqrt{1/70}$
2241-1	$\sqrt{8/35}$

<u>Clebsch-Gordan Index Numbers</u>	<u>Value of Coefficient</u>
44200	$-10/3 \sqrt{1/77}$
442-11	$17/6 \sqrt{1/77}$
442-22	$-4/3 \sqrt{1/77}$
24400	$-\sqrt{20/77}$
2441-1	$\sqrt{3/154}$
2442-2	$3 \sqrt{3/77}$

C. Those with $j_i \geq 4$. These are limited in our work to those coefficients with $j_1 = j_2 = j_3 = 4$. These are not covered by the Condon and Shortley tables but may be evaluated by the special formulas for $c(L_1 L_2 L_3; 00)$ and for $c(LLv; 00)$ given by Rose 3.32 and 3.30, respectively, and the recurrence formula for Clebsch-Gordan coefficients given by Rose 3.27. These are:

$$c(L_1 L_2 L_3 \ 00) = (-)^{\frac{1}{2}(L_1+L_2-L_3)} \left(\frac{2L_3+1}{L_1+L_2+L_3+1} \right)^{1/2} \\ \times \frac{T(L_1+L_2+L_3)}{T(L_1+L_2-L_3) T(L_1-L_2+L_3) T(-L_1+L_2+L_3)}, \quad L_1+L_2+L_3 = \text{even} \quad (4-12)$$

where $T(x) = \frac{(\frac{1}{2}x)!}{\sqrt{x!}},$

$$c(LLv; 00) = \frac{2L(L+1)}{v(v+1) - 2L(L+1)} c(LLv; 1-1), \quad (4-13)$$

and the recurrence relation is

$$\begin{aligned}
 & [j_3(j_3+1) - j_1(j_1+1) - j_2(j_2+1) - 2m(M-m)] c(j_1 j_2 j_3; m, M-m) \\
 & = [(j_1-m+1)(j_1+m)(j_2+M-m+1)(j_2-M+m)]^{1/2} c(j_1 j_2 j_3; m-1, M-m+1) \\
 & + [(j_1+m+1)(j_1-m)(j_2-M+m+1)(j_2+M-m)]^{1/2} c(j_1 j_2 j_3; m+1, M-m-1) \quad (4-14)
 \end{aligned}$$

From (4-12) we obtain

$$c(444; 00) = 9 \sqrt{\frac{2}{1001}} \quad (4-15a)$$

From this last result and (4-13) we obtain

$$c(444; 1, -1) = -\frac{9}{2} \sqrt{\frac{2}{1001}} \quad (4-15b)$$

Finally from (4-14), (4-15a), and (4-15b) we obtain

$$c(444; 2-2) = -\frac{11}{2} \sqrt{\frac{2}{1001}} \quad (4-15c)$$

Appendix 5

SECOND VIRIAL COEFFICIENTS

For convenient reference, the second virial coefficients for the two-centered Lennard-Jones potential which were derived by Sweet and Steele (JCP 47, 3029 (1967)) are tabulated here for $R^* = 0.1$ to 0.4 .

T^*	R^*			
	0.1	0.2	0.3	0.4
0.4	-12.94	-11.08	-9.38	-8.085
0.6	- 5.89	- 5.16	-4.419	-3.807
0.8	- 3.553	- 3.106	-2.626	-2.201
1.0	- 2.401	- 2.075	-1.707	-1.384
1.4	- 1.283	- 1.053	-0.7889	-0.5317
1.8	- 0.7381	- 0.5522	-0.3326	-0.1123
2.0	- 0.5594	- 0.3874	-0.1821	+0.0262
2.2	- 0.4181	- 0.2568	-0.0622	0.1361
2.4	- 0.3035	- 0.1508	+0.0345	0.2252
2.6	- 0.2090	- 0.0634	0.1143	0.2986
2.8	- 0.1298	+ 0.0104	0.1811	0.3606
3.0	- 0.0625	0.0725	0.2378	--
3.2	- 0.0049	0.1258	0.2864	0.4569
3.4	+ 0.0450	--	0.3285	--
4.0	0.1611	0.2804	0.4257	0.5843
5.0	0.2848	0.3927	0.5284	0.6759
6.0	0.3620	0.4627	0.5918	--

Appendix 6

TRIGONOMETRIC FORMS OF SPHERICAL BESSEL FUNCTIONS

$$j_0(x) = \frac{\sin x}{x}$$

$$j_1(x) = \frac{\sin x}{x^2} - \frac{\cos x}{x}$$

$$j_2(x) = \left(\frac{3}{x} - \frac{1}{x}\right) \sin x - \frac{3}{x^2} \cos x$$

$$j_3(x) = \left(\frac{15}{x^4} - \frac{6}{x^2}\right) \sin x - \left(\frac{15}{x^3} - \frac{1}{x}\right) \cos x$$

$$j_4(x) = \frac{\sin x}{x} \left(\frac{105}{x^4} - \frac{45}{x^2} + 1\right) - \left(\frac{105}{x^4} - \frac{10}{x^2}\right) \cos x$$

Asymptotic expression at $x = 0$:

$$x^{-n} j_n(x) = \frac{1}{1 \cdot 3 \cdot 5 \cdots (2n+1)}$$

(provides 4 significant figure accuracy for $j_4(x)$ at $x = 0.1$)

Recurrence formulas:

$$j_n(x) = f_n(x) \sin x + (-)^{n+1} f_{-n-1}(x) \cos x$$

$$f_0(x) = x^{-1}, \quad f_1(x) = x^{-2}$$

$$f_{n-1}(x) + f_{n+1}(x) = (2n+1) x^{-1} f_n(x)$$

PROPOSITIONS

PROPOSITION I

Abstract

Two methods for calculating the third virial coefficient $C(T)$ for nonspherical molecules are discussed. One is the direct evaluation of the cluster integral. The other is an application of statistical mechanical perturbation theory (PT). It is proposed that both sets of calculations be carried out to evaluate $C(T)$ for a modified two-centered Lennard-Jones potential. It is shown that the PT approach must include the second order term and it is suggested that the Barker-Henderson macroscopic compressibility approximation for it be used. Comparison of cluster integral and PT results will allow determination of the temperature below which the perturbation approach is grossly inaccurate, a result that can be extended to other potentials. Finally, $C(T)$ may be expressed as a sum of spherical and nonspherical contributions and a comparison of the two will give the first quantitative estimate of the size of the nonspherical repulsion correlation on $C(T)$.

A fluid equation of state valid in the moderately dense gas region is the virial equation of state. The ability of a particular potential to predict a third virial coefficient that agrees with experimental data is one of the measures of accuracy of the potential. One may note that second virial coefficients are of little or no use in examining the potential, since they are used to determine the parameters which characterize the potential. Third virial coefficients have been studied extensively for spherical potentials of the square well¹ and Lennard-Jones types^{2,3,4}. The calculations of third virial coefficients for nonspherical potentials have strongly

emphasized multipole interactions superimposed on a spherically symmetric repulsive core^{4,5,6}.

Recently work has begun to appear which employs nonspherical repulsive cores^{7,8,9}. The work of Chen and Steele gave values of the second, third, and Percus Yevick fourth virial coefficients for dumbbell-like two-centered hard core molecules (2HC potential). The method of calculation is superior to the earlier multipole work in that the expansions involved do not depend on the particular potential being used. All expressions are given as a function of the Mayer f functions and these may be easily obtained in a separate calculation following the work of Sweet¹⁰. Hence the method may be applied to potentials other than the 2HC potential. One should note, however, that this approach has the significant drawback of being a quite lengthy calculation.

Because of this length a shorter method of calculation would be desirable. One suggested approach is through statistical mechanical perturbation theory⁷. This theory^{11,12} requires that some previous basis calculation has been carried out providing accurate pair distribution functions. Since diatomic hard core calculations have recently been performed, such an attack on nonspherical molecules is now possible.

It is therefore proposed that third virial coefficients be evaluated for a modified two-centered Lennard-Jones potential (mod-2LJ), proceeding later to a true 2LJ potential. This may be accomplished either by applying Chen's cluster integral (CI) method to the mod-2LJ potential or by developing and applying a perturbation


equation. The coefficients would be calculated as a function of temperature and expressed as the sum of a spherically symmetric part and an angular part. Since it has been claimed⁴ that the temperature dependence of the third virial coefficient depends on the angular correlations between molecules, a comparison of these two parts of $C(T)$ would give the first quantitative estimate of the size of nonspherical repulsive effects.

In the following two sections we will review Chen's procedure and then develop a possible perturbation approach. The review of Chen's method will be quite brief, since no modifications are suggested here and his paper contains a good presentation of the theory.


A. Cluster Integral Evaluation (CI)⁷

The cluster integral for $C(T)$ is

$$C(T) = -\frac{1}{3V} \triangle = -\frac{1}{48\pi^2 V} \int f(\underline{R}_1 \underline{R}_2) \text{ (rooted triangle diagram) } d\underline{R}_1 d\underline{R}_2 \quad (1)$$

The CI method involves expanding the rooted triangle diagram, , as

$$\text{ (rooted triangle diagram) } = 4\pi \sum_{\ell \ell' m} t_{\ell \ell' m}(r) Y_{\ell, m}(\Omega_1) Y_{\ell', -m}(\Omega_2) \quad (2)$$

evaluating the coefficients $t_{\ell \ell' m}$, and then performing the integration of (1) for $C(T)$. The evaluation of  proceeds as follows. Multiply both sides of (2) by the complex conjugates of the two harmonics shown and integrate over the Euler angles to give

$$t_{\ell\ell'm}(r) = \frac{1}{16\pi^2} \int \cdots \int f(\underline{R}_1 \underline{R}_3) f(\underline{R}_2 \underline{R}_3) Y_{\ell m}^*(\Omega_1) Y_{\ell' -m}^*(\Omega_2) \times d\Omega_1 d\Omega_2 d\Omega_3 d\underline{r}_3 \quad (3)$$

Harmonic expansions of the two Mayer f functions are substituted into this last expression. The three pairs of spherical harmonics in (3) have their angles expressed in different relative coordinate systems and the angles of each pair must be rotated to a common coordinate system by use of the extended spherical harmonic addition theorem. The resulting expression can be evaluated directly only with great difficulty due to the complicated functional form of the angular variables. Hence $t_{\ell\ell'm}$ is exponentially Fourier transformed; the complex exponential is expanded into a set of angular functions which allows the angular integrations to be performed; and then the expression is back transformed to give $t_{\ell\ell'm}(r)$.

The final expression for $t_{\ell\ell'm}(r)$ involves seven summations over Bessel transforms of the form

$$B(r) = \int_0^\infty b_1(\tau) b_2(\tau) j_s(\tau r) \tau^2 d\tau$$

where b_1 and b_2 are themselves Bessel transforms over Mayer function coefficients. The final expression is manageable because the number of Mayer coefficients that lead to significantly large b functions is relatively small.

B. Perturbation Theory (PT)

In its usual form first order perturbation theory^{11,12} expresses the configurational free energy as

$$A = A_o + \frac{N\rho}{8\pi} \int \cdots \int g_o(\underline{R}_1 \underline{R}_2) u_1(\underline{R}_1 \underline{R}_2) r^2 dr d\Omega_1 d\Omega_2 + O(\beta) \quad (4)$$

The expression has been generalized to include the Euler angles of orientation of molecules 1 and 2; $g_o(\underline{R}_1 \underline{R}_2)$ is the 2HC radial distribution function; and $u_1(\underline{R}_1 \underline{R}_2)$ is the perturbing potential defined by

$$u_1(\underline{R}_1 \underline{R}_2) = u(\underline{R}_1 \underline{R}_2) - u_o(\underline{R}_1 \underline{R}_2) \quad (5)$$

where $u(\underline{R}_1 \underline{R}_2)$ is the total interaction potential and $u_o(\underline{R}_1 \underline{R}_2)$ is the 2HC potential. $u_1(\underline{R}_1 \underline{R}_2)$ is zero when $u_o(\underline{R}_1 \underline{R}_2)$ is infinite. The pressure is related to A by

$$PV = \rho \left(\frac{\partial A}{\partial \rho} \right)_T \quad (6)$$

and so

$$PV = (PV)_o + \frac{N\rho}{8\pi} \frac{\partial}{\partial \rho} \rho \int \cdots \int g_o(\underline{R}_1 \underline{R}_2) u_1(\underline{R}_1 \underline{R}_2) r^2 dr d\Omega_1 d\Omega_2 + O(\beta) \quad (7)$$

The virial coefficients may be identified by substituting the density expansion for $g_o(\underline{R}_1 \underline{R}_2)$ into (7). The expansion is

$$g_o(\underline{R}_1 \underline{R}_2) = e^{-u_o(\underline{R}_1 \underline{R}_2)\beta} \left\{ 1 + \left(\text{diagram 1} \right)_o \rho + \left[\left(\text{diagram 2} \right)_o + 2 \left(\text{diagram 3} \right)_o \right. \right. \\ \left. \left. + \frac{1}{2} \left(\text{diagram 4} \right)_o + \frac{1}{2} \left(\text{diagram 5} \right)_o \right] \rho^2 + \cdots \right\} \quad (8)$$

where the root diagrams are orientation dependent. Hence $C(T)$ is identifiable as the coefficient of ρ^2 in (7) multiplied by β/N :

$$C_1(T) = \frac{1}{4\pi kT} \int \cdots \int (\bigcirc \bigcirc)_0 e^{-u_0(R_1 R_2)^\beta} u_1(R_1 R_2) r^2 dr d\Omega_1 d\Omega_2 \quad (9)$$

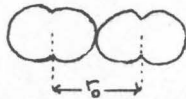
The one subscript on $C_1(T)$ signifies first order perturbation theory. As this integral stands, the integration is over five variables. This may be improved by expanding each of the orientation dependent members of the integrand into the orthonormal expansions of Steele¹³, Eq. (2), or

$$u_1(R_1 R_2) = u_1(r\theta\theta'\phi) = 4\pi\epsilon \sum_{\ell\ell',m} u'_{\ell\ell',m}(r) Y_{\ell,m}(\Omega_1) Y_{\ell',-m}(\Omega_2) \quad (10)$$

$(\bigcirc \bigcirc)_0$ and $e^{-u_0(R_1 R_2)^\beta} - 1 = f_0(R_1 R_2)$ have been tabulated in such a form already by Chen and no new evaluation is required. On the other hand, the perturbing potential $u_1(R_1 R_2)$ must have its $u'_{\ell\ell',m}(r)$ coefficients computed. From (10) the expression for $u'_{\ell\ell',m}(r)$ is

$$u'_{\ell\ell',m}(r) = \frac{1}{2\epsilon} \int_0^{2\pi} \int_{-1}^1 \int_{-1}^1 u_1(r\theta\theta'\phi) P_{\ell,m}(\theta) P_{\ell',-m}(\theta') \\ \times \cos m\phi d \cos \theta d \cos \theta' d\phi$$

For values of r less than the maximum hard core contact distance r_0 ,



it is clear that for certain orientations the hard cores will overlap and the perturbing potential will become discontinuously zero (while the total potential becomes infinite). This presents no real computational problem except that the θ, θ', ϕ grid may have to be small in

this region of r space in order to obtain high accuracy.

Substituting (2), (10), and an expansion similar to (2) for $f_o(\underline{R}_1, \underline{R}_2)$ into (9), one obtains

$$\begin{aligned}
 C_1(T) = & \frac{4\pi\epsilon}{kT} \int t_{000}(r) u'_{000}(r) [1 + f_{000}^o(r)] r^2 dr \\
 & + \frac{16\pi^2\epsilon}{kT} \sum_{\ell\ell'm} \sum_{kk'n} \sum_{jj'p} \int t_{\ell\ell'm}(r) u'_{kk'n}(r) f_{jj'p}^o(r) r^2 dr \\
 & \times \int Y_{\ell,m}(\Omega_1) Y_{kn}(\Omega_1) Y_{jp}(\Omega_1) d\Omega_1 \int Y_{\ell',-m}(\Omega_2) Y_{k',-n}(\Omega_2) Y_{j',-p}(\Omega_2) d\Omega_2
 \end{aligned} \tag{11}$$

The triple harmonic integrals are given by¹⁴

$$\begin{aligned}
 \int Y_{\ell m}(\Omega) Y_{kn}(\Omega) Y_{jp}(\Omega) d\Omega = & (-)^m \left[\frac{(2k+1)(2j+1)}{4\pi(2\ell+1)} \right]^{1/2} \\
 & \times c(jk\ell; pn-m) c(jk\ell; 000)
 \end{aligned} \tag{12}$$

where $c(\)$ is a Clebsch-Gordan coefficient.

Equation (11) may be evaluated by performing a Simpson's integration over the integrals, including as many as is necessary to achieve a desired accuracy of $C(T)$. Calculations of the expansion coefficients⁷ of (\bigwedge_o) have shown that only two coefficients are significant, t_{000} and t_{200} , and hence the $\ell\ell'm$ summations in the second term above may be reduced to include $(\ell\ell'm) = (2,0,0)$ and $(0,2,0)$ only. The Mayer function and most likely $u_1(\underline{R}_1, \underline{R}_2)$ as well will have expansion coefficients up to 400 that will have to be included in the summations above.

When Smith and Alder² applied first order perturbation theory to the third virial calculations of spherical molecules (using a Mod.-LJ potential), they found that the coefficient was in error by about 25% at $T^* = 5.0$ with the error growing rapidly larger as the temperature was decreased. This implied that second order perturbation theory would be required if the temperature range were to be extended to lower temperatures. From work done by Pople and Alder¹⁵ on the mod-LJ potential, one may estimate that $C(T)$ is accurate to about 10% at $T^* = 1.67$ when the second order term is included. Later work by Barker and Henderson¹ on the square well potential showed similar results, obtaining an 8% error in $C(T)$ at $T^* = 1.4$, $\lambda = 1.5$ where $\lambda\sigma$ is the value of the outer wall position. For $\lambda = 2.0$, $C(T)$ began to show error below $T^* = 3.0$. Hence it appears that it will be necessary to include the second order perturbation term for our modified 2LJ potential.

The rigorous expression for the second order perturbation involves three and four body distribution functions which are nearly impossible to evaluate. Fortunately an approximate expression exists which is easy to use; it is the macroscopic compressibility approximation (MC)¹. Pressure calculations from perturbation theory have been performed using this approximation for the square well potential and most recently for mixtures of spherical molecules interacting via a Kihara potential¹⁶. Both works indicate that the approximation is quite good, especially the latter work where agreement with experimental data is excellent.

Using the MC approximation, (4) can be replaced by

$$\begin{aligned}
 A &= A_0 + \frac{N\rho}{8\pi} \int \cdots \int g_0(\underline{R}_1 \underline{R}_2) u_1(\underline{R}_1 \underline{R}_2) r^2 dr d\Omega_1 d\Omega_2 \\
 &\quad - \frac{\beta \rho N}{16\pi} \int \cdots \int [u_1(\underline{R}_1 \underline{R}_2)]^2 kT \left(\frac{\partial \rho}{\partial P} \right)_0 g_0(\underline{R}_1 \underline{R}_2) r^2 dr d\Omega_1 d\Omega_2 + O(\beta^2) \\
 &= A_0 + A_1 + A_2
 \end{aligned} \tag{13}$$

where $\left(\frac{\partial \rho}{\partial P} \right)_0$ is the compressibility of the hard core system. $\left(\frac{\partial \rho}{\partial P} \right)_0$ can be obtained as a density expansion using the Pade' approximant⁷ $P(2,2)$ for the 2HC equation of state or, more simply, by using the 2HC virial expansion. One may write the virial expansion as

$$\frac{P}{kT} = \rho + B_0 \rho^2 + C_0 \rho^3 + \cdots$$

where ρ , B_0 , and C_0 have number density units; hence by differentiation and division

$$\beta^{-1} \left(\frac{\partial \rho}{\partial P} \right)_0 = 1 - 2B_0 \rho + (4B_0^2 - 3C_0) \rho^2 + \cdots \tag{14}$$

The first two terms of (13) lead to $C_1(T)$ as before, while the third term (A_2) gives the second order perturbation contribution, $C_2(T)$.

Hence from $PV = \rho \left(\frac{\partial A}{\partial \rho} \right)_T$,

$$\begin{aligned}
 C_2(T) &= \frac{-\beta^2}{8\pi} \int \cdots \int [u_1(\underline{R}_1 \underline{R}_2)]^2 \left[\left(\bigwedge \right)_0 - 2B_0(T) \right] \\
 &\quad \times e^{-u_0(\underline{R}_1 \underline{R}_2)\beta} r^2 dr d\Omega_1 d\Omega_2
 \end{aligned} \tag{15}$$

This integral may be evaluated in the same fashion as was $C_1(T)$. The only difference is that the integral over $[u_1(\underline{R}_1 \underline{R}_2)]^2 \left(\bigwedge \right)_0 \times$

$[f(R_1 R_2) + 1]$ involves four spherical harmonic expressions and the expansions, although straightforward, will be considerably longer. An expression for

$$\int Y_{\ell m}(\Omega) Y_{kn}(\Omega) Y_{jp}(\Omega) Y_{iq}(\Omega) d\Omega$$

will also have to be derived, but this may easily be accomplished by combining the harmonics in pairs by using the spherical harmonic coupling theorem¹⁴ followed by application of the harmonic orthogonality relation. One may note that the 2HC second virial coefficient required in (15) is known quite accurately, the error apparently running less than 1%¹⁰. The third virial coefficient accurate to second order is thus given by

$$C(T) = C_1(T) + C_2(T)$$

Now that the methods of evaluation have been outlined, only a few comments remain to be made about the $C(T)$ that are finally obtained. As shown by Smith and Alder, the $C(T)$ obtained from perturbation theory will become rapidly divergent from the true $C(T)$ below some temperature T_O^* . Therefore it will be advantageous to compare the $C(T)$ values from the CI and PT calculations to determine what this temperature is. Most likely this T_O^* will also lie near the convergence temperature for other nonspherical potentials. If, contrary to expectation, agreement between the CI and PT $C(T)$ values is poor above T_O^* , then one must doubt the accuracy of the MC approximation when applied to nonspherical systems.

Another comment which must be made concerns the separation of $C(T)$ into spherical and nonspherical parts. Since spherical potentials such as the LJ potential have often been used to describe nonspherical molecules, it might seem appropriate to separate $C(T)$ into a part that depends on the spherical average of the potential (u_{000}) and another part that depends on the angular parts of the potential ($u_{\ell\ell'm;\ell,\ell' \neq 0}$). This kind of separation is very difficult, however, since the spherical average of a given pair function such as \bigtriangleup or $f(\underline{R}_1, \underline{R}_2)$ does not correspond directly to u_{000} . Hence it is convenient to use another separation. It is proposed that the spherical part of $C(T)$ be taken as

$$C_{\text{sph}}(T) = - \frac{1}{3V} \int f_{000}(r_{12}) f_{000}(r_{13}) f_{000}(r_{23}) d\underline{r}_1 d\underline{r}_2 d\underline{r}_3$$

where f_{000} is the spherical average of the Mayer f function for the mod-2LJ potential. The nonspherical contribution may then be represented as

$$C_{\text{nonsph}}(T) = C(T) [\text{Pert. Theory; } T^* > T_o^*] - C_{\text{sph}}(T)$$

Bibliography

1. J. Barker, D. Henderson, JCP 47, 2856 (1967)
2. E. Smith, B. Alder, JCP 30, 1190 (1959)
3. J. Barker, P. Leonard, A. Pompe, JCP 44, 4206 (1966)
4. J. Hirschfelder, C. Curtiss, R. Bird, Molecular Theory of Gases and Liquids, J. Wiley and Sons, New York, 1954
5. H. Levine, D. McQuarrie, JCP 44, 3500 (1966)
6. D. E. Stogryn, JCP 50, 4967 (1969)
7. Y. Chen, W. Steele, JCP 50, 1428 (1969)
8. M. Rigby, JCP 53, 1021 (1970)
9. R. Gibbons, Mol. Phys. 17, 81 (1969)
10. J. Sweet, W. Steele, JCP 47, 3029 (1967)
11. R. Zwanzig, JCP 22, 1420 (1954)
12. J. Barker, D. Henderson, JCP 47, 4714 (1967); 53, 508 (1970)
13. W. Steele, JCP 39, 3197 (1963)
14. M. Rose, Elementary Theory of Angular Momentum, J. Wiley and Sons, New York, 1957, p. 62
15. B. Alder, J. Pople, JCP 26, 325 (1957)
16. B. Rogers, J. Prausnitz, Trans. Far. Soc. 67, 3474 (1971)

PROPOSITION II

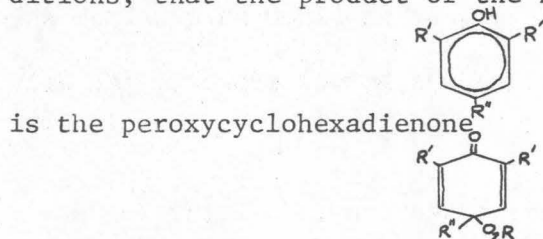
Abstract

It is proposed that the kinetics of the copper (II)-amine catalyzed decomposition of hydroperoxides in the presence of 2,6-di-*t*-butyl-*p*-cresol be thoroughly investigated since this type of antioxidant behavior has not been studied previously. The reaction is to be run using different cupric salts and amines as catalysts and the resulting products are to be analyzed for an expected peroxycyclohexadienone product. Assuming this expected product is formed, a reaction mechanism is proposed that accounts for presently known experimental information. The kinetic equations for this mechanism are derived and the experimental program required for its verification is discussed.

It is well known that many autoxidations proceed by free-radical chain reactions¹. Generally hydroperoxides are formed first and then decompose into alkoxy or peroxy free radicals, these attacking the substrate and propagating the chain reaction. To prevent such chain reactions, substances which form relatively stable free radicals are often added to the reacting medium so that these free radicals will react with the peroxy radicals to form stable decomposition products, thus terminating the chain reaction. It has been known for some time that several of these reactions are catalyzed by certain transition metal ions².

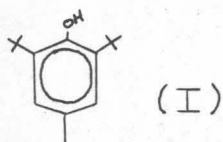
More recently it was discovered that very small amounts of cupric salts and amines in the presence of sterically hindered phenols were extremely effective catalysts, leading to hydroperoxide decomposition rates far in excess of those encountered in earlier work^{3a}. Because of the great speed involved, this reaction becomes important in that it may be used to develop a very efficient antioxidant oil additive.

To date, however, only a minimal amount of information is available about this reaction. Principally this information includes the following: (a) the hydroperoxide decomposition rate is rapid; (b) only catalytic amounts of copper (II) are required; (c) a free radical from the phenol is formed; and (d) the activity of amines is in the order primary > secondary >> tertiary. In fact, when tertiary amines are present, no increase in hydroperoxide decomposition rate is detectable. It is assumed, although not proven for all conditions, that the product of the hydroperoxide, ROOH, and phenol

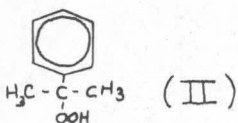


Since so little is known about this reaction, it is proposed that a detailed study be carried out on it. Such a study would have two parts. The first would be to verify the predominance of the peroxy-cyclohexadienone in the product and to see if its contribution varies when different amounts of cupric salts and amines are used. The second part would be to propose a reaction mechanism consistent with the products formed and to conduct experiments to determine its validity.

Initial work on this system employed 2,6-di-*t*-butyl-*p*-cresol (a common oil additive),

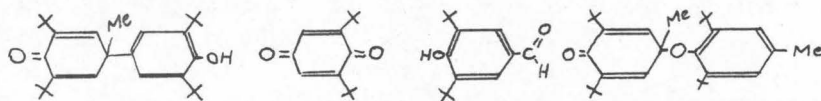


and cumene hydroperoxide,



and these are proposed for use in this study as well (although (II) might be replaced by t-butyl hydroperoxide to reduce absorption in the ultraviolet range [see below]). The solvent material is isooctane. A readily available cupric salt soluble in these solvents is cupric octoate and possible amines are dimethyl amine, cyclohexyl amine, and morpholine.

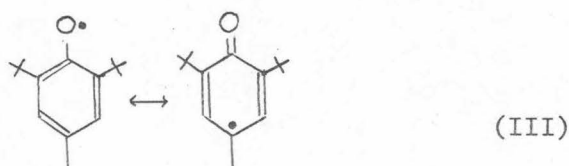
A reactant which must be excluded however is oxygen, since it will compete with the hydroperoxide for phenol and lead to its own set of products. Hewitt⁴ has recently tabulated the products obtained from the system oxygen/(I)/CuCl₂/morpholine in methanol at various CuCl₂ concentrations. These include



Appearance of these compounds in products of the copper amine catalyzed reactions may be indicative of oxygen contamination. Of note is the fact that the various proportions of the oxygen products depended heavily on the CuCl₂ concentration although for certain ranges of reactant concentrations a single component product was obtained. It is possible that such a dependence may also be present in our hydroperoxide system and therefore it is necessary that the products of our reaction be isolated, principally by fractional crystallization, and checked for a similar copper dependence.

While Hewitt's work suggests that several products could be formed, it is expected that this will not be the case if (I) is employed and that a single cyclohexadienone product will be formed. It has been found^{5,6} that RO₂• radicals, derived from hydroperoxides such as (II), will react in the presence of oxygen with the free radical derived

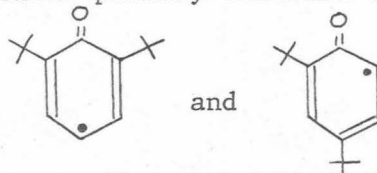
from (I)



to yield

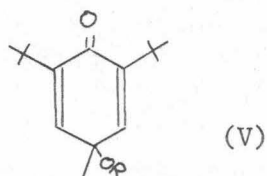


(IV) was produced almost exclusively from (I) under these conditions; other phenols and their phenoxy radicals such as



give mixtures of products of peroxy-phenoxy coupling¹. Thus the study of the copper amine reaction should be limited to the use of (I) in the hope of keeping the product composition simple.

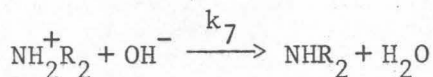
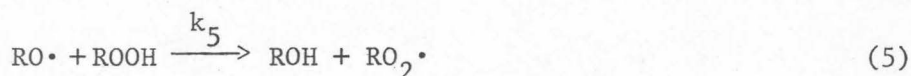
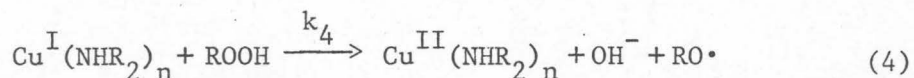
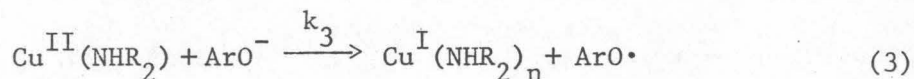
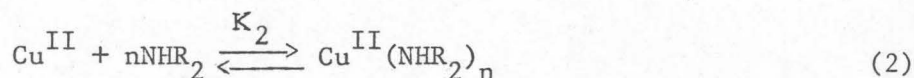
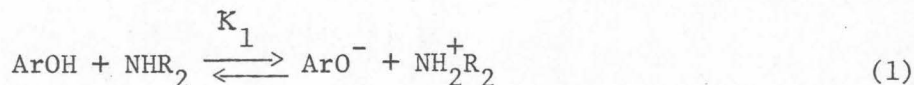
Another product of the copper amine reaction has been suggested^{3a} which involves the coupling of alkoxy radicals, $RO\cdot$, with (III) to give the ether



It has also been found^{3b} that if the final copper amine product mixture were reacted with HI, the same amount of iodine was formed as would be generated from the original hydroperoxide. If one assumed that the only products possible were (IV) and (V), this result indicated that (IV) was formed since (V) was not capable of producing iodine. This does not prove that (IV) is formed since if (V) were formed along with some other compound that produced I_2 from HI, the results would be the same. Such other compounds seem unlikely however and it is presumed

henceforth that (IV) is the principal product.

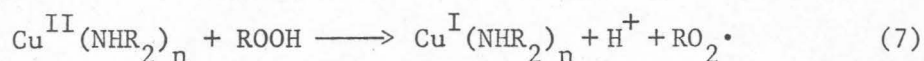
In order to arrive at a complete understanding of the copper amine catalyzed reaction, it would be desirable to determine its reaction mechanism. Based on the information above, a tentative proposal for the mechanism may be made. It is:



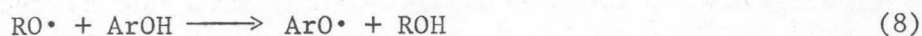
where $\text{ArOH} = (\text{I})$ and $\text{ROOH} = (\text{II})$. This mechanism satisfies the observation that increasing the amine concentration increases the rate of reaction^{3a} since proton abstraction from the phenol is required. It also explains why tertiary amines do not catalyze the reaction since the amine alkyl groups and phenolic t-butyl groups would sterically hinder the abstraction. Reaction (3) is similar to one proposed by Ogata⁷ in the polymerization mechanism of o-cresol. Reaction (4) is well known^{1,8} and applies to many transition metals. The reactive catalyst is the copper amine complex and this correlates with the observation^{3a} that if either the cupric salt or amine is left out of

the reaction, the hydroperoxide decomposition rate shifts from a matter of several minutes to several hours. Before reactions (4) and (5) can begin, some Cu^{I} complex must be produced by reaction (3) and this provides a mechanism for a nearly steady state ArO^\bullet free radical concentration.

Another mechanism that one must consider includes reactions (1), (2), (4) and (6) but would replace reaction (3) with



and reaction (5) with



This alternate route has to be considered at the outset since reactions corresponding to the copper catalysis reactions of equations (4) and (7) have been suggested as intermediate steps in a cobalt catalysis of hydroperoxide decomposition⁹. However, while these reactions account for the peroxy radical formation required for the final product, they seem to lead to difficulty in that they force the ArO^\bullet radicals to be produced from ArOH . This would imply that if the amine concentration were decreased so that reaction (1) would shift to the left, the overall rate of hydroperoxide decomposition would increase. As noted above, this is not what is observed experimentally and it must be concluded that the latter mechanism is incorrect. It is difficult to develop any other hierarchy of equations built around reactions (4) and (7) that will account for the experimental observations, and so it presently appears that the copper catalysis reactions of equations (3) and (4)

are to be preferred.

Having proposed a mechanism it is now possible to indicate how a kinetic study of this reaction would proceed. The first part of such a kinetic study would involve measuring the time-dependent concentrations of two of the reacting compounds. Perhaps the most important one to measure is that of (IV). This may be done by ultra-violet spectroscopy by measuring the dienone absorption peak at 246 m μ ($\epsilon = 15000$ l/mole/cm)¹⁰. (I) and (II) have absorptions in the ultra-violet but their peaks lie at different wavelengths. (II) has its peaks above 246 m μ , the first lying near 260 m μ ¹¹. (I) has a peak at 280 m μ ($\epsilon = 2000$) and another below 230 m μ . It has a minimum at 246 m μ . Both (I) and (II) have extinction coefficients near 200 l/mole/cm at 246 m μ , obviously far less than that of (IV). The phenolate anion of (I) is an interfering compound if its concentration is high, since it has a peak close enough to 246 m μ to account for a high extinction coefficient of about 2000 at this wavelength. However, in view of a hydrogen abstraction study carried out by Coggeshall et al¹², it seems safe to assume that this concentration will remain small because of the blocking effects of the butyl groups (these will even block OH⁻). The phenolate concentration may also be kept low by keeping the amine concentration at or just slightly above catalytic levels. Hence the absorption values at 246 m μ are mainly due to (IV), except near the beginning of the reaction where its concentration is still small. The possibility of solvent interference is eliminated by using isooctane as solvent. Note also that this spectral absorption, combined with evidence for an IR peroxy absorption, could be used to verify the presence of (IV) in the final product mixture.

The second component that should be measured is the phenoxy free radical concentration as a function of time. It has already been observed that this radical is present in sufficient concentration in non-flowing systems to be easily measured by electron spin resonance. If resonance spectra are taken of this radical as a function of time, the ArO^\bullet concentration can be obtained by calibrating the spectra against the stable free radical diphenylpicrylhydrazyl.

The remainder of the kinetic study involves deriving the equation which gives (IV) as a function of time and comparing the predicted behavior of (IV) against that observed experimentally. Although modifications may be called for in the future, a kinetic treatment of the mechanism contained in equations (1) to (6) is now presented.

The basic assumptions of the kinetics are: (a) the RO^\bullet and RO_2^\bullet radical concentrations are steady state; (b) the ArO^\bullet concentration is negligible compared to $[\text{OArO}_2\text{R}] + [\text{ArOH}]$ or $[\text{ROOH}] + [\text{OArO}_2\text{R}]$; (c) the RO^\bullet and RO_2^\bullet concentrations are very small; and (d) the reverse of reactions (3) - (6) are negligible. Using these assumptions, the stoichiometric quantities (denoted by s) of cupric salt and (I) and (II) may be related to other species by:

$$[\text{ArOH}]_s = [\text{ArOH}] + [\text{ArO}^-] + [\text{OArO}_2\text{R}] \quad (9)$$

$$[\text{Cu}^{\text{II}}]_s = [\text{Cu}^{\text{II}}(\text{NHR}_2)] + [\text{Cu}^{\text{I}}(\text{NHR}_2)] + [\text{Cu}^{\text{II}}] \quad (10)$$

$$[\text{ROOH}]_s = [\text{ROOH}] + [\text{OArO}_2\text{R}] \cdot 2 \quad (k_6 > k_5) \quad (11)$$

For simplicity, the amine concentration has been restricted so that there is only a single copper coordination. Also, by a suitable choice of amine, reaction (2) may be chosen to have its equilibrium lie far to

the right, thus rendering $[Cu^{II}]$ negligible in (10) . Hence,

$$[Cu^{II}]_s = [Cu^{II}N] + [Cu^I N] \quad (12)$$

where N denotes NHR_2 .

Steady state conditions lead to:

$$\frac{d[RO\cdot]}{dt} = 0 = k_4[Cu^I N][ROOH] - k_5[RO\cdot][ROOH] \quad (13)$$

$$\frac{d[RO_2\cdot]}{dt} = 0 = k_5[RO\cdot][ROOH] - k_6[RO_2\cdot][ArO\cdot] \quad (14)$$

or by solving (13) and (14)

$$k_6[RO_2\cdot][ArO\cdot] = k_4[Cu^I N][ROOH] \quad (15)$$

In addition to the steady state equations, the ESR study of $ArO\cdot$ provides one with data for $\frac{d[ArO\cdot]}{dt}$. Preliminary data^{3a} indicates that the $ArO\cdot$ concentration changes slowly with time and is nearly linear. Hence

$$\frac{d[ArO\cdot]}{dt} = f(t) = k_3[Cu^{II}N][ArO^-] - k_6[RO_2\cdot][ArO\cdot] \quad (16)$$

Substituting (15) into (16)

$$[Cu^I N] = k_4^{-1}[ROOH]^{-1} \{ [Cu^{II}N][ArO^-]k_3 - f(t) \} \quad (17)$$

and solving (17) and (12)

$$[\text{Cu}^{\text{I}}_{\text{N}}] = \frac{k_4^{-1}[\text{ROOH}]^{-1} \{k_3[\text{Cu}^{\text{II}}]_{\text{s}}[\text{ArO}^-] - f(t)\}}{1 + k_4^{-1}[\text{ROOH}]^{-1} [\text{ArO}^-] k_3} \quad (18)$$

Now the rate of formation of product is described by

$$\frac{d[\text{OArO}_2\text{R}]}{dt} = k_6[\text{RO}_2^\bullet][\text{ArO}^\bullet]$$

which from (11), (15), and (18) becomes

$$\frac{d[\text{OArO}_2\text{R}]}{dt} = \frac{k_3[\text{Cu}^{\text{II}}]_{\text{s}}[\text{ArO}^-] - f(t)}{1 + k_3k_4^{-1}[\text{ArO}^-] \{[\text{ROOH}]_{\text{s}} - 2[\text{OArO}_2\text{R}]\}^{-1}} \quad (19)$$

The only unmeasured quantity in (19) is the $[\text{ArO}^-]$, but this may be obtained by treating (1) as an equilibrium expression and solving

$$\begin{aligned} K_1 &= \frac{[\text{ArO}^-][\text{NH}_2^+\text{R}_2]}{[\text{ArOH}][\text{NHR}_2]} \\ &= \frac{[\text{ArO}^-]^2}{\{[\text{ArOH}]_{\text{s}} - [\text{ArO}^-] - [\text{OArO}_2\text{R}]\} \{[\text{NHR}_2]_{\text{s}} - [\text{ArO}^-] - [\text{Cu}^{\text{II}}]_{\text{s}}\}} \end{aligned} \quad (20)$$

for $[\text{ArO}^-]$ where use has been made of (9) and $[\text{NH}_2^+\text{R}_2]$ has been set equal to $[\text{ArO}^-]$. This is a good approximation if $k_4, k_7 \gg k_3$.

Alternatively, if $k_3, k_7 \gg k_4$, $[\text{NH}_2^+\text{R}_2] = [\text{ArO}^-] + [\text{ArO}^\bullet]$ and this may be used in (20) to solve for ArO^- . If $k_3 \approx k_4$, nearly insuperable difficulties are encountered in solving for ArO^- ; in that case, the only remedy would be to measure $[\text{ArO}^-]$ spectrophotometrically by measuring its peak of 320 mμ¹². However, while (I) will not

interfere at this wavelength, it is possible, even probable, that (IV) will.

In summary, one must verify the product (IV) as the main product of the copper amine reaction. The proposed mechanism for this reaction may then be checked by comparing the kinetic behavior of (IV) against that predicted by (19), provided the rate constants allow one of the $[\text{ArO}^-]$ approximations above to hold or that $[\text{ArO}^-]$ may be measured experimentally. Certainly if (IV) were shown not to be the main product, the mechanism and kinetics would have to be changed. In that event, it is hoped that the study proposed here would serve as an outline for future investigation.

Bibliography

1. K. U. Ingold, Accts. Chem. Research 2, 1 (1969)
2. T. Shiokawa, Sci. Repts. Research Insts. Tohoku Univ. 2, 293 (1950); Goto, Suzuki, ibid. 3, 429,335 (1951)
3. (a) J. R. Miller, Copper/Amine Catalyzed Decomposition of Hydroperoxides, Shell Oil Company, Wood River Laboratory Internal Report, February 1964; (b) J. R. Miller, F. Alsberg, ibid., Sept. 1964.
4. D. G. Hewitt, J. Chem. Soc. 18, 2967 (1971)
5. T. W. Campbell, G. M. Coppinger, JACS 74, 1429 (1952)
6. C. E. Boozer, G. S. Hammond, C. E. Hamilton, J. N. Sen, JACS 77, 3233 (1955)
7. Y. Ogata, T. Morimoto, Tetrahedron 21, 2791 (1965)
8. H. A. Laitinen, Chemical Analysis, McGraw-Hill, New York, 1960, p. 411
9. F. Basalo, R. G. Pearson, Mechanisms of Inorganic Reactions, J. Wiley, New York, 1967
10. J. R. Dyer, Applications of Absorption Spectroscopy of Organic Compounds, Prentice-Hall, Englewood, New Jersey, 1965
11. I. B. Berlman, Handbook of Fluorescence Spectra of Aromatic Molecules, 2nd Ed., Academic Press, New York, 1971
12. N. D. Coggeshall, A. S. Glessner, JACS 71, 3154 (1951)

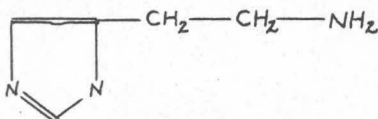
PROPOSITION III

Abstract

It is suggested that various wines be analyzed for their histamine content. The most suitable analytical procedure to be used is outlined. Finished commercial American wines are to be analyzed simply to catalog those which run high in the compound. Grape skins or must, as opposed to grape juice, are to be checked for initial histamine content. Plots of histamine content and cell growth versus time are to be made to determine if yeast cell autolysis is required for histamine release. Finally, wines prepared from a common must at different fermentation temperatures and from different yeast strains are to be analyzed for histamine to see if either temperature or yeast type is a variable which may be adjusted to reduce wine histamine content.

The presence of histamine in wine is an important problem from two standpoints. First, the compound is a known strong vasodilator¹ which in large doses leads to vascular collapse and death. A chronic excess of it leads to mastocytosis, characterized by chronic eruption of brownish papules, headache, dizziness, and hypotension. Certainly if histamine were present as a minimum physiological dose or larger in wine, there could be a possible health hazard to frequent wine drinkers. Secondly, should it generally be decided that the histamine in some wines were physiologically excessive, the sale of wines might be seriously depressed. Since the wine industry is a billion dollar Californian industry², a restriction of wine sales would have a significant effect on the state economy. Thus, from both a health and economic standpoint it is important to know how much histamine is present in various wines and how it is produced.

It has been known for some time that histamine,



is present in wines, one of the first analyses having been carried out

on Sake³. It contained approximately 1 µg/ml. Analyses on grape wines have not been available until comparatively recently. Almost without exception these analyses have been carried out on standard commercial German, French, and Swiss wines. Marquardt, Schmidt, and Spaeth⁴ found "considerable" histamine in white and red table wines, sparkling wines, and beer. De Saint-Blanquat and Derache⁵ found 0.8-0.9 µg/ml in red wines and 0.05-0.5 µg/ml in white wines. Quevauviller and Maziere⁶ analyzed sixty French wines and found values ranging from 0.1 to 30.0 µg/ml. Once again the red wines were found to be highest, with roses second and whites the lowest. Figures for one hundred forty-three Swiss wines showed an average of 3.3 µg/ml for reds and 1.2 µg/ml for whites. It was noted by Hrdlicka and Kubiczek⁷ in a general study of amines in wine as well as by some of the experimentalists above, that the amine content showed a definite dependence on the source of wine. It is therefore suggested that studies of this sort be carried out on American wines as well, in order to catalog those which always run high in histamine.

Analyses of grape juices have also been carried out. Marquardt⁴, Quevauviller⁶, and De Saint-Blanquat have all agreed that little or no histamine is present in grape juice, the latter authors claiming concentrations of less than 0.1 µg/ml. These results apparently refute the results obtained by Millies⁸ who claimed that juices contained from 0.4 to 1.9 µg/ml of histamine, practically the same as in wines. The fact that little histamine is found in grape juices indicates that histamine is formed during fermentation by decarboxylation of histidine, this amino acid being present in large quantities since it is present

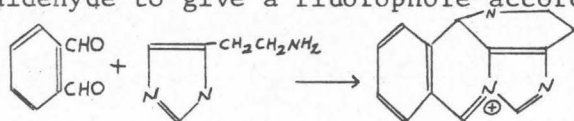
in both grapes and yeast.

The histamine concentrations given above are quite useful in that they allow one to examine the possibility that histamine is present in a large enough quantity in wines so as to give the consumer a "histamine flush"⁹. The Modern Drug Encyclopedia¹ lists histamine (or histamine phosphate) as a diagnostic drug and gives its usual dose as 300-700 µg and states that 0.1 mg of the base, if absorbed rapidly, will cause flushing. Since a wine drinker will usually drink between 300 and 700 ml of wine at a sitting, it is apparent that he will imbibe anywhere from 0.3 to 2.3 mg of histamine. If the drinking is not too slow, he will absorb enough of this to receive a physiological dose and thereby a flush. The long term effects of this level of histamine dose on the body are not known, but it is suspected that they may be adverse; hence the reason for studying wine histamine chemistry.

Several different kinds of analysis for histamine may be carried out with the results typically varying from one another by 0.1 µg/ml or more. A bioassay¹⁰ method is available in which the blood pressure of cats is monitored, or isolated ileum contractions are measured after exposure to the histamine containing solution. Paper chromatography techniques are also available and these compare reasonably well with the bioassay methods^{10,11}. These techniques suffer respectively from being difficult to perform and from lacking reproducibility. The easiest and most accurate technique to use appears to be a fluorescence method¹². The results agree with bioassay results to within about 7%. In this technique the histamine is extracted into n-butanol from an alkaline solution. Any histidine present remains in

the alkaline aqueous phase upon extraction. The histamine is then removed from the butanol by extraction with 0.1N HCl and n-heptane.

Finally the histamine is reacted in strongly alkaline media with o-phthaldehyde to give a fluorophore according to



The fluorophore concentration may be determined by activating the complex at 360 mμ and observing the fluorescence at 450 mμ. Beer's law is followed by the fluorophore in concentrations not exceeding 1.0 μg/ml. A variety of amines and amino acids have been checked for interference reactions. Histidine and ammonia were found to be the only interfering compounds. These present no real problem in grape or wine analysis, since ammonia is present in very small quantities in grapes and histidine is removed by the extraction procedure.

While analyses of histamine content in wines of the type mentioned above provide one with useful information, much remains to be answered. The method by which histamine is produced and introduced into wine still has to be determined. Since this knowledge may be required before good removal techniques can be found, it is an important problem. One study which must be performed is a histamine analysis on grape skins or must. The difference between histamine contents of red and white wines suggests that it is possible that histamine may be extracted from the skins during fermentation over them. It is felt, however, that histamine most probably is not present in the skins since grape juice would be expected to contain skin-extracted histamine in greater concentrations than 0.1 μg/ml, particularly in pressed

juice. But since no careful determination has been made, the study should be made to be absolutely positive that this is not a source of histamine. To make extraction of components from the skin easier, one would store the grapes under increased carbon dioxide pressure for a few days², causing the grapeskin cells to die and freeing the internal components for extraction.

The most likely source of histamine is the action of yeast histamine decarboxylase on histidine. We note that red wines would be expected to contain higher histamine concentrations since more histidine is available to enzymatic attack in the fermenting must due to extraction of the amino acid from the skins. The histamine may be formed enzymatically in two ways. The first would be for the decarboxylase to react continuously with histidine either interior or external to the cell membrane but releasing histamine to the solution throughout the entire fermentation. The second would be for the decarboxylase to form and store histamine completely within the yeast cell membrane. As the yeast culture aged and cells began to die, autolysis of these cells would release histamine to the developing wine.

Assuming that one of these pathways is predominant, a test that could be applied to distinguish between the two is the following. A freshly prepared grape juice would be inoculated with the standard *Saccharomyces cerevisiae* and the fermentation would be allowed to proceed. At regular intervals samples would be withdrawn and immediately filtered through a 1 μ filter. This would remove the yeast cells (typically 4-8 μ in breadth, 5-15 μ in length)¹³ and prevent the release of more decarboxylase and histamine either by diffusion or autolysis

from the cells. Each sample should be cooled immediately to slow the histidine-decarboxylase reaction and extracted with butyl alcohol and analyzed as above. Simultaneously, samples would be withdrawn, treated with phenol to inhibit further yeast growth, and counted with the aid of a hemocytometer¹⁴. One could then plot numbers of yeast and histamine concentration versus time.

Since yeast grow according to the typical S-shaped growth curve¹⁵, it may be surmised that few cells are autolyzing during the early fast growth phase whereas a great number are autolyzing in the later plateau phase. Hence if the histamine content does not increase until the plateau region is reached, there would be a strong indication that autolysis must occur for histamine release. On the other hand, if the histamine content climbs in proportion to the number of yeast cells in the fast growth region, then a continuous release of histamine is indicated.

If it were found that autolysis is required for a high histamine content, this suggests that one may keep the content low in wines by allowing fermentations to proceed only while the yeast cultures are young. In fact a procedure bordering on this is used currently in the preparation of some still wines where temperatures tend to run high during the racking when excessive temperature encourages unwanted autolysis. The new wine is separated from the yeast even before the fermentation is complete. Except for minor clarification problems, no difficulties are encountered in this approach. The young yeast technique would not be without problems however, since some wines produced only from young yeast would lack certain flavors due to the omission of

the frequently used process of aging on the lees. Champagnes would be particularly susceptible to this since more favored varieties are bottle-aged on the yeast for at least a year².

Still other studies remain. The effect of fermentation temperature on the production of histamine is not known. Accordingly, wines from a common must produced at fermentation temperatures of 45°F to 85°F should be analyzed for histamine content. Especially if cold fermentations reduce the final histamine content, a very good commercial method for histamine removal would be available.

It is also possible that various yeast strains will produce varying amounts of histamine when all other factors are held constant. There certainly are large variations between species as to the amount of certain chemicals produced such as glycerol and higher alcohols¹⁵. Studies designed to investigate the behavior of various yeasts have a great number of yeast strains available to them, but relatively few are as well adapted to wine making as the standard *Saccharomyces cerevisiae* var. *ellipsoideus*. However, a set that will produce as much alcohol and as quickly as this standard strain includes the following: *S. rosei*, the *S. cerevisiae* strains of *alpinus*, *turbidans*, and *orasti*, *S. oviformis*, and *S. acidifaciens*¹⁵. Histamine analysis of finished wines from these yeasts should be performed. Perhaps one of these yeasts or a combination of them will give the desired flavors as well as a reduced histamine content.

Bibliography

1. A. Lewis, M.D., Editor, Modern Drug Encyclopedia, 11th Ed., Yorke Med. Group Publ., New York, 1970, p. 349.
2. M. A. Amerine, V. L. Singleton, Wine, An Introduction for Americans, U. of California Press, Berkeley, 1965.
3. T. Higashi, Sci. Papers of the Inst. of Phys. and Chem. Research (Japan), No. 727, 1937.
4. P. Marquardt, H. Schmidt, M. Spaeth, Arzneimittel Forsch. 13, 1100-1102 (1963).
5. G. DeSaint-Blanquat, R. Derache, Trav. Soc. Pharm. Montpellier 28(1), 23-26 (1968).
6. A. Quevauviller, M. Maziere, Ann. Pharm. Fr. 27(6), 411-414 (1969).
7. J. Hrdlicka, J. Kubiczek, Kvsony Prumysl 9, 35-38 (1963).
8. K. Millies, Int. Fruchtsoft-Union, Ber. Wiss. Tech. Komm. 7, 125-134 (1966).
9. F. Drawert, Vitis 5(2), 127-130 (1965).
10. H. W. J. Werringboer, Arzneimittel Forsch. 16(12), 1654-1656 (1966).
11. H. G. Maier, Fresenius' Z. Anal. Chem. 244(4), 256 (1969).
12. A. Beall, Intern. Arch. Allergy Appl. Immunol. 26(1), 1-17 (1965); P. Shore, A. Burkhalter, V. Cohn, J. Pharmacol. and Exper. Therap. 127, 182 (1959).
13. W. Roman, Ed., Yeasts, Dr. W. Junk Publishers, The Hague, 1957.
14. A. Guilliermond, F. Tanner, The Yeasts, J. Wiley, New York, 1920.
15. M. A. Amerine, H. Berg, W. Cruess, The Technology of Wine Making, 2nd Ed., The Avi Publ. Co., Westport, 1967.

PROPOSITION IV

Abstract

A brief review is given of the theories that have been advanced to explain the behavior of alkali metal ammonia solutions. Because structural differences characterize each of the theories, it is proposed that they be studied by analyzing x-ray scattering data taken on metal ammonia solutions. A discussion of the Fourier inverse of the intensity data shows that cesium ammonia solutions in the 1.5 to 7.0M range provide the most information about possible metal ion clustering. If clustering is present, it is argued that Cs-Cs peaks in the distribution function will show little change in position as the concentration is changed.

Metal ammonia solutions have been under study for over seventy years and work is still continuing on them¹⁻⁴. They are of present day interest because of their structural uniqueness. In low concentrations of dissolved metal, the solutions are ionic in character and closely resemble salt solutions. As the metal concentration increases, their properties change in a continuous fashion from ionic to metallic.

Currently several theories exist that attempt to account for this behavior. Since different structures of the solutions are suggested in the various theories, it is proposed that these theories be investigated where possible by studying the x-ray diffraction patterns of these solutions. The remainder of this proposition includes a brief summary of the current theories, followed by a description of how an x-ray experiment might be carried out to examine these theories.

In low concentrations of metal (less than 0.05M), it is thought that the metal dissociates to metal cations and electrons⁵. The electrons are then trapped in a spherical cavity formed by ammonia

molecules (an e_1 cavity), presumably with the molecules oriented so that the hydrogens are directed toward the center of the cavity. In order to account for the volume expansion which occurs when metal is dissolved in ammonia, the radius of these cavities has been estimated to be about 4Å. Support for the cavity model comes from the fact that if energies are calculated for a cavity of this radius, it is found that the lowest transition accounts for the 7000 cm^{-1} absorption band always found in dilute metal ammonia solutions. Evidence of the electrons being merely solvated and not bound to other species is found in the large transference number of the negative carrier in conduction experiments; the negative carrier accounts for nearly 86% of the total current.

In intermediate concentrations (0.05M to 1M), the structure is less well understood. One theory⁶ (BLA) proposes that the basic unit is composed of the solvated cation and the electron trapped in the potential of the charged cation and its surrounding solvent shell. The cation-electron unit is termed a monomer. Since the solution is diamagnetic in this concentration range, the electron spins must be paired and hence it has been suggested that two monomers are bound together to form a chemically bonded dimer. Symons¹ has indicated that at low concentrations the dimer must break up into solvated cations and electrons with very little monomer formation in order to correctly describe the conductivity of these solutions.

An extension of the cavity theory accounts for the diamagnetism in this range by assuming that two paired electrons can exist in a single cavity (an e_2 cavity). A visible absorption band at 15000 cm^{-1}

has been assigned to transitions within the e_2 cavity. The cations remain solvated and do not pair.

Still another theory, advocated by Jolly³, is that the monomer unit is an ion pair of solvated cations and electrons bound together by coulombic attraction and the dimer species is a quadrupolar ionic assembly of two ammoniated cations and two ammoniated electrons. The wavefunctions of the two electrons are presumed to overlap sufficiently to insure pairing. This theory was advanced to account for the fact that the 7000 cm^{-1} peak unexpectedly followed Beer's law up to 0.05M, this upper limit being a region where dimer formation was extensive and changes in the spectrum had been expected as the BLA dimer absorbed radiation instead of the e_1 cavity.

At still higher concentrations (greater than 1M), little is known about the structure of metal ammonia solutions. Electron spin resonance data⁷ shows that sodium ammonia solutions doped with very small amounts of cesium have relaxation times that are characteristic of cesium ammonia solutions rather than the sodium solutions. Since the electrons must all have access to the cesium atoms for this to be true, a lattice structure with delocalized electrons is indicated. The detailed structure of this lattice is unknown. It may be diffuse with solvated cations spread fairly evenly throughout the solution or it may consist of reasonably well defined clusters of solvated metal ions.

Since the cavity and BLA theories predicted different spatial arrangements of the metal ions and thus different x-ray spectra in intermediate concentrations, Schmidt⁸ and Brady⁹ undertook the measurement of the low angle x-ray scattering of sodium ammonia solutions. In

both works, it was expected that a peak would appear at about 0.05 radians (2θ) if the dimer species (approximately 15Å long) were present. The peak would be absent if only cavities were present. Unfortunately, the two experiments are in strong disagreement, Schmidt's work confirming the existence of dimers and Brady's work refuting them.

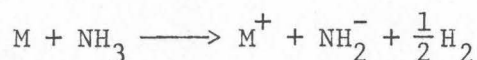
Because of the doubt raised about the existence of groupings of the metal ions, it is desirable that new x-ray experiments be performed to search for them. Unlike the earlier work, however, it is suggested that large angle x-ray scattering techniques be employed. In order to obtain the results in the low angle work, the researchers had to push the method close to its error limit. As will be seen, information may be extracted from the large angle data with less error provided the metal concentration is kept high enough. Besides answering the general question about whether metal groupings exist, there is reasonable hope that if they do exist some of the metal-metal distances in these structures may be determined. Hence, it is expected that the scattering results will help define just what the lattice is that Chan⁷ claims must exist in concentrated solutions.

Since the aim of the x-ray experiment is to search for persistent metal-metal spacings characteristic of clustering, it is desirable to weight the spectrum with scattering from the metal rather than solvent. This can be done by choosing a metal with a large number of electrons since, to first order, scattering is proportional to the square of the number of electrons. Cesium would thus be the metal of choice, since it is the highest atomic numbered alkali metal

that can be readily obtained. Cesium ammonia solutions have the further advantage of showing no liquid-liquid two phase region as do sodium or potassium ammonia solutions¹⁰. Hence, separation or equilibration of phases will not be an important experimental problem.

Two special experimental problems of cesium ammonia solutions must be considered. First, cesium ammonia solutions are highly reactive and one must be careful to choose a sample cell whose materials will not be attacked. Beryllium is the standard window material used in the construction of x-ray cells, but since all other alkaline earths are known to dissolve in ammonia, there was doubt as to whether it would be suitable for these solutions. Fortunately, tests¹¹ have shown that Be samples will stand up to sodium-ammonia solutions for twenty-four hours with no detectable weight change. Stainless steel (18-8,304) also resists attack over this time period and may be used for the non-window parts of the cell.

Secondly, one must check the solutions for possible decomposition according to



Since this reaction is quite fast (it is self-catalyzing)¹⁰ and since an x-ray experiment requires containment of the solution for about twenty-four hours, it is possible that the solution could be badly decomposed by the end of the run if the reaction ever got started. Ordinarily this decomposition is prevented by careful exclusion of impurities, but one should always check to see if it really has been prevented by condensing the ammonia from the cesium ammonia solution with liquid nitrogen and measuring any remaining hydrogen with the

small volume McCloud-Toepler equipment described by Naiditch¹². The amount of hydrogen produced defines the degree of decomposition by the equation above.

The experimental data may be obtained by following the relatively standard procedures^{13a,b} used in the data acquisition from argon samples. The methods of temperature control, normalization, and correction of data for polarization and absorption are quite general and may be carried over with only minor modification for use with cesium ammonia solutions.

Once the scattering data is obtained, it must be interpreted and in order to do this one must know the scattering species in solution. In the case of cesium ammonia solutions, one may assume that there are two scatterers, Cs^+ and NH_3 . Cs^0 may be ignored since it is completely dissociated into Cs^+ ions and electrons; the electrons scatter so little of the radiation relative to other species that they may be neglected.

An observation of some importance is that the ammonia molecules are non-spherical and should have their scattering described by orientation dependent scattering factors. While this is rigorously true, it appears that the higher coefficients of the harmonic expansion of the factor¹⁴, if centered on the nitrogen atom, allow one to neglect scattering differences due to orientational changes of the molecule. Hence, to a first order approximation, cesium ammonia solutions may be treated (for x-ray purposes) as a binary mixture composed of spherical Cs^+ and NH_3 scatterers.

The analysis of the scattering data from the mixture may be carried out by following either one of two formalisms. One is due to Warren, Krutter, and Morningstar¹⁵ (WKM) and the other is due to Pings and Waser¹⁶ (PW). In either approach, it is impossible to invert the data for a full description of the mixture. In the case of cesium ammonia solutions, three pair correlation functions appear in the expression for the intensity $g_{\text{Cs}^+, \text{Cs}^+}$, $g_{\text{Cs}^+, \text{NH}_3}$, and $g_{\text{NH}_3, \text{NH}_3}$, and it is immediately apparent that one experiment will not provide enough information to determine all of these functions uniquely. At best some superposition of these functions is all that can be obtained.

Both the WKM and PW formalisms begin with the expression

$$I(\kappa) = \sum_i x_i f_i^2(\kappa) + \sum_i \sum_j x_i x_j f_i(\kappa) f_j(\kappa) \rho \int [g_{ij}(r) - 1] j_0(\kappa r) 4\pi r^2 dr$$

for total coherently scattered intensity, where i and j denote the various scattering species. The WKM approach makes the approximation that there is a general $f(\kappa)$ curve shape common to all atomic scattering factors and $f_i(\kappa) = K_i f(\kappa)$. K_i is approximately the atomic number of species i . The expression above may then be transformed to give

$$\begin{aligned} & r \sum_i \sum_j x_i x_j K_i K_j [g_{ij}(r) - 1] \\ &= \frac{1}{2\pi^2 \rho} \int \kappa \frac{I(\kappa) - f^2(\kappa) \sum_i x_i K_i^2}{f^2(\kappa)} \sin(\kappa r) d\kappa = rD(r) \end{aligned}$$

The PW approach does not make any approximation and by means of a convolution analysis gives

$$r \sum_i \sum_j x_i x_j H_{ij}(r) = \frac{1}{2\pi^2 \rho} \int_0^\infty \kappa \frac{I(\kappa) - \sum_i x_i f_i^2(\kappa)}{[\sum_i x_i f_i(\kappa)]^2} \sin(\kappa r) d\kappa = rH(r)$$

In cases where the Morningstar approximation is valid, it can be seen that the right-hand sides of both of these equations become equal to one another except for a factor of $(\sum_i x_i K_i)^2 = F$. Hence an interpretation for $H_{ij}(r)$ is available which shows that it is closely related to $K_i K_j [g_{ij}(r) - 1] / F$. Note that inversion of the experimental data only leads to a sum of $H_{ij}(r)$ functions and does not evaluate each one. Either theory may be applied to cesium ammonia solutions although care must be taken to verify the Morningstar approximation if the WKM approach is used. The best check will be to perform both inversions and check on the agreement between $D(r)/F$ and $H(r)$.

It is to be noted that there is no difficulty in evaluating the Fourier transform integrals above. The spherical $f(\kappa)$ that would be used for ammonia has recently been calculated¹⁴ and it contains no zeros provided the center of the scattering factor is placed on the nitrogen nucleus. Hence the denominator of the Fourier kernel in the expression above cannot go to zero and the difficulties stemming from such a development may be avoided.

It is apparent that if cesium dimers or large clusters were present, H_{Cs^+, Cs^+} would possess peaks at distances corresponding to cesium-cesium separations. Such peaks should be quite noticeable in

$H(r)$ or $D(r)$ for concentrated solutions, which may be verified as follows. At a concentrated solution level of 4N, the NH_3/Cs mole ratio is 7.88¹⁰. Hence $\frac{1}{F} \sum_i \sum_j x_i x_j K_i K_j$ (all $g_{ij} - 1$ are assumed constant and equal for this rough calculation) becomes

$$\begin{aligned} & \left[\left(\frac{1}{8.88} \right)^2 (55)^2 + 2 \left(\frac{7.88}{8.88} \right) \left(\frac{1}{8.88} \right) (10)(55) + \left(\frac{7.88}{8.88} \right)^2 (10)^2 \right] \\ & \times \left[\frac{1}{\frac{7.88}{8.88} (10) + \frac{1.00}{8.88} (55)} \right]^2 \\ & = \left(\frac{1}{133.8} \right)^2 (3025 + 8668 + 6209) \end{aligned}$$

from which one can see that the Cs-Cs contribution is about 17% of the total. To be more accurate the g_{ij} term would have to be included. Since this function would have peaks at r values corresponding to any Cs-Cs spacings present in solution and since Cs- NH_3 or NH_3 - NH_3 spacings presumably would occur at different r values, it is likely that the Cs-Cs contribution could be raised well above this 17% level in the region of Cs-Cs separation distances. If the calculation is repeated at 1.5N (mole ratio of 25.5), an average contribution of about 3% is found instead of 17%; g_{ij} peak effects may raise this to a measurable level. It is apparent, however, that concentrations below 1.5N will yield information on Cs-Cs spacings with rapidly increasing difficulty, and one must conclude that the large angle x-ray scattering is most useful for concentrated solutions above 1.5N.

An experimental program would thus involve obtaining scattering data for solutions near saturation and then for solutions of decreasing cesium concentration down to about 1.5N. In each case the $H(r)$

function would be obtained and the positions of peaks noted. As the concentration is reduced, those peaks corresponding to cesium-cesium spacings will generally decrease (as x_{Cs}^2 decreases) whereas those corresponding to $\text{NH}_3\text{-NH}_3$ spacings will increase. This will allow one to make general species assignments to the peaks. Evidence of clustering (lattice structure) will be found if the locations of the Cs-Cs peaks change little upon dilution. If no clustering were present, the cesium ions would be distributed equally throughout the solution and the average distance between cesium ions would be proportional to the minus one-third power of the concentration. If clusters were present, at least two of the metal ions would be held at a nearly constant spacing corresponding to a potential minimum and the Cs-Cs peak would not be greatly shifted as the concentration was lowered. Of course, its height may change because of cluster dissociation. If evidence for clustering were found at high concentrations, it may be viewed as evidence for smaller groupings, such as dimers, existing at intermediate concentrations.

Bibliography

1. M. Symons, Quart. Rev. (London) 30, 1628 (1959)
2. T. Das, Advan. Chem. Phys. 4, 303 (1962)
3. G. Lepoutre, M. Sienko, Metal-Ammonia Solutions, W. Benjamin, Inc. New York, N. Y., 1964.
4. R. Gould, Solvated Electron, Adv. in Chem. Series 50, Am. Chem. Soc., Washington, D. C., 1965
5. (a) R. Ogg, JCP 14, 114 (1946); (b) J. Kaplan, C. Kittel, *ibid.* 21, 1429 (1953); (c) W. Lipscomb, *ibid.* 21, 52 (1953); (d) M. Gold, W. Jolly, K. Pitzer, JACS 84, 2264 (1962)
6. E. Becker, R. Lindquist, B. Alder, JCP 35, 971 (1956)
7. S. Chan, J. Austin, O. Paez, Proc. International Conf. on Metal Ammonia Solutions, Cornell University, Ithaca, N.Y., 1969.
8. P. Schmidt, JCP 27, 23 (1957)
9. G. Brady, J. Varimbi, JCP 40, 2615 (1964)
10. J. Hodgins, Can. J. Res. 27, 861 (1949)
11. This laboratory, unpublished results.
12. S. Naiditch, J. Vac. Sci. and Tech. 3 (5), Oct. 1966
13. (a) S. Smelser, "An X-Ray Diffraction Study of the Structure of Argon in the Dense Liquid Region", Thesis, California Institute of Technology, 1969; (b) B. Kirstein, "An X-Ray Diffraction Study of Liquid Argon" (in preparation), Thesis, California Institute of Technology, 1972
14. L. Blum, J. Comp. Phys. 7, 592 (1971)
15. B. Warren, H. Krutter, O. Morningstar, J. Am. Ceramic Soc. 19, 202 (1936)
16. C. Pings, J. Waser, JCP 48, 3016 (1968)

PROPOSITION V

Abstract

It is proposed that a sample of bottle-aged champagne be investigated to determine if the protein colloids present in it resulting from yeast autolysis are responsible for its increased ability to dissolve and retain carbon dioxide. The champagne is to be decarbonated and then divided into two samples. One will retain the colloid and the other will have it removed by ultracentrifugation or ultrafiltration. Each of the resulting solutions is to be placed in a PVT apparatus, mixed with known amounts of carbon dioxide, and measured for bubble point pressures as a function of added carbon dioxide. Only if the colloid is interacting with the carbon dioxide/carbonate equilibria will the bubble point pressure-carbon dioxide curves differ between the colloid present and colloid free solutions.

A process that the wine industry would like to develop further is the carbonation of still wines to produce sparkling wines^{1a}. The principal reason for employing this process is to reduce production costs. Bottle fermented champagne must be aged for at least a year during which time much labor goes into the riddling procedure. Furthermore, the final product is taxed at the rather high rate of \$3.40/gal (1965)^{2b}. Carbonated wine eliminates the riddling labor and much of the storage time. Perhaps of greatest importance is that it is taxed at only \$2.40/gal.

Carbonation, although used occasionally in the past, is not widely used presently even though the above-mentioned financial inducements exist. The principal reason for this is that carbonated wines

have lost status relative to other sparkling wines because they have historically been priced as high but were inferior in quality. One of the main quality differences is the ability of champagne type² wines to dissolve more carbon dioxide at fixed volume and pressure than carbonated wines^{1c}. Liotta³ has shown that commercial carbonated wines lose about twice as much carbon dioxide as champagne types if left open at one atmosphere.

The cause of the solubility difference is not understood. It has been proposed^{1c,4,5} that the colloidal proteins which are introduced into champagne when the yeast autolyzes are responsible for binding carbon dioxide or its carbonate derivatives to its surface, thus increasing the carbon dioxide solubility. A possible mechanism for this binding is that the carbon dioxide will form hydronium and bicarbonate ions and the colloid, being generally positively charged in the acidic pH of the wine, will trap some of these bicarbonate ions in the double layer surrounding it. In a study⁴ of the differences between bottle and tank fermented champagnes, some evidence for this effect has been found. When these two wines were ultrafiltered, it was found that the carbon-dioxide release ratio changed in rough proportion to the amount of colloidal nitrogen removed.

Of course other mechanisms are present which may account for increased carbon dioxide solubility in champagne. Besides adding to the colloid content of the wine, autolysis also produces increased levels of other non-colloidal components such as amino acids. When carbon dioxide is added to solutions containing these substances, new acid-base equilibria favoring solubility may be established.

Furthermore, increased amounts of substances such as glycerol may change the ability of the solution to retain gas since this would result in a change in the carbon dioxide Henry's constant.

In order to determine the importance of the colloidal protein in binding carbon dioxide, it is proposed that the bubble point pressure be measured as a function of carbon dioxide added to two degassed samples of champagne, one containing colloid and the other lacking it. The bubble point pressure depends strongly on the mole fraction of the most volatile component present in a solution, in this case carbon dioxide. Of course this mole fraction is not equal to the amount of gas added to a sample, since there will always be a CO_2 /carbonate equilibrium. It is known from the work of Jahnke and Röhr⁴ that the amount of colloidal protein present in champagne is relatively small (less than 9.6 mg colloidal N/l); hence the mole fraction compositions of the degassed colloid containing and colloid free samples would be nearly identical. Thus, if on the one hand it is assumed that upon carbon dioxide addition no interactions between colloid and CO_2 /carbonate equilibria occur, the two samples will have nearly identical equilibria, nearly identical carbon dioxide mole fractions, and hence nearly identical bubble point pressures. If, on the other hand colloid interactions do exist, the mole fraction of carbon dioxide will be reduced as the CO_2 equilibria shift to accommodate the colloid binding, and the bubble point pressure will be reduced. The degree of difference between bubble point pressures of the colloid containing and colloid free samples will thus serve to determine the significance or, in fact, the very existence of the carbon dioxide binding action of

the colloid.

Three steps are involved in carrying out this study. Before PVT measurements can be carried out on the wine, it is first necessary to remove all the carbon dioxide from the champagne. This is easily done by bubbling nitrogen gas through the solution until no more carbon dioxide comes off. Carbon dioxide may be monitored in the nitrogen outflow by either chemical means or gas chromatography. Loss of other volatile components in the nitrogen stream is unimportant provided the amounts are kept small.

The decarbonated solution must then be divided into two parts and one part must have its colloid removed. This removal may be effected by either ultracentrifugation or ultrafiltration. In either case, the colloid free wine must also be free of nitrogen before proceeding to the PVT measurements, since nitrogen would pass out of solution along with the carbon dioxide at the bubble point if it were not removed. In the case of ultracentrifugation, nitrogen may be removed before centrifugation by applying a slight vacuum to the (undivided) decarbonated wine. Transfers of the wine into and out of the centrifuge tube would then be done under its own vapor pressure, taking care not to reintroduce nitrogen into the system. In the case of ultrafiltration, the wine would be filtered under about 15 atm compressed nitrogen⁶ and would then have its nitrogen removed by vacuum. Loss of components such as water or ethanol in this degassing procedure would lead to a compositional difference between the filtered and nonfiltered wine and such losses would have to be minimized.

Finally, the PVT measurements would have to be carried out in a suitable apparatus. Micro-sized chambers are practically required

if ultracentrifugation is employed, since the tubes have a maximum capacity of only a few cubic centimeters. A good micro apparatus has been developed by Reamer and Sage⁷ and with minor modifications can be adapted for use with this system. The carbon dioxide/wine pressure data of Vogt^{1d} is available for equipment design. The data would be taken in the following way. After a small volume (approx. 0.1 cc) of degassed nonfiltered wine was introduced into the chamber, a small amount of carbon dioxide would be added to it. The mixture would be compressed until a single liquid phase was obtained. The liquid would then be slowly expanded and a plot of pressure versus volume made for this composition. A discontinuity would be obtained in the plot at the bubble point pressure. After obtaining enough data to adequately determine this pressure, the mixture would be expanded, more carbon dioxide would be introduced, and the procedure would be repeated to determine the bubble point pressure of this more concentrated carbon dioxide mixture. After several carbon dioxide additions, one could make a plot of bubble point pressure versus total carbon dioxide added. The entire procedure would then be repeated for the degassed filtered wine. The two plots of bubble point pressure versus carbon dioxide added would be the desired data.

If it should be found that protein colloids do affect the solubility of carbon dioxide in wine, then a large number of future experiments would be indicated. The first of these would involve identifying the colloid size range most responsible for this effect. Later experiments would involve separating these colloids as concentrates from sources such as wine and yeast liquors. The colloid

concentrates would then be added to still wines and the mixture carbonated. Carbon dioxide retention in these colloid enriched still wines could then be compared against that characteristic of tank and bottle fermented champagnes. Sensory comparisons would also be required, since the concentrates might contain odorous materials.

Bibliography

1. M. Amerine, H. Berg, W. Cruess, The Technology of Wine Making, 2nd Ed., Avi Publ., Westport, Conn., 1967; (a) p. 461; (b) p.749; (c) p. 214; (d) p. 456.
2. Champagne type wines are those which pick up their carbon dioxide charge from a second fermentation (either in bottle or tank), whereas the carbonated wines pick it up from an outside source. The sparkling wine designation includes both types.
3. C. Liotta, "Interim Report Concerning Experiments on Naturally and Artificially Carbonated Wines", Internal Revenue Service, Washington, D. C., 1956
4. A. Jahnke, M. Röhr, Mitt. Rebe u. Wein, Serie A (Klosterneuberg) 10, 111 (1960); 10, 210 (1960)
5. J. Anderson, Comm. Masters Brewers Assoc. America 20, Nos. 1-2, 3-7, 15 (1959)
6. L. Ambard, S. Trautmann, Ultrafiltration, C. Thomas Publ., Springfield, Ill., 1960
7. H. Reamer, B. Sage, Am. Jour. Phys. 9, 310 (1941); 25, 58 (1957)